Republic of Iraq

Ministry of Higher Education & Scientific Research

University of Kerbala

College of Engineering

Civil Engineering Department

Finite Difference Analysis of Geogrid Reinforced Load Transfer Platform Over Rigid Inclusions

A Thesis Submitted to the Council of the Faculty of the College of the Engineering/University of Kerbala in Partial Fulfillment of the Requirements for the Master Degree in Infrastructure Engineering

By:

Alaq Khalil Ibraheem

Supervisors

Asst. Prof. Dr. Mahdi Abbas Mahdi

Asst. Prof. Dr. Saif Mohammed Jawad

September - 2025 Rabi' al-Thani - 1447

بسم الله الرحمن الرحيم

يَرْفَعِ اللَّهُ الَّذِينَ آمَنُوا مِنكُمْ وَالَّذِينَ أُوتُوا الْعِلْمَ دَرَجَاتٍ

صدق الله العلي العظيم

(المجادلة: من الآية 11)

Examination committee certification

We certify that we have read the thesis entitled **"Finite Difference Analysis of Geogrid Reinforced Load Transfer Platform Over Rigid Inclusions"** and as an examining committee, we examined the student **"Alaq Khalil Ibraheem"** in its content and in what is connected with it and that, in our opinion, it is adequate as a thesis for the degree of Master of Science in Civil Engineering.

Supervisor

Signature:
Name: **Asst.Prof.Dr. Mahdi Abbas Mahdi**
Date: / / 2025

Supervisor

Signature:
Name: **Asst.Prof.Dr. Saif Mohammed Jawad**
Date: / / 2025

Member

Signature:
Name: **Asst.Prof.Dr. Raid R. A. Almuhanna**
Date: 23/ 9/ 2025

Member

Signature:
Name: **Dr. Mustafa Naeem Kareem**
Date: 23/ 9 / 2025

Chairman

Signature:
Name: **Prof.Dr. Qassun S. Mohammed Shafiqu**
Date: / / 2025

Signature:
Name: **Asst. Prof. Dr. Aysar Tuama Al-Awadi**
Head of the Department of Civil Engineering
Date: / / 2025

Signature:
Name: **Prof. Dr. Haider N. Azziz**
Dean of the Engineering College
Date: / / 2025

Supervisor certificate

We certify that the thesis entitled **"Finite Difference Analysis of Geogrid Reinforced Load Transfer Platform Over Rigid Inclusions"** was prepared by **Alaq Khalil Ibraheem** under our supervision at the Department of Civil Engineering, Faculty of Engineering, University of Kerbala as a partial of fulfilment of the requirements for the Degree of Master of Science in Civil Engineering.

Signature:

Asst. Prof. Dr. Mahdi Abbas Mahdi

Date: / / 2025

Signature:

Asst. Prof. Dr. Saif Mohammed Jawad

Date: / / 2025

Linguistic certificate

I certify that the thesis entitled **"Finite Difference Analysis of Geogrid Reinforced Load Transfer Platform Over Rigid Inclusions,"** which has been submitted by **Alaq Khalil Ibraheem,** has been proofread, and its language has been amended to meet the English style.

Signature:

Dr. Awad Ali Sagheer

Date: / / 2025

Undertaking

I certify that research work titled **"Finite Difference Analysis of Geogrid Reinforced Load Transfer Platform Over Rigid Inclusions"** is my own work. The work has not been presented elsewhere for assessment. Where material has been used from other sources, it has been properly acknowledged / referred.

Signature:

Alaq Khalil Ibraheem

Date: / / 2025

Dedication

To my dearest mother, whose unwavering love, prayers, and support have been the cornerstone of my perseverance.

And to my beloved husband, whose steadfast encouragement and understanding have strengthened my resolve to achieve this work.

With deepest gratitude, I dedicate this thesis to both of you in recognition of your sacrifices and enduring faith in my journey.

Acknowledgments

First and foremost, I would like to express my deepest gratitude and sincere appreciation to my supervisors, Asst. Prof. Dr. Mahdi Al-Naddaf and Asst. Prof. Dr. Saif Jawad, for their invaluable guidance, continuous support, and insightful feedback throughout the course of this research. Their expertise, patience, and encouragement have been instrumental in the successful completion of this thesis.

I would also like to extend my heartfelt thanks to Asst. Lecturer Sajjad Emad Rasheed and all the faculty members of the Department of Civil Engineering for their generous assistance, constructive advice, and enriching discussions, which have significantly contributed to my academic and professional development.

Finally, I am deeply thankful to my family for their unwavering love, sacrifices, and constant encouragement, which have been my greatest source of strength throughout this journey.

Abstract

The construction of embankments and foundation systems over weak or compressible soils often requires advanced ground-improvement techniques to ensure stability and serviceability. Geosynthetic-Reinforced Load Transfer Platforms (GRLTP) combined with rigid inclusions have proven effective in redistributing vertical stresses and minimizing differential settlements. Nevertheless, a clear gap exists in previous research regarding the combined influence of applied vertical stress, trapdoor displacement magnitude, trapdoor geometry and arrangement, footing dimensions and location, and the inclusion of geosynthetic reinforcement on load transfer platforms under localized subsidence. Earlier studies rarely examined these factors simultaneously within a rigorous finite-difference framework.

This study addresses that gap by employing the finite difference method (FDM), implemented in FLAC3D, to perform an advanced three-dimensional numerical investigation of GRLTPs over rigid inclusions subjected to trapdoor-induced subsidence and surface loading. A suite of calibrated models explored the effects of displacement, trapdoor width and multiplicity, footing size and offset, and reinforcement depth and configuration. Validation against published laboratory trapdoor tests demonstrated good agreement, with a root mean square error (RMSE) about 3.18%, confirming the robustness of the models.

The results showed that soil arching mobilizes rapidly at relatively small displacements, effectively redirecting stresses toward adjacent supports. However, arch efficiency progressively degrades with continued displacement or under high surface loads, as vertical stresses re-concentrate

above the yielding zones. Reinforcement was found to significantly enhance stability, with single geogrid layers positioned near the settlement plane achieving a Stress Reduction Ratio (SRR) of about 0.75 and TC–SE stress intersection about 70 kPa, corresponding to a good performance rating. Furthermore, multiple reinforcement layers provided even greater improvements, where double reinforcement achieved a 60% increase in performance compared to the single-layer baseline, raising the TC–SE intersection from 70 kPa to 110 kPa and yielding an excellent cost–benefit ratio. However, the addition of a third reinforcement layer resulted in only marginal gains, with poor cost–benefit efficiency.

The study further revealed that increasing the number of trapdoors fundamentally alters the load transfer mechanism. In double- and triple-trapdoor systems, intermediate supports subdivided the embankment into multiple interacting arching zones, reducing the direct load on trapdoors and enhancing stress uniformity across supports. Wider footings and increased offset from the trapdoor center further improved load transfer efficiency. Collectively, these findings provide a comprehensive understanding of LTP behavior under multi-trapdoor subsidence, offering refined insights for optimizing pile-supported embankment design.

Table of Contents

List of Tables

List of Figures

List of Abbreviations

AFDP	Arching Full Degradation Pressure
BS	British Standard
DEM	Discrete Element Method
FDM	Finite Difference Method
FEA	Finite Element Analysis
FLAC3D	Fast Lagrangian Analysis of Continua in 3 Dimensions
GRLTP	Geosynthetic Reinforced Load Transfer Platform
GRPS	Geosynthetic Reinforced Pile-Supported (Embankment)
LTP	Load Transfer Platform
MSC	Middle Support Center
MSE	Middle Support Edge
RMSE	Root Mean Square Error
RIs	Rigid Inclusions
SAR	Soil Arching Ratio
SE	Side (Edge) Support
SRR	Stress Reduction Ratio
TC	Trapdoor Center
TE	Trapdoor Edge
3D	Three-Dimensional
TER	Right Trapdoor Edge
TEL	Left Trapdoor Edge
SEL	Left Edge Support
SER	Right Edge Support

List of Symbols

a	Width of pile cap or trapdoor
B	Footing/Trapdoor width
c	Soil cohesion
E	Elastic modulus
Ea	Arching effectiveness
H	Embankment or fill height
K	Coefficient of lateral pressure at rest
Kp	Coefficient of passive earth pressure
q	Applied uniform surcharge
R	Radius of soil arch
s	Pile or trapdoor center-to-center spacing
s′	Clear spacing between piles/trapdoors (s − a)
σ_v	The average measured vertical pressure above the yielding base
σ'_v	The average measured vertical pressure beneath the geosynthetic reinforcement
t	Vertical displacement of trapdoor
T	Maximum tension in geosynthetic reinforcement
ε	Strain in geosynthetic reinforcement
φ	Internal friction angel
ψ	Dilatancy angle
γ	Unit weight of embankment soil

Chapter I

Introduction

Chapter One: Introduction

1.1 General

This chapter establishes the foundation of the research by contextualizing the engineering challenges associated with constructing embankments and foundation systems over weak or compressible soils. It introduces the phenomenon of soil arching as a fundamental mechanism governing stress redistribution in such conditions and emphasizes the role of rigid inclusions and geosynthetic reinforcement in enhancing stability and serviceability. This chapter presents by articulating the research problem, objectives, and scope, while also outlining the organization of the thesis to provide a clear framework for the subsequent chapters.

Expanding upon the conceptual foundation outlined in the introduction, the following section provides an in-depth examination of geosynthetic-reinforced load transfer platforms (GRLTP). It synthesizes their historical development, governing mechanisms, and documented limitations in current research, thereby consolidating the rationale for undertaking the present finite difference investigation into their performance under localized subsidence.

1.2 Geosynthetic-Reinforced Load Transfer Platform (GRLTP)

In recent decades, the design and construction of embankments and foundations over soft or compressible soils have posed significant challenges in geotechnical engineering. To overcome issues related to excessive settlements and low bearing capacity, composite foundation systems that combine rigid inclusions with Geosynthetic-Reinforced Load Transfer Platforms (GRLTPs) have become increasingly prevalent (Han and Gabr, 2002) (Van Eekelen and Brugman, 2016) . This approach has proven highly effective in redistributing loads from embankments or structural elements to

deeper, stiffer strata while mitigating differential settlements and enhancing overall stability (Al-Naddaf and Han, 2021).

The performance of geosynthetic-reinforced load transfer platform (GRLTP) systems is governed primarily by two fundamental mechanisms: soil arching and the tensioned membrane effect of the geosynthetic reinforcement (Rui *et al.*, 2022). The soil arching mechanism enables the redistribution of vertical stresses away from yielding zones—such as trapdoors or weak soil pockets—toward adjacent rigid inclusions or stable support regions. This stress transfer reduces the direct load imposed on the underlying compressible subsoil (Karl Terzaghi, 1943) and (Hewlett and Randolph, 1988). Concurrently, the geosynthetic reinforcement contributes to system stability by intercepting the residual stresses and redistributing them laterally. Acting as a tensioned membrane, it enhances the overall load transfer capacity and minimizes differential settlement (Han and Gabr, 2002).

While extensive research has been conducted through physical model tests and field case studies to explore these mechanisms (Al-Naddaf, 2017) and (Al-Naddaf, 2019), most numerical investigations have primarily utilize two-dimensional analyses, which cannot fully capture the inherently three-dimensional nature of soil-structure interactions under localized subsidence conditions (Van Pham and Dias, 2021). Parameters such as the magnitude of trapdoor displacement, the number and arrangement of trapdoors, footing width and position, and the characteristics of the geosynthetic reinforcement critically influence the mobilization and degradation of soil arching, yet these factors have not been comprehensively studied within a robust three-dimensional numerical framework (Al-Naddaf and Han, 2021).

Consequently, a detailed understanding of how these interacting variables affect stress redistribution and load transfer mechanisms is essential

to optimize the design and ensure the long-term performance of LTP. To address this research gap, the present study employs advanced finite difference modeling to systematically investigate the behavior of geosynthetic-reinforced load transfer platforms over rigid inclusions subjected to localized subsidence scenarios. The outcomes aim to contribute valuable insights for improving current design guidelines and practices in the context of pile-supported embankments and similar composite foundation systems.

1.3 Problem Statements

Load transfer platforms (LTP) constructed over rigid inclusions have gained significant attention in recent years due to their ability to enhance ground stability and mitigate differential settlements. While considerable research has been undertaken through field studies, laboratory experiments, and finite element simulations, comprehensive finite difference analyses remain limited.

In particular, a notable gap exists in the literature concerning the interaction among critical factors governing the performance of LTP systems under localized subsidence scenarios, such as those simulated in trapdoor tests. Previous studies have seldom explored the combined influence of applied vertical stress, the magnitude of trapdoor displacement, the number and arrangement of trapdoors, the width of the trapdoor, the dimensions and location of footing loads, and the inclusion of geosynthetic reinforcement within a rigorous finite difference framework.

Consequently, current understanding of how these parameters collectively affect stress redistribution, load-transfer mechanisms, and soil-arching behavior within the platform remains insufficient, underscoring the

need for refined analyses to optimize LTP design in practical engineering applications.

1.4 Aim and Objectives of This Research

The principal aim of this research is to undertake a rigorous numerical investigation into the behaviour of load transfer platforms constructed over rigid inclusions and subjected to localized subsidence, employing advanced finite-difference modelling through the FLAC 3D software to establish a robust analytical framework for assessing stress redistribution, load-transfer mechanisms, and overall system stability.

In pursuing this research aim, the study is setting the following objectives:

1. Evaluating the stress distribution and deformation patterns within the load transfer platform under varying applied vertical stress levels.
2. Examining the influence of trapdoor displacement magnitude on the stress transfer mechanism and soil arching effect.
3. Assessing the impact of the width, number, spacing, and arrangement of trapdoors on platform behaviour.
4. Investigating the effect of footing width and its position relative to the platform center on stress concentration and load distribution.
5. Comparing the performance of platforms with and without geosynthetic reinforcement under identical conditions.

1.5 Scope of The Work

This research adopts a numerical approach utilizing FLAC 3D, a finite difference-based numerical modeling software, to simulate a series of trapdoor experiments representing localized subsidence beneath load transfer platforms.

The methodology involves:

1.5.1 Model Setup

Developing three-dimensional numerical models representing the load transfer platform both unreinforced and reinforced with geosynthetics over rigid inclusions. The model incorporates a trapdoor mechanism to simulate subsidence beneath the platform.

1.5.2 Limitations

The numerical investigation is limited to a granular fill represented by medium-dense Kansas River sand, characterised by a unit weight of approximately 18 kN/m³, a peak friction angle of about 36°, zero cohesion, an elastic modulus near 25 MPa, and a Poisson's ratio of 0.30.

Accordingly, the applicability of the findings to cohesive soils or materials with markedly different strength, stiffness, or compressibility lies beyond the scope of this study.

1.5.3 Analysis

Monitoring and analyzing stress distribution, displacement fields, and load transfer paths within the platform under different test scenarios.

1.5.4 Validation

Validating the numerical model outcomes by comparing with available laboratory trapdoor test data from published literature.

1.5.5 Parametric Study

Systematically varying key parameters, including:

1. Applied vertical stress levels ranging from 10 kPa to 110 kPa.
2. Magnitudes of trapdoor displacement.
3. Number and arrangement of trapdoors.

4. Width of the trapdoor.
5. Width of the applied footing load.
6. Position of the applied footing load relative to the platform center.
7. Presence or absence of geosynthetic reinforcement.

1.5.6 Results Interpretation

Interpreting the results to evaluate the effects of different parameters on the load transfer mechanisms and providing practical recommendations for GRLTP design under localized ground movement conditions.

1.6 Thesis Layout

1. Chapter One: Introduction

This chapter is establishing the study's foundation by outlining the background, research problem, objectives, scope, and limitations, while presenting soil arching, rigid inclusions, and geosynthetic reinforcement as key concepts.

2. Chapter Two: Literature Review

This chapter is synthesizing relevant studies on soil arching, load transfer platforms, and geosynthetics, critically reviewing experimental, analytical, and numerical approaches, and identifying gaps motivating the present investigation.

3. Chapter Three: Numerical Simulation by Finite Difference Method

This chapter is presenting the research methodology, describing numerical modelling in FLAC 3D software, constitutive models, boundary conditions, and calibration, while designing a parametric study to evaluate trapdoor displacement, footing geometry, and reinforcement effects.

4. Chapter Four: Results and Discussions

This chapter is analysing and interpreting the numerical results, discussing how key variables influence stress redistribution, deformation, and soil arching, and comparing findings with experimental and analytical benchmarks.

5. Chapter Five: Conlusions and Recommendations

This chapter is summarizing the principal conclusions, formulating design recommendations, and proposing directions for future research, including long-term performance and field validation.

Chapter II

Literature Review

Chapter Two: Literature Review

2.1 Introduction

This chapter provides a comprehensive review of the state of knowledge concerning soil arching, trapdoor testing, and the performance of geosynthetic-reinforced load transfer platforms. It synthesizes experimental findings, analytical models, and numerical simulations, critically evaluating their contributions to understanding soil–structure interaction mechanisms. Special emphasis is placed on the evolution of research from classical trapdoor experiments to advanced discrete and finite element approaches. Gaps in the literature, particularly the scarcity of three-dimensional studies addressing multi-trapdoor systems and reinforcement configurations, are explicitly identified. These knowledge gaps form the basis for the present investigation, underscoring its novelty and scientific significance.

2.2 Pile-Supported Embankments

Since the early 1960s, piles have been widely employed to enhance the bearing capacity of soft soils and to reduce post-construction settlements in embankments(Magnan, 1994). Through the mobilization of soil arching caused by differential settlements between piles and surrounding soft ground, piles are capable of supporting up to 60% of the embankment weight with as little as 10% pile coverage area (Hewlett and Randolph, 1988). Installation of piles can also densify and stiffen the foundation soil, further decreasing settlement (Hewlett and Randolph, 1988). To improve load transfer and limit differential settlements, geosynthetics have been introduced into pile-supported (PS) embankments, forming geosynthetic-reinforced pile-supported (GRPS) systems (Han and Gabr, 2002). Their inclusion enables larger pile spacing and smaller caps, thus reducing construction costs (Jones

et al., 1992), while mitigating both primary and long-term settlements (Bell *et al.*, 1994) and eliminating the need for excessively thick embankments (Broms and Wong, 1985). Practical applications of GRPS embankments have been reported in Scotland (Reid and Buchanan, 1984) London (Card and Carter, 1995), and Philadelphia (Collin, 2003). In GRPS systems, the reinforced platform transfers loads from the soft foundation to stiffer piles through a combination of soil arching and the tensioned membrane effect (Han *et al.*, 2012). Soil arching, however, remains the principal mechanism governing load transfer in PS and GRPS embankments.

2.3 Geosynthetic in Geotechnical Application

Geosynthetics refer to planar products crafted from polymeric materials, strategically employed in conjunction with soil, rock, and other geotechnical elements, seamlessly integrated into artificial projects, structures, or systems. These versatile materials, composed of diverse polymers, serve to augment, enhance, or modify the behavior of various civil engineering constructions. Geosynthetics are produced in various types and materials, each designed for particular engineering purposes. Their versatility allows for extensive application in geotechnical projects, transportation systems, hydraulic engineering, and private construction developments. Their applications span a wide array, encompassing roads, airfields, embankments, retaining structures, reservoirs, canals, dams, erosion control, sediment control, landfill liners, landfill covers, mining, and agriculture. Geosynthetics play a pivotal role in ground stabilization, supporting pavements like roads, parking bays, and runways, especially in bearing heavy vehicle loads. They prove indispensable in the development of robust pavements for ports and harbors, as well as in railway projects. Additionally, geosynthetics find crucial

application in erosion control, retaining walls, bridge abutments, and, notably, in enhancing building foundations. The multifaceted utility of geosynthetics underscores their significance in modern civil engineering practices (Gorai, 2022).

2.3.1 Types of Geosynthetics

Geosynthetics represent a broad category of synthetic materials utilized in geotechnical, environmental, and civil engineering applications to enhance the performance and stability of soil and structures. These materials are manufactured from polymeric substances and are primarily employed for functions such as separation, reinforcement, filtration, drainage, and containment. Among the widely recognized types of geosynthetics are geotextiles, which are permeable fabrics used for separation and filtration, and geogrids, which are grid-like structures primarily designed for soil reinforcement. Geonets are net-shaped products used for drainage applications, while geomembranes are impermeable sheets applied for fluid containment and barrier systems. Geosynthetic clay liners combine geotextiles with bentonite clay to create hydraulic barriers, and geocells, also known as geo web members, are three-dimensional honeycomb-like structures used for soil stabilization and erosion control. Additionally, geopipes serve drainage and fluid transport purposes, and geofoam refers to lightweight blocks employed for fill and insulation. Geocomposites integrate multiple geosynthetic types to fulfill combined functions such as drainage and reinforcement. Other specialized forms include geotubes for dewatering and shoreline protection, geocellular confinement systems for load support, geoblankets for surface erosion control, geomats for root reinforcement and erosion prevention, geomattresses for underwater and embankment

protection, geostrips and geobars for reinforcement applications, and electrokinetic geosynthetics, which facilitate soil improvement through electrokinetic processes. The selection of an appropriate geosynthetic type depends on the project's specific functional and environmental requirements, underscoring the versatility and essential role of geosynthetics in contemporary engineering practice (Gorai, 2022). Figure 2.1 shows the types of geosynthetics (Patel, 2019).

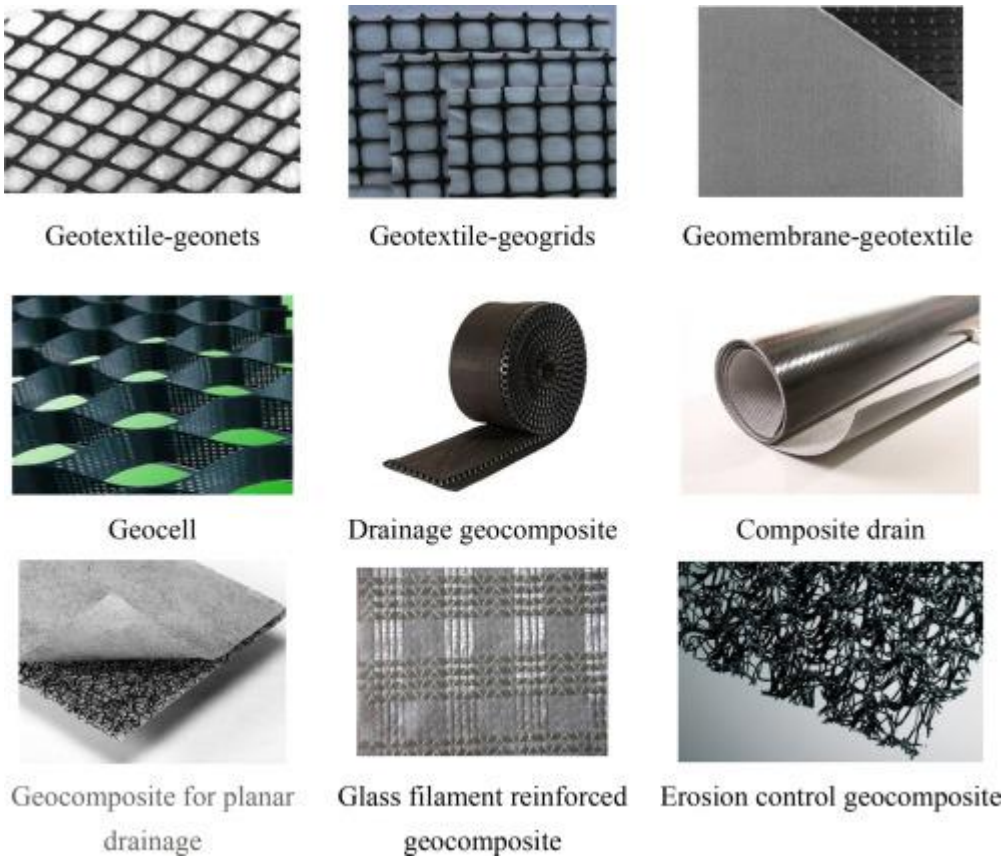

Figure 2.1 Types of geosynthetics (Patel, 2019)

2.4 Load Transfer Mechanisims

2.4.1 Soil Arching

Numerous models have been developed to delve deeper into the mechanisms governing the transfer of loads in piled embankments. Within this context, the concept of "soil arching" stands out as a prevalent and crucial phenomenon. It plays a vital role in transferring vertical stress from the soft surrounding soil to the comparatively rigid piles. This transfer of stress occurs due to differential settlement, as extensively discussed in references (Karl Terzaghi, 1943), (Hewlett and Randolph, 1988), (Zhuang and Wang, 2018), (Anh Tran *et al.*, 2019), (Alonso *et al.*, 2022), (Lai *et al.*, 2020), (Rui *et al.*, 2020), and (Pham and Dias, 2021). The soil arching effect brings about a notable advantage by mitigating localized differential settlements in piled embankments. Among the various models proposed to understand soil arching, the consideration of arching within an equal settlement pattern holds particular significance. This is pivotal for ensuring the overall functionality and serviceability of the embankment. One of the key parameters in this context is the critical height, denoted as "Hcr." This critical height is often recommended as a means to estimate the potential behavior of soil arching, as outlined in references (Rui, van Tol, *et al.*, 2016), (Rui, Van Tol, *et al.*, 2016), (Jenck *et al.*, 2005), (Yun-min *et al.*, 2008), and (Lai *et al.*, 2016). (Hewlett and Randolph, 1988), in their work, have put forth an interesting perspective on this matter. They suggest that in a three-dimensional context, the crown of the arch resembles a hemisphere. Importantly, they establish that its radius is equal to half the diagonal spacing between piles arranged in a square pattern. As a result of this understanding, the critical height, denoted as "Hcr," is typically calculated as 1.4 times the clear spacing between the pile caps. This calculation aligns with the assumption found in (British Standards Institution.,

2010), a recognized reference in the field. By adhering to this guideline, engineers and designers can effectively address the soil arching phenomenon in piled embankments, contributing to their stability and performance.

2.4.2 Tension Membrane Effect

A reinforced granular mattress functions as a load transfer platform, possessing the capability to transfer loads through two principal mechanisms: arching and tension membrane. A potential method for improvement entails the insertion of a geosynthetic layer within the interface between soft soil and the granular platform. This geosynthetic layer plays a pivotal role in facilitating the transmission of tensile forces to the piles, specifically for the portion of the load that has not already been transferred via soil arching, as shown in Fig. 2.2. The technical nomenclature for this phenomenon is the 'membrane effect,' as elucidated by (Le Hello and Villard, 2009).

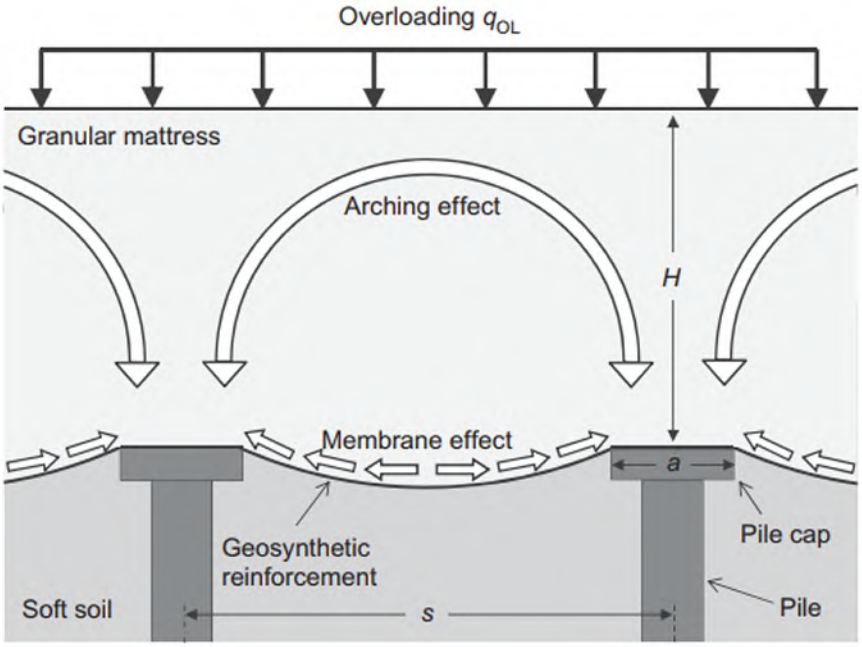

Figure 2.2: Load transfer mechanisms in GRPS (Blanc *et al.*, 2014)

2.4.3 Beam Effect

The Collin Method, also known as the Guido Method, presents an alternative approach to constructing Load Transfer Platforms (LTPs). This method utilizes multiple reinforcement layers to create a sturdy reinforced soil mass, functioning akin to a beam. The key assumptions based on beam theory for the Collin Method include the incorporation of a minimum of three reinforcement layers, spaced at 200 to 450 mm intervals, a platform thickness equal to or greater than half the clear span between piles, and the presence of a fully developed soil arch within the platform's depth. In contrast to the catenary technique using typical geosynthetics, the Collin Method allows for more substantial spacing between columns. This is achieved by the Collin Method, enabling a smooth shift from column to column over the platform to the piles beneath. Notably, the catenary technique generally requires higher strength reinforcement under similar design conditions compared to the beam method. This emphasizes the effectiveness of the Collin Method in optimizing column-to-column spacing and improving overall stability and load distribution within the reinforced soil structure (Gangatharan, 2014).

2.5 Rigid Inclusions

This increasingly utilized ground improvement technique, known by several names such as piled embankment, column-supported embankment, and geosynthetic reinforced pile-supported (GRPS) embankment, involves the use of vertical rigid inclusions (RIs) combined with a granular load transfer platform (LTP) to redistribute loads from embankments or structural elements to deeper, competent bearing strata. These rigid inclusions, which may be referred to as columns or settlement-reducing piles, are installed using various methods, including deep mixing, jet grouting, or vibro concrete

techniques, and can feature enlarged heads or caps to improve load transfer efficiency. A key characteristic of this system is the absence of a direct structural connection between the inclusions and the superstructure, distinguishing it from piled raft foundations. The load transfer platform (LTP), usually made of well-graded granular material, is essential for distributing loads from the embankment fill to the rigid inclusions and underlying soil. Its design must ensure sufficient shear strength, proper compaction, and may include reinforcements like geosynthetics or stabilized soils when necessary. Maintaining ductile behavior in the LTP is crucial for effective shear-based load transfer. Furthermore, the structural configuration of the system is notably affected by the presence or absence of a rigid slab or raft foundation. In configurations lacking a rigid slab, load transfer is primarily facilitated through shear resistance within the load transfer platform (LTP). However, when a rigid slab is incorporated, it actively participates in the redistribution of loads, inducing a non-uniform stress distribution across the underlying system. This complexity necessitates meticulous consideration in the design phase to ensure accurate representation of load paths and to maintain overall structural integrity (Simon and Terrasol, 2012).

2.6 Previous Studies on Geosynthetic Rienforced Load Transfer Platform

2.6.1 Physical Studies

2.6.1.1 Model Test

The study that was conducted by (Al-Naddaf, 2017), investigated the mobilization and stability of soil arching under self-weight and surface loading using trapdoor model tests conducted in plane strain conditions. Static and cyclic footing loads were applied to simulate traffic loading scenarios.

The findings revealed that soil arching developed as trapdoor displacement increased, leading to a reduction in pressure on the trapdoor and a corresponding transfer of load to the supports. In unreinforced embankments, the soil arching effect began to deteriorate once the trapdoor displacement exceeded 2.5% of its width. However, geosynthetic reinforcement was found to effectively preserve the stability of the soil arching mechanism even at a displacement level of 4%, primarily due to its capacity to provide lateral confinement and to mobilize the tensioned membrane effect. In addition to enhancing arching stability, geosynthetics substantially reduced differential settlement. Under a static surface load of 80 kPa, a single layer of reinforcement decreased footing settlement by approximately 23% to 39%, while the implementation of a double-layer system yielded a settlement reduction of up to 71%. Furthermore, the use of biaxial geogrids significantly increased the degradation pressure threshold of the soil arching mechanism, achieving improvements of up to 99.6%. Geosynthetics also demonstrated the ability to mitigate the detrimental effects of cyclic loading on settlement behavior. Notably, double-layer geosynthetic configurations exhibited a beam-like structural response, contributing to further reductions in settlement; however, this configuration was associated with a slight reduction in soil arching stability when subjected to higher load intensities. These results underscore the effectiveness of geosynthetic reinforcement in stabilizing soil arching and improving the load-bearing performance of embankments under both static and cyclic loading conditions.

In addition, (Al-Naddaf, 2019) investigated the load transfer mechanisms, with a focus on soil arching, over a scaled-down buried culvert and the potential of Expanded Polystyrene (EPS) geofoam in alleviating vertical pressure on such structures. Through a series of laboratory tests

conducted under both static and cyclic loading conditions, the research evaluates how soil arching behaves and how the properties of EPS geofoam, such as its stiffness and thickness, influence the distribution of vertical stress. The results demonstrate that EPS geofoam significantly reduces the pressure on the culvert, with low-density geofoam reducing the vertical pressure by up to 45% and high-density geofoam by 31% under static loading conditions. Thicker geofoam was found to be less effective due to its higher stiffness. Additionally, trapdoor tests simulating subsidence were used to examine both the mobilization of soil arching and the performance of geosynthetic reinforcements, such as single- and double-layer geosynthetics. These reinforcements were shown to enhance load transfer, reduce pressure on the trapdoor, and slow the degradation of soil arching, especially under higher applied pressures. The study introduces the concept of the Arching Full Degradation Pressure (AFDP), which identifies the pressure level at which soil arching ceases. The presence of geosynthetics increased AFDP by up to 143% in double-layer systems compared to unreinforced soil. Furthermore, numerical models were employed to validate experimental data, revealing that while cyclic loading diminished the effectiveness of soil arching at lower pressures, it promoted shear stresses and enhanced load transfer at higher pressures. Flexible trapdoors demonstrated a more even pressure distribution compared to rigid ones, underscoring their influence on the behavior of soil arching. These findings underscore the importance of optimizing EPS geofoam and geosynthetics to improve load transfer in buried structures subjected to diverse loading conditions.

Another study that was conducted by (Zhang *et al.*, 2024), which was consisted of five centrifuge tests. The performance of cement fly ash gravel (CFG) supported composite foundations, encompassing both nonconnected

piled raft foundation systems (NPRF) and geosynthetic-reinforced pile-supported (GRPS) systems, in high-speed railway applications over silty clay soil was examined. The research systematically discussed the findings regarding the load-bearing characteristics and deformation behaviors of these composite foundations, considering variations in load transfer platforms and substratum stiffness. Key observations from their study revealed that the majority of embankment surface settlement occurred during the filling phase, with minor additional settlements during the resting and operating phases. Additionally, higher substratum stiffness was linked to reduced settlement at varying depths, with the operational (load application) phase significantly influencing deformation, particularly at the central region of the embankment. Notably, NPRF exhibited downward deformation, while GRPS displayed upward deformation approximately 5 meters from the embankment's edge. The choice of load transfer platform played a crucial role in determining the failure mode of NPRF and GRPS, particularly when subjected to increased additional stress. Furthermore, the incorporation of raft or geosynthetic reinforcement in the composite foundation enhanced stress transfer to the pile, with NPRF exhibiting greater pile efficiency compared to GRPS. This efficiency exhibited variations with filling height and the type of load transfer platform used, which were influenced by substratum stiffness. Pressure distribution consistently demonstrated lower values further from the subgrade center. Along the embankment width, NPRF displayed higher pile-soil stress ratios and efficiencies than GRPS, with these variations linked to the specific action form of the load transfer platform. Lastly, distinct differences in axial force were observed between end-bearing and floating piles, particularly pronounced in GRPS, where the pile body exhibited negative friction due to issues related to differential settlement.

Additionally, (Dieguez *et al.*, 2020) have investigated geosynthetic-reinforced pile-supported systems (GRPS) construction under plane-strain conditions. This study employed different hand-operated compactors: a vibrating plate (referred to as the "light compactor") and a vibratory tamper (referred to as the "heavy compactor"). The vibrating plate applied lower vertical stresses than the vibratory tamper. The models aimed to monitor settlements, reinforcement tensions, and vertical stress at the pile caps-soil interface. Using both the vibrating plate and vibratory tamper resulted in fewer settlements compared to using only the vibrating plate. Higher soil compaction reduced differential settlements. Interestingly, regardless of compaction type (heavy or light), soil arching efficiency reached its maximum and remained stable in both Type 1 and Type 2 compaction tests. This stability was attributed to the use of large pile caps, which enhanced soil arching mechanisms.

Furthermore, the study conducted by (Blanc *et al.*, 2013) specifically investigated the enhancement of load transfer mechanisms through the incorporation of a geosynthetic reinforcement layer within a granular mattress positioned above rigid inclusions. It investigated various mattress thicknesses (H = 35, 50, and 90 mm) and two networks of rigid inclusions that its area ratio ($\alpha = 4.91\%$ and 2.47%) using the geo-centrifuge with a mobile tray setup. Without geosynthetic reinforcement, load transfer relied on arching effects within the mattress (Fig. 2.3(a)). Thicker mattresses and smaller α values reduced surface differential settlement because they provided more space for the mattress to absorb pile loads without punching. The effectiveness of arching was linked to "distance s-a," (s= pile c/c spacing and a= pile diameter) representing the mattress thickness needed for full arching, assuming semi-cylindrical arches. Geometric factors played a significant role, with thicker

mattresses and lower area ratios showing better arching effects. When a geosynthetic layer was added directly on the mobile tray's surface, it transferred some embankment weight through the "membrane effect," adapting to tension loads (Fig. 2.3(b)). This effect improved over time as the subsoil settled beneath the geosynthetic. While both membrane and arching effects enhanced load transfer mechanisms, no significant differential settlement improvement was observed when tested with the mobile tray device. This was due to continuous monitoring, contrasting in-situ conditions where efficacy increased and soft soil settlement decreased. The study noted that applying initial pretension to the geosynthetic could enhance secant stiffness but was insufficient to significantly enhance its performance in this context.

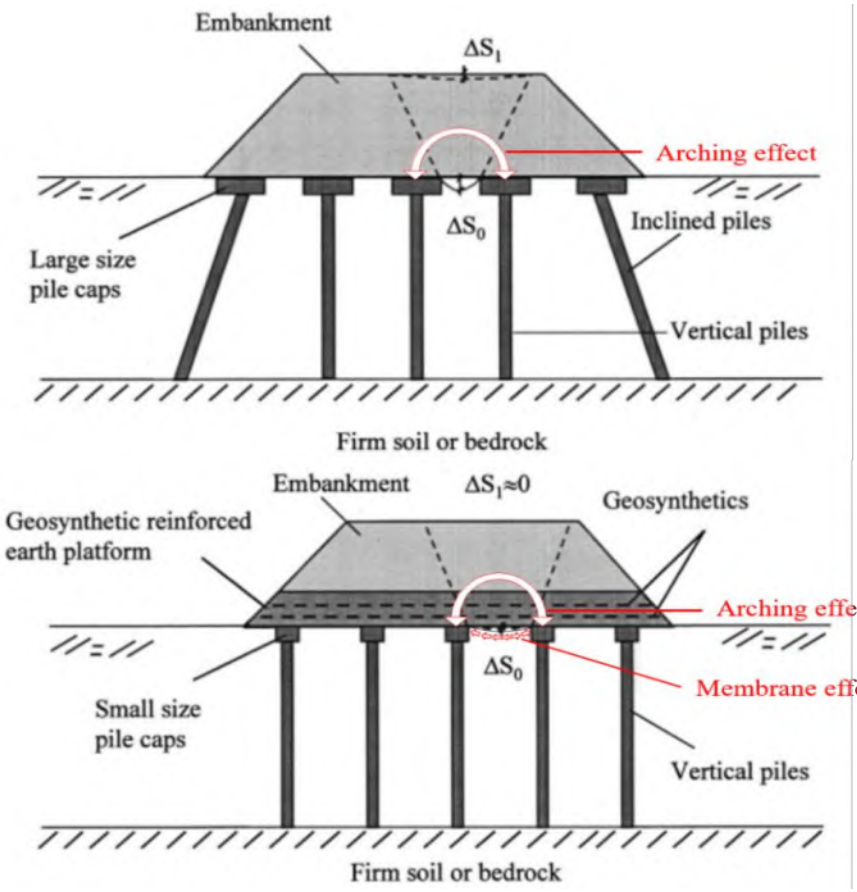

Figure 2.3: Load transfer mechanisms in pile support embankment – (a) without geosynethetics – (b) with geosynethetics (modified from (Han and Gabr,

2.6.1.2 Field Test

The paper examined by (Briançon *et al.*, 2015) presented a case study within the domain of industrial construction, featuring a relatively low improvement area ratio of 2.18%. The study leveraged field observations and a sophisticated three-dimensional finite difference back-analysis to investigate the behavior of the site. One notable finding from this investigation was the rapid dissipation of excessive positive pore-water pressures, which facilitated the application of drained calculations. This observation was particularly significant in gaining insights into the site's soil dynamics. Furthermore, the study provided substantial evidence of the effective transfer of loads from the surrounding soil to the underlying piles, primarily attributable to the phenomenon known as soil arching. When a surcharge load was incrementally raised to 50 kPa, it resulted in an approximate 17 kPa increase in soil surface pressures, representing approximately 34% of the surcharge load. Impressively, the pressure at the pile heads surged to 180 kPa, nearly three times the magnitude of the surcharge load. Moreover, it was evident that the contact pressure at the pile heads exceeded that between adjacent piles by a factor of 6.7. This disparity in pressure distribution had a substantial impact on the load-bearing behavior of the system. As the surcharge load was increased, both the measured and back-analyzed stresses exhibited corresponding increments. Piles played a pivotal role in shouldering the majority of the embankment load and efficiently transferring it to deeper soil layers. This efficient load transfer mechanism had the desirable effect of significantly reducing settlement, a critical factor in ensuring the structural stability and performance of construction projects. Of particular interest was the observation that the vertical strain within the piles reached nearly 100 $\mu\varepsilon$ (micro-strains),

indicating the extent of deformation experienced by the piles during the process. The validated numerical model utilized in the study suggested that the incorporation of rigid inclusions effectively improved the soft soil's load-bearing capacity, enabling it to support the load without encountering problematic differential settlement issues beneath the concrete raft.

In addition to that, (Briançon and Simon, 2012) have conducted a full-scale experiment to assess the performance of an embankment reinforced with geosynthetics and rigid piles over soft soil, as part of a French research project. Four experimental sections with different reinforcement solutions were tested using the same fill height. Instrumentation consistency was ensured by cross-verifying data from various sensors in similar positions. Stress measurements on soil and piles revealed significant improvements in load transfer to the piles when a reinforced granular platform was present. Despite moderate soil compressibility, incorporating piles and geosynthetics substantially reduced settlement. Initial differential settlement occurred during embankment construction, but sections with a load-transfer platform maintained relatively constant differential settlement after construction. Geosynthetic strain measurements showed variations in strain distribution depending on the reinforcement configuration, emphasizing the benefits of using two geogrid layers to achieve uniform stress distribution and reduce differential settlement. This full-scale experiment provides valuable insights into pile and geosynthetic behavior, highlighting the importance of a quality load-transfer layer for enhanced efficiency and settlement reduction in embankment construction. These findings offer valuable considerations for design evaluations.

Furthermore, an analysis of post-construction data obtained from a Geosynthetic-Reinforced Column-Supported Embankment (GRCSE) located

in Melbourne, Australia, spanning a period of over 2 years, reveals the time-dependent evolution of arching stresses in the post-construction phase. These arching stresses are attributed to sub-soil settlement occurring between the columns of the embankment. This relationship between arching stresses and sub-soil settlement has been observed in laboratory experiments and small-scale models, as documented in references (Karl Terzaghi, 1936), (LADANYI B and HOYAUX B, 1969), (Evans, 1984), (Iglesia *et al.*, 2011), (Iglesia *et al.*, 2014), (Ellis and Aslam, 2009a), (Ellis and Aslam, 2009b), and (Yun-min *et al.*, 2008), and is now demonstrated at the field scale in this study. (King *et al.*, 2017) successfully predicted reductions in stress levels during the maximum arching phase using various methods, with the GRC (geosynthetic-reinforced column) method proving particularly effective in describing the development of arching stresses from the initial stages to the maximum phase and even in predicting future developments. The concept of arching development occurring in distinct phases, including the critical load recovery phase, is considered valuable for comprehending the behavior of load transfer platforms (LTP) and for informing design considerations. The breakdown of arching stresses as sub-soil settlement increases carries significant implications for the design of geogrid layers and the long-term performance of embankments, particularly in relation to surface settlement in shallow embankments. It is therefore recommended that further research be conducted to explore the role of sub-soil settlement in the development of arching stresses, particularly in the context of the load recovery phase. Such investigations can provide valuable insights into optimizing embankment designs and enhancing their overall stability and performance over time.

2.6.2 Numerical Studies

2.6.2.1 Finite Element and Finite Difference Method

Literature reviews showed that several numerical studies have been carried out to investigate the behavior of embankments supported by deep foundations. (Dang *et al.*, 2018) has discussed a 2D Finite Element Model (FEM) used to analyze the behavior of an embankment supported by deep cement mixing (DCM) columns, both with and without a fiber-reinforced load transfer platform (FRLTP). The FRLTP, made from natural fibers and lime, helps transfer higher loads to the DCM columns and reduces the load transferred to the foundation soil between the columns, thereby decreasing excess pore water pressure in the soft soil layer. The combination of fiber-reinforced load transfer platform and DCM columns effectively prevents both overall and differential settlements of the embankment when compared to embankments supported only by DCM columns. Additionally, this investigation highlights the potential to use agricultural and industrial waste by-products such as coconut coir fiber, bagasse fiber, and jute fiber as construction fill materials for sustainable development in infrastructure foundations.

The numerical analyses also provided valuable insights into the behavior of granular fill under cyclic loading conditions, particularly regarding the role of geosynthetic reinforcement. In a study that was conducted by (Zhang *et al.*, 2018), key findings highlighted the significance of a complete soil arch, where a critical height of 1.5 times the clear spacing was identified for load transfer between stationary and movable sections under both static and cyclic loading as shown in Fig. 2.4. Cyclic loading was found to diminish the effectiveness of load transfer mechanisms, leading to a greater concentration of stresses on the yielding zone and an associated

increase in differential settlement when compared to static loading conditions. Geosynthetic reinforcement proved effective in mitigating these effects, particularly in cases involving thin fill. The study also revealed distinct soil arch characteristics in thin and thick fill conditions, resembling Terzaghi's trench arch model in the former (1943) and forming a parabolic shape in the latter, with defined upper and lower boundaries. Additionally, geosynthetic reinforcement reduced soil plastic strain during cyclic loading. The introduction of a modified factor allowed for a more accurate assessment of cyclic loading's influence on the soil arching effect, showing that geosynthetics helped maintain stability regardless of fill height, particularly when the normalized height (fill height/clear spacing) reached 2.5, minimizing the cyclic load's impact on the soil arching ratio. These findings collectively enhance our understanding of soil behavior in cyclically loaded granular fills and emphasize the effectiveness of geosynthetic reinforcement in improving structural stability under such conditions.

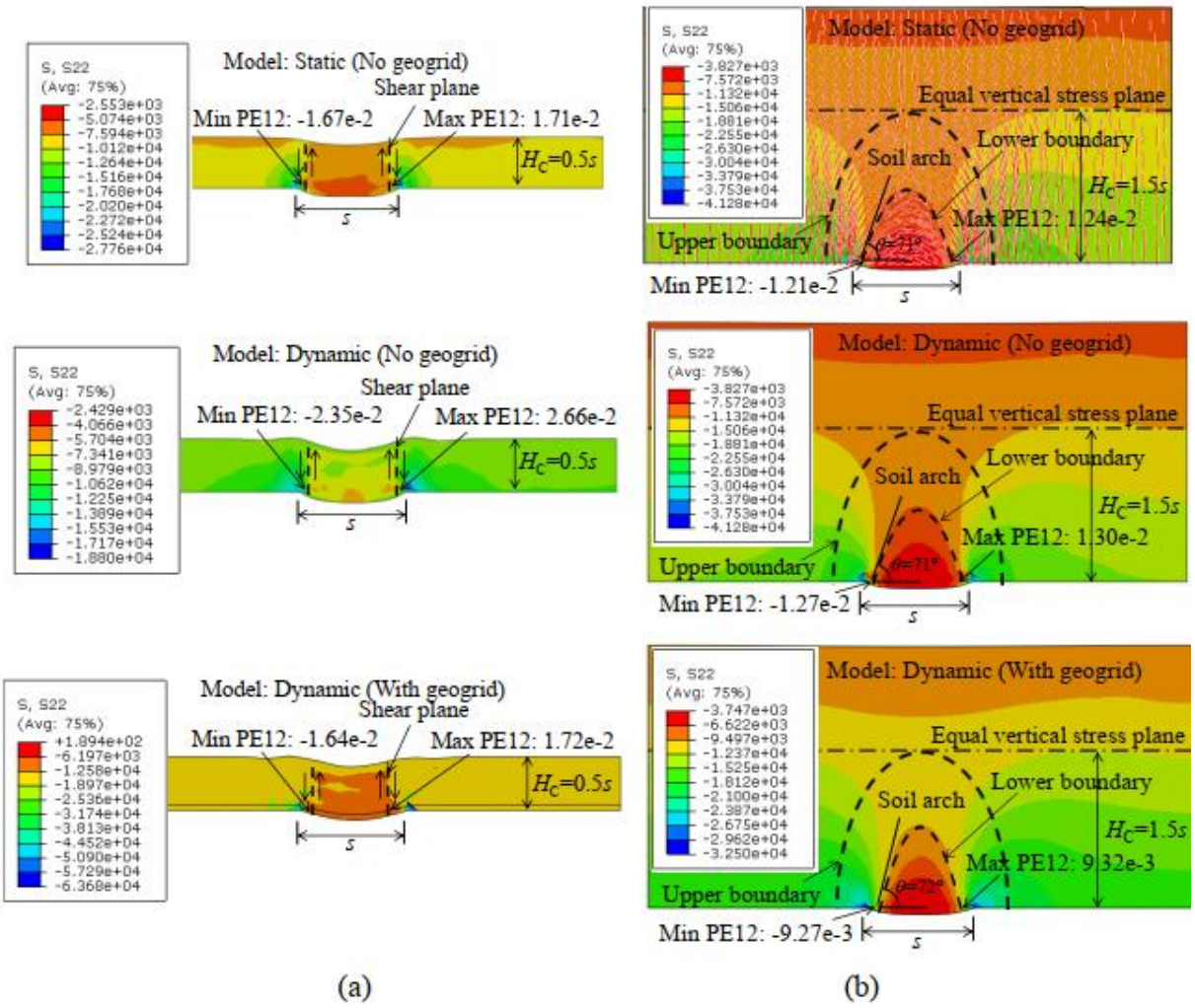

Figure 2.4: Contours of vertical stresses at 100 load cycles: (a) thin fill (H/s=0.5); (b) thick fill (H/s=2.5) (Zhang *et al.*, 2018)

Another study that was conducted by (El-Gendy *et al.*, 2020) utilized finite element analysis to replicate a well-instrumented laboratory model of soft soil enhanced with rigid inclusions. The research involved a comprehensive exploration of appropriate geotechnical parameters for the model and employed a hardening soil constitutive model to simulate the behavior of the soft deposit. Comparisons were made between the outcomes of the developed numerical model, the laboratory model, and previously published numerical analyses from the literature. The primary focus of these

comparisons was on load distribution between the rigid inclusions and associated vertical displacements. The analyses demonstrated the capacity of the sophisticated numerical model to closely mimic the real behavior observed in the laboratory test. Furthermore, the results indicated that this developed model outperforms other published numerical studies in accurately predicting settlement values at various locations. Specifically, previous models (T.J.M. den Boogert, 2011) produced lower vertical displacement values than those observed in the laboratory. Additionally, one of the models (der Peet, 2014) displayed inconsistent behavior regarding load distribution and vertical displacement. A parametric study using the validated numerical model revealed that increasing the internal angle of friction of the embankment improved the arching effect, resulting in reduced vertical displacements.

A more sophisticated analysis, 3-D finite difference model, was employed by (Mánica Malcom *et al.*, 2016) to investigate the impact of rigid inclusions on the seismic response of a particular site. Two different techniques for modeling these inclusions were evaluated, with solid zones requiring high discretization for accurate representation of bending stiffness, while beam elements effectively reproduced axial and bending stiffness. Various inclusion configurations were studied, and some analyses included surface buildings to consider inertial effects. The results showed that rigid inclusions alone had limited impact on seismic ground response, but when combined with surface structures, they led to additional reductions in spectral ordinates and decreased dynamic vertical stress in the soft soil. The analyses revealed significant dynamic axial force increments in the inclusions due to rocking motions in the structures, but shear forces and bending moments along inclusion lengths were generally small, except in areas with substantial soil stiffness contrasts. Variations in support conditions, length, and spacing

had relatively minor effects on ground response compared to changes in the dynamic characteristics of surface structures, which dominated soil-structure interaction. The study is location-specific, and further research is recommended to explore different ground conditions and consider elastoplastic constitutive models, especially near failure.

Van Pham and Dias, (2021) conducted a three-dimensional numerical study (Fig. 2.5) to analyze the behavior of soft soils reinforced with rigid inclusions when subjected to both monotonic and cyclic loading. The load transfer platform (LTP) was modeled using the hypoplastic constitutive model (HYP model), allowing for a detailed representation of the granular material's mechanical response under varying loading conditions. The research compares numerical and experimental results concerning pile effectiveness and cumulative settlements. Under monotonic loading, increasing surcharge leads to greater settlements, with a good agreement between numerical and experimental data. The HYP model performs better than the Cap-Yield (CYsoil) model in replicating settlements. In the context of cyclic loading, the results reveal a progressive reduction in the stress experienced at the head of rigid inclusions and a marginal increment in the stress within the soft soil, resulting in reduced pile effectiveness as load cycles progress. The type of cyclic loading has minimal impact on soil arching, and cumulative settlements at the LTP base decrease gradually with the number of load cycles. Additionally, over-consolidated soft soils experience fewer cumulative settlements than normally consolidated ones under cyclic loading. The presence of rigid slabs was found to increase cumulative settlements by approximately 50% compared to configurations without slabs, due to their influence on stress redistribution. In contrast, a moderate reduction in mattress thickness was observed to enhance the efficiency of the rigid inclusions and

contribute to a decrease in overall cumulative settlements, indicating improved load transfer performance. However, it's noted that precise calibration of parameters, which may require additional laboratory tests, is essential for accurate numerical analysis using the sophisticated HYP constitutive model.

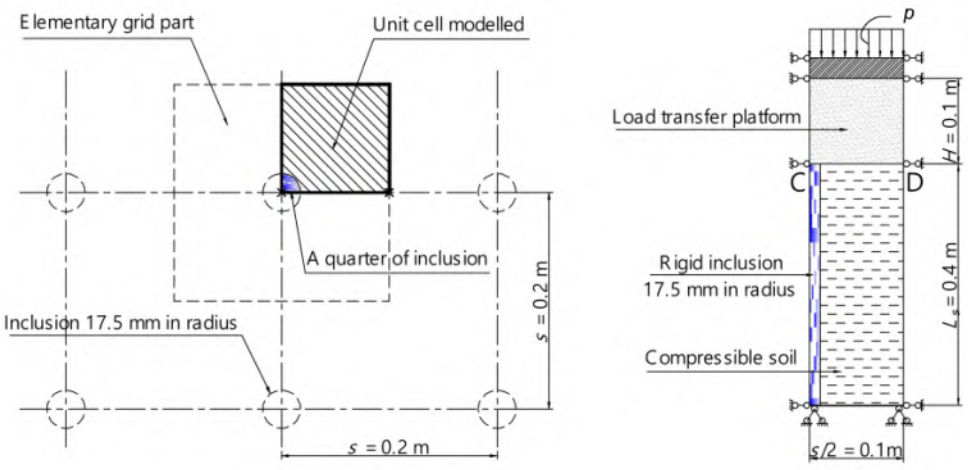

Figure 2.5: Elementary volume model used for 3D numerical analyses (Van Pham and Dias, 2021)

2.6.2.2 Discrete Element Method (DEM)

Recently, researchers have turned to the Discrete Element Method (DEM) to model soil arching phenomena within piled embankments (Lai *et al.*, 2020), (Chevalier *et al.*, 2012), (Jenck *et al.*, 2009), (Han *et al.*, 2012), and (Chen *et al.*, 2020). These investigations have illustrated the effectiveness of DEM simulations in capturing the qualitative aspects of soil arching behavior within piled embankments (Chen *et al.*, 2020). It is important to note, however, that the majority of these DEM simulations primarily focus on identifying soil arching based on the deformation patterns observed in the embankment, rather than delving into the analysis of stress redistributions or

contact force chains (Lai *et al.*, 2020). In a broader context, soil arching within piled embankments plays a crucial role in improving the transfer of loads from soft surrounding soil to the comparatively rigid piles (Alonso *et al.*, 2022), (Rui *et al.*, 2020), (Jenck *et al.*, 2005), (Yun-min *et al.*, 2008), (Lai *et al.*, 2016), (Al-Naddaf, 2019), (Zhuang and Wang, 2018), (Anh Tran *et al.*, 2019), and (He *et al.*, 2018). With this in mind, (Wang *et al.*, 2021) employed the PFC (Particle Flow Code) discrete element software to investigate the soil arching effect, particularly in the context of an equal settlement pattern. Their study specifically examined vertical displacement and vertical stress and explored how soil arching influences the formation of this pattern by varying key parameters such as embankment height (H) and pile cap width (a). To establish a realistic initial stress state, they proposed a novel specimen preparation method that combines improved multilayer compaction and multilayer under-compaction techniques. The analysis indicates that, under conditions of uniform settlement, the progressive descent of the trapdoor induces the gradual formation of a semi-elliptical soil arch within the embankment. This arching mechanism evolves with continued displacement and ultimately stabilizes at a height corresponding to approximately 0.7 times the difference between (s) and (a), as depicted in Fig. 2.6. Additionally, their study underscores the substantial influence of embankment height (H) and pile cap width (a) on pattern formation. Lower embankment height and larger pile cap width result in more pronounced differential settlement and the emergence of a slip surface, which hinders the formation of the equal settlement pattern.

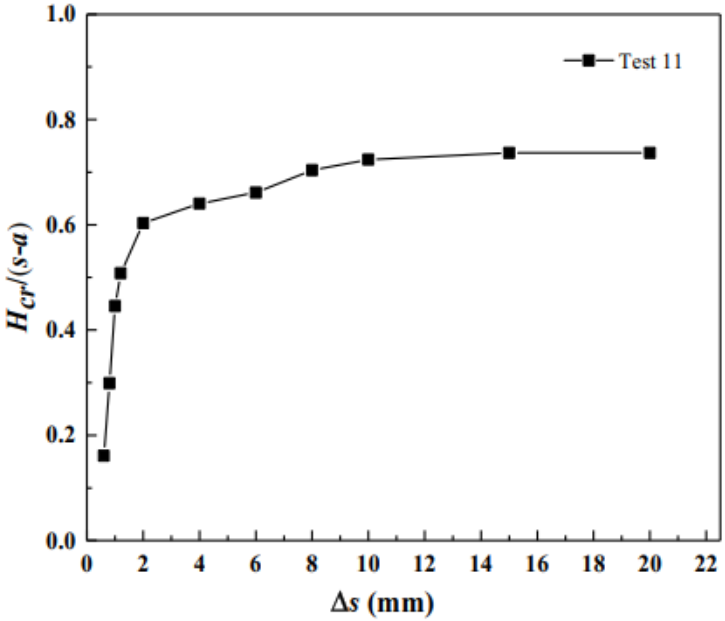

Figure 2.6: Moving of equal settlement with the increase in Δs (Wang *et al.*, 2021)

The evolution of soil arching in embankments with the increase of surcharge was studied using two-dimensional DEM numerical simulations. (Lai *et al.*, 2014) has revealed that soil arching in the embankment is primarily formed by contacts in a strong force network (SN), functioning as load-carrying chains, while contacts in a weak force network (WN) provide support. Three stages of soil arching development are observed as surcharge increases: (a) gradual strengthening of soil arching, leading to increased efficacy; (b) full mobilization of soil arching with a "forming-failure-reforming" process, characterized by step-shaped reductions in efficacy; and (c) a stage where no new stable soil arching forms, resulting in a gradual decrease in efficacy. However, in geogrid-reinforced embankments, there is no Stage_3 failure mode, and the presence of geogrid enhances load transfer efficacy and soil arching stability. Pile spacing significantly influences soil

arching development, while subsoil stiffness and embankment fill grain composition have minimal effects.

Moreover, a study conducted by (Zhang *et al.*, 2021) delved into a comparison between three different types of embankments: one without reinforcement, one with geogrid reinforcement, and one with fixed geogrid reinforcement. The investigation employed the Discrete Element Method (DEM) to scrutinize the mechanism of load transfer in a pile-supported embankment with geogrid reinforcement, as depicted in Figure (2.7). The analysis encompassed multiple factors, including embankment settlement, the relative displacement between piles and subsoil as depicted in Figure (2.8), soil stress distribution, deformation of the reinforcement, and the evolution of contact force chains. The findings of the study demonstrated that the fixed geogrid technique significantly enhances the control of differential settlement between rigid inclusions and the underlying subsoil. This approach yielded notable reductions in both total and differential settlements when compared to conventional geogrid-reinforced embankment systems, thereby indicating superior performance in load transfer and deformation control. Furthermore, it promotes a more uniform distribution of stress along the interface between the embankment and the soil, thereby enhancing the efficiency of load transfer and limiting the displacement of soil particles. Notably, the fixed geogrid technique also reduces the proportion of load transferred to the piles through soil arching. This results in a 10% increase in the effectiveness of the piles, achieved through the combined influence of fixed reinforcement and soil arching. This study sheds light on the advantages and underlying mechanics of the fixed geogrid technique in enhancing the stability of embankments and improving the efficiency of load transfer within such structural configurations.

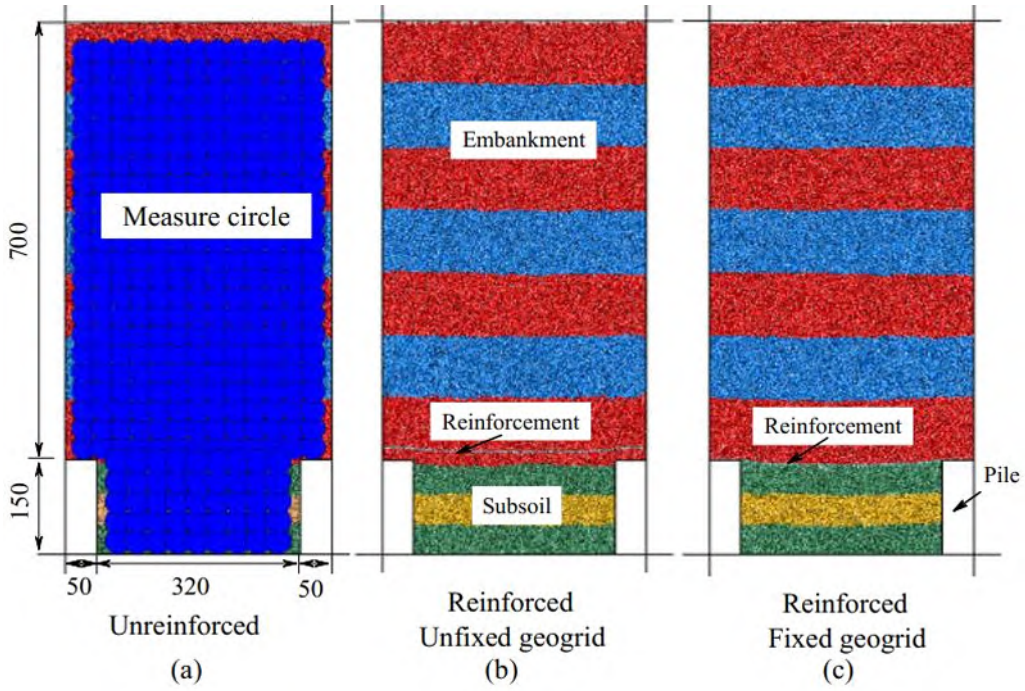

Figure 2.7: DEM models of the embankment arrangements (unit:mm) (Zhang *et al.*, 2021)

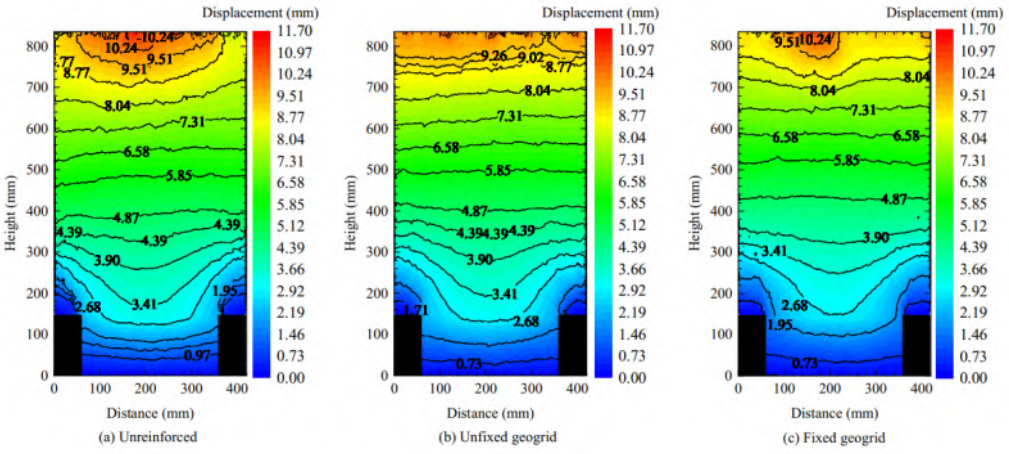

Figure 2.8: Comparison of the particle displasements of the embankements (surcharge load =100 kPa) (Zhang *et al.*, 2021)

2.7 Available Design Methods

Numerous design approaches exist for creating geosynthetic-reinforced and pile-supported (GRPS) embankments. It's important to note that not all of these methods were originally conceived for the specific purpose of designing GRPS embankments; instead, they were subsequently modified for this application. This section will provide an overview of many currently accessible design methods for GRPS embankments. Fig. 2.9 shows arching theory according to three of these methods.

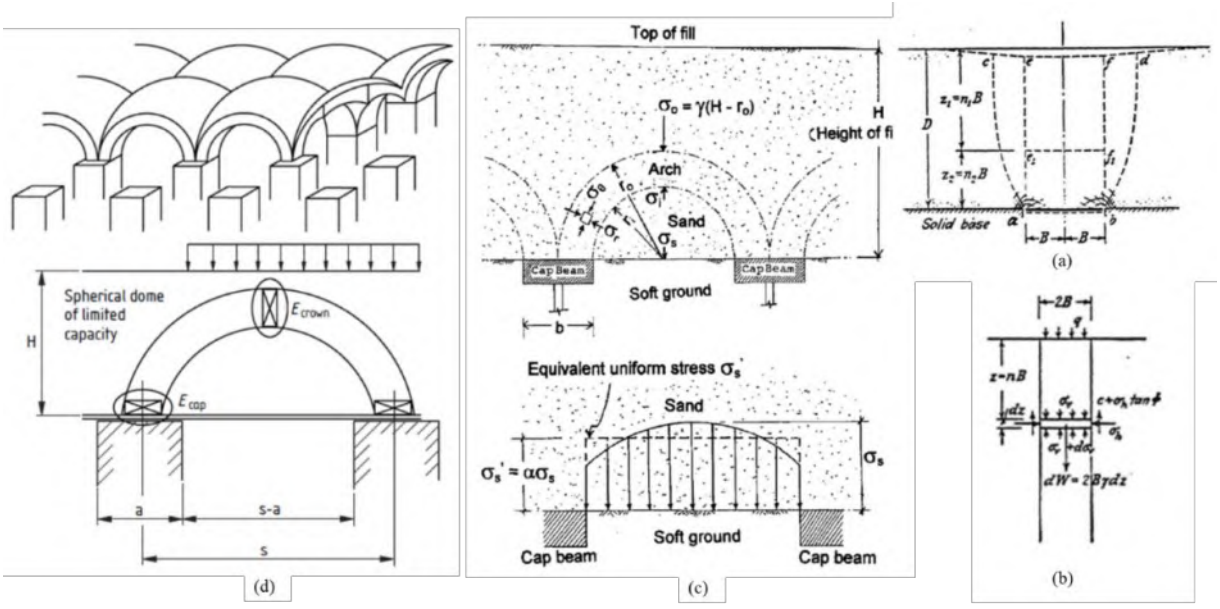

Figure 2.9: Arching theory according to (a) Terzaghi's investigation in sand proposed failure of downward movement in a trapdoor test (Karl Terzaghi, 1943) (b) Terzaghi's investigation in sand free body diagram for a slice of soil within the yielding zone (Karl Terzaghi, 1943) (c) (Low *et al.*, 1994) (d) (British Standards Institution., 2010)

2.7.1 Load Calculation Method

The calculation of loads in piled embankment systems is a fundamental aspect of geotechnical design, with various methodologies developed over time to capture the arching behavior and load transfer mechanisms. One of the earliest and most influential approaches is Terzaghi's arching theory (1943),

derived from his trapdoor experiment, which illustrates how vertical stresses redistribute when soil is allowed to deform (Karl Terzaghi, 1943). Building on this concept, Russell and Pierpoint (1997) formulated a three-dimensional equation to evaluate the stress reduction ratio in geosynthetic-reinforced pile-supported (GRPS) embankments, introducing parameters such as pile spacing, cap width, embankment height, and earth pressure coefficients (Russell and Pierpoint, 1997). The resulting equation is as follows:

$$S_{3D} = \frac{(s^2-a^2)}{4HaK\tan\emptyset'}\left(1 - e^{\frac{(-4HaK\tan\emptyset')}{(s^2-a^2)}}\right) \qquad \textbf{(2.1)}$$

Where:

s = the pile spacing

a = the pile cap width

H = the embankment height

K = the coefficient of earth pressure at rest, where $K = (1 - \sin\emptyset')$

The British Standard BS 8006 (British Standards Institution., 2010) is widely employed in practice for its pragmatic simplicity. It provides two methods for estimating the load on geosynthetic reinforcement: one based on Marston's theory and another derived from the work of (Hewlett and Randolph, 1988). The latter uses observed arching patterns represented by hemispherical domes to evaluate arching efficiency (Ea), which denotes the proportion of load carried directly by piles. The equations distinguish between failure occurring at the arch crown and the pile cap, with Ea influencing the residual load carried by reinforcement and subsoil. The maximum tensile force in the geosynthetic is then computed based on vertical stress due to arching and design strain assumptions, typically 5%, although variations can be incorporated via equilibrium-based adjustments as suggested by (Pham, 2020).

In Germany, the EBGEO guidelines (Bräu, 2012) utilize lower-bound plasticity theory, pilot experiments, and numerical modeling, incorporating (Kempfert *et al.*, 2004) ground arching equilibrium concept. The model assumes a triangular pressure distribution and uses elastic subgrade support to derive vertical stresses in the soil beneath the reinforcement. The method further allows estimation of arching efficiency based on embankment dimensions, pile spacing, and surcharge conditions.

The Dutch design approach, outlined in CUR226 (2016) (Van Eekelen and Brugman, 2016), adopts the Concentric Arches model developed by (Van Eekelen *et al.*, 2012), (Van Eekelen *et al.*, 2013), and (van Eekelen *et al.*, 2015) as depicted in Fig. 2.10. This method distinguishes between load parts: the portion directly transferred to the pile cap and the remainder sustained by geosynthetic strips and the subsoil. The model considers arch geometry in both 2D and 3D and differentiates between triangular and uniform load distributions depending on the presence of subsoil support. The tensile force in the geosynthetic is calculated through either analytical expressions or design charts, using assumptions about strain distribution and deformation geometry.

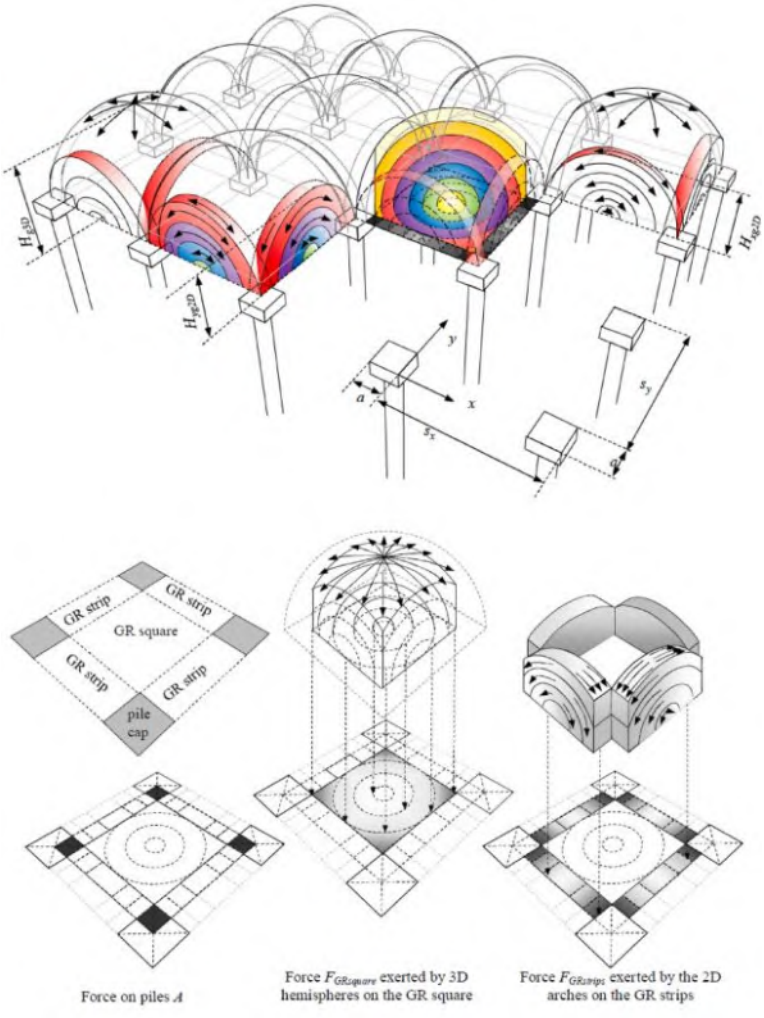

Figure 2.10: Concentric arc model according (Van Eekelen *et al.*, 2013).

The Nordic guideline (NGG, 2004) adopts a more simplified soil arching model by assuming a 30°-angled soil wedge forming an arch between pile caps. The resulting average vertical stress on the geosynthetic and subsoil is then used to determine the arching efficiency, similar in conceptual basis to other methods but differing in geometric and analytical simplicity (Fig. 2.11).

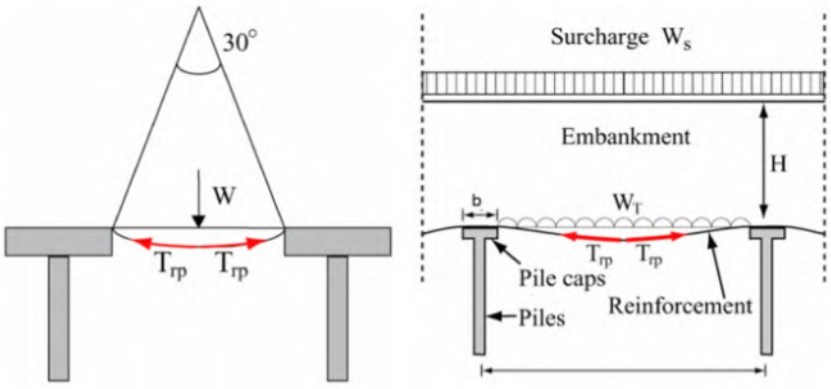

Figure 2.11: Calculation model used in (NGG, 2004)

An advanced analytical method was proposed by (Low *et al.*, 1994), expanding upon Hewlett and Randolph's semi-cylindrical arching concept (Hewlett and Randolph, 1988). Their approach incorporates geosynthetic tension, soil stiffness, and deformation geometry, with the reinforcement assumed to form a circular arc. The model introduces iterative procedures to resolve the equilibrium of forces and deformation compatibility. This framework offers a more refined estimation of tensile forces and vertical displacements in the geosynthetic, accounting for the interaction between reinforcement and foundation soil.

In conclusion, while the fundamental principle across all methods is the redistribution of vertical loads due to soil arching, each design guideline incorporates unique assumptions about arch geometry, material behavior, and load distribution. Terzaghi's original concept remains foundational, but modern standards (such as BS 8006, EBGEO, CUR226, NGG, and the method by Low et al.) offer increasingly complex yet precise tools for engineers to evaluate the performance of geosynthetic-reinforced pile-supported embankments under various loading and subsoil conditions. These methods

allow for better estimation of load transfer mechanisms, ensuring safer and more efficient embankment designs.

2.7.1.1 Related Previous Studies

Depending on German EBGEO method (Bräu, 2012), a parametric study was conducted by (Blanc *et al.*, 2014) using instrumented centrifuge models to investigate composite foundations, specifically those comprising vertical rigid inclusions and a reinforced dense granular load transfer platform. In these experiments, conducted under 20 times gravity conditions (20g) using a mobile tray device, a surcharge (representing scenarios like embankment construction or tank filling) was applied while simulating soft soil settlement through downward tray displacement. The study explored three main parameters: mattress thickness (H), area ratio or pile spacing (s), and the presence or absence of a geosynthetic layer at the mattress's bottom. The results revealed several significant observations regarding the inclusion of a geosynthetic reinforcement layer. Notably, its presence enhanced overall system efficiency, reduced the vertical stress transmitted to the soft soil interface, and led to a marked decrease in differential settlement across the mattress surface, particularly in configurations with lower embankment heights (H). The efficiency gains reached up to 75%, underscoring the effectiveness of geosynthetic inclusion in improving load transfer behavior. Furthermore, the study incorporated a comparative analysis against the EBGEO (German) guidelines in scenarios where the geosynthetic layer was not in direct contact with the soft subsoil. This comparison offered valuable insights into variations in deflection patterns and stress redistribution. The experimental findings demonstrated strong agreement with the expected load

transfer mechanisms within the granular mattress, thereby providing a robust dataset for the calibration and validation of numerical models.

In addition, in order to compare the four current methods for GRPS embankment design (the Dutch design guideline (CUR226 2016) (Van Eekelen and Brugman, 2016), also known as (Van Eekelen *et al.*, 2013) technique, the German design guideline (Bräu, 2012), the British standard (British Standards Institution., 2010), and the Nordic design guideline (NGG, 2004)) a study that was conducted by (Pham *et al.*, 2024) presented the results of three-dimensional numerical modelling for geosynthetic-reinforced and pile-supported embankments. The findings indicate that the efficacy of the load transfer mechanism in GRPS embankments can be enhanced by raising the embankment height, decreasing subsurface stiffness, raising the density of embankment soils, and raising geosynthetic stiffness. Increased loads transferred onto piles due to the geosynthetic tensioned membrane effect lessen differential settlements and soil yielding above pile heads. The study also shows that one needs to take into account how subsurface stiffness affects settlement prediction and arching in analytical models. Among the various methodologies, the CUR226 method performs the best in terms of soil arching and geosynthetic deformation prediction.

2.7.2 Strain and Tension of Geosynthetic

The determination of geosynthetic strain and tension in pile-supported embankments is a key aspect of geotechnical design, governed by several standards and analytical methods. The British Standard BS 8006 (British Standards Institution., 2010) provides a widely used formulation to estimate tensile force in the reinforcement based on the distributed load between piles, reinforcement strain, and geometric parameters. Corrections by (van Eekelen

et al., 2011) refined the load calculations by eliminating double-counting, with separate equations for full and partial arching conditions.

Several researchers proposed alternative methods to compute geosynthetic tension, such as (Russell and Pierpoint, 1997), (Kempfert *et al.*, 2004), and (Low *et al.*, 1994), using stress reduction ratios or strain-based equilibrium. Most methods adopt a design strain of 5%, although some standards, such as BS 8605, recommend stricter limits (e.g., 2% for long-term creep) depending on embankment height and expected settlement.

Graph-based methods from EBGEO (Bräu, 2012), CUR 226 (Van Eekelen and Brugman, 2016), and Nordic guidelines (NGG, 2004) estimate strain by considering subsoil support and arching behavior. Deflection of the geosynthetic is commonly modeled as parabolic, with maximum deflection linked to strain. Methods such as those by (Abusharar *et al.*, 2009) further refine the analysis by incorporating surcharge effects and pile spacing.

Overall, while different approaches vary in complexity and assumptions, they converge on the principle that geosynthetic tension depends on load distribution, deformation geometry, and reinforcement properties. Accurate estimation ensures effective load transfer and structural stability in geosynthetic-reinforced embankments.

2.8 Summary

This chapter provides a critical synthesis of research concerning soil arching, trapdoor testing, and the behaviour of geosynthetic-reinforced load transfer platforms (GRLTPs). It reviews experimental investigations, analytical formulations, and numerical studies—encompassing finite element, finite difference, and discrete element methods—to elucidate the mechanisms

governing stress redistribution and deformation in pile-supported embankments. Particular attention is devoted to the roles of soil arching, the tensioned membrane effect, and beam action in facilitating load transfer. The chapter also evaluates the contribution of geosynthetics to enhancing stability, mitigating settlements, and improving stress uniformity within reinforced platforms. Finally, it identifies notable gaps in existing research, most prominently the limited availability of rigorous Finite Difference analyses addressing multi-trapdoor configurations and reinforcement arrangements, thereby establishing the rationale for the present study.

Chapter III

Numerical Simulation by Finite Difference Method

Chapter Three: Numerical Simulation by Finite Difference Method

3.1 Introduction

This chapter details the development of the numerical framework employed in this study, constructed using FLAC3D. The model geometry, boundary conditions, constitutive soil properties, and reinforcement parameters are systematically presented, along with the implementation of trapdoor displacement and surface loading. Verification of the numerical model is achieved by comparison with benchmark laboratory trapdoor tests, ensuring its capacity to replicate stress redistribution and soil arching phenomena with acceptable accuracy. This methodological foundation validates the reliability of the numerical approach and establishes the platform for the subsequent parametric analyses.

3.2 Description of the Case Study

The experimental programme conducted by (Al-Naddaf, 2017) is being adopted as the primary case study for this research. Its detailed trapdoor tests, comprehensive stress and deformation measurements, and inclusion of reinforced and unreinforced configurations provide a reliable benchmark for calibrating and validating the finite-difference numerical models. Al-Naddaf, (2017) conducted a series of physical model experiments at the Geotechnical Laboratory of the University of Kansas at USA to examine the development and stability of soil arching within embankments subjected to both static and cyclic loading conditions. The experiments were performed in a controlled testing environment using a model box measuring 1760 × 460 × 1480 mm, equipped with a transparent Plexiglas front panel to facilitate direct visual monitoring of soil displacement. The embankment was constructed from

Kansas River sand, classified as poorly graded sand (SP), and compacted to a relative density of 75% in seven successive layers, each 100 mm thick, employing the mass-volume control method, as illustrated in Figure 3.1. The experimental program consisted of two principal phases: (1) a trapdoor test and (2) a surface loading test. In the first phase, a trapdoor system measuring 360 mm in width and 460 mm in length was incrementally lowered from the base of the embankment to initiate soil arching, while vertical earth pressures were recorded by pressure cells strategically installed across the trapdoor and adjacent fixed supports. One pressure transducer (TC) was located along the centerline of the trapdoor, with four additional sensors (TE and SE) placed symmetrically at distances of 130 mm and 230 mm from the centerline. The full mobilization of soil arching was identified by the peak pressure readings at the stationary supports. Upon completion of the trapdoor phase, a rigid steel footing, identical in dimensions to the trapdoor, was subjected to surface loading through a hydraulic jack. Eight tests were conducted under static loading, with pressure increments of 7 kPa maintained for seven minutes at each stage. For cyclic loading, a frequency of 0.1 Hz was applied, with 100 cycles per load increment. Displacement transducers recorded the movements of both the footing and the trapdoor, while pressure cells continuously monitored the redistribution of stresses within the embankment. To validate the reliability of the numerical model, a simulation was initially calibrated against the results of a selected laboratory test involving a trapdoor displacement of 15 mm, which was adopted as the reference case for model verification.

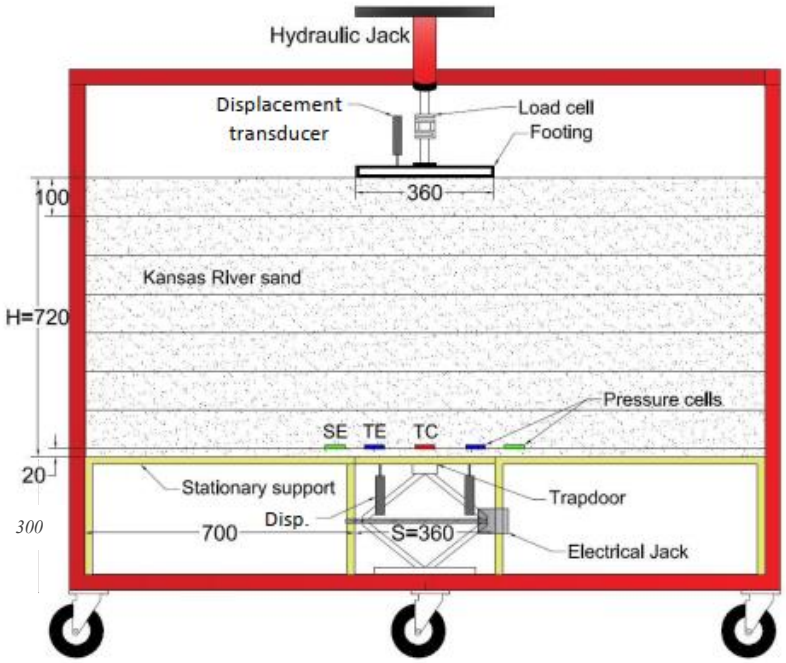

Figure 3.1: Setup for the experimental test displaying the trapdoor, measuring devices, and dimensions (unit:mm) (Al-Naddaf, 2017) .

3.3 Numerical Modeling

3.3.1 Numerical Software

The numerical simulations in this study were conducted using the finite difference software FLAC3D (Itasca Consulting Group, Inc.), which is widely utilized for geotechnical and soil-structure interaction analyses. The software's capabilities allow for the simulation of three-dimensional stress redistribution and displacement behavior under both static and dynamic loading conditions.

3.3.2 Typical Numerical Model

The numerical model was constructed to replicate the previously described physical model tests. The model geometry consists of alternating stationary supports and a central trapdoor block positioned at the base of the

embankment, extending uniformly along the y-direction. Above this foundation system, soil layers were incrementally placed, with each layer measuring approximately 0.10 m in thickness, except for the final layer, which was slightly thicker at 0.12 m. Upon completion of the embankment, a rigid steel footing, identical in width to the trapdoor and with a thickness of 0.05 m, was positioned at the soil surface. The footing was centrally aligned with the trapdoor to ensure symmetric loading and stress distribution. Figures 3.2 and 3.3 illustrate the typical numerical model configuration developed for this research.

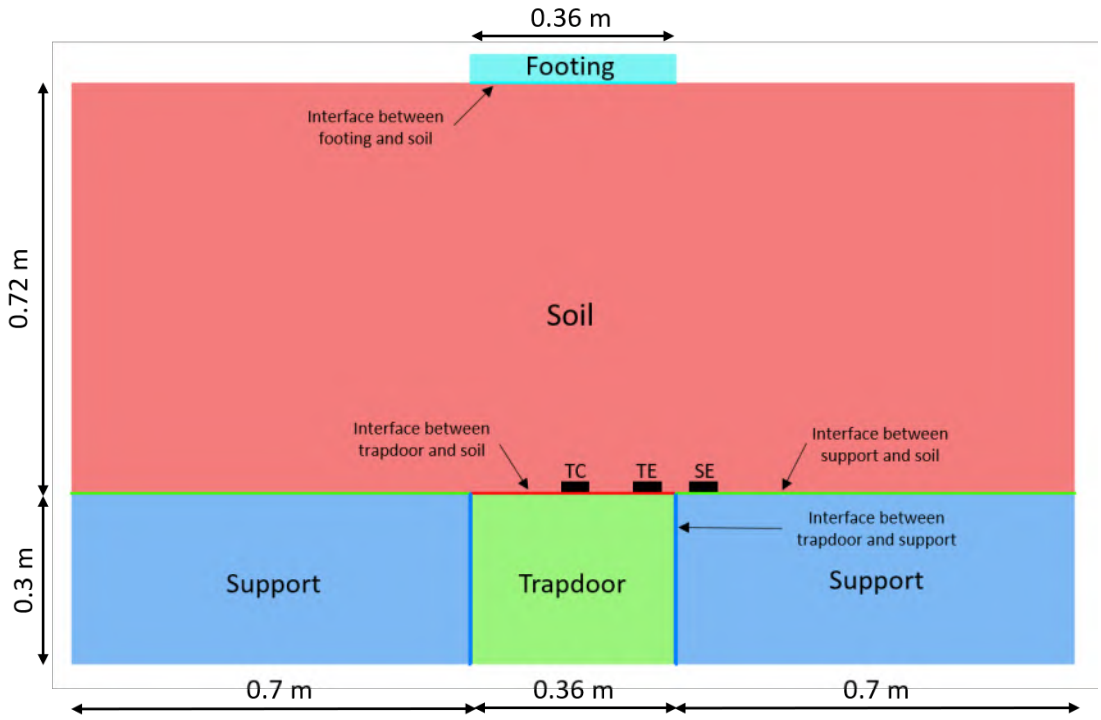

Figure 3.2: Numerical model discription and boundary layout-Front view

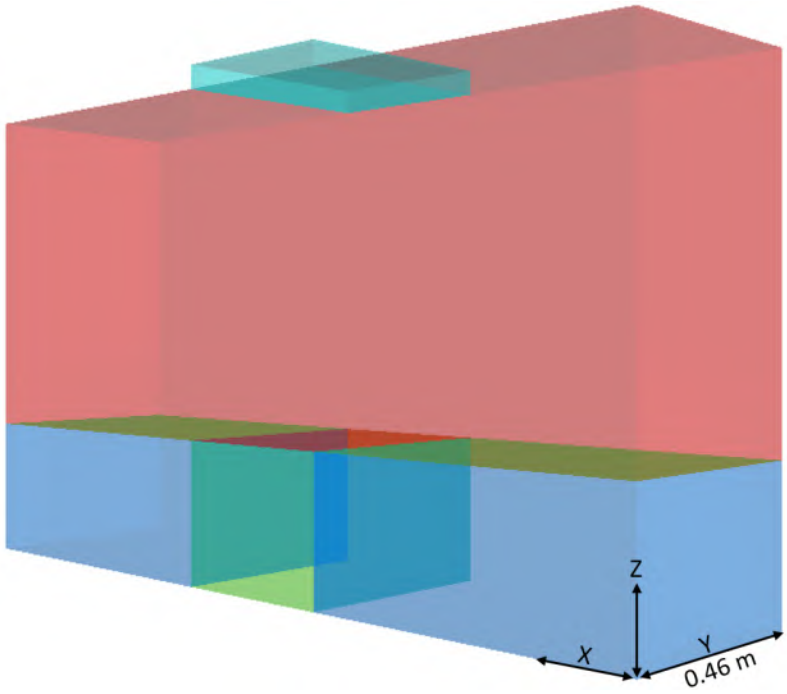

Figure 3.3: Numerical model discription-3D view

3.3.3 Constitutive Models

Two primary constitutive modeling frameworks were employed to characterize the mechanical behavior of different model components:

3.3.3.1 Structural Elements (Footing, Trapdoor, and Supports):

A linear elastic constitutive model was adopted to represent these rigid elements. In this model, the relationship between stress and strain is linear, characterized by the elastic modulus (E) and Poisson's ratio (ν), ensuring elastic, non-yielding behavior under applied loads.

3.3.3.2 Fill Material:

The embankment soil was simulated using a linear elastic-perfectly plastic model incorporating the Mohr-Coulomb (MC) failure criterion. This model governs the soil's behavior under loading by defining yield conditions through five key parameters: internal friction angle (ϕ), cohesion (c), dilatancy

angle (ψ), elastic modulus (E), and Poisson's ratio (ν). The values adopted for these parameters are summarized in Table 3.1, while a comprehensive overview of all constitutive models, material types, and their mechanical properties is provided in Table 3.2.

Table 3.1: Material properties of fill used in numerical models – All values in SI units (Al-Naddaf, 2017).

Parameters	Unit	Value
Peak friction angle (ϕ)	Degree	36
Cohesion (c)	kPa	0
Dilation angle (ψ)	Degree	0
Elastic modulus (E)	MPa	25
Poisson's ratio (ν)	-	0.3

Table 3.2: Material properties used in the numerical models (Al-Naddaf, 2017)

Zone	Model	Type	Property
Fill Material	Mohr-Coulomb	Soil (sand)	E= 25 MPa; v=0.3
Trapdoor	Linear elastic	Wood	E= 12.5 GPa; v=0.25
Stationary Supports	Linear elastic	Wood	E= 12.5 GPa; v=0.25
Footing	Linear elastic	Steel	E= 25 GPa; v=0.3

3.3.3.3 Reinforcement

In the numerical model, a geogrid layer was incorporated to represent the reinforcing effect within the embankment soil above the trapdoor. The reinforcement was simulated using FLAC3D liner structural elements with orthotropic tensile stiffness to capture the anisotropic mechanical behaviour characteristic of biaxial geogrids. The orthogonal stiffness values in the principal reinforcement directions were derived from the material's tensile properties, ensuring that the numerical model reproduced the realistic load–strain response of the geosynthetic. A membrane constitutive matrix of (1, 0, 0) was employed, enabling the element to resist in-plane tensile forces while

eliminating bending stiffness, thus reflecting the flexible nature of the geogrid.

The geogrid was assigned a nominal thickness and installed horizontally at an elevation of z = 0.34 m within first soil layer, positioned above the trapdoor level. This placement ensured that the reinforcement fully spanned the trapdoor opening and extended into the adjacent support zones, providing sufficient anchorage for tensile force mobilisation. Interaction between the geogrid and the surrounding soil was modelled using liner–zone interfaces applied to both its upper and lower faces. The interface normal and shear stiffness parameters were chosen to maintain full contact under normal loading while permitting slip once the interface shear strength was reached, thereby enabling a realistic simulation of soil–geogrid load transfer mechanisms.

3.3.4 Interfaces

In FLAC3D, various types of interface elements are available—such as bonded interfaces, slip-while-bonded, and Coulomb sliding—that can be positioned between zone faces where relative movement or separation might occur. These interfaces are crucial for realistically simulating the mechanical interaction between different material zones. In this study, interface elements were introduced to control the interaction between adjacent zones, including the contacts between the footing and the fill, the trapdoor and the fill, the supports and the fill, and between the trapdoor and the supports. The behavior of these interfaces was governed by Coulomb sliding and shear bonding mechanisms, incorporating properties such as friction angle, cohesion, dilation angle, normal and shear stiffness, as well as tensile and shear bond strengths.

3.3.5 Boundary Conditions

To accurately replicate the experimental setup, boundary conditions were carefully applied to the numerical model. Vertical gravitational loading was imposed in the negative z-direction, while lateral displacements were restrained at the model boundaries: movements in the x-direction were fixed at both ends along the x-axis, and similarly, displacements in the y-direction were restricted at both ends along the y-axis. At the model base ($z \approx 0$), all translational degrees of freedom were fixed to simulate a rigid foundation, ensuring plane strain conditions and preventing boundary-induced distortions in the results.

3.3.6 Mesh

A mesh sensitivity analysis was also performed to determine an optimal element size for the model. A refined mesh with an element size of approximately 0.0225 m was implemented in areas expected to experience high stress gradients, particularly around the trapdoor and surrounding soil zones. While coarser meshes were sufficient for capturing overall stress redistribution patterns, the finer discretization was essential for accurately resolving localized stress concentrations and displacement behaviors. The model achieved convergence at a mechanical convergence ratio of 2×10^{-5}, with additional mesh refinements producing negligible differences in the results, confirming that the chosen mesh density provided an effective balance between computational efficiency and solution accuracy.

3.4 Calibration of Numerical Simulation

Calibration of the numerical model parameters was performed based on the experimental data to ensure reliable simulation of the physical behavior. The mechanical properties of the fill material, including the Mohr-Coulomb

parameters, were adjusted to replicate the observed responses from (Al-Naddaf, 2017) laboratory test with a trapdoor displacement of 15 mm, which served as the reference case for model validation.

3.5 Simulation Procedure

The simulation process was divided into several sequential stages:

3.5.1 Soil Embankment Construction

Soil layers were incrementally added to the model, with gravitational loading applied after each layer to establish in-situ stress equilibrium.

3.5.2 Trapdoor Displacement

The trapdoor was progressively lowered in small increments using prescribed velocity boundary conditions to simulate subsidence and initiate soil arching above the void. During this phase, vertical stress and displacement data were collected at designated monitoring points within the embankment.

3.5.3 Footing Loading

Following trapdoor displacement, a vertical surface load was incrementally applied to the rigid footing. Load increments were maintained while vertical displacements and stress redistributions were continuously monitored, allowing for a detailed analysis of soil arching mechanisms and footing-soil interaction behavior.

This comprehensive modeling approach facilitated a detailed investigation of the behavior of soil under combined subsidence and surface loading conditions, with particular emphasis on arching mechanisms and the associated load transfer processes.

3.6 Monitoring Points

Stress and displacement data were recorded at strategically placed monitoring points to capture the arching effect and stress transfer within the embankment. These included a central point (TC) along the trapdoor's centerline, and two additional points (TE and SE) symmetrically located at distances of 130 mm and 230 mm from the centerline. The collected data were compiled for subsequent post-processing, analysis, and visualization.

3.7 Parametric Study

To comprehensively assess the influence of key factors governing soil arching behavior in unreinforced and reinforced embankments, a detailed parametric study was conducted using three-dimensional finite difference analyses. The study aimed to investigate the effects of varying trapdoor displacements, footing positions, footing sizes, trapdoor sizes, and multiple trapdoor configurations on the load transfer mechanisms and stress redistribution within the embankment system. A total of thirty-six numerical simulations were performed, systematically grouped according to the primary variable under consideration, as outlined in Figure 3.4. Initially, a baseline test was conducted by applying surface loading without any trapdoor displacement. Subsequent tests examined the embankment response under different trapdoor displacement magnitudes, various footing locations relative to the trapdoor center, and multiple footing and trapdoor sizes. Additional cases involving two and three trapdoors arranged in different configurations were analyzed to capture the interaction effects between adjacent voids and to better represent realistic subsidence scenarios. Furthermore, a series of reinforced models incorporating single- and multiple-layer geogrid reinforcement at different depths was developed to evaluate the role of

geosynthetics in enhancing soil arching mobilization and reducing stress transfer to the underlying subsoil. Among these models, a reference case (Test 4) featuring a single trapdoor displaced by 15 mm, a footing size equal to 1B (where B is the trapdoor width), and a footing location directly above the trapdoor centerline (0B offset) was selected for direct comparison with the corresponding experimental test. This comparison model was employed to validate the accuracy and reliability of the numerical simulations in replicating the observed physical behavior, providing a solid basis for subsequent parametric evaluations.

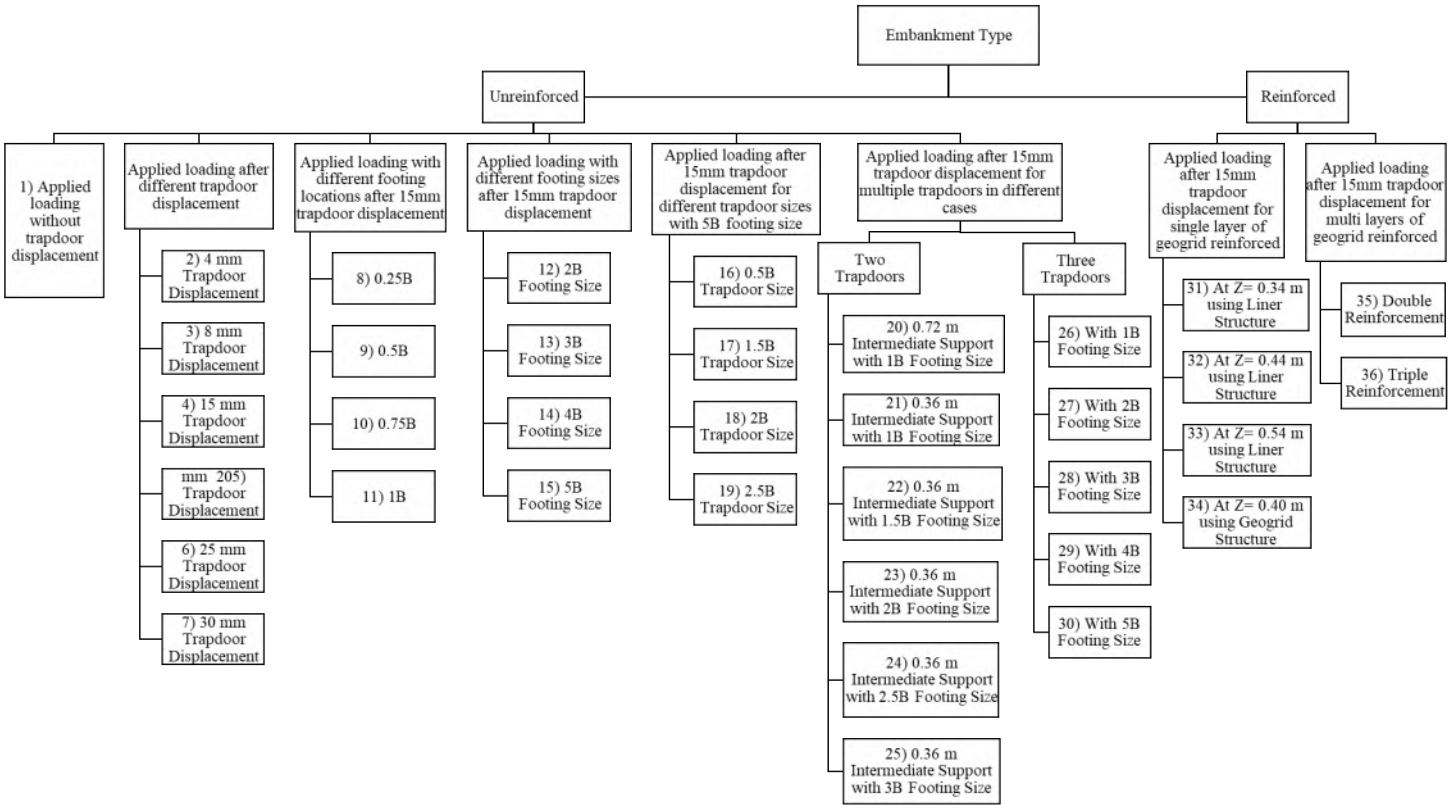

Figure 3.4: Plan of test cases

It is important to note that the surface loading simulations for all test cases (from 8 to 36) were also conducted under conditions of zero trapdoor

displacement in order to calculate the corresponding soil arching ratio (SAR) and stress reduction ratio (SRR) values.

3.8 Soil Arching

The soil arching ratio (SAR) is a widely used parameter to evaluate the extent of soil arching development in both unreinforced and geosynthetic-reinforced pile-supported embankments (Al-Naddaf and Han, 2021) (Rui *et al.*, 2022). It is defined as the ratio of the average vertical pressure measured above a yielding base (which, depending on the case, refers to either the trapdoor in unreinforced tests or the geosynthetic reinforcement in reinforced tests) to the sum of the overburden pressure, calculated as the product of the unit weight of the fill material and the fill height (γH), and any applied uniform surcharge (q), as expressed in Equation (3.1).

$$SAR = \frac{\sigma_v}{(\gamma H + q)} \qquad (3.1)$$

where:

σ_v = the average measured vertical pressure above the yielding base (kPa)

γ = the unit weight of the embankment fill material (kN/m³)

H = the embankment fill height above the yielding base (m)

q = the applied uniform surcharge (kPa).

In addition to SAR, the stress reduction ratio (SRR) is frequently employed to assess the combined effect of soil arching and the tensioned membrane behavior provided by the geosynthetic reinforcement in pile-supported embankments (Low *et al.*, 1994) (Al-Naddaf, 2019) (Ye *et al.*, 2023). The SRR is determined as the ratio between the average measured pressure below the geosynthetic reinforcement (and directly on the trapdoor) and the total vertical pressure exerted by the overburden and any applied

surcharge, as shown in Equation (3.2). In the absence of reinforcement, as in unreinforced trapdoor tests, the SRR is equal to the SAR since no geosynthetic membrane is present to influence the stress distribution.

$$SRR = \frac{\sigma'_v}{(\gamma H + q)} \qquad (3.2)$$

Where:

σ'_v = the average measured vertical pressure beneath the geosynthetic reinforcement (kPa).

During the construction of the embankment fill in this study, no additional surface surcharge was applied, and therefore, the value of q was set to zero during this phase. It should be noted that, based on the definitions of both SAR and SRR, the denominator in Equations (3.1) and (3.2) represents the initial vertical pressure on the yielding base prior to any soil arching mobilization. Accordingly, for localized surface loading scenarios, the surcharge value used in the SAR and SRR calculations was considered based on the average measured vertical pressure on the trapdoor obtained from reference test (Test 1), in which the trapdoor remained stationary throughout the loading process.

Figure 3.5 illustrates the variation of the Soil Arching Ratio (SAR) with respect to the trapdoor displacement. As shown, the SAR initially has a high value of approximately 0.98 at zero displacement, indicating that most of the applied vertical stress is being transferred directly to the trapdoor. This is expected since no soil arching mechanism is yet mobilized at this stage, and the soil behaves as a continuous medium.

As the trapdoor displacement increases from 0 mm to approximately 2 mm, a rapid decrease in the SAR is observed. The SAR drops from 0.98 to approximately 0.23 within this small range of displacement. This sharp

reduction signifies the quick mobilization of the soil arching effect, where part of the vertical stress is redistributed to the surrounding soil rather than being directly transferred to the yielding trapdoor.

Beyond a displacement of 4 mm, the SAR stabilizes at a nearly constant value of 0.232 despite further increases in trapdoor displacement up to 15 mm. This plateau suggests that the soil arching mechanism has fully developed, and a stable arching system is established within the fill material. In this condition, the stress transfer mechanism reaches a steady state where further displacement no longer contributes to additional redistribution of stresses.

Moreover, the constant SAR value after 4 mm implies that the trapdoor has undergone sufficient movement to activate the ultimate soil arching capacity. Additional displacement does not significantly influence the vertical stress distribution, as the arching structure effectively channels the stresses to the adjacent stationary zones.

In practical terms, this behavior emphasizes the efficiency of soil arching mechanisms in reducing loads on yielding or deformable substructures with minimal settlement. It also highlights the importance of understanding the threshold displacement required for full arching mobilization in geotechnical designs involving trapdoor systems, piled embankments, or reinforced foundations.

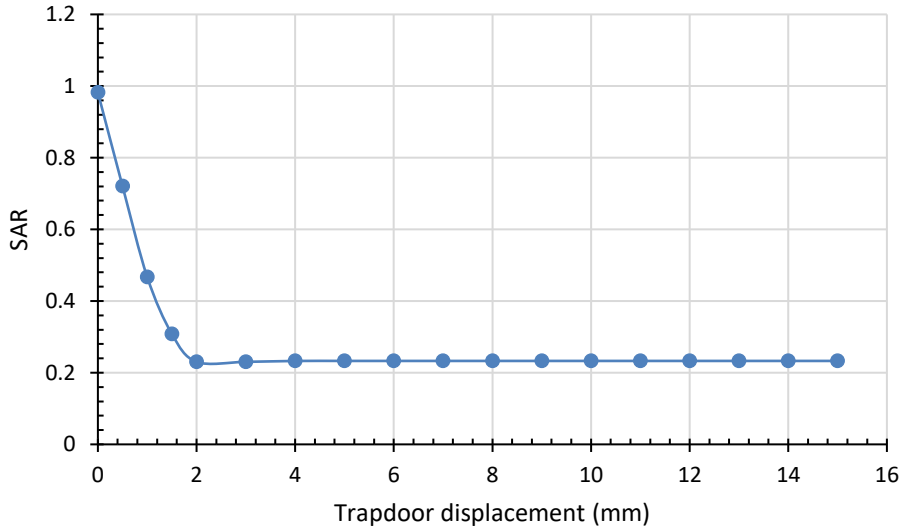

Figure 3.5: Soil arching ratio versus trapdoor displacement

Figure 3.6 presents the relationship between the Soil Arching Ratio (SAR) and the applied footing pressure, ranging from 0 to 110 kPa. At the initial unloaded state, the SAR value was approximately 0.23, indicating highly effective soil arching, where a significant portion of the vertical stress was transferred laterally to the adjacent soil. According to the classical soil arching theory, SAR values less than 1 signify active arching behavior, where the mobilized shear strength along potential slip surfaces enables the redistribution of stresses away from the yielding zone , in this case, under the footing. As the applied footing pressure increased to 50 kPa, the SAR value rose progressively from 0.232 to approximately 0.68. This stage exhibited a relatively rapid increase in SAR, reflecting a gradual loss in arching efficiency as the soil's ability to carry additional redistributed stress diminished under higher loads.

Between 50 and 100 kPa, the SAR continued to increase but at a slower, nonlinear rate, approaching 0.86 at 110 kPa. This progressive increase in SAR

with applied pressure highlights the combined effects of stress concentration above the trapdoor and the reduction of mobilized arching action due to the breakdown of soil arch formation under increased surcharge. It is important to note that throughout the entire pressure range, the SAR values remained below 1.0, confirming the continuous presence of soil arching. In the context of geotechnical practice, SAR values exceeding 1 would indicate that the applied vertical stress surpasses the natural overburden stress and surcharge capacity, causing excessive stress concentration on the yielding zone, and suggesting ineffective or failed arching action.

From a design perspective, the ability of the soil to sustain SAR values below 1 under pressures up to 110 kPa demonstrates a favorable performance of the embankment system, where soil arching effectively reduces vertical stress concentration on the underlying soft layer or reinforcement system. Additionally, the diminishing rate of SAR increase at higher pressures suggests the system may approach a stabilized stress redistribution state, beyond which further loading would not significantly degrade arching action, or the soil reaches a limit equilibrium state.

In summary, the presented results demonstrate that while the soil arching mechanism weakens progressively with increasing applied pressure, it remains effective throughout the examined range, mitigating excessive stress transfer to the trapdoor area. This behavior reinforces the importance of accounting for both surcharge magnitude and soil arching capacity when assessing the performance and design safety of embankments, footings, and geosynthetic-reinforced systems constructed over yielding or soft foundations.

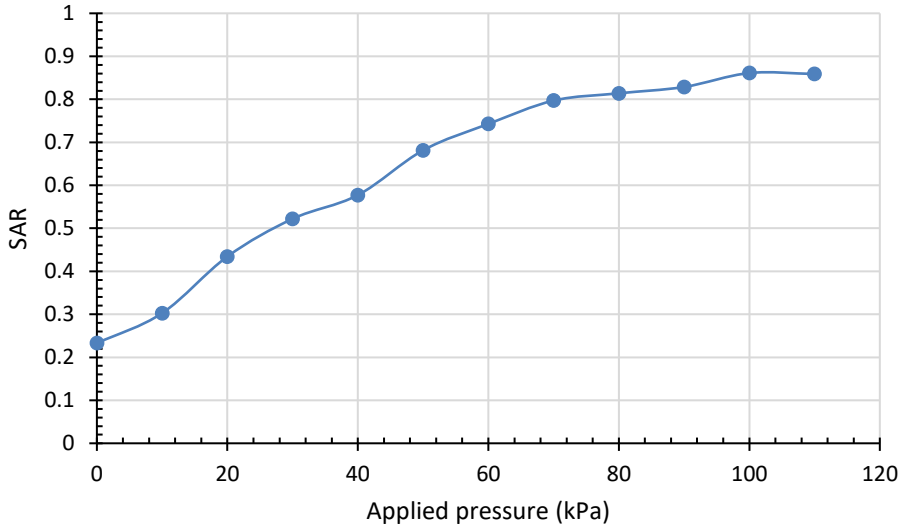

Figure 3.6: Soil arching ratio versus applied pressure

3.9 Validation of Numerical Models

To ensure the reliability of the subsequent parametric study, the reference numerical model (Test 4) was first validated by comparing its outcomes with available experimental data and theoretical expectations.

3.9.1 Comparisons with Analytical Solution

The validation process was first conducted during the soil construction stage, where relationship between fill height and vertical pressure, as presented in Figure 3.7, exhibits a consistent linear trend across the numerical simulation outcomes and the theoretical calculation based on the unit weight of the fill material (γH). This linearity aligns with classical geotechnical theory, where vertical stress under a self-weighted fill increases proportionally with depth, in the absence of significant arching effects or lateral constraints.

A detailed comparison indicates excellent agreement between the numerical model predictions and theoretical values at all examined fill heights. The computed vertical pressures from the numerical simulation closely follow the theoretical data, with negligible discrepancies throughout the range of 100 mm to 700 mm fill height. This observation is further supported by the Root Mean Square Error (RMSE) expressed as a percentage of the mean, calculated to be 3.18%, which is considered highly acceptable within geotechnical numerical modeling practice. An RMSE value of this magnitude indicates that the numerical model reliably captures the essential stress distribution behavior under self-weight loading conditions.

Overall, the strong correlation observed between the numerical and theoretical results provides confidence in the validity of the baseline numerical model. Consequently, it is deemed appropriate for use in the subsequent parametric studies investigating the effects of various parameters on soil arching behavior and pressure redistribution mechanisms.

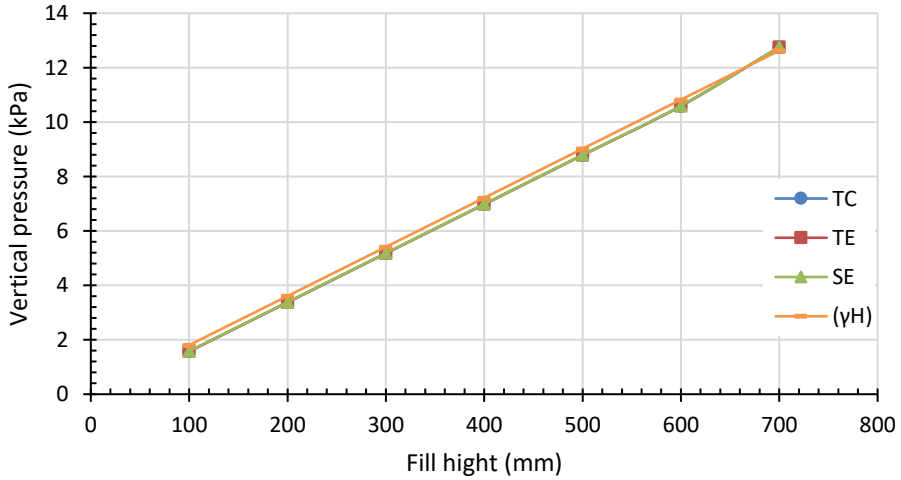

Figure 3.7: Comparison of vertical stress in relation to fill height at three monitoring points during soil construction

3.9.2 Comparisons with Experimental Test- for Unreinforced Model

A verification process was conducted to evaluate the accuracy of the numerical model by comparing its results at a trapdoor displacement of 15 mm with the corresponding experimental measurements at two distinct stages.

3.9.2.1 During Trapdoor Displacement

During the trapdoor displacement stage, as illustrated in Figure 3.8, the comparison revealed a strong agreement between the numerical predictions and the experimental observations, particularly at the stationary support locations. Both the experimental (SE exp.) and numerical (SE num.) values followed a similar trend and converged to comparable final values, thereby validating the numerical model's capability to simulate the soil arching mechanism effectively.

However, slight deviations were observed at the center and edges of the trapdoor, where the numerical model tended to slightly overestimate the vertical stress values relative to the experimental results. These discrepancies are likely due to inherent simplifications in the numerical approach, including the assumption of idealized boundary conditions, homogeneous soil properties, and the adoption of a linear elastic-perfectly plastic Mohr-Coulomb constitutive model. Such assumptions may not fully capture the complex, nonlinear, and stress-dependent behavior of soil during the development of arching.

To quantitatively assess the model's predictive performance, the root mean square error (RMSE) was calculated and expressed as a percentage of the mean experimental values. The results indicated an RMSE of approximately 12.5% at the trapdoor and 8.8% at the stationary support. These relatively low error margins further support the adequacy and reliability of the

numerical model in replicating the stress distribution and arching response of soil under trapdoor-induced displacement.

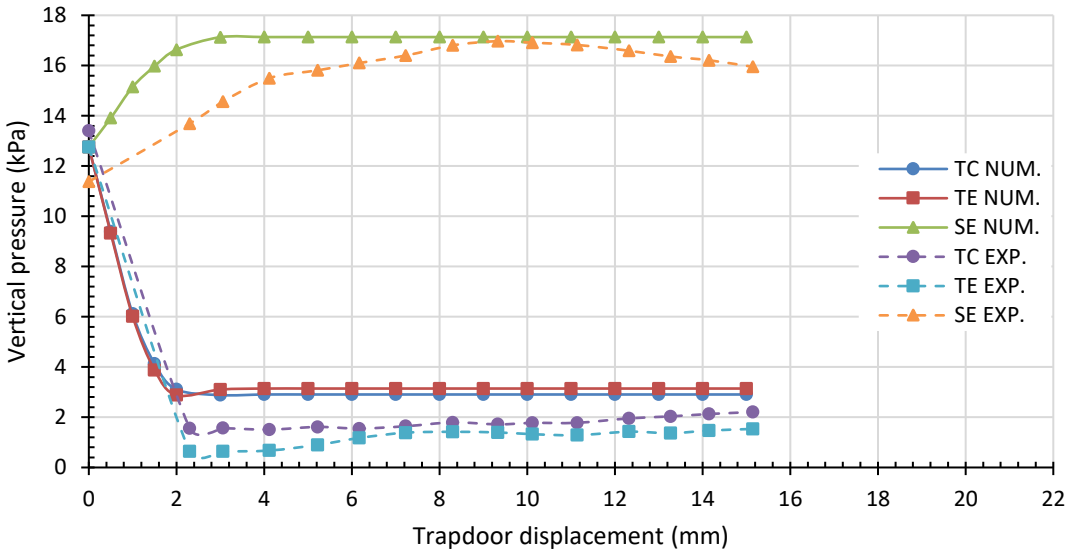

Figure 3.8: Comparison of vertical stress in relation to trapdoor displacement at three monitoring points-Numerical model verification with experimental test

3.9.2.2 Under Incremental Surface Loading

After the trapdoor displacement reached stabilization, the vertical stress responses under incremental surface loading were compared between the numerical simulation and the experimental results, as depicted in Figure 3.9. The comparison demonstrates a generally good agreement, indicating the numerical model's competence in replicating the arching mechanism behavior. Initially, the vertical stresses recorded at the stationary support (SE) were higher than those at the trapdoor center (TC) in both datasets. This pattern reflects the typical arching effect, where stresses are transferred laterally towards the trapdoor edges, resulting in reduced stress at the center.

With the progression of surface loading, the stress values at TC and SE gradually approached each other, signifying the degradation of the arching

structure and a redistribution of stresses across the entire system. Notable differences were observed at the trapdoor edge (TE) under higher load levels, where the numerical model slightly overestimated the stress values compared to the experimental data. This overprediction can be attributed to the limitations of the Mohr-Coulomb constitutive model, particularly its inability to accurately capture strain-softening, post-yield behavior, and localized stress concentrations that were evident in the experimental setup.

To further evaluate the accuracy of the numerical model, the root mean square error (RMSE) was calculated as a percentage of the mean experimental values. The RMSE was found to be 14.15% at the trapdoor and 6.32% at the stationary support. These values indicate that the numerical model achieved an acceptable level of accuracy, especially at the support, and effectively represented the overall stress distribution during the surface loading phase, despite some localized discrepancies.

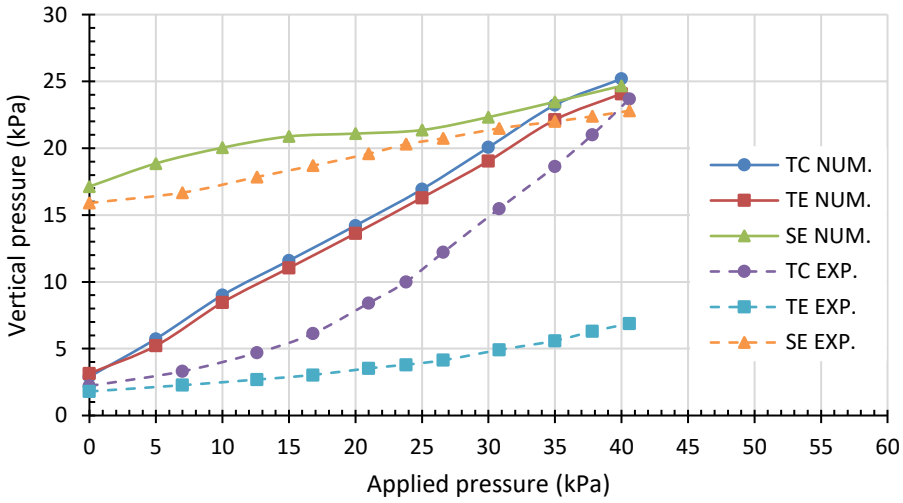

Figure 3.9: Comparison of vertical stress in relation to monotonic static footing pressure in the loading test at three monitoring points- Numerical model verification with experimental test

3.9.3 Comparisons with Experimental Test- for Reinforced Model

A verification process was conducted to evaluate the accuracy of the numerical model by comparing its results at a trapdoor displacement of 15 mm and single geogrid reinforcement in the first layer, with the corresponding experimental measurements at two distinct stages.

3.9.3.1 During Trapdoor Displacement

The comparison between experimental and numerical results for the single-trapdoor case with a geogrid in the first layer shown in Figure 3.10 demonstrates strong agreement in capturing the fundamental stress redistribution trends during trapdoor displacement. At the trapdoor center (TC) and edge (TE), both approaches show a rapid stress reduction from an initial ~13 kPa to ~0.5 kPa within the first 3 mm of displacement, reflecting the swift mobilization of the arching mechanism and load diversion toward the supports. The numerical model slightly underestimates the residual stresses at larger displacements, producing flatter tails compared to the experimental curves, which retain marginally higher values—likely due to partial load transfer along the geogrid–soil interface in the physical test. At the support location (SE), the agreement is particularly strong, with both datasets showing a rapid increase in vertical stress from ~12-13 kPa to ~17–18 kPa within the first few millimeters, followed by stabilization. However, the experimental results exhibit a gradual continued rise to ~21 kPa at maximum displacement, whereas the numerical values plateau earlier, suggesting that tensile stiffening or strain-hardening effects of the geogrid in the physical test were not fully replicated numerically. Overall, the numerical simulation successfully reproduces the dominant load transfer mechanisms—

stress relief at the yielding zone and stress concentration at the supports—while the minor discrepancies in residual and ultimate stress magnitudes can be attributed to idealized modeling assumptions, boundary conditions, and the absence of certain geogrid material non-linearities present in the experimental setup.

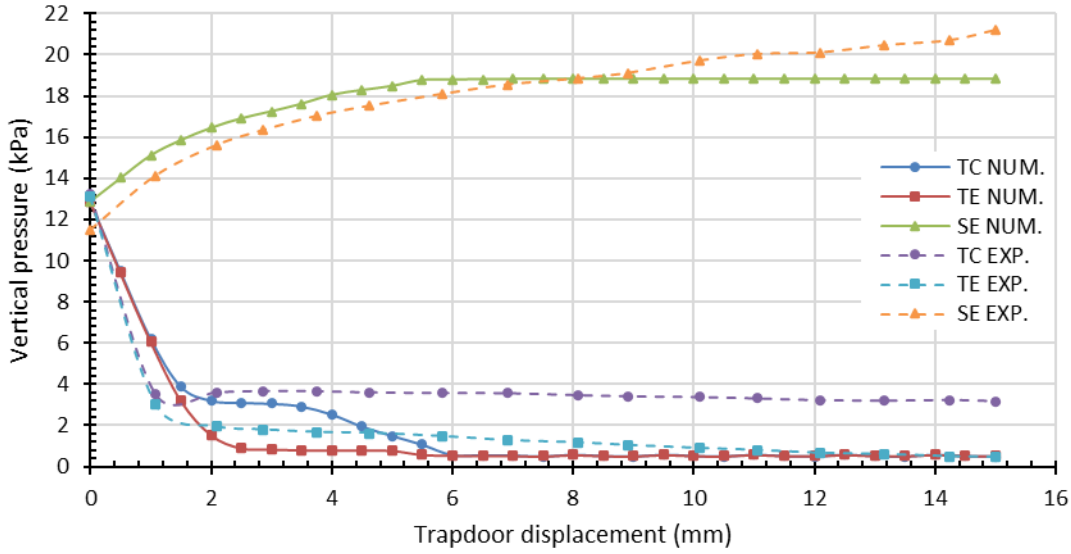

Figure 3.10: Comparison of vertical stress in relation to trapdoor displacement at three monitoring points-Numerical model verification with experimental test for geogrid reinforced model

3.9.3.2 Under Incremental Surface Loading

The comparison between the experimental and numerical results for the single-trapdoor case with a geogrid in the first layer under applied surface loading shows generally consistent trends, with minor deviations in magnitude and stiffness response (Figure 3.11). At the trapdoor center (TC), both datasets capture the expected steady increase in vertical stress with applied load, reflecting progressive direct load transmission to the yielding zone. The numerical results show a more linear stress–load relationship,

reaching ~55 kPa at 100 kPa applied load, whereas the experimental curve exhibits a slightly lower stiffness in the early stages but catches up, converging with the numerical prediction at around 90 kPa. At the support location (SE), both datasets indicate an initial dominance of load transfer to the supports, with the experimental results starting higher (~21 kPa) and showing a more pronounced early stiffness, reaching ~45 kPa by 80 kPa applied load. The numerical results, although starting lower (~19 kPa), increase more gradually, ultimately approaching 47 kPa at the maximum load. The higher initial SE stress in the experimental test suggests that the physical geogrid mobilized tensile resistance earlier, possibly due to pre-tensioning effects or soil–geogrid interlock not fully replicated in the numerical model. Overall, both approaches successfully reproduce the qualitative load-sharing mechanism, where the geogrid enables substantial stress redirection toward the supports while allowing controlled stress growth at the trapdoor center. The small quantitative differences are likely attributable to modeling simplifications, particularly in simulating geogrid– non-linear tensile stiffening, and boundary condition influences present in the physical test.

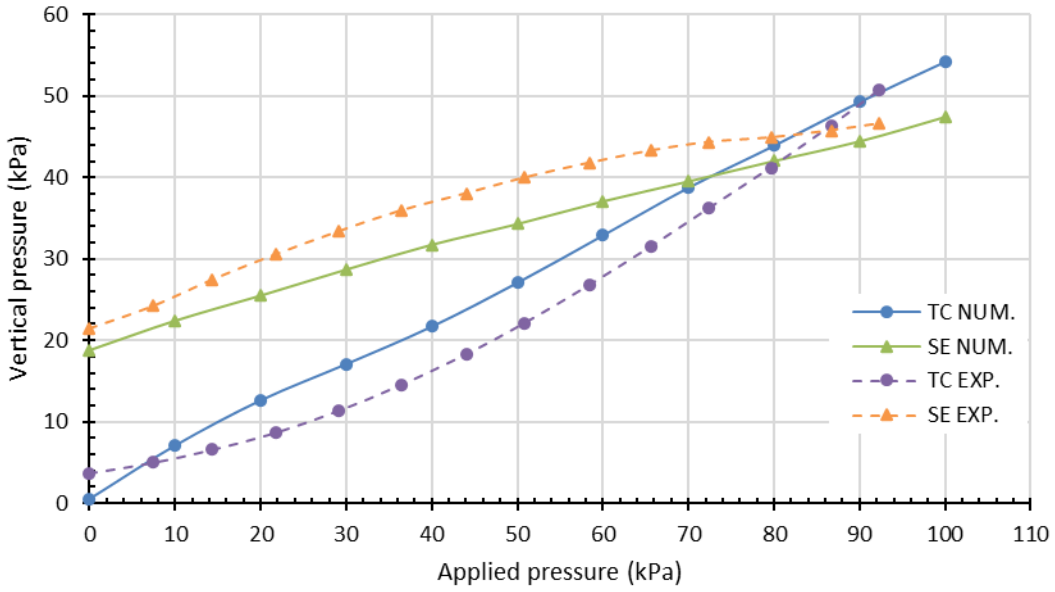

Figure 3.11: Comparison of vertical stress in relation to monotonic static footing pressure in the loading test at three monitoring points-Numerical model verification with experimental test for geogrid reinforced model

Chapter IV

Results and Discussion

Chapter Four: Results and Discussion

4.1 Introduction

This chapter presents the outcomes of the numerical analyses for both single and multiple trapdoor systems, with and without geogrid reinforcement. It first examines single trapdoor cases, establishing baseline behavior by evaluating the effects of displacement, width, and footing position on stress redistribution and soil arching ratio (SAR). The discussion then extends to double- and triple-trapdoor systems, where intermediate supports are shown to enhance stress uniformity, load transfer efficiency, and arch stability. Finally, the influence of geogrid reinforcement is assessed, focusing on the effects of reinforcement depth, layering, and structural representation. The integrated results provide a comprehensive three-dimensional understanding of soil arching mechanisms and the factors governing their mobilization and degradation.

4.2 Effect of Trapdoor Displacement

4.2.1 During Trapdoor Displacement

Figure 4.1 present the relationship between trapdoor displacement and vertical pressure measured at three critical points: directly above the trapdoor center (TC), at the edge of the trapdoor (TE), and at the soil edge (SE). The vertical pressure response exhibits a consistent pattern across all model configurations. At the onset of displacement (0 to approximately 3 mm), a sharp decrease in vertical pressure is observed at both TC and TE. Concurrently, a marked increase in pressure occurs at SE, indicating the initiation and rapid mobilization of the soil arching mechanism.

Beyond approximately 4 mm of displacement, the pressures at TC and TE stabilize at small values estimated 2.9 and 3.1 kPa respectively, while the

pressure at SE remains relatively constant at value 17 kPa. This stabilization confirms the full development of the arching structure, effectively transferring the applied loads from the trapdoor zone to the surrounding soil mass.

The similarity in pressure trends across all displacement cases suggests a consistent formation of soil arches under the applied conditions.

The contour plots shown in Figure 4.2 corroborate this observation, highlighting a reduction in stress at the center and a corresponding increase toward the edges.

The development of the soil arching ratio (SAR) with respect to trapdoor displacement is illustrated in Figure 4.3. In all cases, SAR exhibits a sharp decline during the initial displacement stage, reaching a stable, near-constant value after approximately 3 to 5 mm of displacement. The final SAR values recorded fall within a narrow range of 0.21 to 0.24.

This behavior further corroborates the early mobilization of arching action within the soil mass. The rapid decrease in SAR corresponds to the redistribution of vertical stress from the trapdoor region to the soil edge as the arch forms. The subsequent plateau in SAR indicates the establishment of a stable arching mechanism capable of maintaining a consistent stress distribution throughout the remainder of the displacement process.

The close agreement in the final SAR values across the different cases suggests that the arching phenomenon is relatively insensitive to minor changes in the displacement range tested in this study. This consistency underlines the robustness of the soil arching effect under trapdoor conditions, particularly for displacements exceeding 5 mm.

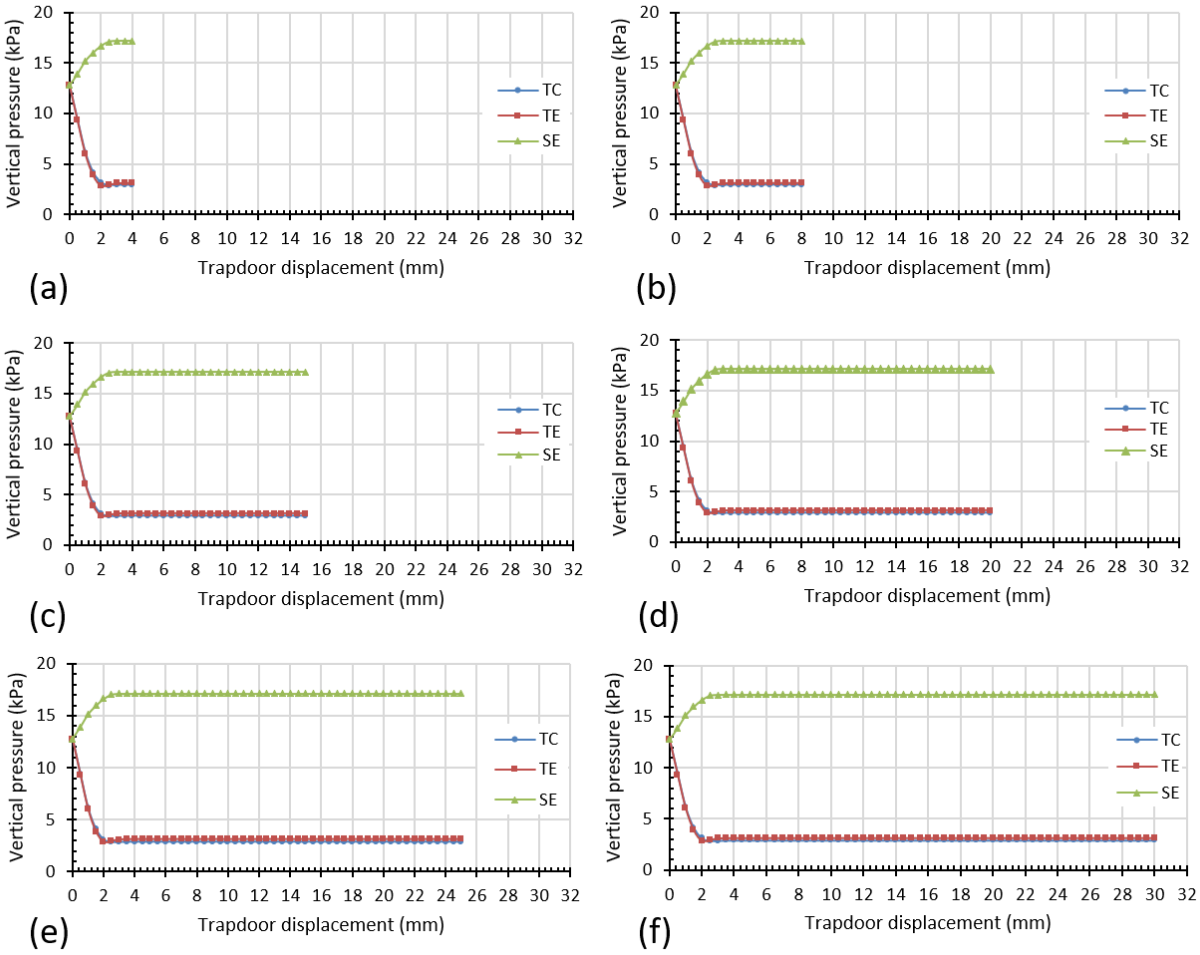

Figure 4.1: Comparison of vertical stress in relation to trapdoor displacement at three monitoring points, (a) Test 2 (4mm displacement); (b)Test 3 (8mm displacement); (c) Test 4 (15mm displacement); (d) Test 5 (20mm displacement); (e) Test 6 (25mm displacement); and (f) Test 7 (30mm displacement)

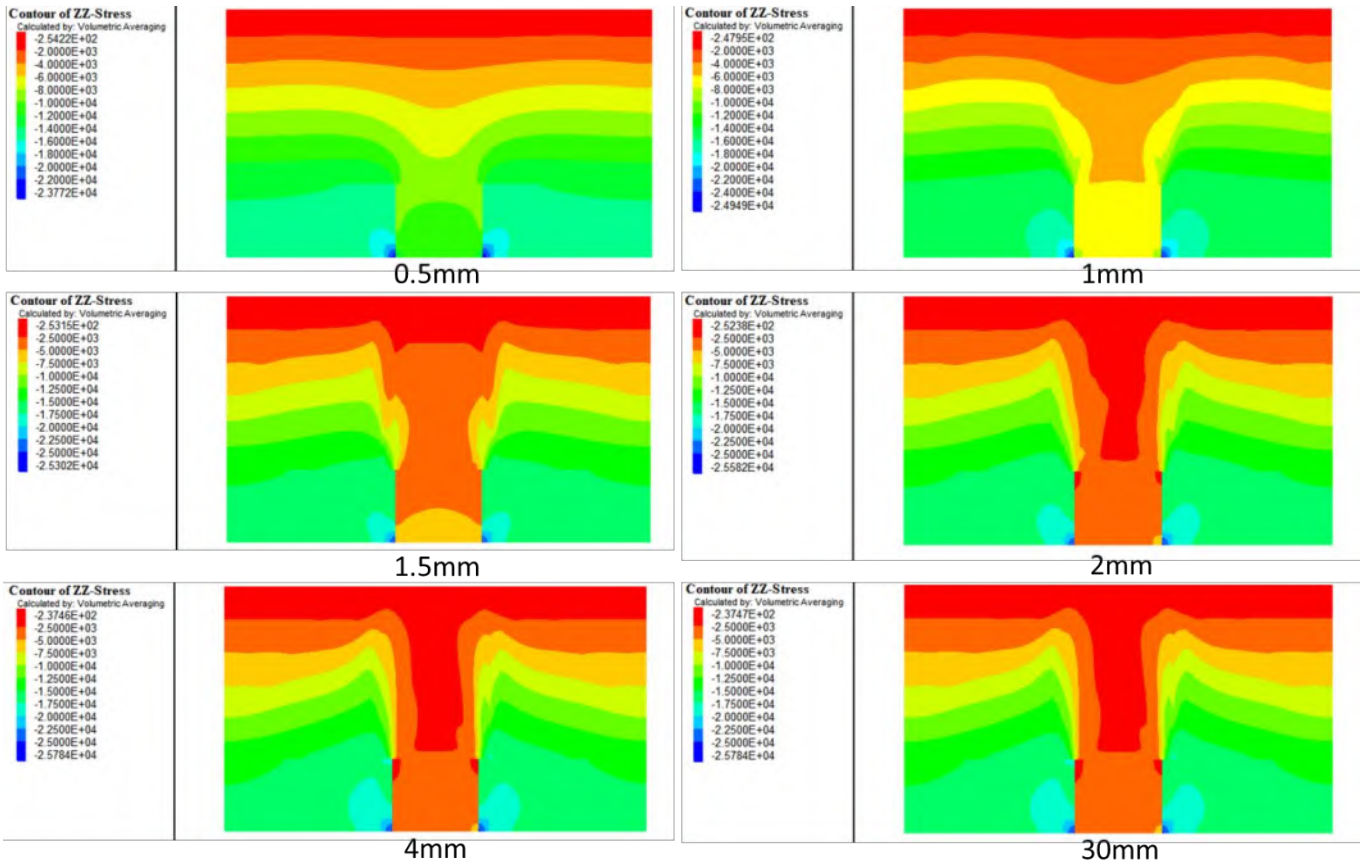

Figure 4.2: Pressure distribution of numerical model during trapdoor displacements

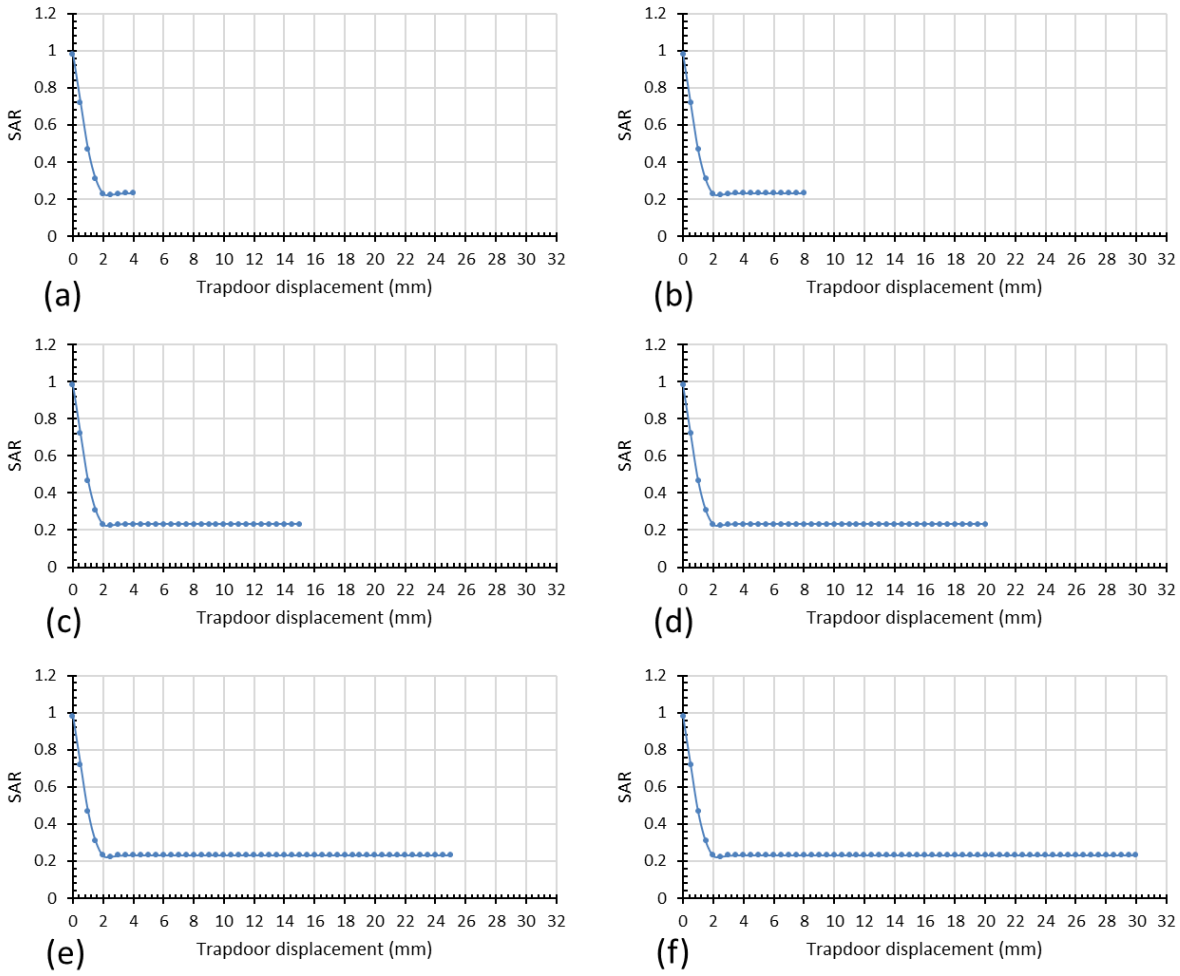

Figure 4.3: Comparison of SAR in relation to trapdoor displacement, at (a) Test 2 (4mm displacement); (b) Test 3 (8mm displacement); (c) Test 4 (15mm displacement); (d) Test 5 (20mm displacement); (e) Test 6 (25mm displacement); and (f) Test 7 (30mm displacement)

4.2.2 During Footing Loading

The variation of vertical pressure beneath the footing with increasing applied load across the different displacement cases reveals the progressive mobilization and subsequent degradation of the soil arching mechanism Figures (4.4 and 4.5). In the early stages of loading, specifically within the 0-30 kPa range, the vertical pressure recorded at the soil edge (SE) was consistently higher than the pressures at both the trapdoor center (TC) and trapdoor edge (TE) in all cases, indicating effective activation of the soil arching effect. This behavior confirms that, regardless of the magnitude of

trapdoor displacement, the arching mechanism initially facilitated the lateral redistribution of stresses from the unsupported trapdoor region toward the adjacent soil mass. As the applied footing pressure increased beyond approximately 30-40 kPa, a noticeable shift in stress distribution occurred. The vertical pressure at SE began to stabilize, while the pressures at TC and TE continued to increase nearly linearly with the applied load, reducing the stress differential. This convergence signifies a progressive degradation in the efficiency of the soil arching mechanism.

This evolution is further supported by the trends observed in the Soil Arching Ratio (SAR) Figure (4.6). Initially, SAR increased rapidly in all cases, particularly within the 0-30 kPa range, reflecting the efficient mobilization of arching pathways. However, beyond 40–50 kPa, the rate of SAR increase diminished across all displacement scenarios, with the effect more pronounced in cases (d) through (f). Notably, for all cases, SAR values approached approximately 0.8 at applied pressures of 55-60 kPa, signifying that the arching mechanism's capacity to redistribute additional stresses was compromised. The combined interpretation of vertical pressure and SAR trends demonstrates that while soil arching plays a critical role in stress redistribution under moderate footing loads and displacements, its effectiveness progressively declines with increasing applied load and trapdoor displacement due to the cumulative effects of soil deformation, reduced lateral confinement, and degradation of the internal arch structure. These findings align with established theoretical and experimental research, emphasizing the necessity of considering both applied load and displacement magnitude when

evaluating soil arching behavior in foundation systems over voids or discontinuities.

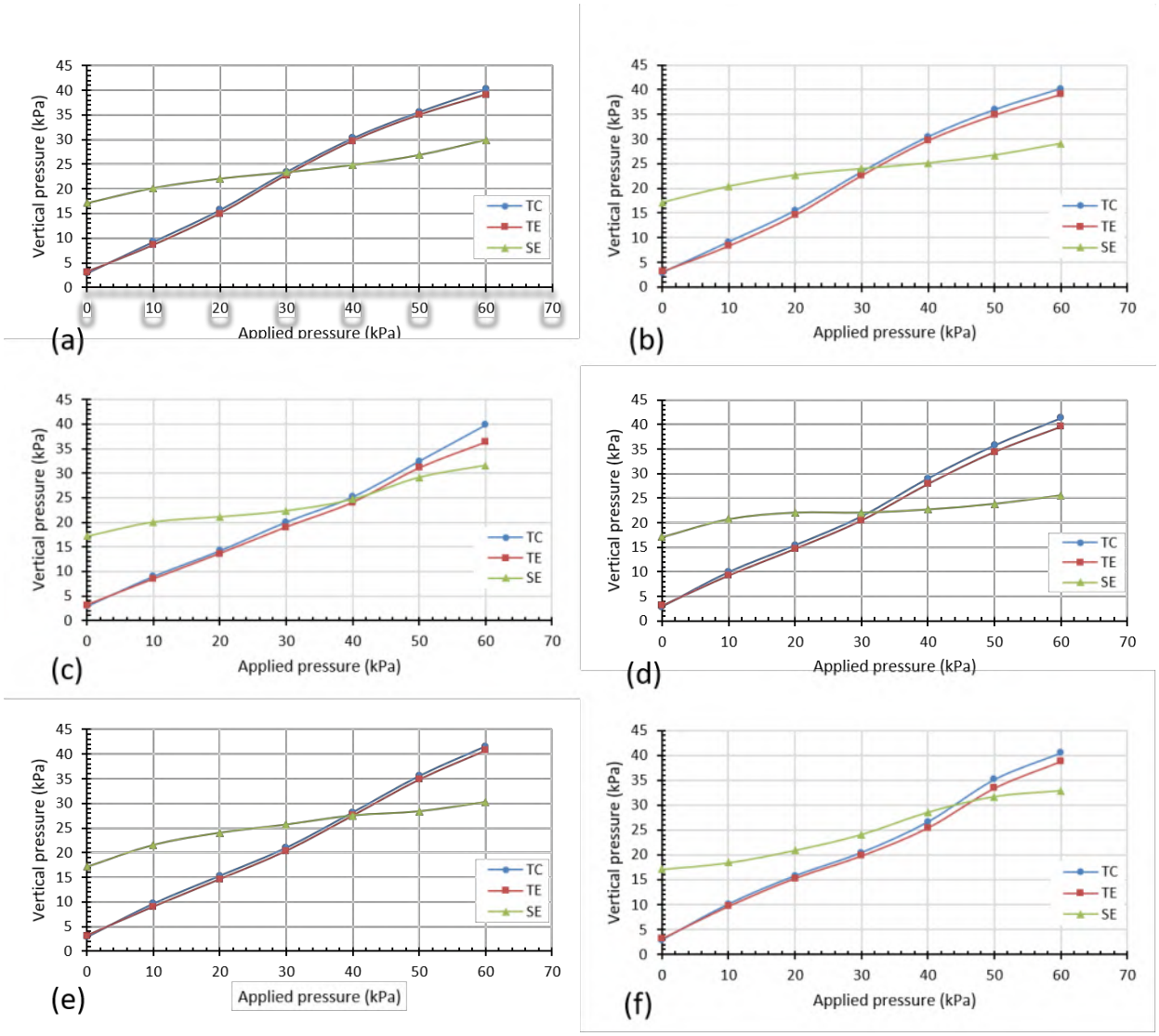

Figure 4.4: Comparison of vertical stress in relation to monotonic static footing pressure in the loading test at three monitoring points, (a) Test 2 (4mm displacement); (b) Test 3 (8mm displacement); (c) Test 4 (15mm displacement); (d) Test 5 (20mm displacement); (e) Test 6 (25mm displacement); and (f) Test 7 (30mm displacement)

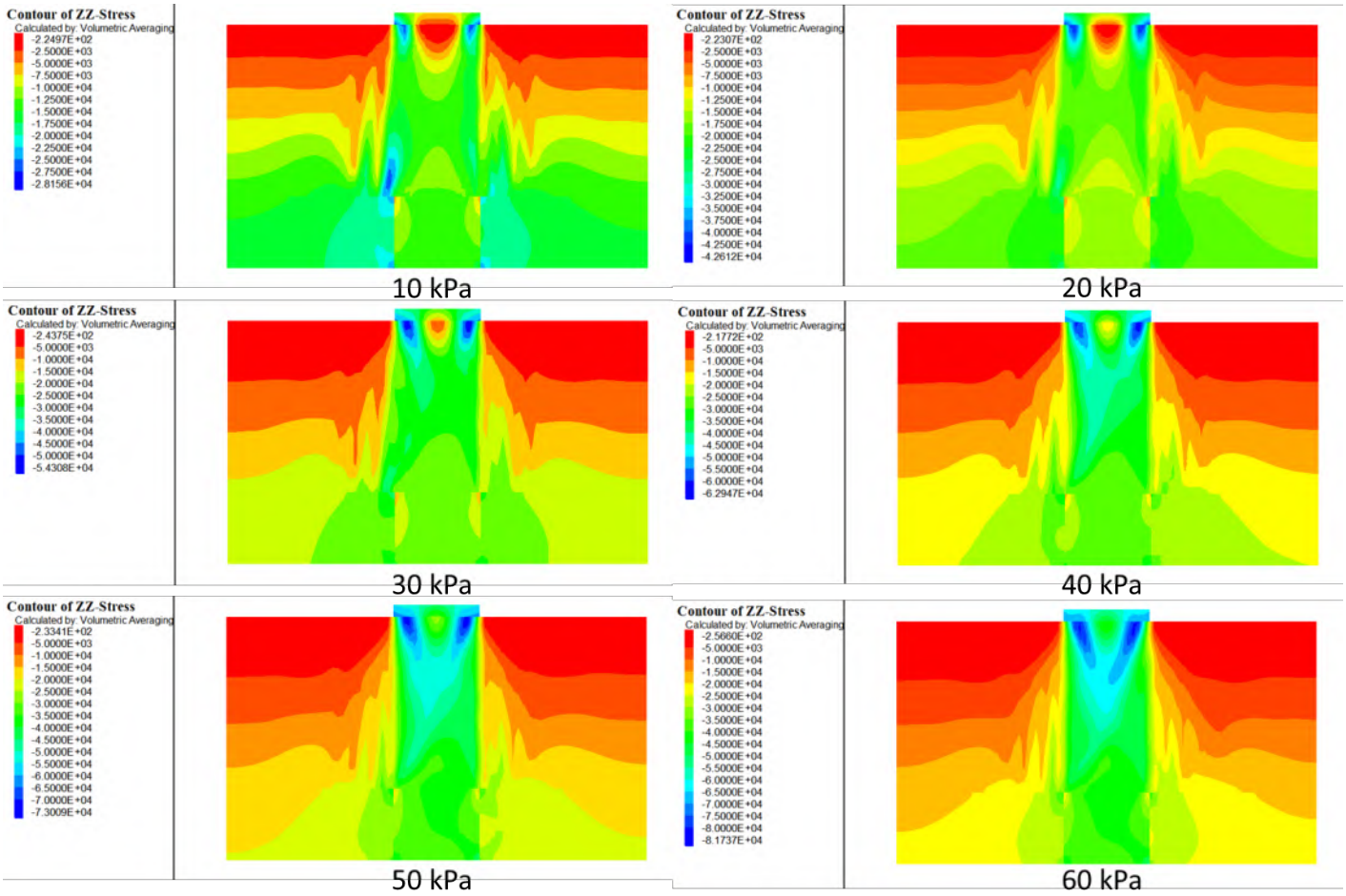

Figure 4.5: Pressure distribution of numerical model under applied loads for a 15 mm displacement model (Test 4)

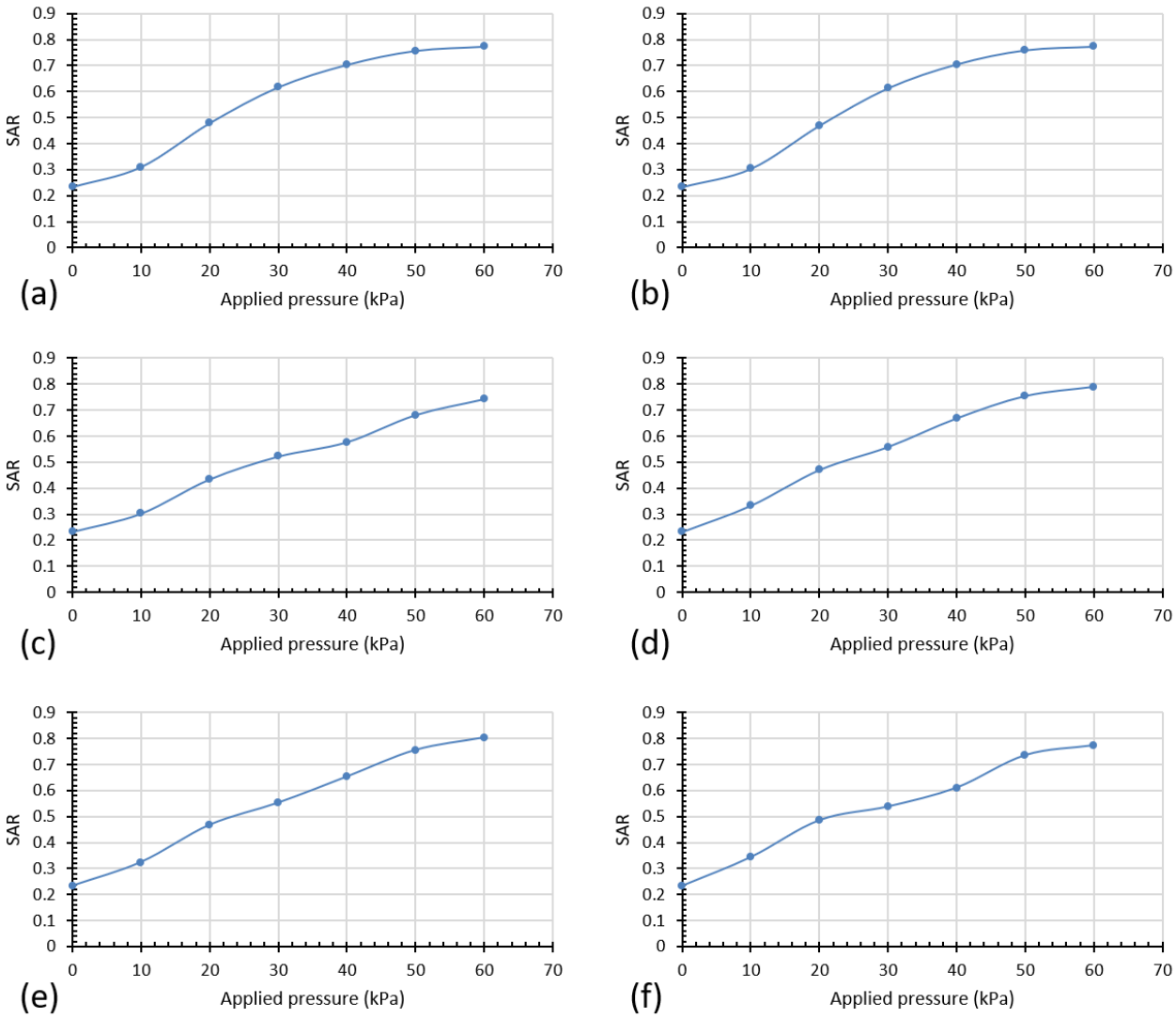

Figure 4.6: Comparison of SAR in relation to applied pressure, at (a) Test 2 (4mm displacement); (b) Test 3 (8mm displacement); (c) Test 4 (15mm displacement); (d) Test 5 (20mm displacement); (e) Test 6 (25mm displacement); and (f) Test 7(30mm displacement)

4.3 Effect of Footing Location

4.3.1 During Footing Loading

The numerical findings distinctly demonstrate the significant influence of footing offset on the development, stability, and eventual degradation of the soil arching mechanism under varying surface loads. Figures (4.7 and 4.8) shows that, in all offset scenarios, the initial application of low pressures (around 20 kPa) resulted in a well-defined arching effect, characterized by

higher vertical stresses at the side supports (SE) and markedly lower stresses at the trapdoor center (TC), indicative of effective stress transfer away from the yielding zone. At this stage, SAR values remained well below unity, confirming the arch's structural efficiency in distributing loads toward the stable soil regions. As surface pressures increased to moderate levels (~60 kPa), the response of the arch began to diverge between cases. In the 0.25B and 0.5B configurations, although arching persisted, a gradual rise in TC stress signaled the onset of degradation, as the mobilized soil strength and interparticle friction progressively diminished. This trend was accentuated under higher loads (100–110 kPa), where in both cases, TC stresses approached or exceeded those at SE, with SAR values nearing or surpassing 0.85, reflecting a substantial loss in arching effectiveness and increased direct load transfer to the trapdoor region. In contrast, the 0.75B and 1.0B offset cases demonstrated superior arch durability, with stress concentrations remaining predominantly at SE throughout the loading sequence. Notably, in the 1.0B scenario, even at maximum applied pressures, TC stress remained significantly lower than at SE, and no stress reversal occurred, maintaining SAR values within a range that indicated reliable arching action. This behavior highlights how increasing the lateral distance between the footing and the trapdoor reduces the direct influence of surface loading on the trapdoor area, allowing the arching mechanism to sustain its load transfer function effectively. The results underscore the critical role of optimized footing placement in enhancing both the load redistribution capacity and long-term performance of soil systems governed by arching, with practical implications for the design of embankments, load transfer platforms, and piled embankment systems where differential settlements and localized yielding are concerns.

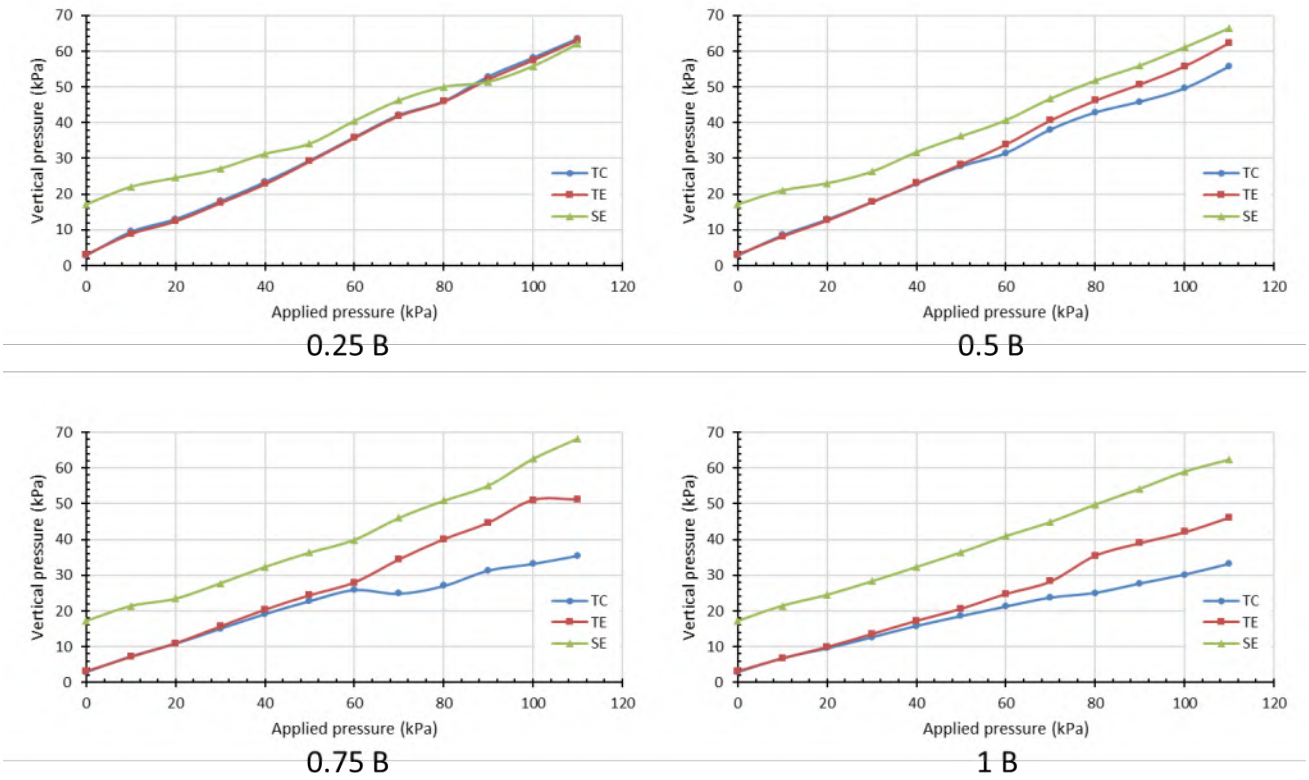

Figure 4.7: Comparison of vertical stress in relation to monotonic static footing pressure in the loading test at three monitoring points, for: Test 8 (0.25B) ; Test 9 (0.5B); Test 10 (0.75B); and Test 11 (1B)

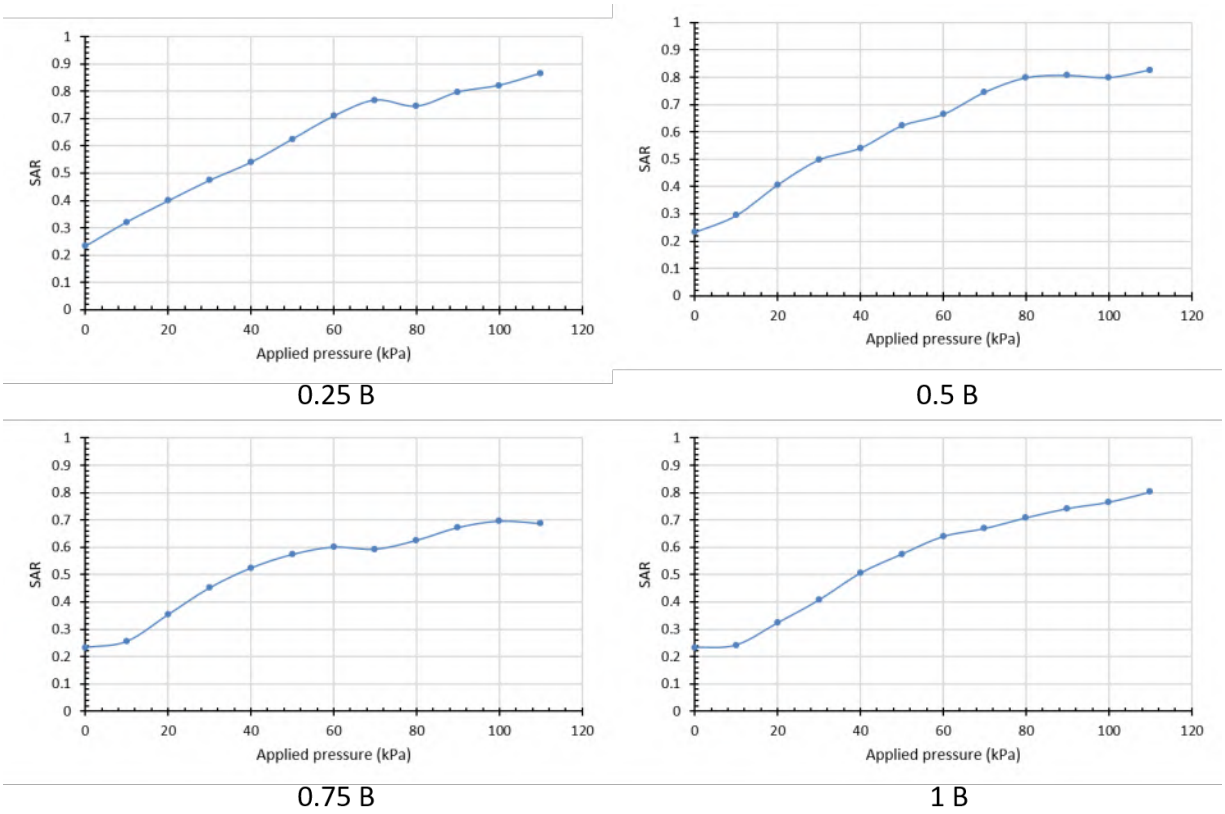

Figure 4.8: Comparison of SAR in relation to applied pressure for: Test 8 (0.25B); Test 9 (0.5B); Test 10 (0.75B); and Test 11 (1B)

The vertical stress distribution illustrated in the contour plots shown in Figures (4.9,4.10,4.11, and 4.12) provides a clear depiction of how stress fields evolve within the soil mass under varying applied pressures and different footing locations relative to the trapdoor. At an applied pressure of 20 kPa, all cases exhibit localized stress concentrations directly beneath the footing. In the first case, these stresses form distinct arch-like pathways curving outward toward the adjacent support zones, indicative of early-stage soil arching. In contrast, this pronounced arching pattern is not clearly observed in the other offset cases. For the 0.75B and 1.0B offsets, where the footing is positioned farther from the trapdoor center, the region above the trapdoor remains largely unstressed, maintaining a well-defined low-stress

zone. As the applied pressure increases to 60 kPa, the stress bulbs beneath the footing expand noticeably, and in the 0.25B and 0.5B cases, the stress contours begin to extend toward the trapdoor, indicating the onset of arch degradation and progressive stress transmission to the yielding area. Conversely, in the 0.75B and 1.0B configurations, the stress pathways maintain their arching form, effectively diverting stresses laterally toward the stable support regions while continuing to protect the trapdoor zone. This behavioral divergence becomes increasingly evident at an applied pressure of 80 kPa. The 0.25B and 0.5B cases exhibit substantial stress intensification over the trapdoor, with stress contours merging between the loaded area and the yielding region, signifying a considerable weakening of the arching mechanism. In contrast, the 0.75B and 1.0B offset cases sustain their arch-shaped stress trajectories, with peak stress concentrations remaining well-distributed at the side supports, minimizing stress transmission to the trapdoor. Under the highest applied pressure of 110 kPa, the stress contours in the 0.25B and 0.5B cases display a near-complete merging of stress fields over the trapdoor, indicating substantial arch collapse and direct load transfer to the yielding zone. Meanwhile, in the 0.75B and especially the 1.0B cases, the stress distribution remains structurally efficient, with elevated stresses confined to the side supports and the area directly beneath the footing, and minimal encroachment over the trapdoor. These findings clearly emphasize the critical influence of footing position on the spatial stress distribution within trapdoor systems and its consequent effect on the formation, stability, and degradation of soil arching under increasing surface loads.

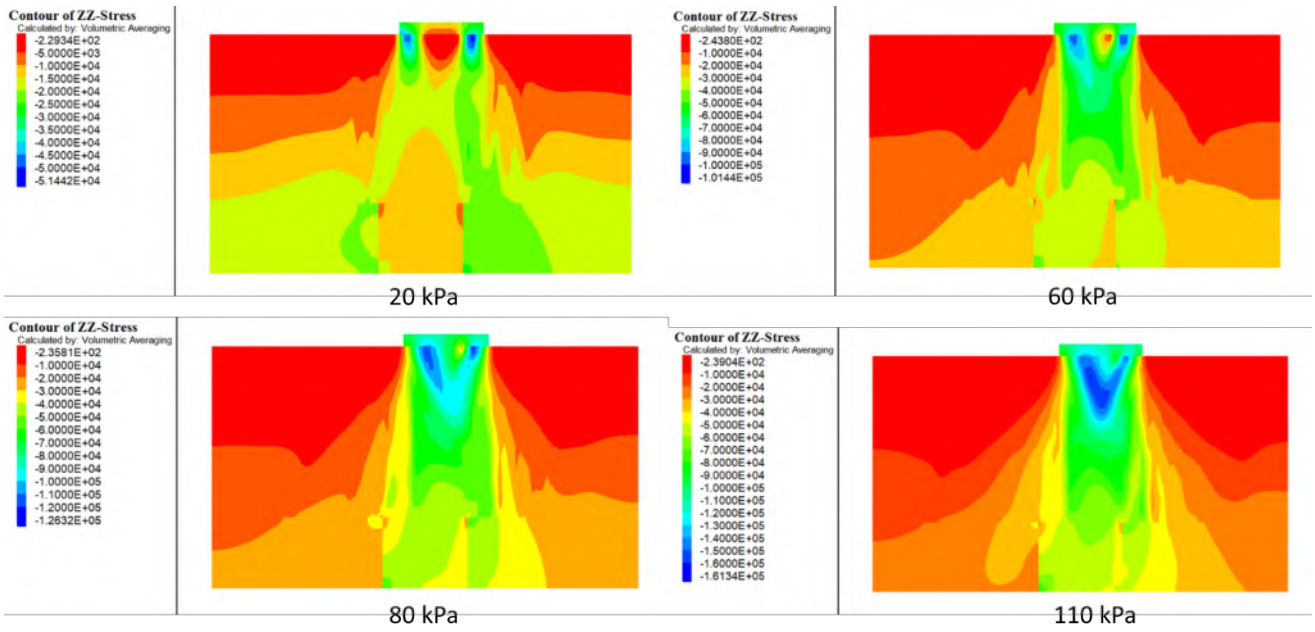

Figure 4.9: Pressure distribution of numerical model under applied loads for Test 8 (0.25B)

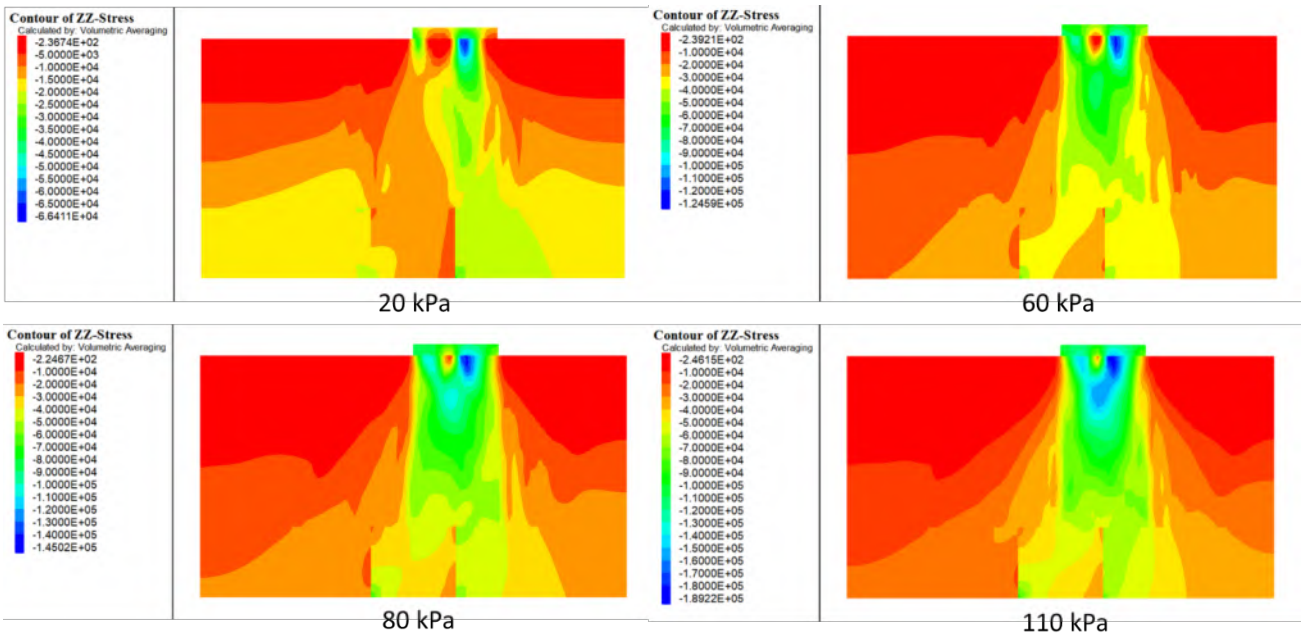

Figure 4.10: Pressure distribution of numerical model under applied loads for Test 9 (0.5B)

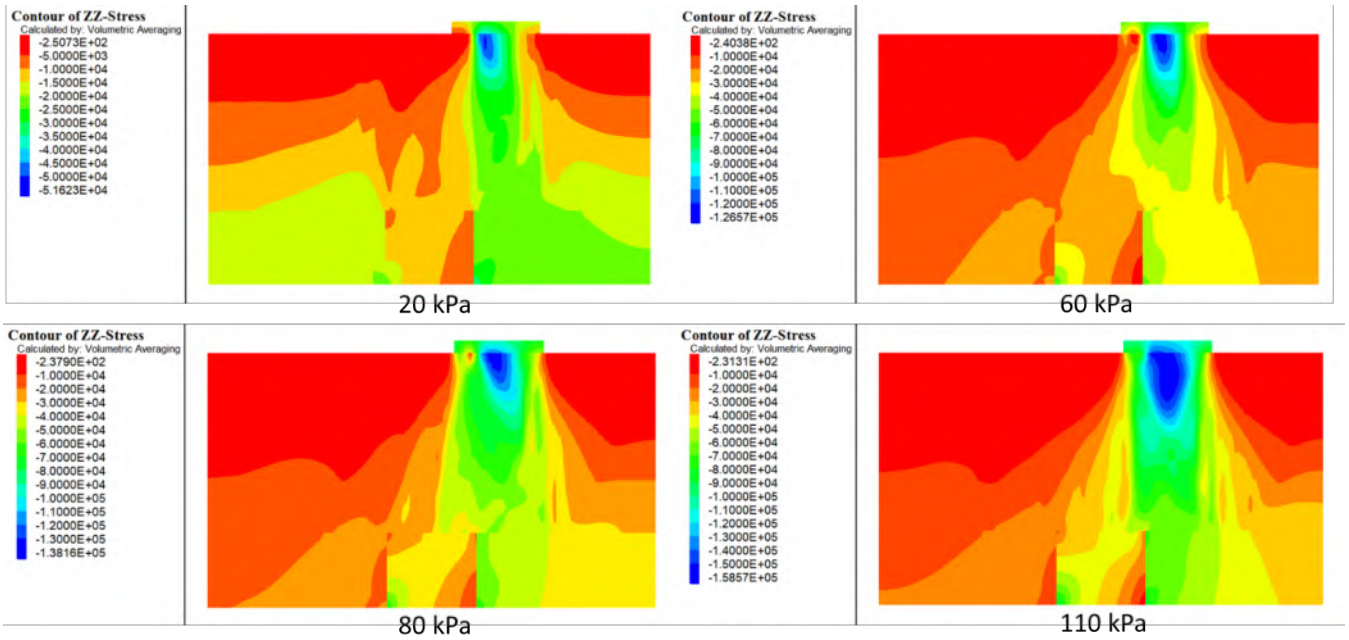

Figure 4.11: Pressure distribution of numerical model under applied loads for Test 10 (0.75B)

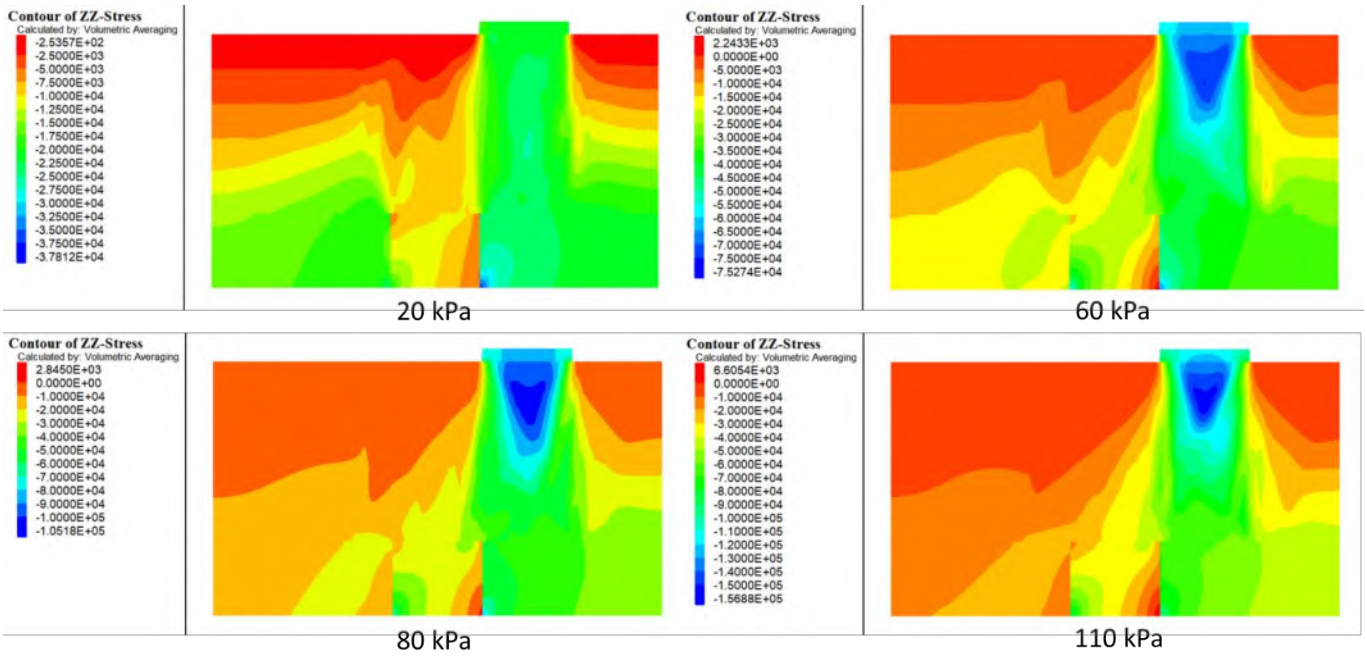

Figure 4.12: Pressure distribution of numerical model under applied loads for Test 11 (1.0B)

4.4 Effect of Footing Size

4.4.1 During Footing Loading

The comprehensive numerical analysis, supported by SAR charts shown in Figures (4.13 and 4.14) , clearly demonstrates that increasing the footing width relative to the trapdoor span markedly enhances the development and resilience of the soil arching mechanism under progressive surface loading. At lower applied pressures of 20–40 kPa, the narrower footing configuration (2B) shows localized stress concentrations directly above the trapdoor, with the trapdoor center (TC) carrying approximately 16–29 kPa while the stationary support (SE) bears 28–42 kPa, indicating that although arching is initiated, its effectiveness remains limited. In contrast, the wider footing cases (3B to 5B) already exhibit broader and shallower stress bulbs at these stages, accompanied by slightly reduced TC stresses and increased SE stresses, reflecting more robust early-stage lateral load transfer to the stable supports. As the surface pressure rises to 60 kPa, this difference becomes more evident: for 2B, TC reaches about 45 kPa and SE about 57 kPa, whereas for the 5B footing, TC increases more moderately to 61 kPa while SE rises to 77 kPa, illustrating that the wider footing engages a larger volume of stable soil, distributing the load more efficiently. This trend persists and intensifies at higher load levels; at 80 kPa, the 2B model shows TC and SE stresses of around 62 kPa and 73 kPa, respectively, while the 5B configuration maintains a shallower, wider stress arch with TC at 79 kPa and SE at 96 kPa. At the maximum applied pressure of 110 kPa, the 2B footing records a TC stress of approximately 89.5 kPa and SE stress of 99.4 kPa, with a corresponding soil arching ratio (SAR) of about 0.82, signifying that a

substantial fraction of the load is still transmitted directly through the trapdoor region. By contrast, the 5B footing achieves the most extensive lateral load redistribution and the lowest SAR, stabilizing near 0.77, with TC and SE stresses of approximately 105.1 kPa and 124.5 kPa, respectively, demonstrating a more effective and sustained soil arching action even under high loading.

The accompanying stress contours shown in Figures (4.15, 4.16, 4.17, and 4.18) corroborate this behavior, clearly illustrating that increasing the footing width transforms the stress field from a deep, vertically concentrated zone into a broader, more horizontally dispersed arch that efficiently redirects applied loads toward the stable supports. These validated results confirm that designing a footing with sufficient width relative to the underlying weak zone significantly improves the load transfer mechanism, mitigates excessive vertical stress concentrations on the yielding trapdoor, and enhances overall stability and serviceability of embankment and load transfer systems subjected to heavy surface loading.

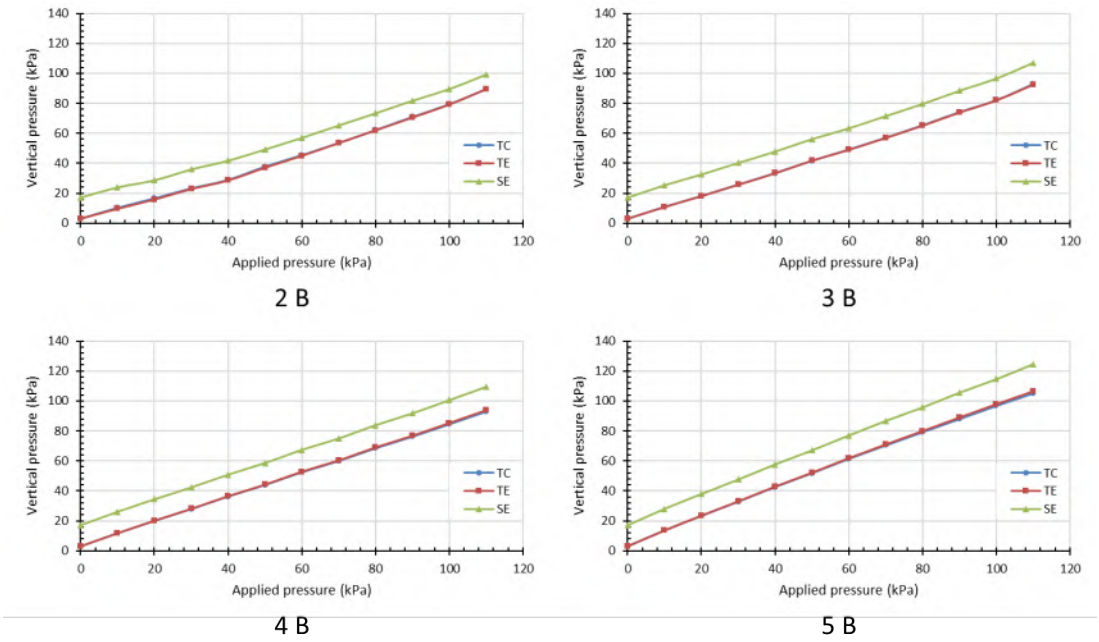

Figure 4.13: Comparison of vertical stress in relation to monotonic static footing pressure in the loading test at three monitoring points, for: Test 12 (2B) ; Test 13 (3B); Test 14 (4B); and Test 15 (5B)

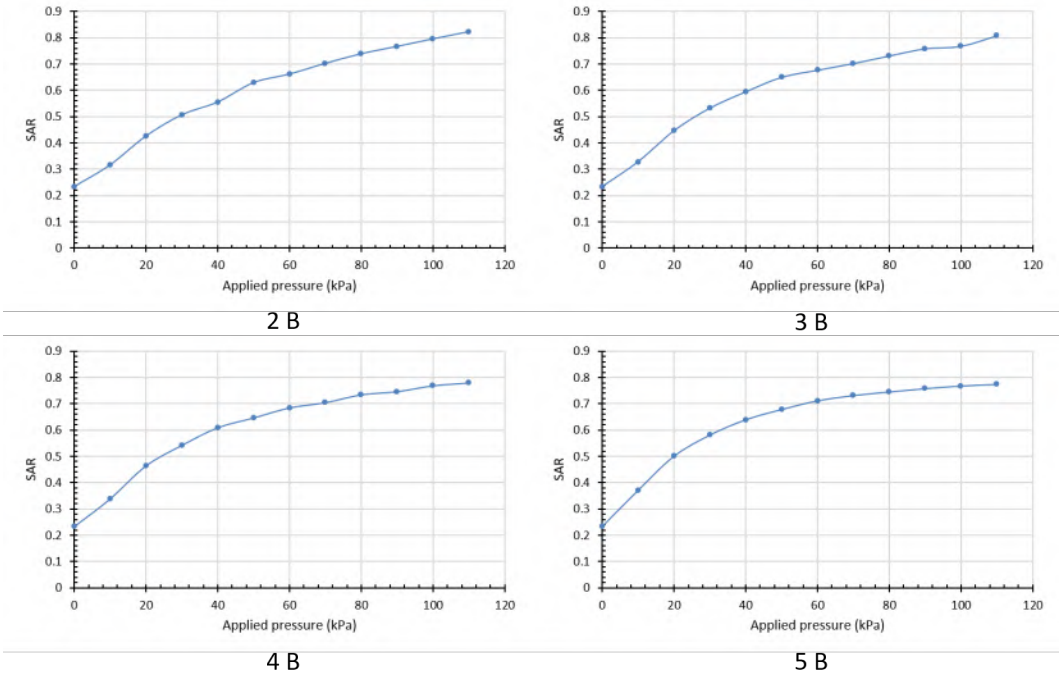

Figure 4.14: Comparison of SAR in relation to applied pressure for: Test 12 (2B) ; Test 13 (3B); Test 14 (4B); and Test 15 (5B)

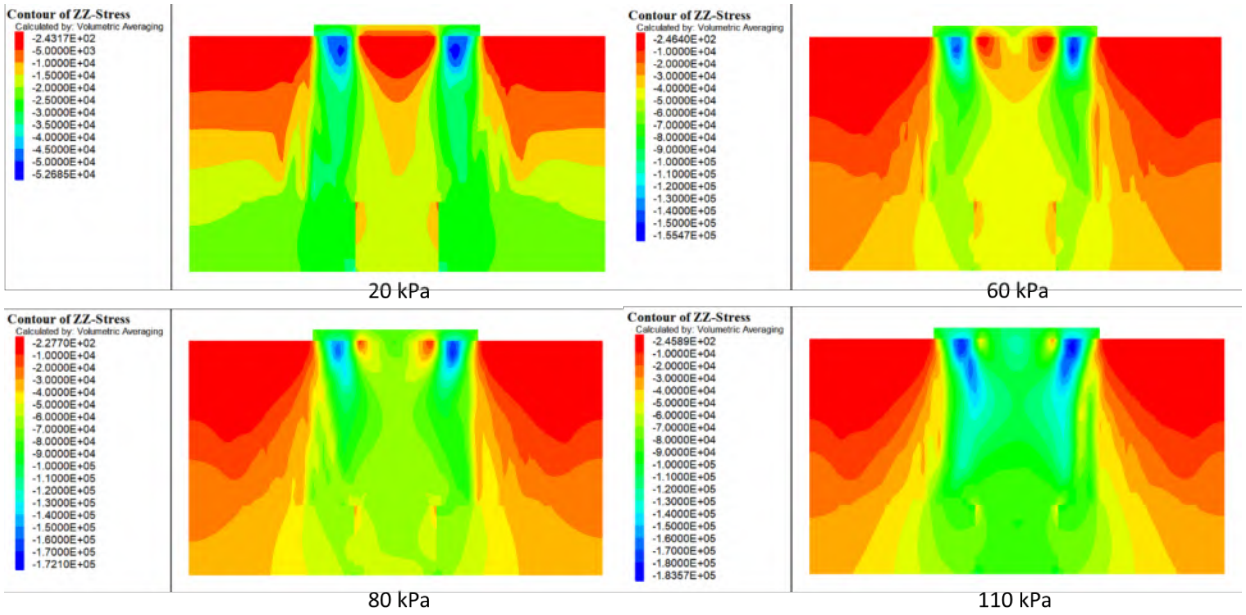

Figure 4.15: Pressure distribution of numerical model under applied loads for Test 12 (2B)

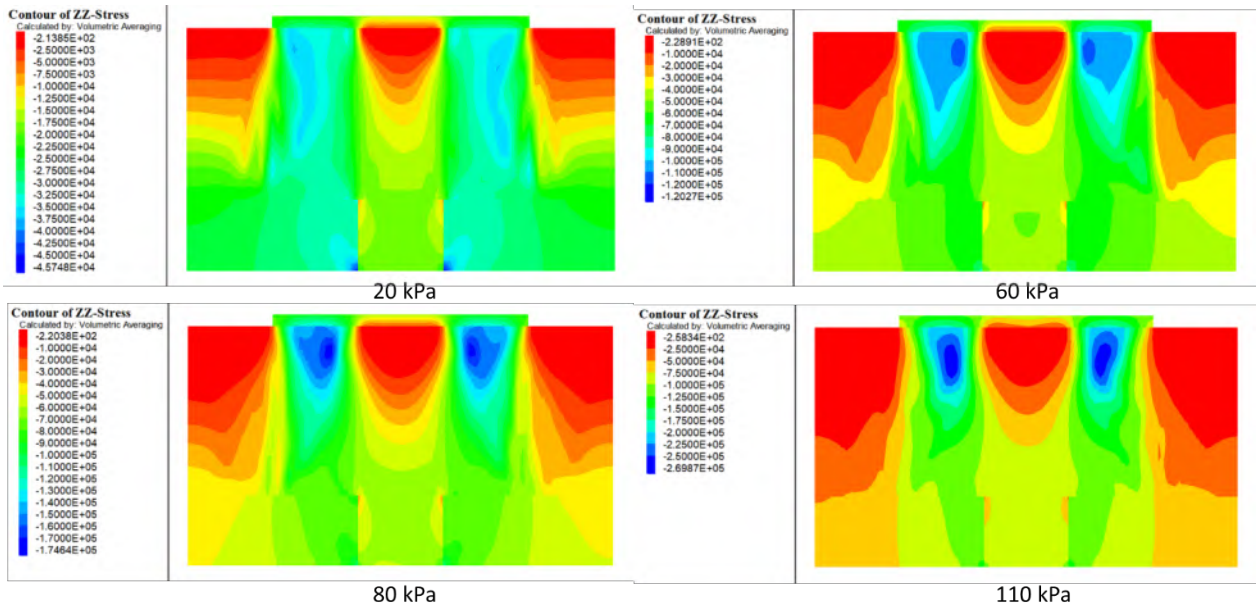

Figure 4.16: Pressure distribution of numerical model under applied loads for Test 13 (3B)

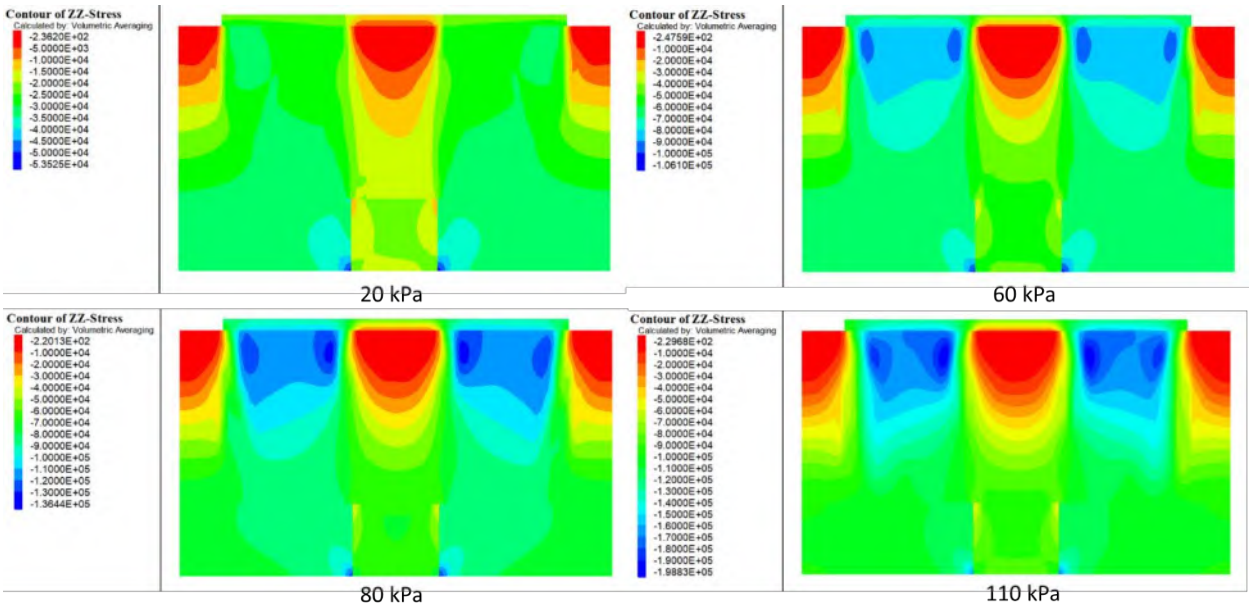

Figure 4.17: Pressure distribution of numerical model under applied loads for Test 14 (4B)

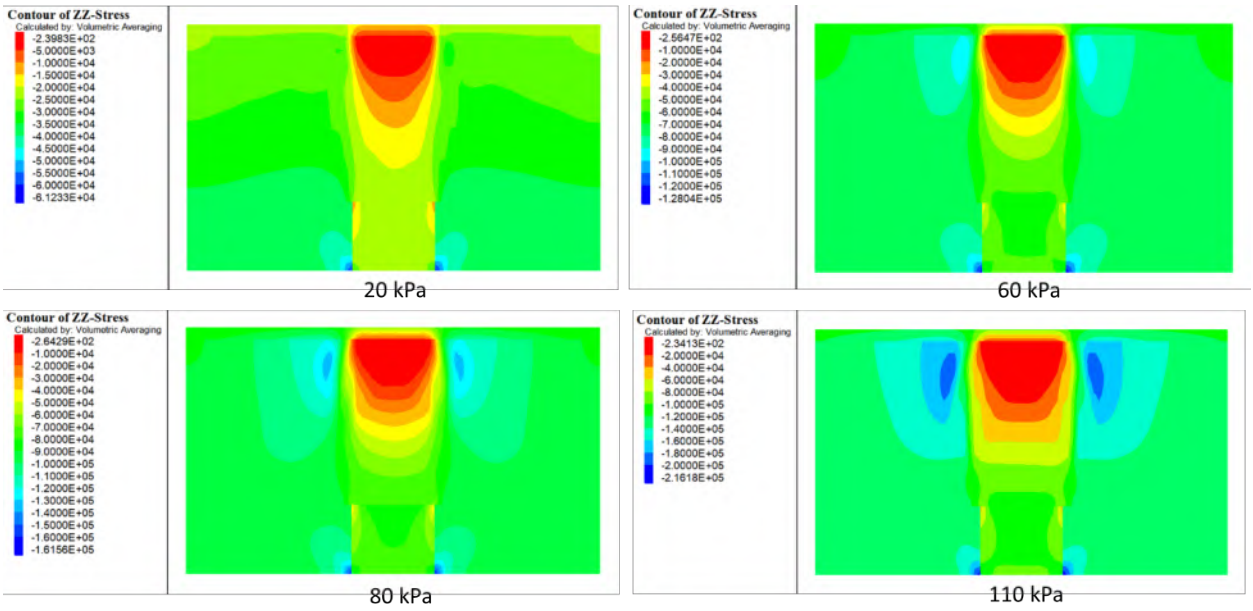

Figure 4.18: Pressure distribution of numerical model under applied loads for Test 15 (5B)

4.5 Effect of Trapdoor Size

4.5.1 During Trapdoor Displacement

A comprehensive comparison between the base model (trapdoor width equal to B) and the parametric cases with varied trapdoor widths (0.5 B, 1.5 B, 2 B, and 2.5 B) offers clear evidence of the critical influence of trapdoor width on the mobilization and effectiveness of the soil arching mechanism during the displacement stage prior to the application of external surface loading. In the base model (Test 4), the stress-displacement response reveals that as the trapdoor begins to settle, the vertical stress at the trapdoor center (TC) and trapdoor edge (TE) rapidly decreases, stabilizing at a low residual value of approximately 3kPa, while the stationary support (SE) efficiently absorbs the redistributed load, reaching a steady-state stress near 17 kPa. This behavior exemplifies the classical development of a well-formed soil arch, wherein the mobilized passive resistance in the surrounding soil transfers the overburden weight away from the yielding region toward the stable supports. The corresponding soil arching ratio (SAR) drops sharply within the first few millimeters of displacement and remains constant around 0.23, indicating that only a minor fraction of the overburden stress is transmitted through the trapdoor once full arching is established.

Figures (4.19 and 4.20) show, when the trapdoor width is reduced to 0.5 B, this favorable behavior is further accentuated. The TC and TE stresses decline even more abruptly and stabilize at lower residual values about 1.4 and 1.8 kPa, while the SE stress reaches a peak of about 15 kPa. The SAR curve for the 0.5 B case confirms this trend, stabilizing at the lowest observed value of approximately 0.13, highlighting the enhanced efficiency of the arching mechanism when the unsupported span is minimized relative to the footing width. This demonstrates that narrower trapdoors enable rapid and

complete mobilization of arching, resulting in more effective stress bypass and improved load transfer to the stable boundaries.

In contrast, increasing the trapdoor width to 1.5 B leads to a slight reduction in arching efficiency relative to the base case. The TC and TE stresses do not decrease as sharply and remain marginally higher during displacement, its value about 5.9 and 5.4 kPa, while the SE stress reaches a comparable value but exhibits a slightly delayed stabilization. Consequently, the SAR for the 1.5 B configuration levels off at a modestly higher value of approximately 0.44, indicating that the wider opening inhibits the full development of the arch and allows a greater portion of the stress to be carried directly by the yielding zone.

This diminishing trend in arching effectiveness becomes more pronounced when the trapdoor width is increased to 2 B and 2.5 B. In these wider cases, the vertical stresses at the trapdoor center (TC) and trapdoor edges (TE) decrease at a slower rate during trapdoor displacement and stabilize at relatively high stresses values. This behavior indicates that, even after arching develops, a considerable portion of the load continues to be carried directly above the trapdoor, resulting in incomplete stress transfer to the supports. Although the SE stress still increases, it achieves a slightly lower peak compared to narrower trapdoor scenarios, reflecting a reduced capacity of the stable supports to absorb the redistributed load when the trapdoor span is larger. Accordingly, the SAR for the 2 B configuration stabilizes around 0.6, while for 2.5 B it approaches 0.69 (more than double the residual SAR of the base model) thus confirming a notable degradation in the arching mechanism with increasing trapdoor width.

Overall, this parametric analysis unequivocally demonstrates that reducing the trapdoor width relative to the footing span promotes the rapid

formation of a stable soil arch, optimizes lateral stress transfer to the stable supports, and minimizes vertical stress concentration within the yielding zone. Conversely, enlarging the trapdoor span under a constant wide footing footprint impedes the complete development of the arching mechanism, prolongs the direct load path through the trapdoor, and results in higher sustained stress within the weak region during displacement. These findings underscore the critical role of trapdoor geometry in controlling soil arching behavior and provide essential guidance for the design and optimization of embankments and load transfer platforms constructed over voided or weak subsurface zones.

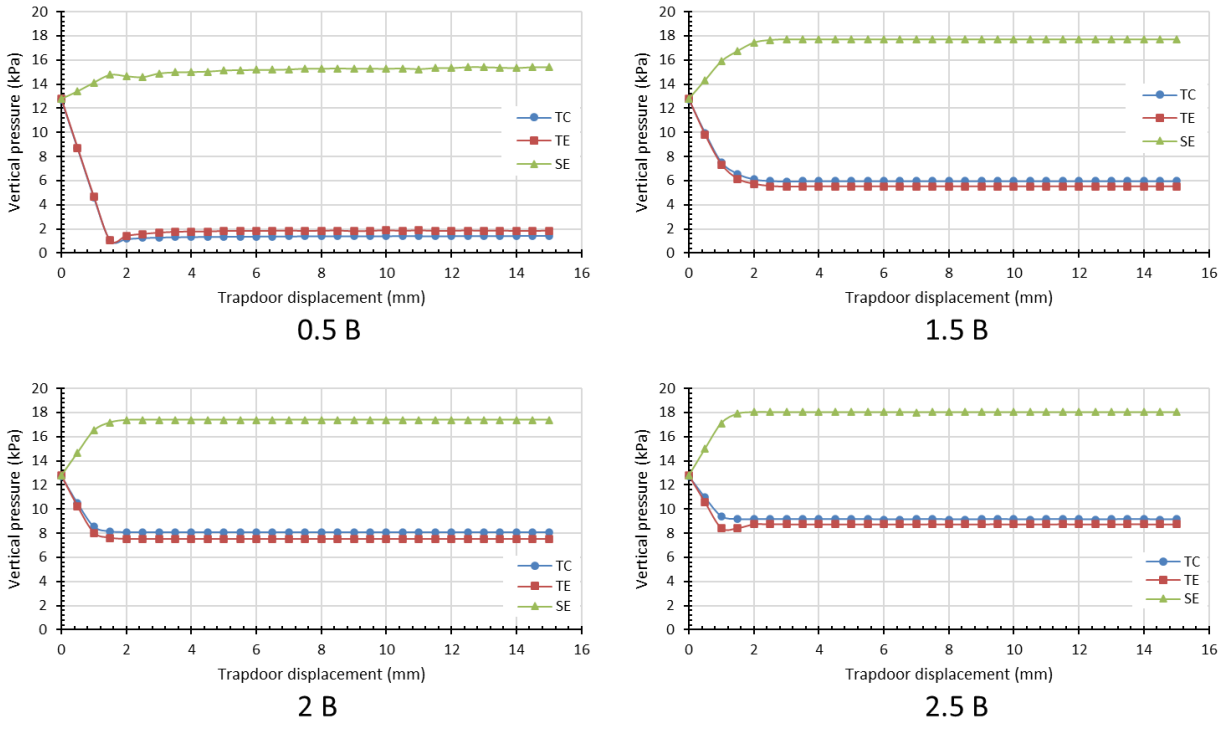

Figure 4.19: Comparison of vertical stress in relation to trapdoor displacement at three monitoring points, for: Test 16 (0.5B); Test 17 (1.5B); Test 18 (2B); and Test 19 (2.5B)

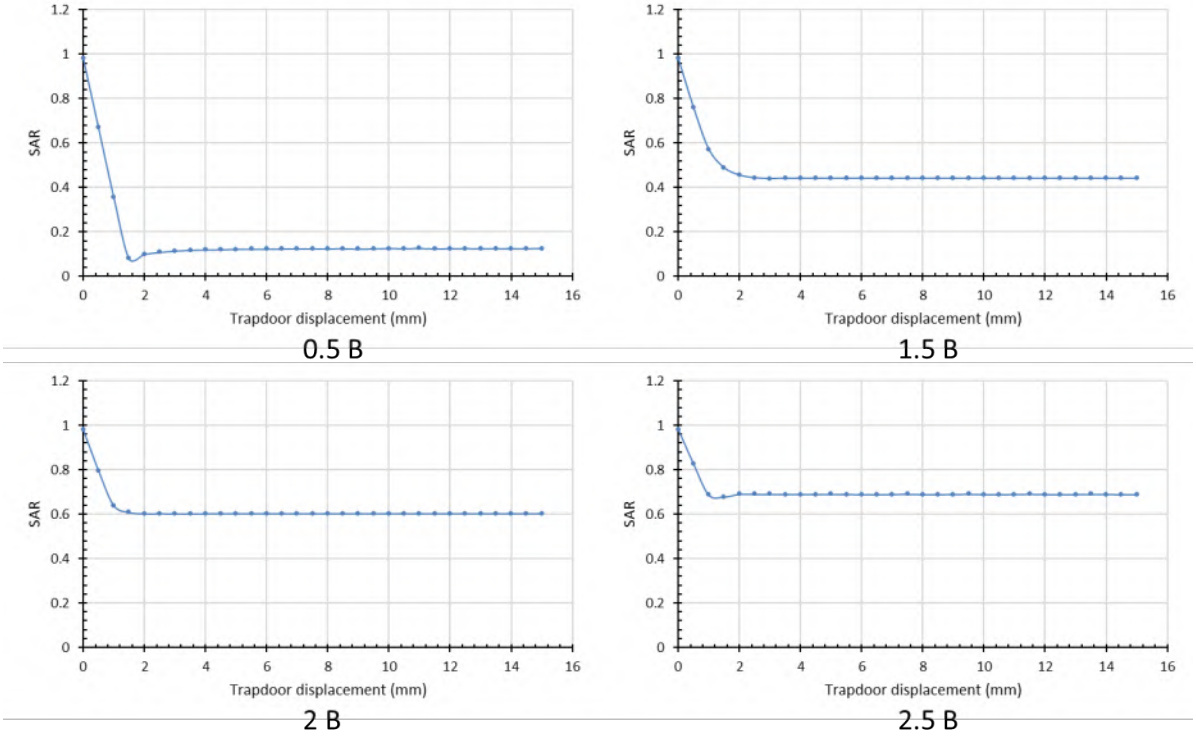

Figure 4.20: Comparison of SAR in relation to trapdoor displacement, for:Test 16 (0.5B); Test 17 (1.5B); Test 18 (2B); and Test 19 (2.5B)

The stress contour plots shown in Figure (4.21) corresponding to a displacement of 15 mm further substantiate the observed trends in the numerical stress–displacement curves and SAR values. For the narrowest trapdoor width (0.5 B), the contours clearly depict a well-developed, narrow arching zone with a pronounced stress transfer pathway redirecting the overburden load laterally toward the stable supports. The stress bands above the trapdoor are steeply inclined and compact, signifying effective confinement and minimal vertical stress concentration within the yielding zone. In contrast, for the 1.5 B configuration, the arching zone appears wider and slightly more diffused, with stress contours spreading further horizontally, indicating that a larger portion of the soil mass is engaged but with slightly

less confinement efficiency compared to the narrower case. This pattern continues for the wider trapdoors (2 B and 2.5 B), where the contours reveal a more dispersed and flatter arching structure. The stress distribution becomes shallower and the high-stress bands extend deeper into the yielding zone, suggesting incomplete stress redirection and increased reliance on the trapdoor itself to carry the overburden load. Notably, for the 2.5 B scenario, the arching effect is visibly weakened, as evidenced by the broader stress bulbs directly above the trapdoor and the less distinct curvature of the stress pathways, which indicates that the passive resistance offered by the adjacent soil is insufficient to fully mobilize a stable arch across the wider opening. These contour observations at the final displacement stage thus visually corroborate the quantitative findings, affirming that narrower trapdoors facilitate a more efficient and stable soil arch, whereas increasing the trapdoor width progressively undermines the arching mechanism and allows greater stress penetration into the weak zone above the trapdoor.

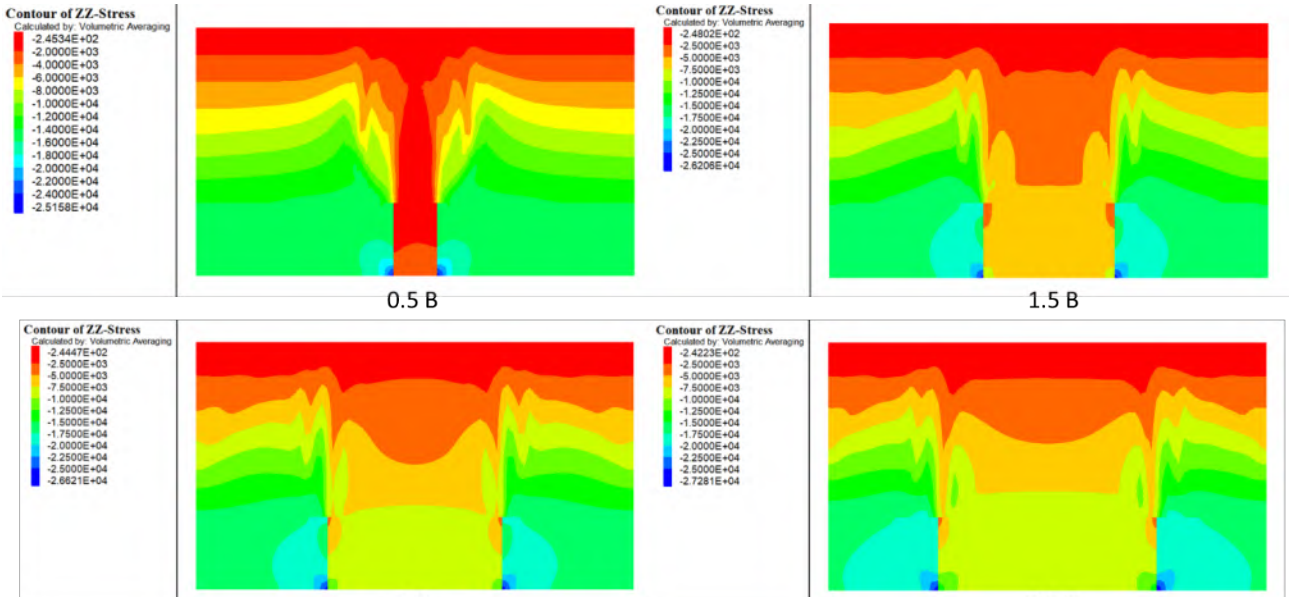

Figure 4.21: Pressure distribution of numerical model at 15mm trapdoor displacement for: Test 16 (0.5B); Test 17 (1.5B); Test 18 (2B); and Test 19 (2.5B)

4.5.2 During Footing Loading

A comprehensive evaluation of the vertical stress measurements (Figure 4.22), Soil Arching Ratio (SAR) trends (Figure 4.23), and corresponding stress contour plots (Figures 4.24, 2.25, 2.26, and 4.27) provides clear evidence of the critical role of trapdoor width in governing the mobilization and stability of the soil arching mechanism beneath the footing.

For the reference model (Test 15) and the narrower trapdoor condition (0.5 B), the results consistently demonstrate the successful formation of a robust soil arch. This is evident from the pronounced vertical stress differential observed between the stationary support (SE) and the trapdoor center (TC) and edge (TE) across the full range of applied surface loads. For instance, in the 0.5 B model, at an applied load of 20 kPa, the SE stress reaches approximately 35.7 kPa, whereas the TC and TE register notably lower values of 21.6 kPa and 21.9 kPa, respectively. Even at the maximum surface load of 110 kPa, the SE continues to sustain a higher stress of about 118.9 kPa, while the TC and TE remain lower at about 104 kPa. Correspondingly, the SAR for this narrow trapdoor configuration rises from approximately 0.13 at low loads to 0.76 at peak load, indicating that a significant proportion of the applied load is effectively transferred laterally to the stable supports rather than being carried directly through the yielding trapdoor zone. This efficient stress redirection is clearly reflected in the stress contour plots, which show compact, well-defined arch-shaped isobars spanning the trapdoor area and connecting seamlessly to the adjacent stable soil, confirming the full mobilization of the arching mechanism.

In contrast, as the trapdoor width is increased to 1.5 B, 2 B, and 2.5 B, the results reveal a distinct change in arching behavior. Although the SAR values for these wider trapdoor cases are lower-decreasing to approximately

0.65–0.67 at high loads-this does not indicate enhanced arching performance. Rather, it signifies that the soil arching mechanism does not fully develop in these configurations due to insufficient lateral confinement. For instance, in the 2.5 B model at an applied load of 20 kPa, the stress at the stationary support (SE) is about 42.8 kPa, which remains noticeably higher than the stresses recorded at the trapdoor center (TC) and edge (TE), measured at 24.4 kPa and 29.3 kPa, respectively. This difference indicates that a portion of the vertical stress is already being transferred outward toward the stable supports, signifying the initial stages of soil arch formation. As the surface load increases to 110 kPa, the SE stress rises substantially to approximately 139.0 kPa, while the TC and TE also increase to 77.7 kPa and 106.2 kPa. Despite this increase, the fact that the SE consistently carries the highest stress confirms that the arching mechanism is partially active, enabling the redistribution of some load away from the center of the trapdoor toward the more stable surrounding soil.

This incomplete arch formation is further substantiated by the stress contour plots for the wider trapdoor cases. Unlike the clear, curved isobars observed for the base and narrow trapdoor models, the contours for 1.5 B, 2 B, and 2.5 B become increasingly diffuse and vertically elongated, with less pronounced arch shoulders. This indicates that the passive resistance provided by the soil adjacent to the trapdoor is insufficient to confine the deforming zone, preventing the development of a well-defined arch and allowing a greater proportion of the applied stress to penetrate directly downward.

The noticeable difference between TC and TE stresses in these wider trapdoor cases indicates that the vertical stress is not uniformly distributed across the trapdoor span. Instead, the stress tends to concentrate more near the edges (TE) where the local confinement provided by the adjacent stable soil

remains relatively stronger, while the central portion (TC) experiences comparatively lower stress due to the lack of sufficient confinement. This non-uniform pattern reflects that, in wide trapdoor configurations, the arching effect is incomplete, and the load transfer mechanism relies more heavily on the trapdoor edges rather than maintaining a balanced distribution across the entire width.

Overall, the integrated evidence from the stress trends, SAR data, and stress contour plots clearly demonstrates that excessive trapdoor widening does not lead to stronger or more effective soil arching. Instead, it inhibits the complete formation of the arch from the outset, resulting in lower SAR values that reflect a predominantly direct load path through the trapdoor region rather than lateral stress transfer. This behavior increases the risk of local settlement and reduces the load transfer efficiency that the arching mechanism is intended to provide.

In conclusion, these findings underscore the importance of optimizing the trapdoor width relative to the footing width. To ensure robust soil arch formation and stable load redistribution, the trapdoor must be sufficiently narrow to allow the surrounding soil to mobilize adequate passive resistance and develop a fully formed arch that can sustain increasing surface loads effectively.

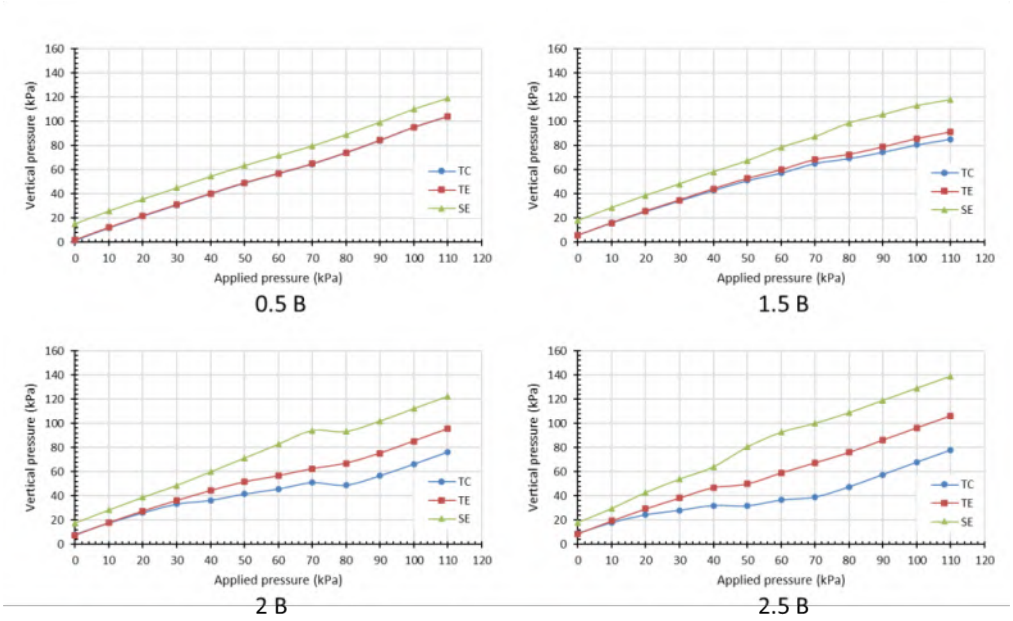

Figure 4.22: Comparison of vertical stress in relation to monotonic static footing pressure in the loading test at three monitoring points, for: Test 16 (0.5B), Test 17 (1.5B), Test 18 (2B), and Test 19 (2.5B)

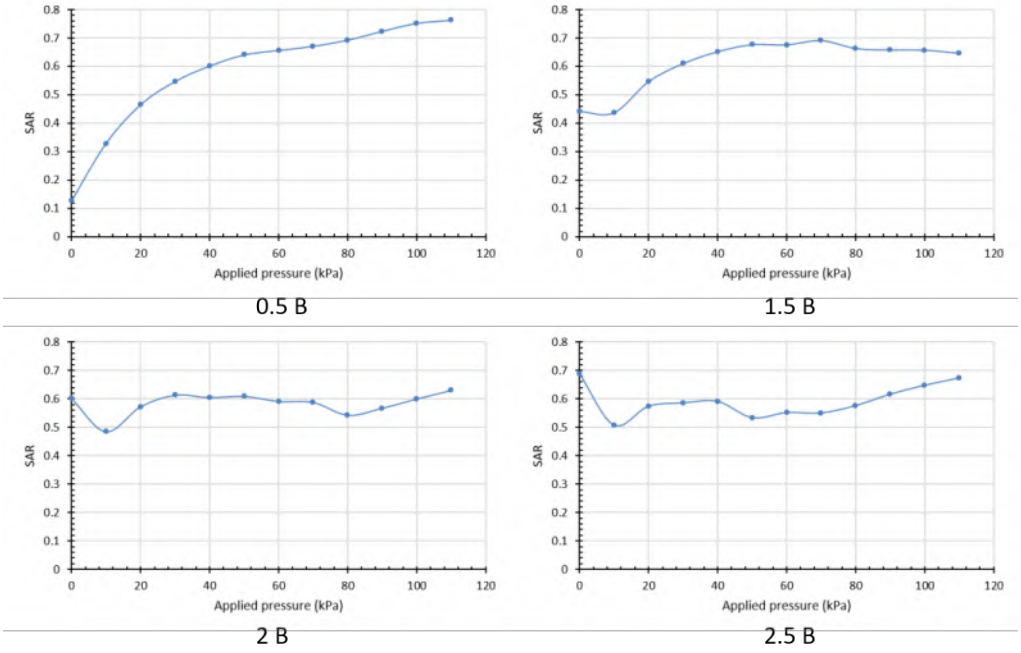

Figure 4.23: Comparison of SAR in relation to applied pressure for: Test 16 (0.5B), Test 17 (1.5B), Test 18 (2B), and Test 19 (2.5B)

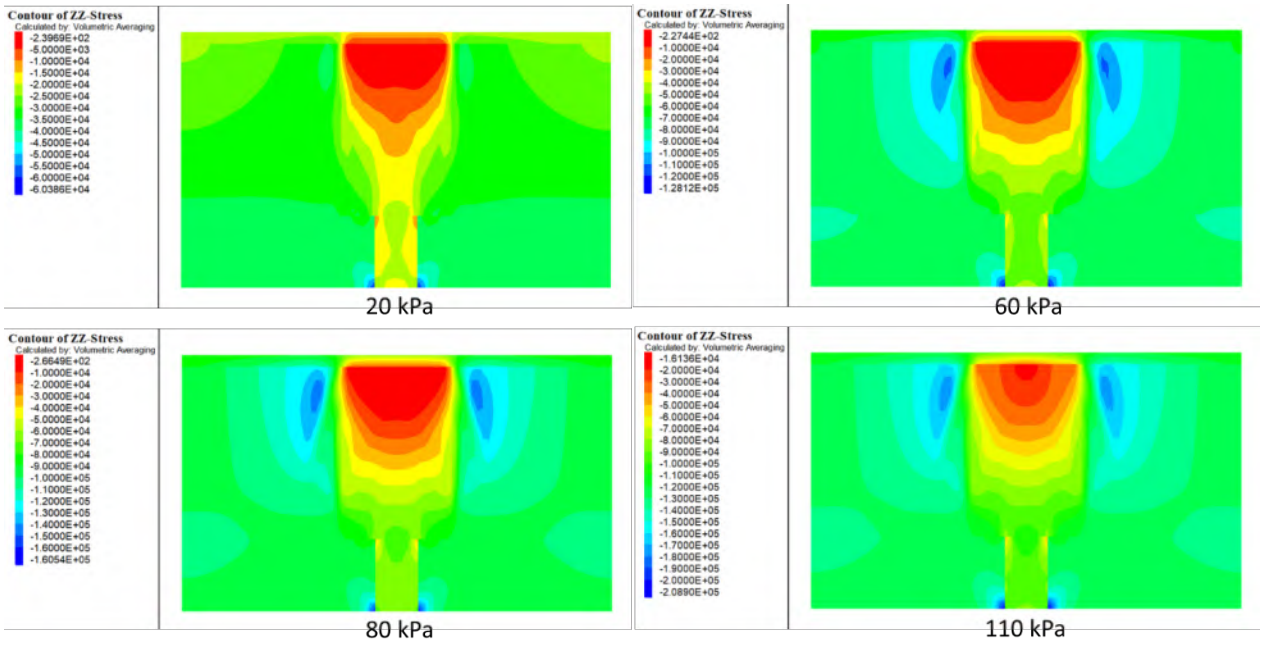

Figure 4.24: Pressure distribution of numerical model under applied loads for Test 16 (0.5B)

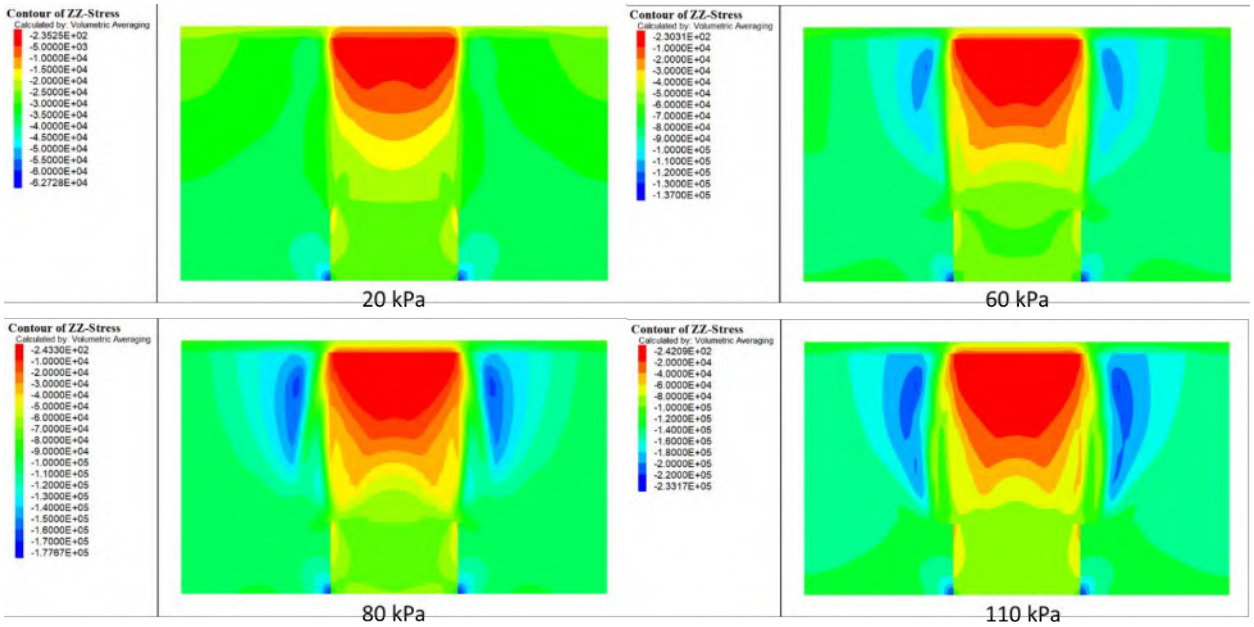

Figure 4.25: Pressure distribution of numerical model under applied loads for Test 17 (1.5B)

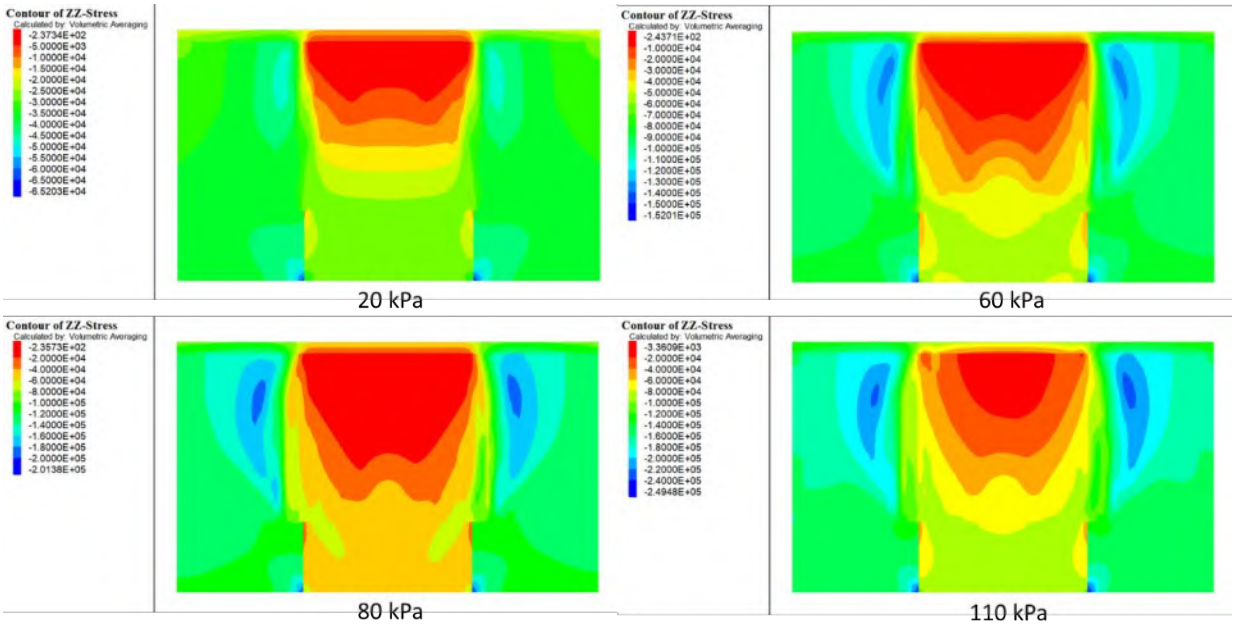

Figure 4.26: Pressure distribution of numerical model under applied loads for Test 18 (2B)

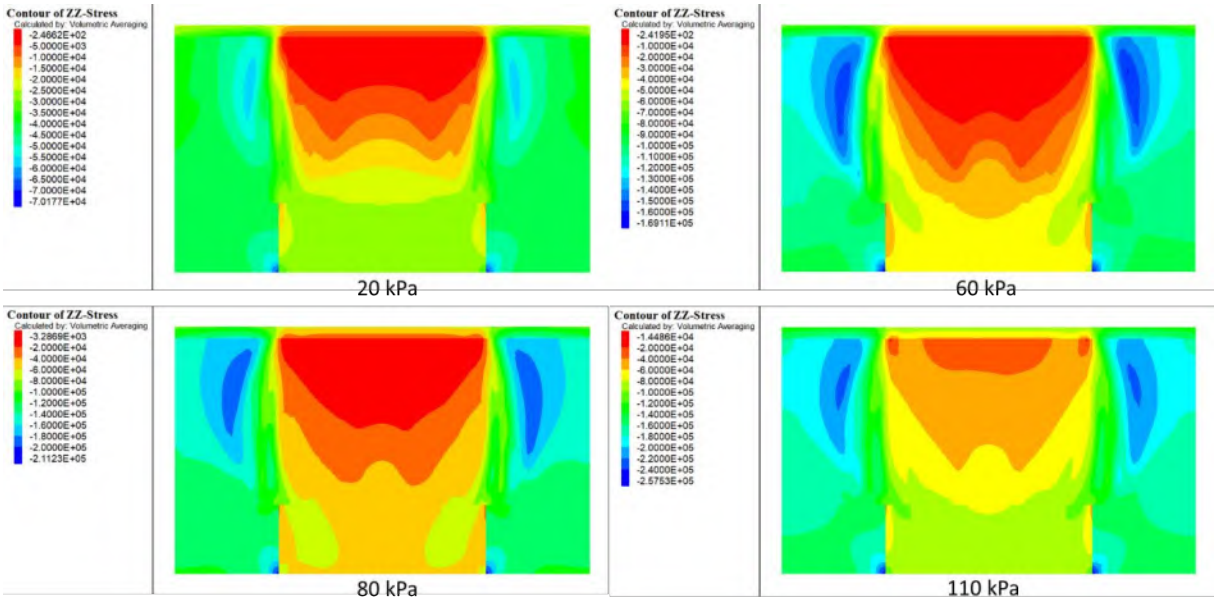

Figure 4.27: Pressure distribution of numerical model under applied loads for Test 19 (2.5B)

4.6 Effect of Multiple Trapdoors

4.6.1 Two Trapdoors

4.6.1.1 During Trapdoors Displacement

The numerical results for the case with two trapdoors and a middle support of equal width to the edge supports (0.72 m) show a strong soil arching response under trapdoor displacement.

Vertical stress evolution shown in Figure (4.28) presents that as the trapdoors begin to displace, the vertical stress directly above them (TC and TE) declines sharply from an initial ~12.7 kPa to about 2.96 kPa and 2.77 kPa at a displacement of 4 mm. Meanwhile, the surrounding stable regions (namely the edge supports (SE) and the wide middle support (MSC and MSE)) experience a clear stress increase, stabilizing around 17.9 kPa, 17.5 kPa, and 18 kPa. This immediate stress redistribution indicates that a substantial portion of the overburden load is effectively transferred to the stable supports very early in the displacement process.

The Soil Arching Ratio (SAR) shown in Figure (4.29), which drops rapidly from ~0.98 to a plateau near 0.22, further confirms the prompt formation of an efficient arch. The stable SAR beyond 3 mm displacement suggests that the load transfer mechanism remains consistent throughout the entire settlement stage, minimizing further stress variation on the trapdoor itself.

The contour plots shown in Figure (4.30) clearly illustrate this arch development process. At an early displacement of 0.5 mm, the stress distribution remains relatively uniform vertically; however, by 1 mm and 1.5 mm, arch-like stress trajectories begin to emerge above each trapdoor, curving towards both the edge and the middle support. With further displacement (2 mm, 4 mm, and up to 15 mm), the stress contours become

increasingly curved and the high-stress zones concentrate along the supports while stress above the trapdoors remains significantly relieved. The wide middle support effectively acts as a strong intermediate pier, allowing the arches to span over each trapdoor without merging prematurely, and preventing excessive stress accumulation directly above the voids.

This behavior confirms that using multiple trapdoors with an adequately wide intermediate support not only sustains the integrity of the soil arching system but also prevents localized failure above the voids. The similarity in stress magnitude between the middle and edge supports (with MSC and MSE stabilizing near 17.5 kPa and 18.05 kPa) demonstrates that the middle support is fully engaged in load bearing, minimizing differential stress across the span.

Overall, the combined evidence from the stress charts, SAR curve, and stress contours confirms that multiple trapdoors combined with a wide middle support significantly enhance the development and stability of the soil arching mechanism. This configuration distributes loads more uniformly, reduces the risk of excessive settlement, and ensures effective stress transfer to stable zones-crucial design insights for foundations, embankments, and void bridging in geotechnical practice.

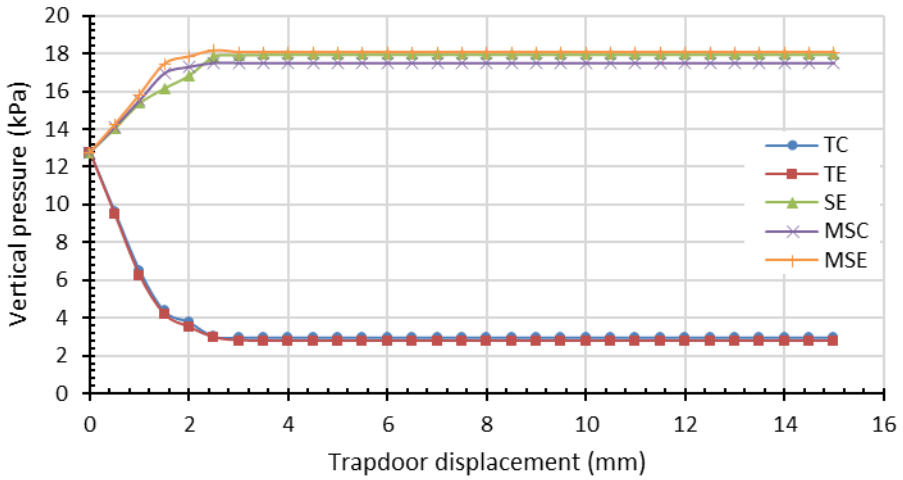

Figure 4.28: Comparison of vertical stress in relation to trapdoor displacement at five monitoring points, for Test 20 (Two Trapdoors with 0.72m Intermediate Support-1B)

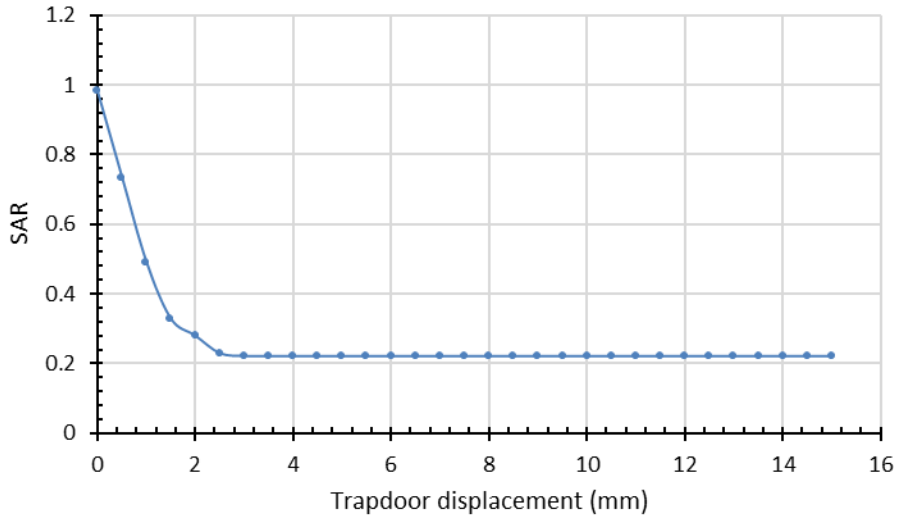

Figure 4.29: Comparison of SAR in relation to trapdoor displacement for Test 20 (Two Trapdoors with 0.72m Intermediate Support-1B)

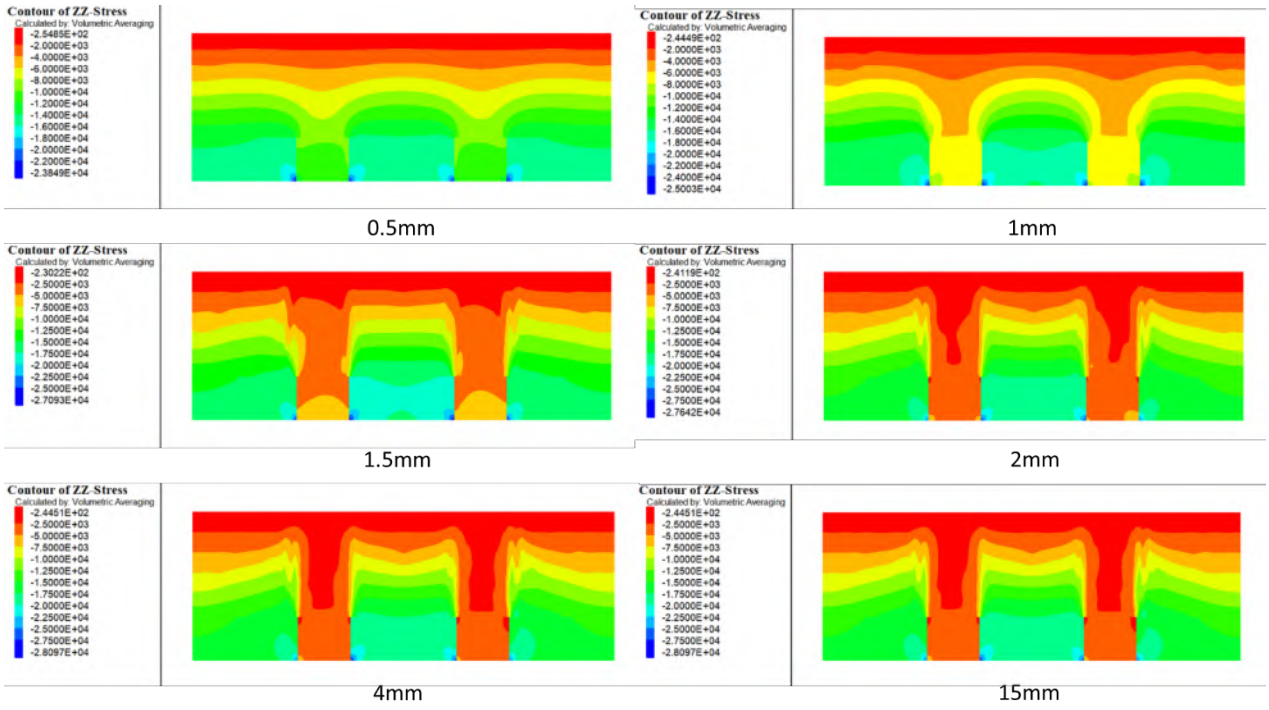

Figure 4.30: Pressure distribution of numerical model during 15mm trapdoor displacements for Test 20 (Two Trapdoors with 0.72m Intermediate Support-1B)

The numerical investigation of the dual trapdoor configuration with a narrow intermediate support (equal to the trapdoor width, 0.36 B) provides deeper insight into how the middle support's geometry influences the development and stability of the soil arching mechanism during trapdoor displacement.

The vertical stress chart shown in Figure(4.31) reveals a clear trend: as the trapdoor displacement progresses, the edge supports (SE) consistently attract a high stress, stabilizing around 18.0 kPa, while the stresses measured at the middle support center (MSC) and middle support edge (MSE) gradually reach approximately 23.3 kPa and 23.4 kPa, respectively. Simultaneously, the trapdoor center (TC) and trapdoor edge (TE) drop sharply and remain near

2.5 kPa and 2.2kPa, indicating significant stress relief within the moving trapdoor zones.

The corresponding Soil Arching Ratio (SAR) trend supports this observation (Figure 4.32): the SAR decreases rapidly from an initial value near 0.98 to about 0.18, remaining nearly constant thereafter. Although this low SAR may numerically suggest a high degree of arching, a closer inspection of the stress distribution and contour plots reveals the opposite. The stress contours for various displacement stages show that, unlike a well-formed arch bridging continuously across voids and supports, the narrow intermediate support fails to adequately intercept the load. Instead, stress pathways are deflected predominantly toward the edge supports, resulting in a segmented arch form with local stress concentration around the support edges and a pronounced stress deficit over the narrow column (Figure 4.33).

This incomplete arch formation is a direct consequence of insufficient bearing width at the middle support, which cannot mobilize enough passive resistance to anchor the downward load effectively. As a result, the soil arch remains partially developed, with larger localized deformation potential and limited lateral stress dispersion toward the centerline.

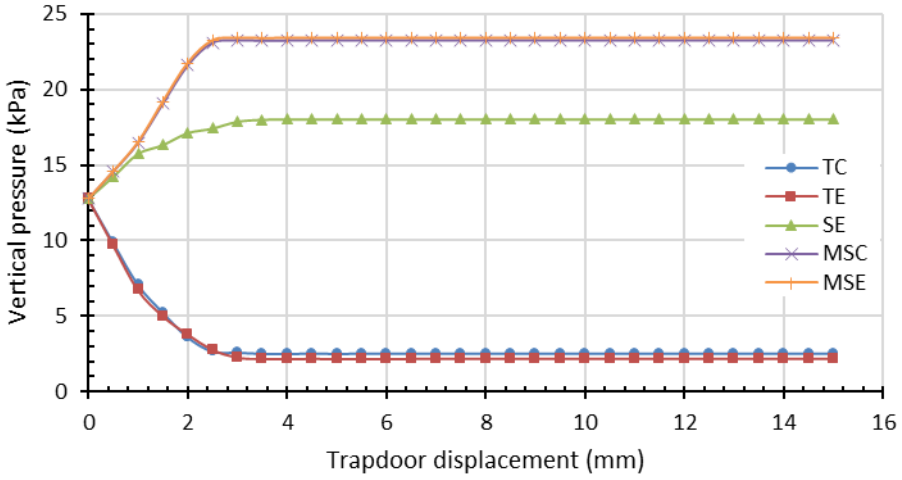

Figure 4.31: Comparison of vertical stress in relation to trapdoor displacement at five monitoring points, for Test 21 (Two Trapdoors with 0.36m Intermediate Support-1B)

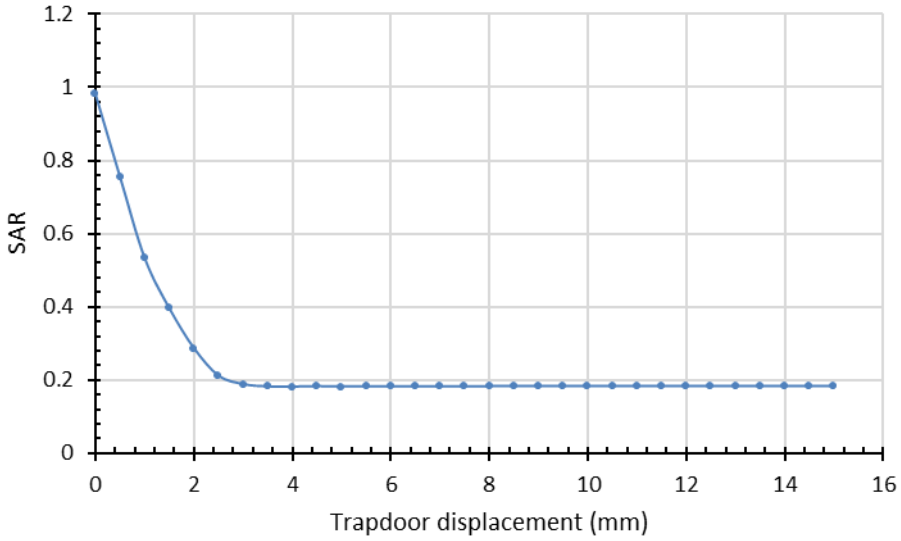

Figure 4.32: Comparison of SAR in relation to trapdoor displacement for Test 21 (Two Trapdoors with 0.36m Intermediate Support-1B)

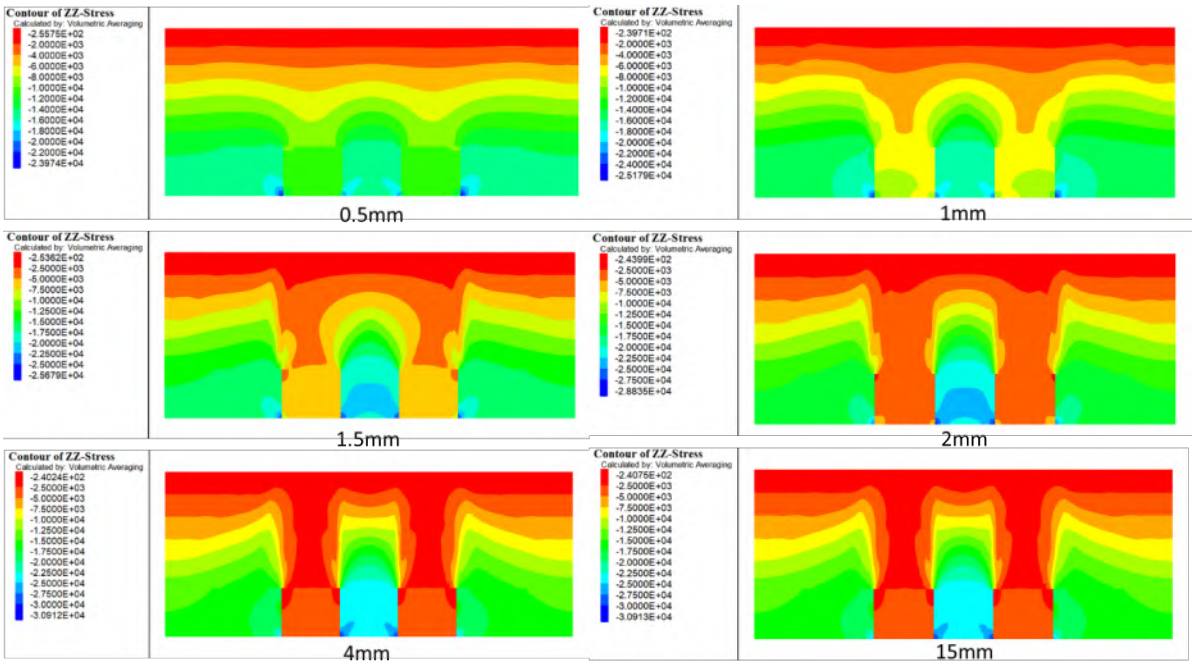

Figure 4.33: Pressure distribution of numerical model during 15mm trapdoor displacements for Test 21 (Two Trapdoors with 0.36m Intermediate Support-1B)

When compared to the wide middle support configuration (0.72 B), the functional importance of adequate intermediate support width becomes more evident. In the wide support case, the vertical stress distribution demonstrates more balanced load sharing: the MSC and MSE achieve stress levels comparable to the SE, each sustaining about 18.0 kPa after full displacement, and the SAR stabilizes at a slightly higher value near 0.22. Although this SAR is numerically larger, it reflects a more effective soil arch that fully cross over the trapdoors and engages both the middle and edge supports in redistributing loads. In contrast, the narrow support model exhibits a larger discrepancy between SE and MSC/MSE, with the central support unable to mobilize its full capacity. This behavior is confirmed by the contour plots: the wide support generates smooth, continuous stress arches that span the voids and anchor at both intermediate and edge supports, whereas the narrow support

produces segmented stress bands that dissipate mainly into the edge zones, leaving the central region more vulnerable to local settlement. These findings clearly demonstrate that wider intermediate supports significantly enhance soil arching effectiveness in multi-void systems, ensuring more uniform stress redistribution and improved overall stability. While the narrow support reduces SAR values numerically, it does so at the expense of arch continuity, resulting in stress concentration at the edges and inefficient load interception in the mid-span.

4.6.1.2 During Footing Loading

A comparative evaluation of the vertical stress distributions, soil arching ratio (SAR) trends, and stress contours clearly demonstrates the significant role played by the intermediate support width in governing the efficiency of load transfer and the mobilization of the soil arching mechanism in a double trapdoor system after apply load. As shown in Figure (4.34), the model with a wider intermediate support (0.72 m), the stress charts reveal that a substantial proportion of the applied load is redistributed towards the intermediate support, as evidenced by the markedly higher stress values recorded at the middle support center (MSC) and edge (MSE). For example, at an applied pressure of 110 kPa, the MSC stress reaches approximately 64 kPa, and the MSE about 44 kPa, whereas the trapdoor center (TC) and trapdoor edge (TE) remain comparatively lower at about 21.4kPa and 15.4 kPa, respectively. And for the end support SE, the stress is about 22.5kPa at 100kPa applied load,and then begins to decrease at 110kPa to reach about 22.2kPa. This indicates that the wider intermediate support acts as a strong load-bearing element, promoting load transfer away from the central trapdoor region. While, in the narrower support case (0.36 m), the MSC and MSE

stresses are peaking at about 64.7 kPa (MSC) and 62 kPa (MSE) at 110 kPa. Meanwhile, the TC and TE values increase more rapidly and approach 35.6 kPa and 28.5kPa, respectively. And for the end support SE, the stress is about 24.5kPa at 110kPa applied load.This pattern indicates that the narrower intermediate support is less effective at attracting load, causing more stress to remain directly above the trapdoor zones.

The SAR curves shown in Figure (4.35) reinforce this interpretation. For the wider support configuration, the SAR remains lower across the loading range (e.g., ~0.52 at 110 kPa) compared to the narrower support case, where SAR rises more sharply, reaching about 0.74 at the same load level. This suggests that the wider intermediate support facilitates a more robust soil arching effect by diverting a larger share of the load to stable regions and reducing direct transfer to the trapdoors. In contrast, the higher SAR in the small support case implies incomplete arching, with more stress passing vertically through the movable trapdoor elements.

The contour plots provide further insight into the spatial development of the stress arch. In the wide support model (Figure 4.36), stress concentration bands are clearly observed spanning from the loaded surface towards the intermediate support, forming well-defined load transfer paths that bridge over the trapdoors even at higher loads. The arching pattern appears more continuous and the stress bulb beneath the trapdoor is noticeably weaker. In contrast, for the narrow support (Figure 4.37), the contours show that stress arches are less pronounced and tend to be confined closer to the trapdoor regions, with deeper stress penetration underneath the trapdoors, signifying that the intermediate support is insufficient to intercept and redirect a significant portion of the load.

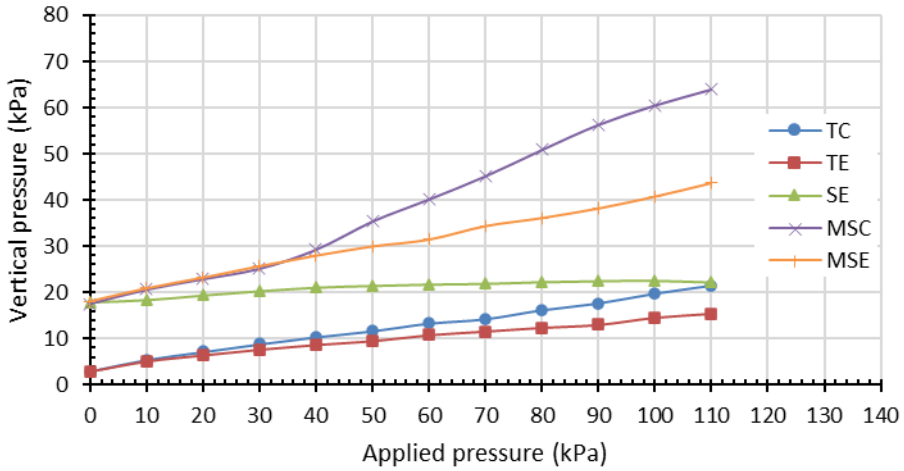

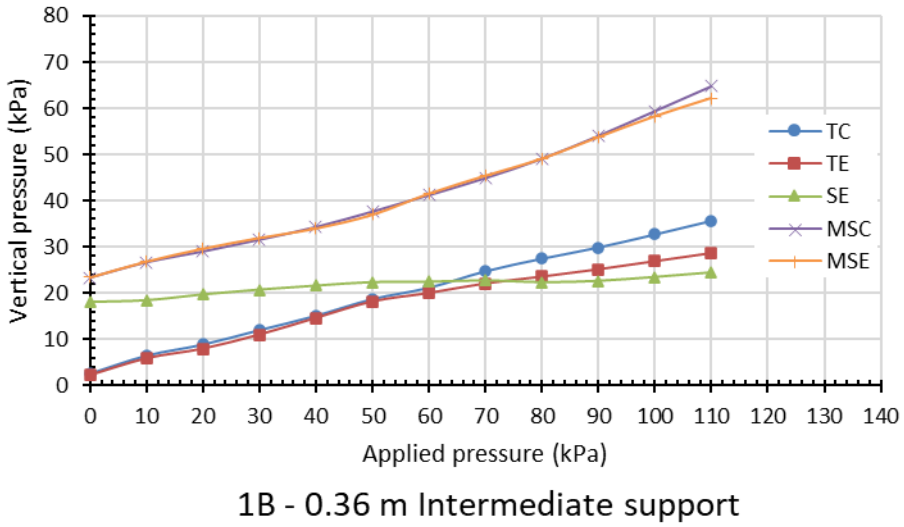

Figure 4.34: Comparison of vertical stress in relation to monotonic static footing pressure in the loading test at five monitoring points, for Test 20 (0.72m Intermediate support- 1B) and Test 21 (0.36m Intermediate support- 1B)

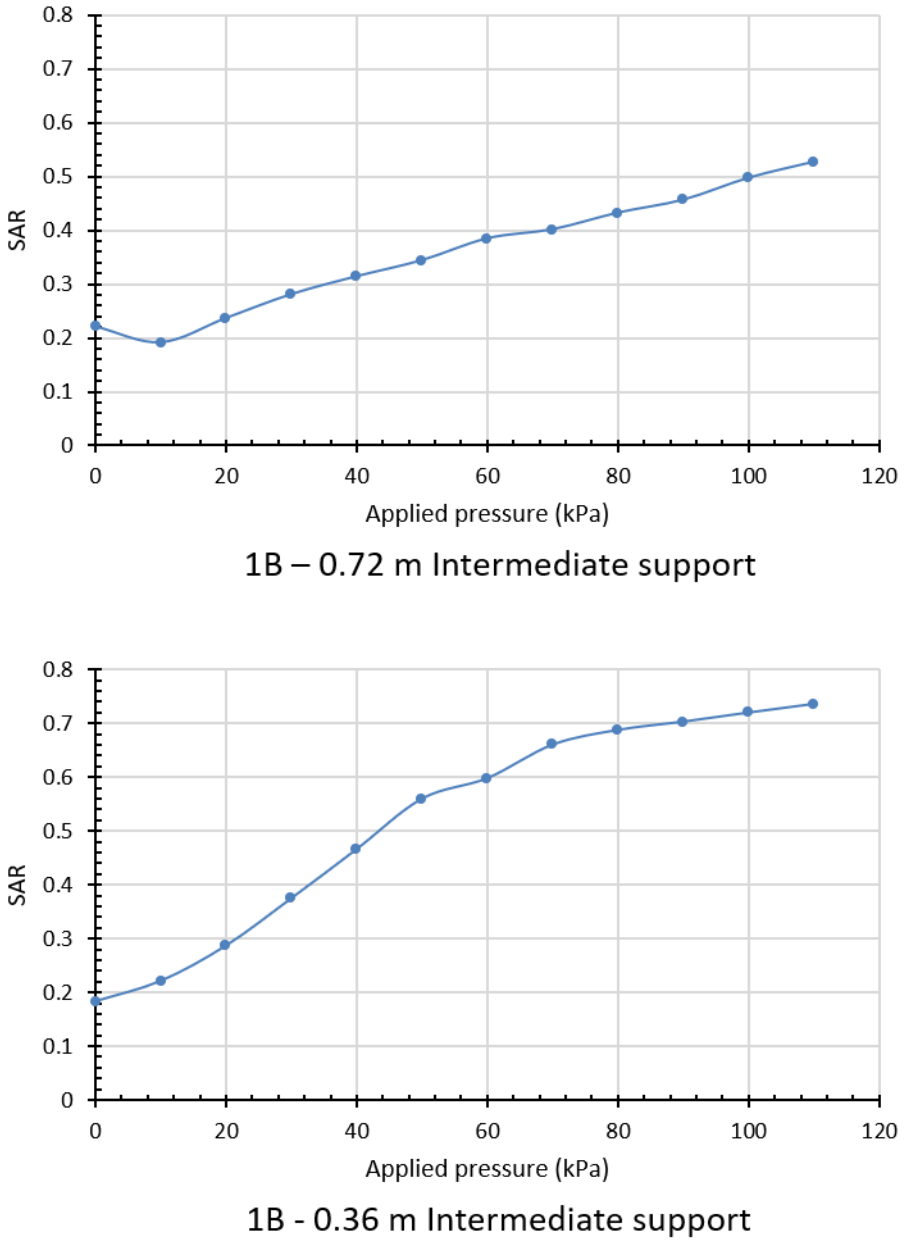

Figure 4.35: Comparison of SAR in relation to monotonic static footing pressure in the loading test for Test 20 (0.72m Intermediate support- 1B) and Test 21 (0.36m Intermediate support- 1B)

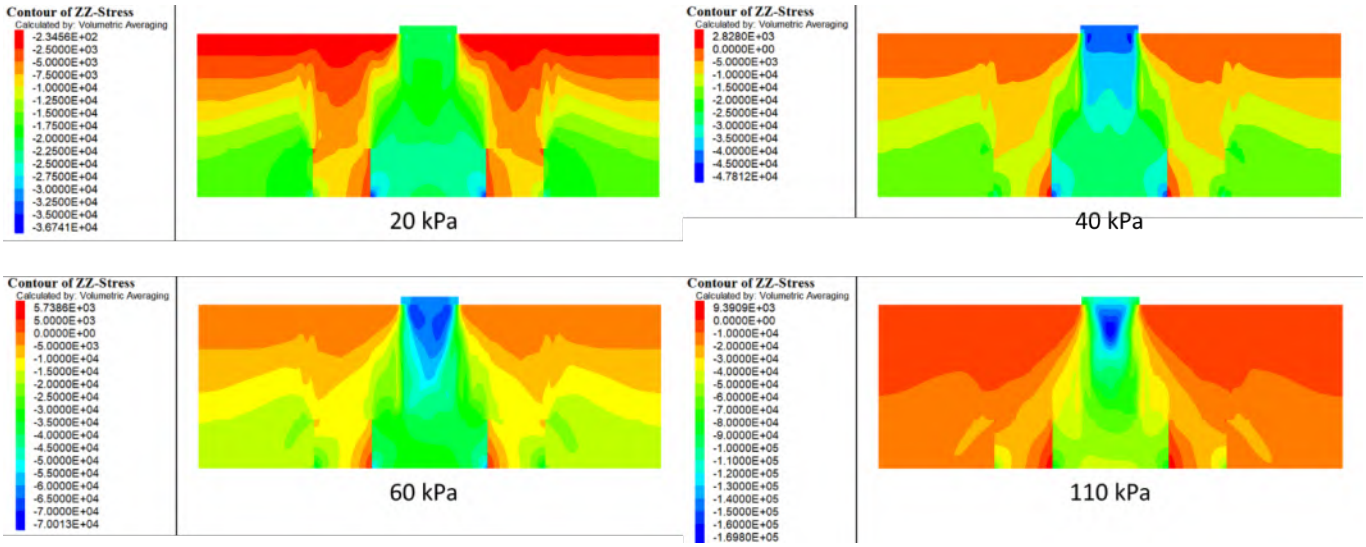

Figure 4.36: Pressure distribution of numerical model under applied loads for Test 20 (0.72m Intermediate support- 1B)

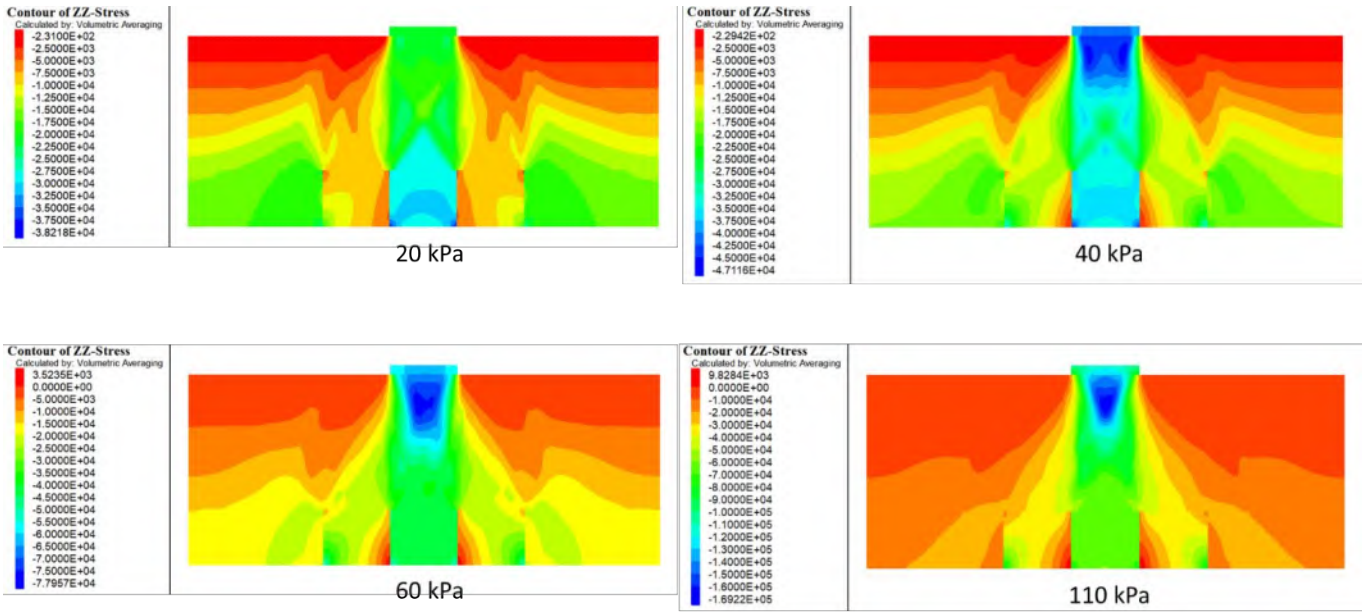

Figure 4.37: Pressure distribution of numerical model under applied loads for Test 21 (0.36m Intermediate support- 1B)

The progressive increase in footing width (1.5 B, 2 B, 2.5 B, and 3 B) with a fixed narrow intermediate support of 0.36 m reveals clear trends in how vertical stress redistributes among the trapdoor center (TC), the edge support (SE), and the middle support, represented by both its centre (MSC) and edge (MSE).

Figure (4.38) shows that, at the initial loading stage (10–20 kPa), the SE (edge support) consistently bears the largest share of the applied load compared to the trapdoor center (TC) and edge (TE), indicating that the soil preferentially redirects stress outward to the stable margins before the arching structure stabilizes. For example, at 20 kPa, the SE values increase progressively with footing width: (1.5 B: 20.73 kPa, 2 B: 21.5 kPa, 2.5 B: 21.95 kPa, and 3 B: 21.29 kPa) showing a slight increase then stabilization as width grows. This reflects that wider footings promote more lateral stress transfer but also begin to expand the arch's span, slightly reducing peak edge stress concentration. Simultaneously, MSC and MSE demonstrate steady load accumulation early on, with notable increments for larger footings. At 20 kPa, MSC grows from 31.8 kPa (1.5 B) to 34.8 kPa (2 B) to 38.8kPa (2.5B) and up to 43.1 kPa (3 B), confirming that wider footings enhance the intermediate support's role as a secondary load path, thereby stabilizing the soil arch and controlling downward displacement. A critical transitional point occurs where the stress carried by TC intersects with SE. For the 1.5 B case, TC intersect with SE at apply load about 45kPa . For 2 B, TC starts catching up near 30 kPa; for 2.5 B, the intersection becomes more distinct at about 25kPa, and for 3 B, TC surpasses SE clearly beyond 20 kPa. This behavior indicates that with larger footing widths, the central trapdoor increasingly resists more load directly, as the soil arch's lateral span becomes more extensive and less efficient at transferring load solely to the edges. At the final applied pressure

(110 kPa), the edge support SE still exhibits a gradual increase with footing width: (1.5 B: 30.17 kPa, 2 B: 35.9 kPa, 2.5 B: 48.37 kPa, and 3 B: 59.46 kPa). This demonstrates that, despite some stress being absorbed by the growing TC and intermediate supports, the edge region remains a critical zone for load transfer especially for wider footings, due to arch expansion and the need to stabilize a larger soil block. For the intermediate supports, MSC and MSE show the most significant load increase among all zones as the footing expands. At 110 kPa: MSC: rises from 86.2 kPa (1.5 B) to 127.9 kPa (3 B), and MSE: grows from 80.8 kPa (1.5 B) to 122.5 kPa (3 B). This confirms that wider footings with a fixed intermediate support width intensify stress at the mid-span supports, ensuring they carry a larger portion of the load. This efficient load sharing is fundamental for preserving soil stability beneath expansive foundations.

The SAR trend shown in Figure (4.39) corroborates this behavior: at initial stages, SAR is low (~0.18) for all widths, signifying weak arching. As loading progresses, SAR grows more rapidly with increased footing width, reaching 0.95 for 1.5 B and stabilizing slightly lower (0.77) for 3 B. This indicates that while wider footings expand the arch span, they also distribute stresses more broadly, slightly lowering the peak arching ratio but providing greater overall load-sharing stability across the supports.

The ZZ-stress contour plots shown in Figures (4.40, 4.41, 4.42, and 4.43) vividly illustrate the progressive development and spatial distribution of the soil arching mechanism within the double-trapdoor system featuring an intermediate support. At the early loading stages (e.g., 20 kPa), the contours clearly reveal that vertical stress is initially concentrated directly above each trapdoor, with stress bulbs extending laterally toward both the adjacent edge supports (SE) and the central intermediate support (MSC and MSE). This

indicates that from the onset of loading, the intermediate support actively participates in transferring load, effectively subdividing the entire footing system into two interactive arching zones rather than a single continuous arch. As the applied pressure increases, the stress concentration beneath the trapdoors intensifies and expands vertically, while lateral stress bands connecting the trapdoors to the intermediate support become more prominent and continuous. This pattern demonstrates that the intermediate support plays a pivotal role in intercepting and redistributing vertical stress that would otherwise transmit directly through the trapdoors to the underlying subsoil. This behavior is particularly evident in wider footing configurations (from 1.5 B to 3 B), where the contour plots show an increasingly well-defined stress bridge forming between each trapdoor and the intermediate support. Consequently, the intermediate support effectively reduces the load carried directly by the trapdoors themselves, mitigating localized settlement and enhancing the uniformity of stress transfer toward the stable edge supports.

In conclusion, increasing the footing width while maintaining an intermediate support, enhances the role of the edge support SE at low loads, but its relative dominance reduces as TC and MSC rise with larger footing widths, and significantly raises the stress in the intermediate supports (MSC and MSE), which become increasingly vital for sustaining stability under wider footings.Also elevates SAR during loading but with a slight diminishing return as the footing widens, due to less efficient lateral load shedding in very wide footing.

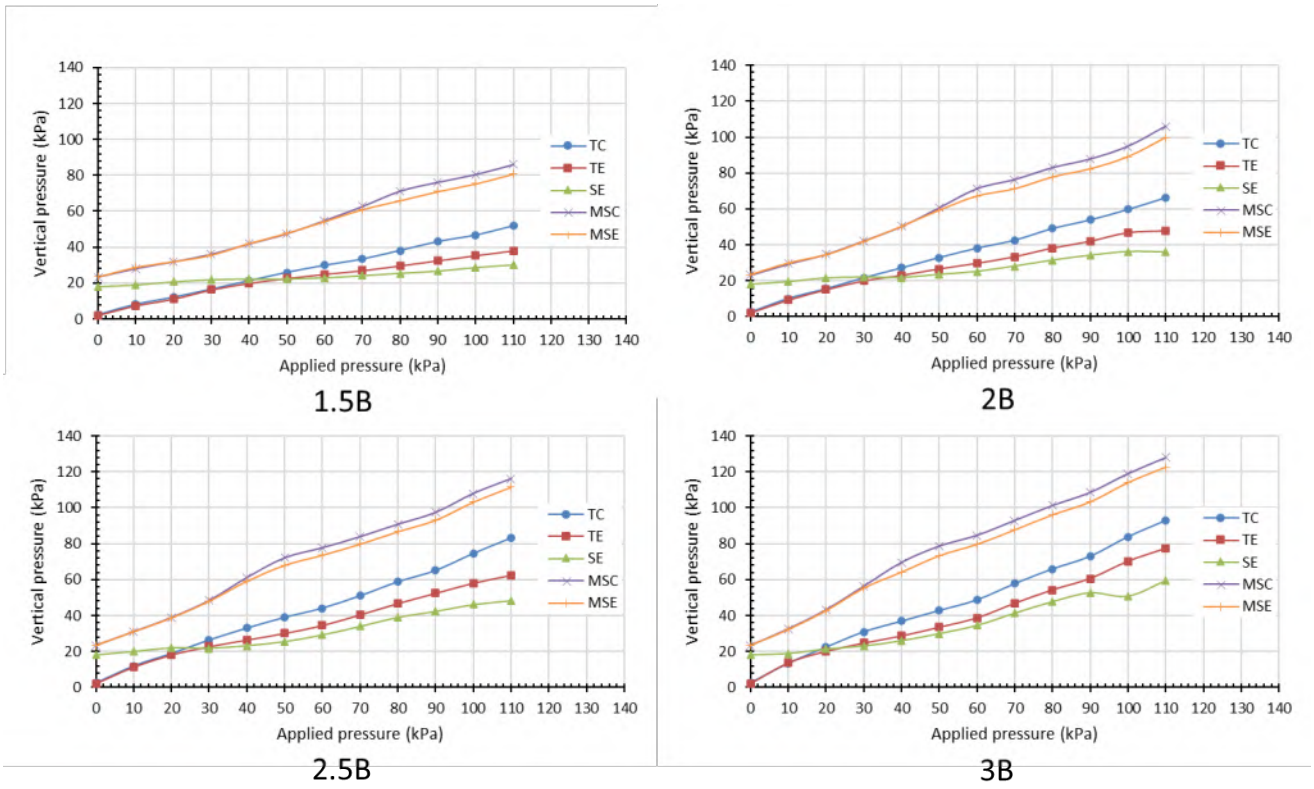

Figure 4.38: Comparison of vertical stress in relation to monotonic static footing pressure in the loading test at five monitoring points, for Test 22 (0.36m Intermediate support- 1.5B), Test 23 (0.36m Intermediate support- 2B), Test 24 (0.36m Intermediate support- 2.5B), and Test 25 (0.36m Intermediate support- 3B)

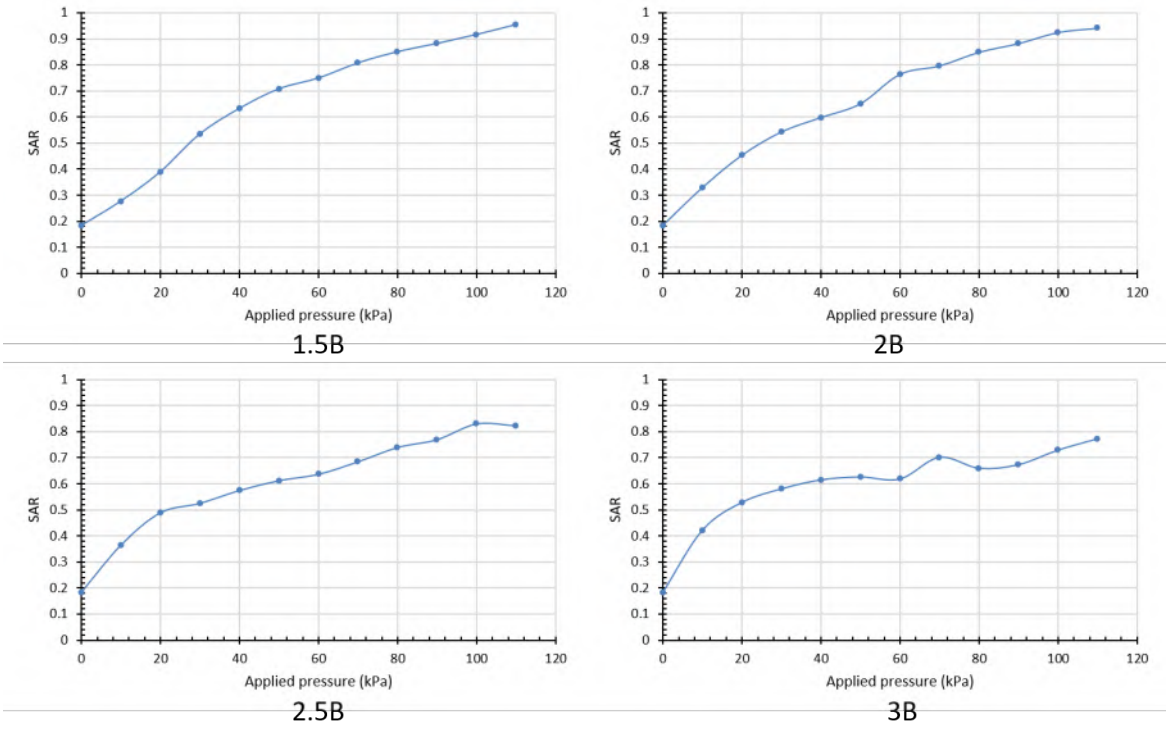

Figure 4.39: Comparison of SAR in relation to monotonic static footing pressure in the loading test for Test 22 (0.36m Intermediate support- 1.5B), Test 23 (0.36m Intermediate support- 2B), Test 24 (0.36m Intermediate support- 2.5B), and Test 25 (0.36m Intermediate support- 3B)

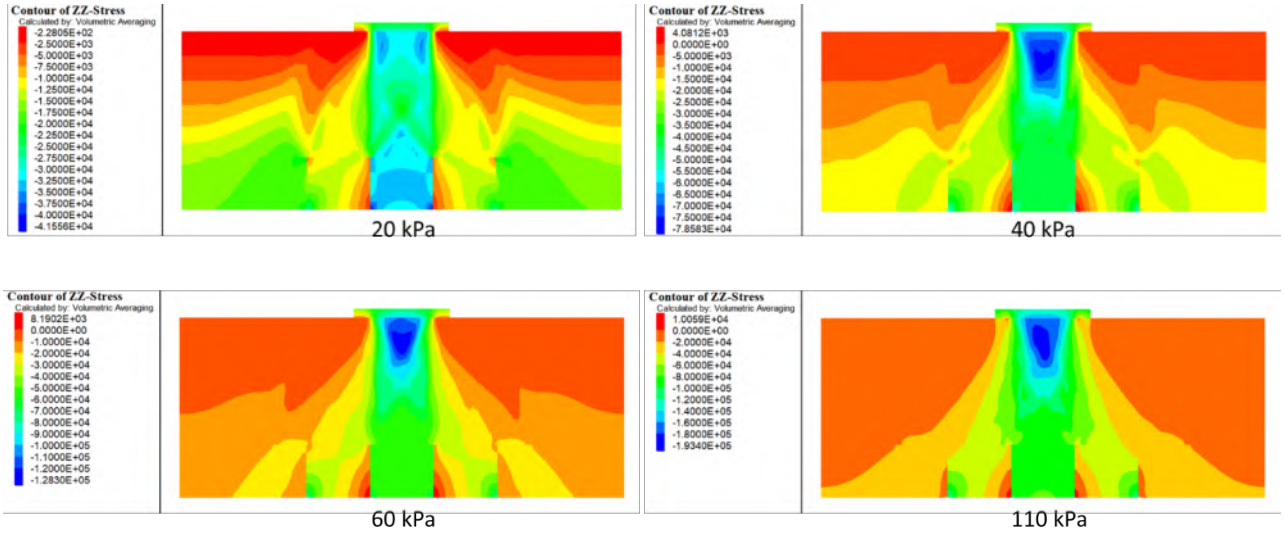

Figure 4.40: Pressure distribution of numerical model under applied loads for Test 22 (0.36m Intermediate support- 1.5B)

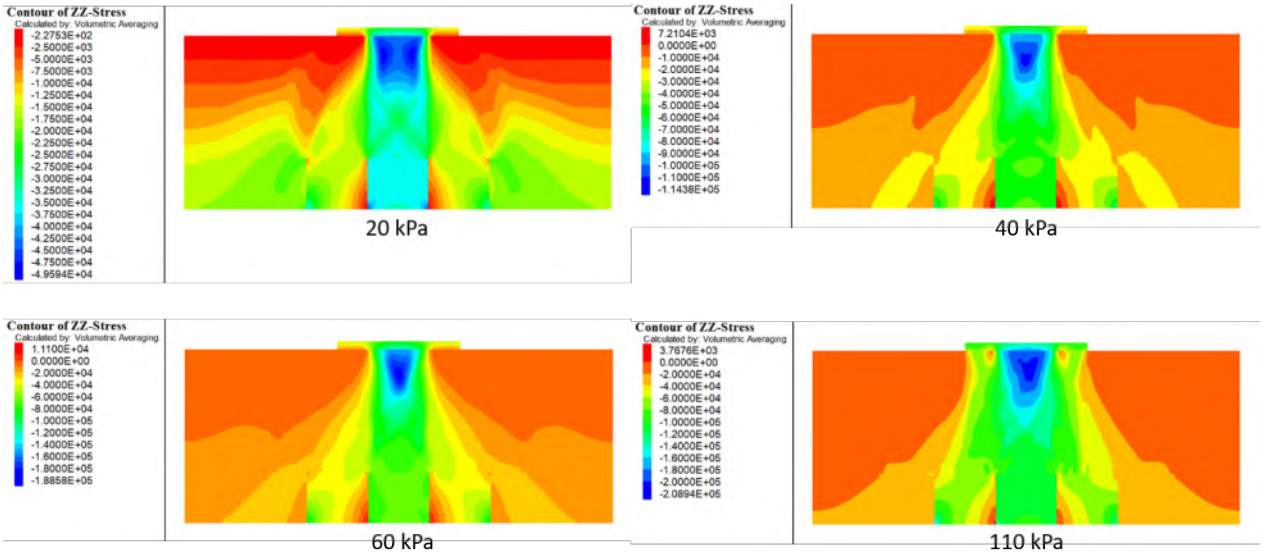

Figure 4.41: Pressure distribution of numerical model under applied loads for Test 23 (0.36m Intermediate support- 2B)

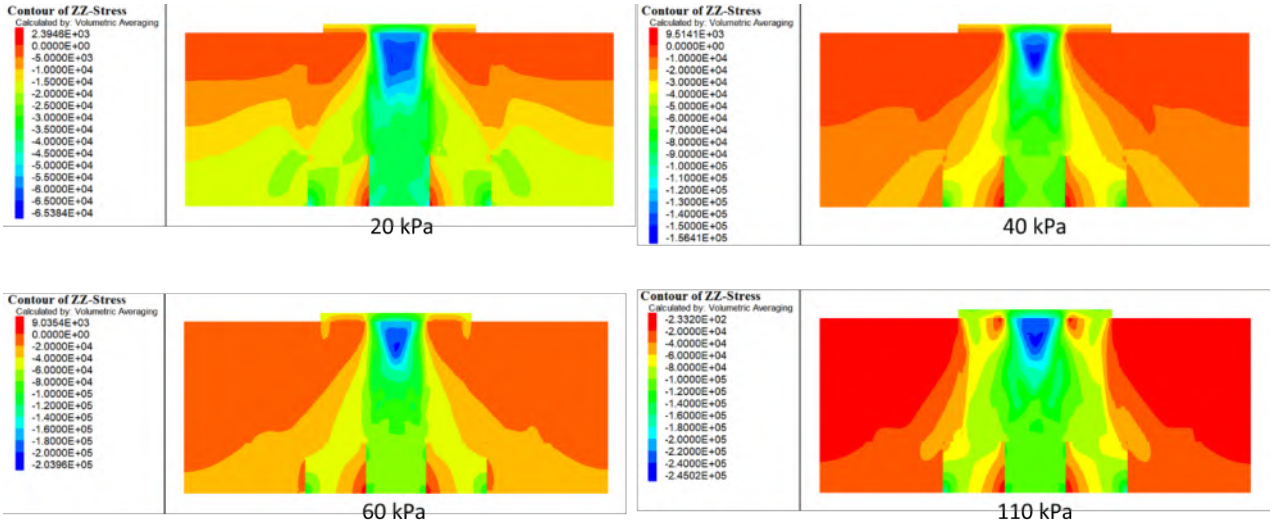

Figure 4.42: Pressure distribution of numerical model under applied loads for Test 24 (0.36m Intermediate support- 2.5B)

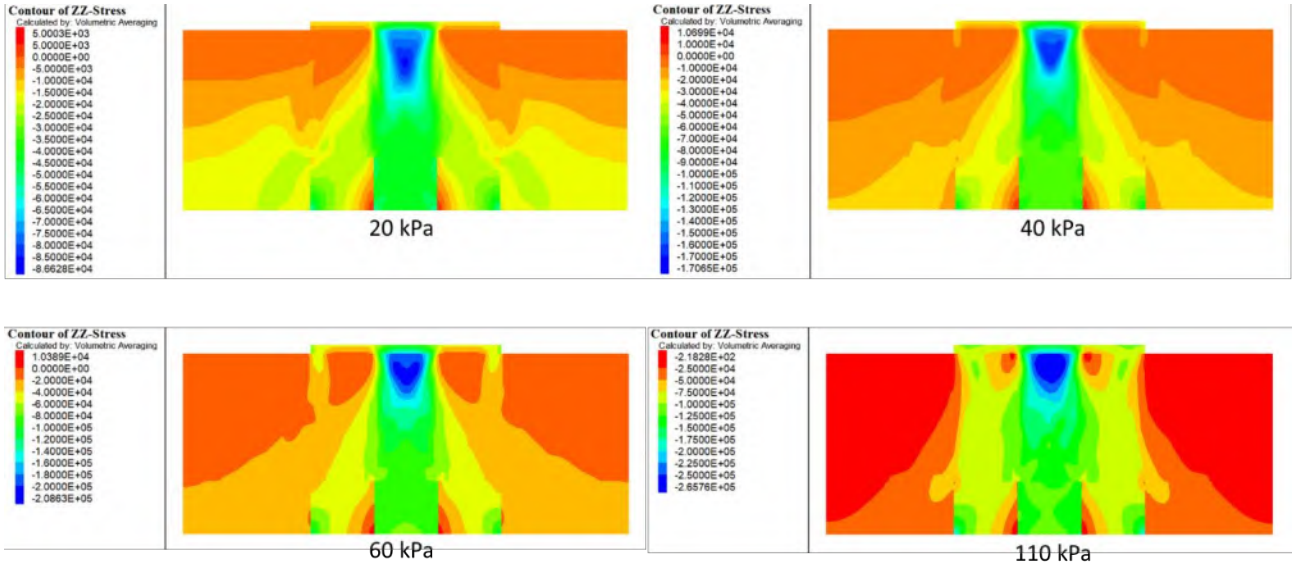

Figure 4.43: Pressure distribution of numerical model under applied loads for Test 25 (0.36m Intermediate support- 3B)

4.6.2 Three Trapdoors

4.6.2.1 During Trapdoors displacement

The vertical stress evolution during trapdoor displacement in the three-trapdoor configuration (Figure 4.44) reveals sophisticated multi-arch development under self-weight loading conditions. The stress-displacement relationships demonstrate enhanced arching mobilization compared to single and dual-trapdoor systems, consistent with (Karl Terzaghi, 1943)'s fundamental observations that multiple yielding zones create more complex stress redistribution patterns. The trapdoor center response (TC1) shows rapid stress reduction from approximately 12.7 kPa to 2.9 kPa within the first 3 mm of displacement, demonstrating immediate arch mobilization. This behavior aligns with (Jenck *et al.*, 2005)'s experimental observations in multi-pile systems, where they documented that stress relief over yielding zones occurs more rapidly in denser pile arrangements due to enhanced lateral confinement.

The support center performance (SC1) exhibits progressive stress increase to approximately 22.7 kPa, indicating effective load interception by intermediate supports. (Low *et al.*, 1994) demonstrated in their analytical work that intermediate supports in multi-pile configurations experience higher stress concentrations due to their role in anchoring multiple arch systems simultaneously. The edge support engagement (SER1, SEL1) shows balanced stress accumulation to 22.8 and 23 kPa across both edge supports, confirming uniform load distribution throughout the support system. This symmetrical response validates (Hewlett and Randolph, 1988)'s theoretical framework for multi-pile arching, where they predicted that properly spaced supports would share loads equally under uniform settlement conditions.

The stress stabilization patterns reveal critical multi-arch interactions not observed in simpler configurations. All support elements (SC1, SEL1, SER1) reach similar final stress levels (about 23 kPa), indicating coordinated load sharing among the three arching zones. Briançon and Simon (2012) observed similar stress equalization in their full-scale pile-supported embankment, attributing this behavior to the redundant load paths created by multiple support elements. The effective span between adjacent supports in the three-trapdoor configuration is reduced compared to dual-trapdoor systems, promoting more stable arch geometries. (Zhuang and Wang, 2018) demonstrated through finite element analysis that reduced clear spacing enhances arch stability by decreasing the required shear strength mobilization in the soil mass. The multiple intermediate supports provide increased lateral restraint, enabling more effective passive pressure mobilization, as shown by (Chevalier *et al.*, 2012) in their discrete element modeling studies of granular materials.

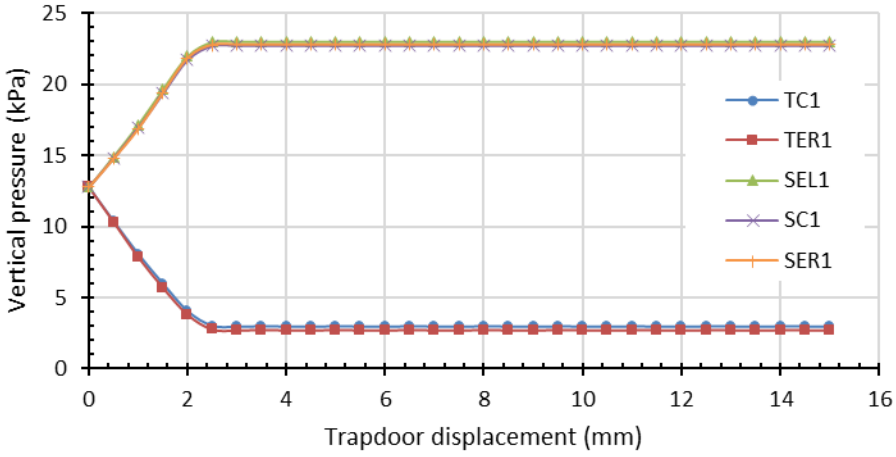

Figure 4.44 Comparison of vertical stress in relation to trapdoor displacement at five monitoring points, for Tests 26-29 (three trapdoors)

The SAR evolution during trapdoor displacement (Figure 4.45) demonstrates superior arching efficiency in the three-trapdoor configuration. The SAR exhibits accelerated development, decreasing from unity to approximately 0.20 within 2-3 mm displacement. The sharp SAR decline in the first 2 mm indicates immediate stress redistribution upon trapdoor movement. (Lai *et al.*, 2020) observed similar rapid SAR mobilization in their discrete element analyses of dense pile arrangements, attributing this behavior to the immediate activation of inter-particle friction in well-confined granular materials.

The SAR reaches a stable plateau at 0.20, indicating that 80% of the overburden load is effectively transferred to support elements while only 20% remains over the yielding zones. This efficiency exceeds the performance of both single-trapdoor (SAR = 0.23) and most dual-trapdoor configurations (SAR = 0.22-0.25). The SAR remains constant beyond 3 mm displacement, confirming robust arch stability under continued settlement. (Van Eekelen *et*

al., 2013) predicted similar SAR stabilization in their Concentric Arches model for dense pile arrangements, where reduced clear spacing promotes stable arch geometries. The three-trapdoor configuration achieves intermediate performance between wide and narrow dual-trapdoor supports, suggesting that multiple intermediate supports provide optimal load distribution without the sensitivity to support width observed in dual-trapdoor systems. This behavior confirms the theoretical predictions of (Wang *et al.*, 2021) in their discrete element analysis of pile-supported embankments, where they demonstrated that increased pile density leads to more stable stress redistribution patterns.

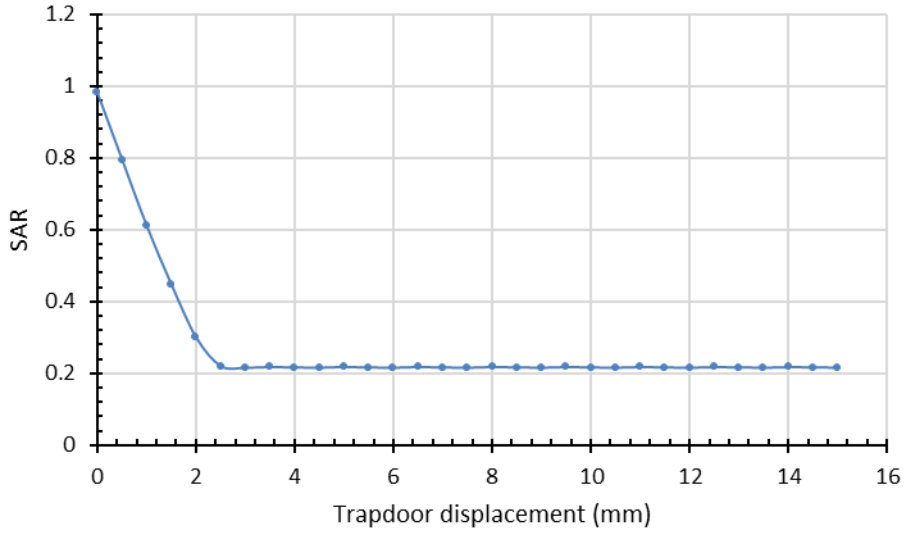

Figure 4.45 Comparison of SAR in relation to trapdoor displacement for Tests 26-29 (three trapdoors)

The stress contour evolution for the three-trapdoor (Figure 4.46) configuration illustrates the sequential formation and stabilization of multiple soil arches during displacement. At the early stage (0.5–1 mm), only initial stress relief zones appear above each trapdoor with minimal lateral transfer, indicating arch shoulders have not yet formed. By the intermediate stage (1–2 mm), distinct semi-elliptical arches develop between trapdoors and supports, showing clear load transfer paths. In the advanced stage (>2 mm), arches are fully stabilized, with concentrated stresses at supports and minimal stress above trapdoors, confirming effective and balanced load redistribution. The contours reveal progressive lateral stress diffusion and coordinated arch interaction, with overlapping stress fields enhancing mutual stability—an effect well-documented in multi-pile studies. This coordinated three-arch system achieves more uniform stress distribution and greater stability than simpler configurations, validating its superior load transfer efficiency.

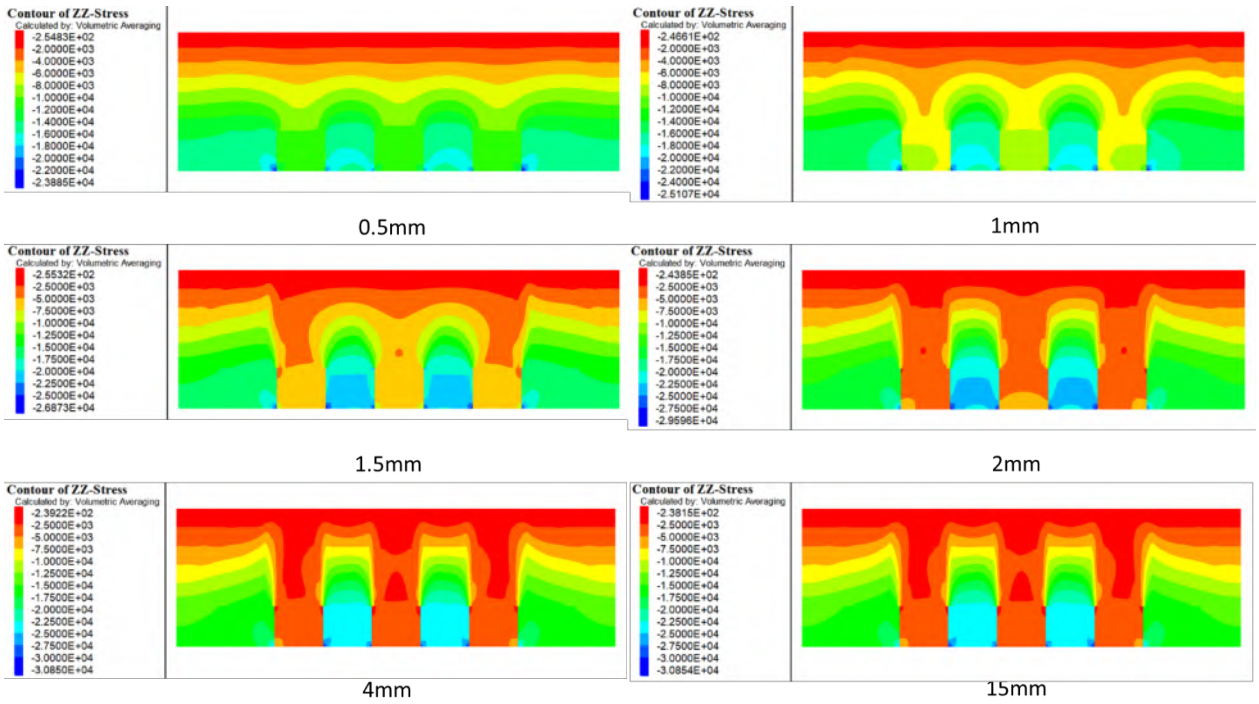

Figure 4.46 Pressure distribution of numerical model during 15mm trapdoor displacements for Tests 26-29 (three trapdoors)

4.6.2.2 During Footing Loading

The vertical stress evolution under progressive applied loading in the three-trapdoor configuration - 1B (Figure 4.47) demonstrates complex stress redistribution patterns that differ significantly from the displacement-only phase. The stress-load relationships reveal the progressive mobilization and subsequent degradation of the soil arching mechanism under increasing surface pressures, consistent with the theoretical framework established by Terzaghi (1943) for multiple yielding zones under external loading. At low applied pressures (0–20 kPa), the middle trapdoor center (TC1) records a steep increase in vertical stress, reaching approximately 20 kPa by mid-range loading. This early and rapid rise reflects the direct influence of the footing load and the immediate mobilization of the soil arch above the central opening. The adjacent central support (SE1) sustains high stresses from the

onset, confirming its dominant role in carrying the redistributed load. The trapdoor edge (TE1) shows a steady increase in stress, indicating progressive arch shoulder development and lateral load spreading toward SE1 and SE2.

In contrast, the edge trapdoor region experiences significantly lower vertical stresses throughout loading. TC2 remains far below TC1, not exceeding ~13 kPa even at maximum applied pressure, confirming that the overlying central arch effectively shields the edge trapdoor from direct loading. SE2, located adjacent to the edge trapdoor, carries moderate stress levels that increase gradually with loading, reflecting secondary load transfer from the central arch system. TE2 shows a limited stress rise, indicating that only a portion of the redistributed load reaches the edge arch shoulders.

The SAR response reinforces these observations. For the middle trapdoor (T1), SAR increases sharply from ~0.2 to ~0.7 within the first 40 kPa of loading, stabilizing at ~0.85 for higher loads. This plateau reflects a stable and efficient load transfer mechanism, with approximately 80% of the load above the central trapdoor being redirected to the supports, leaving only 20% acting directly over the yielding zone. For the edge trapdoor (T2), SAR initially dips slightly under very low loads, then rises slowly to a maximum of ~0.35 at peak pressure. This modest efficiency reflects the reduced demand placed on the edge arch due to the dominant load interception by the central arch system.

Overall, the results confirm that a footing directly over the middle trapdoor produces a highly efficient and stable central arch due to symmetrical confinement and bilateral support, while simultaneously reducing the load mobilization requirements for the edge trapdoor. This behavior is consistent with multi-trapdoor and multi-pile studies, where load placement governs the relative mobilization and stability of adjacent arches, with central loading

favoring the directly supported arch and limiting activation of peripheral arches.

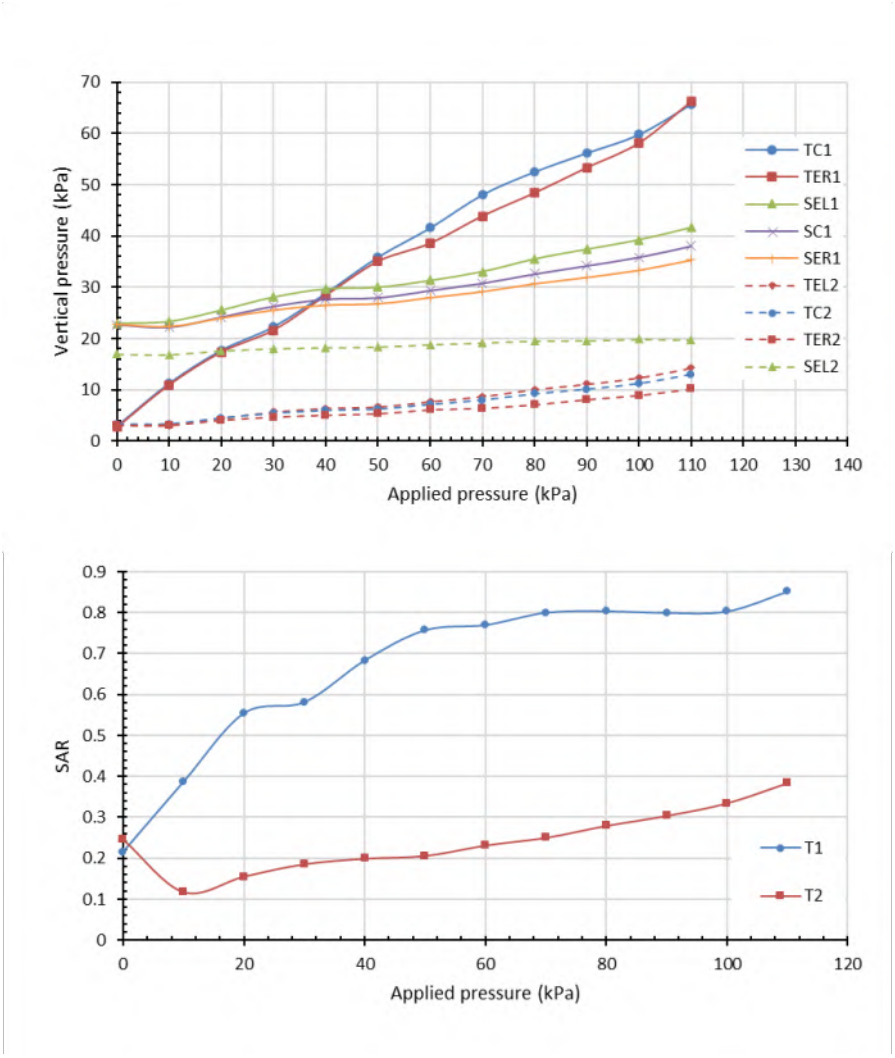

Figure 4.47 a) Comparison of vertical stress in relation to monotonic static footing pressure in the loading test at nine monitoring points and b) Comparison of SAR in relation to monotonic static footing pressure in the loading test , for Test 26

The stress contour evolution under loading for the three-trapdoor configuration illustrates the progressive degradation of the arching system while highlighting its resilience (Figure 4.48). At low load (20 kPa), well-defined arches remain intact, with clear stress relief zones above trapdoors and curved trajectories directing loads to supports. As loading increases to 40–60 kPa, stress bulbs expand—particularly above the central trapdoor under the footing—while stress paths begin to straighten, signaling reduced lateral transfer efficiency. At maximum load (110 kPa), arches are largely degraded, replaced by more direct vertical stress transmission, though some lateral spreading persists, preventing complete failure. The central trapdoor experiences the greatest stress concentration, while peripheral regions retain better distribution, confirming that multi-trapdoor systems can sustain partial functionality even when individual arches weaken. Low et al. (1994) predicted similar spatial degradation patterns in their analytical model, where they demonstrated that the failure of individual arches in multi-pile systems does not necessarily lead to global system failure.

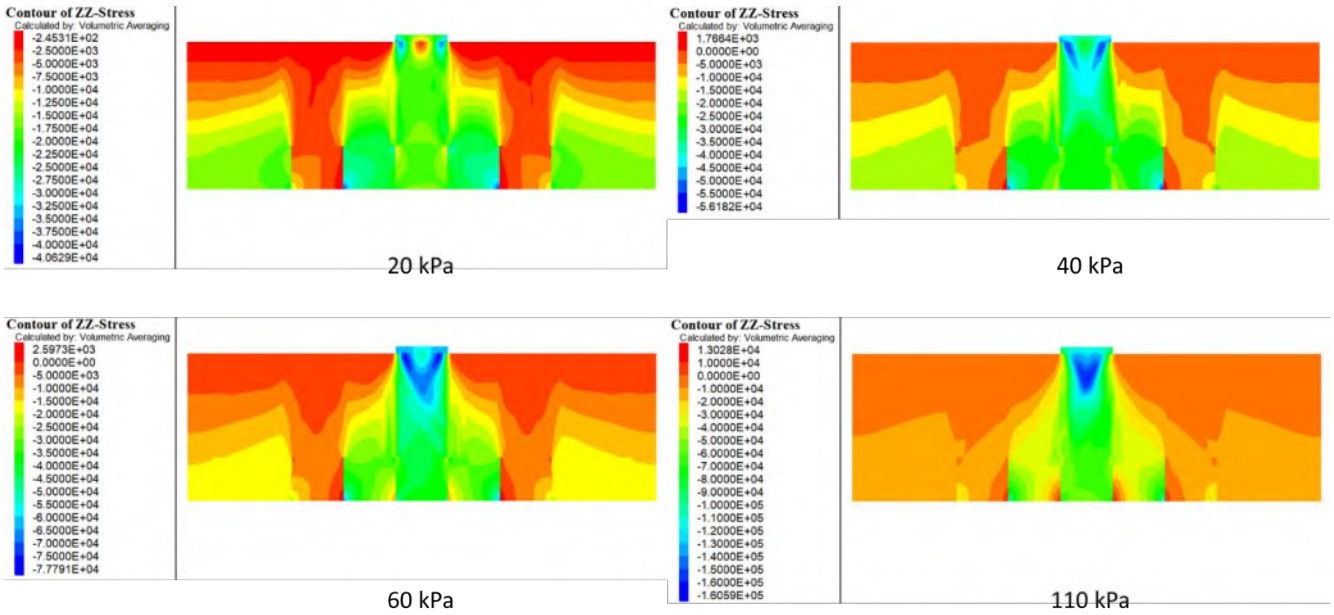

Figure 4.48 Pressure distribution of numerical model under applied loads for Test 26 (three trapdoors- 1B)

The progressive increase in footing width from 2B to 5B markedly influences the stress redistribution mechanisms within the three-trapdoor system, transitioning from a localized, centrally dominated arching response to a fully integrated multi-arch load transfer mechanism (Figure 4.49).

For the smallest width (2B), where the applied load is concentrated directly above the middle trapdoor, vertical stresses at the central trapdoor center (TC1) rise sharply with applied pressure, reflecting the dominant role of the central arch in load transfer. The adjacent support (SE1) sustains the highest stresses in the system, while the edge trapdoor center (TC2) and its associated support (SE2) experience minimal stress, confirming the shielding effect of the central arch and the limited engagement of peripheral arches under narrow loading conditions.

Increasing the width to 3B partially extends the loading influence toward the edge trapdoors. This is reflected in higher stress magnitudes at

TC2, TE2, and SE2, accompanied by a noticeable reduction in the disparity between TC1 and TC2 stresses. While the middle trapdoor arch still governs the load transfer, the edge arches begin to mobilize more effectively, resulting in a more distributed load-sharing pattern between the central and peripheral supports.

At 4B, the applied load spans across the middle and edge trapdoors, producing a substantial increase in TC2 stresses and elevating SE2 to levels comparable with SE1. The stress curves at TE1 and TE2 also become more closely aligned, indicating that lateral stress transfer pathways are fully activated. This stage marks a functional transition toward coordinated arching across the system, with the central arch no longer the sole dominant load path.

Under the 5B condition, the footing covers all three trapdoors, resulting in a highly uniform stress distribution. Stresses at TC1 and TC2 converge closely. This uniformity indicates that the arches above both the central and edge trapdoors are fully mobilized and operating in a coordinated manner, with balanced load transfer to all support elements. The system at this stage exhibits a mature multi-arch response, minimizing localized stress concentrations and enhancing global stability.

Overall, the results confirm that footing width is a critical parameter in multi-trapdoor systems. Narrow widths promote localized arching and concentrated load transfer, while increasing the width progressively engages peripheral arches, culminating in a uniformly distributed and stable multi-arch configuration. This behavior aligns with theoretical predictions for pile-supported and multi-opening systems, where increased load coverage promotes synchronous arch mobilization and improved load distribution efficiency.

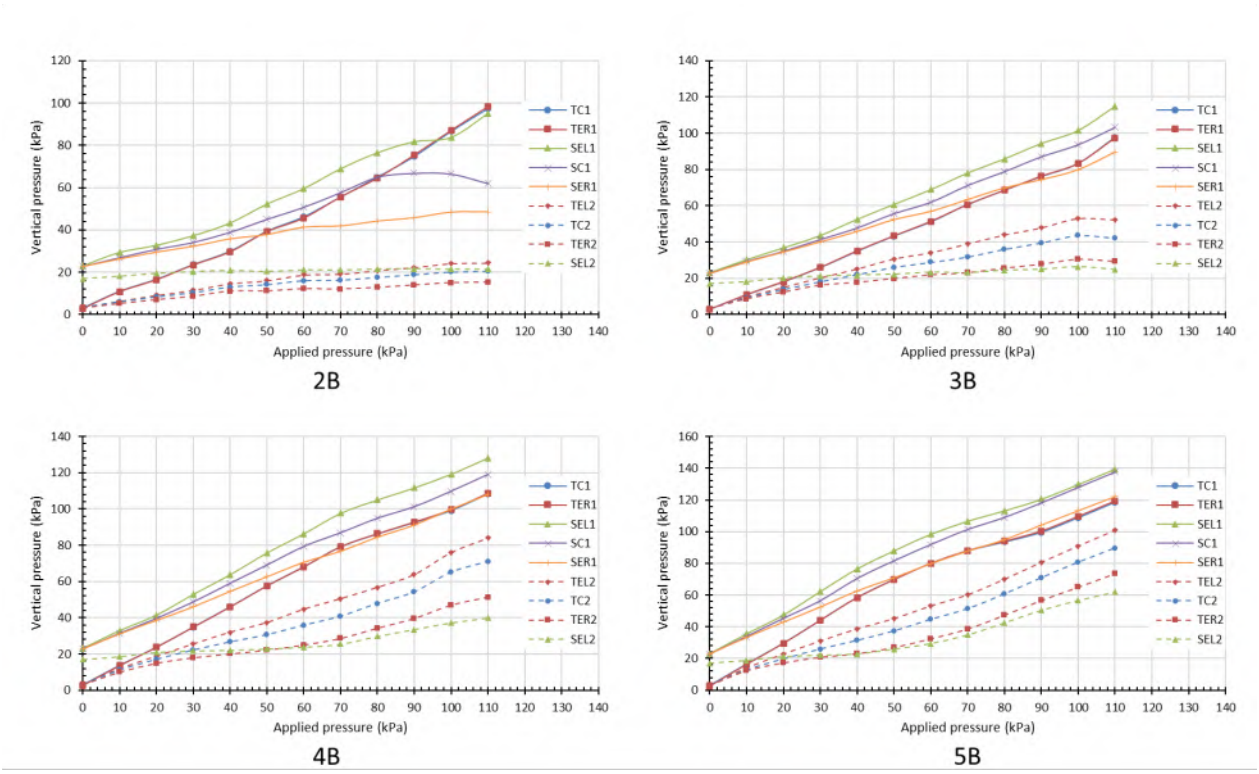

Figure 4.49: Comparison of vertical stress in relation to monotonic static footing pressure in the loading test at nine monitoring points , for Tests 27-29 (three trapdoors- 2-5B)

The Soil Arching Ratio (SAR) results for varying footing widths reveal a clear progression from localized load transfer dominance to balanced multi-arch engagement as the applied load coverage increases from 2B to 5B (Figure 4.50).

For the 2B footing width, where the applied load is concentrated above the middle trapdoor, SAR for the central arch (T1) rises steadily from ~0.25 at low loads to ~0.85 at peak pressure, indicating efficient and progressive mobilization of load transfer to the supports. In contrast, SAR for the edge trapdoor (T2) remains substantially lower, starting near 0.20 and plateauing around 0.55, reflecting limited engagement due to shielding by the central arch. The large SAR disparity between T1 and T2 confirms the dominance of the centrally located arch under narrow loading.

When the footing width increases to 3B, the SAR disparity between T1 and T2 is significantly reduced, with both curves rising in parallel and converging at ~0.8–0.85. This indicates that the load now engages both the middle and edge arches almost equally, and lateral stress transfer pathways are fully activated at relatively low applied pressures. The symmetrical performance reflects the partial overlap of the footing load with the edge trapdoors, promoting coordinated mobilization of both arches.

At 4B, SAR for T1 shows rapid initial growth, reaching ~0.8 by 50 kPa before stabilizing, while T2 exhibits a steady increase to ~0.82 at peak pressure. The reduced gap between T1 and T2 compared to the 2B case highlights the transition toward more uniform load sharing. This configuration still shows slightly higher efficiency in T1, likely due to its central location and bilateral support confinement, but both arches contribute significantly to the global load transfer mechanism.

Under the 5B condition, with the footing spanning the entire three-trapdoor system, T1 achieves a rapid SAR peak of ~1.0 by mid-range loading (≈ 40 kPa), before showing a slight decline at higher pressures, likely due to progressive arch degradation under sustained loading. T2 exhibits the highest SAR achieved in any configuration for the edge trapdoor (~0.78), confirming that full footing coverage promotes near-synchronous mobilization of both central and edge arches. This uniformity in SAR trends reflects the integrated multi-arch system behavior, where all arches actively contribute to load redistribution without the pronounced dominance of any single arch.

Overall, the SAR results confirm that increasing footing width enhances the engagement of peripheral arches and transitions the system from localized central arch dominance toward balanced, cooperative load transfer across all trapdoors. Narrow footings concentrate arching efficiency above the

loaded zone, whereas full-width footings promote global stability and uniform stress redistribution. These findings align with multi-pile and multi-opening system studies, where increased load coverage improves the uniformity of load sharing and reduces vulnerability to localized arch failure.

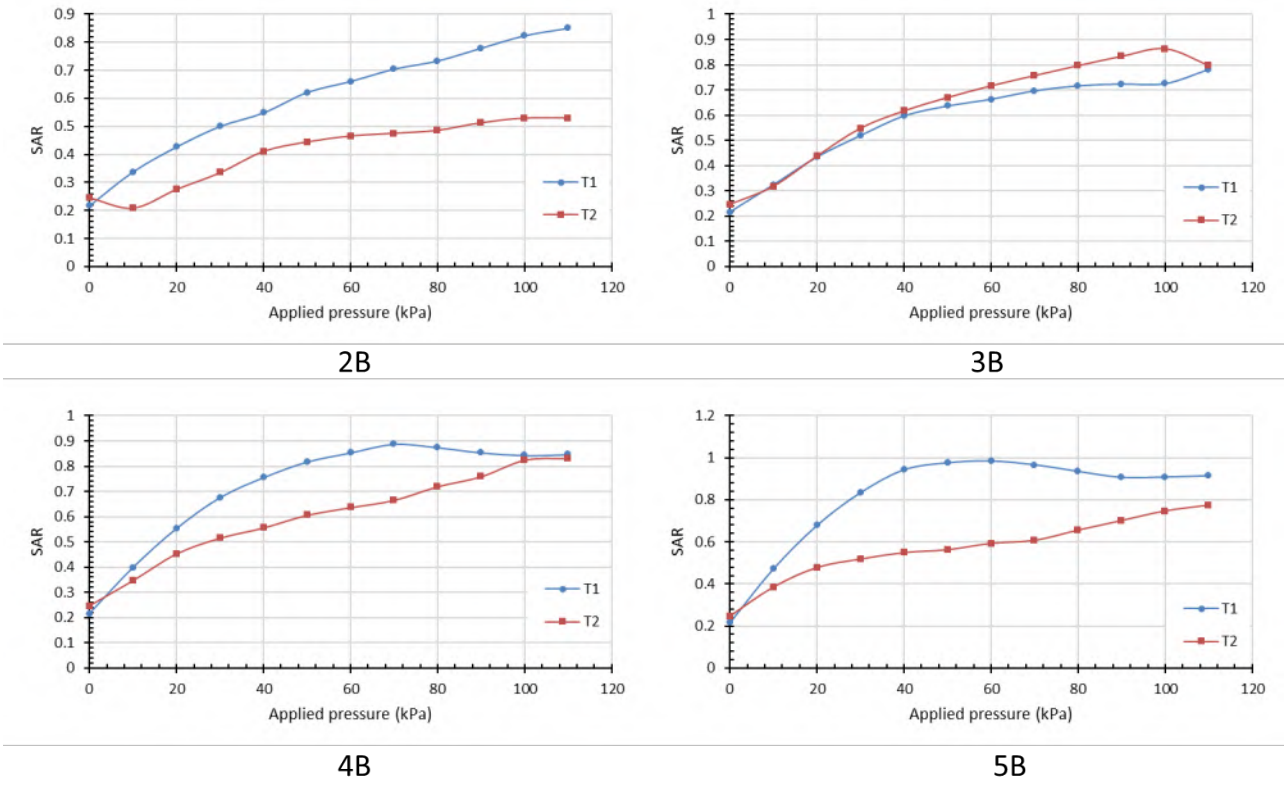

Figure 4.50: Comparison of SAR in relation to monotonic static footing pressure in the loading test at nine monitoring points , for Tests 27-29 (three trapdoors- 2-5B)

The stress contour evolution for footing widths ranging from 2B to 5B illustrates the progressive transformation of the load transfer mechanism in the three-trapdoor configuration, from localized arching above the loaded region to fully integrated multi-arch mobilization (Figures 4.51-4.54).

For the 2B footing width, where the load is concentrated above the middle trapdoor, the initial stage at 20 kPa shows distinct stress bulbs above the central opening, with curved trajectories extending toward the adjacent supports (SE1). The edge trapdoors remain largely inactive, with minimal stress penetration above TC2. At 40–60 kPa, the central arch maintains its shape, but stress intensity increases sharply within the yielding zone, indicating partial degradation of the curved load paths. At 110 kPa, significant vertical stress penetration occurs above TC1, while only limited lateral spreading reaches the edge supports, confirming that the narrow footing width constrains load transfer primarily to the central arch system.

Increasing the width to 3B partially overlaps the loading with the edge trapdoors. At 20 kPa, the contours reveal active arches above both central and edge openings, with stress relief zones forming in each. At 40–60 kPa, the stress bulbs expand more uniformly across the three trapdoors, with the edge arches showing greater engagement than in the 2B case. By 110 kPa, although vertical stress penetration is visible above all trapdoors, significant lateral stress transfer persists toward both SE1 and SE2, indicating a more balanced distribution of load between arches.

At 4B footing width, the applied load covers most of the span across the three trapdoors. From the early stages, the contours display nearly simultaneous activation of central and edge arches, with overlapping stress influence zones that promote coordinated load transfer. As the load increases to 60–110 kPa, stress trajectories remain curved for longer before

straightening, and the supports on both sides exhibit similar stress concentrations. This symmetry marks a transition toward a globally mobilized arching system.

Under the 5B condition, the footing spans the entire three-trapdoor width, producing a fully integrated multi-arch response from the onset. At 20 kPa, stress relief zones appear above all trapdoors, with lateral spreading toward both edges. By 40–60 kPa, the arches merge into a continuous stress transfer network, and at 110 kPa, although the curved stress patterns degrade under high load, lateral redistribution remains strong, preventing localized overload. The edge and central trapdoors share the load almost equally, and the supports sustain similar stress magnitudes, confirming a fully balanced load-sharing mechanism.

Overall, the contour analysis confirms that increasing footing width enhances the engagement of peripheral arches and transitions the system from a single-arch-dominated mechanism (2B) to a stable, cooperative multi-arch system (5B). Wider footing coverage not only improves stress distribution uniformity but also delays the onset of localized arch degradation, consistent with theoretical predictions for multi-opening and multi-pile-supported systems under broad load application.

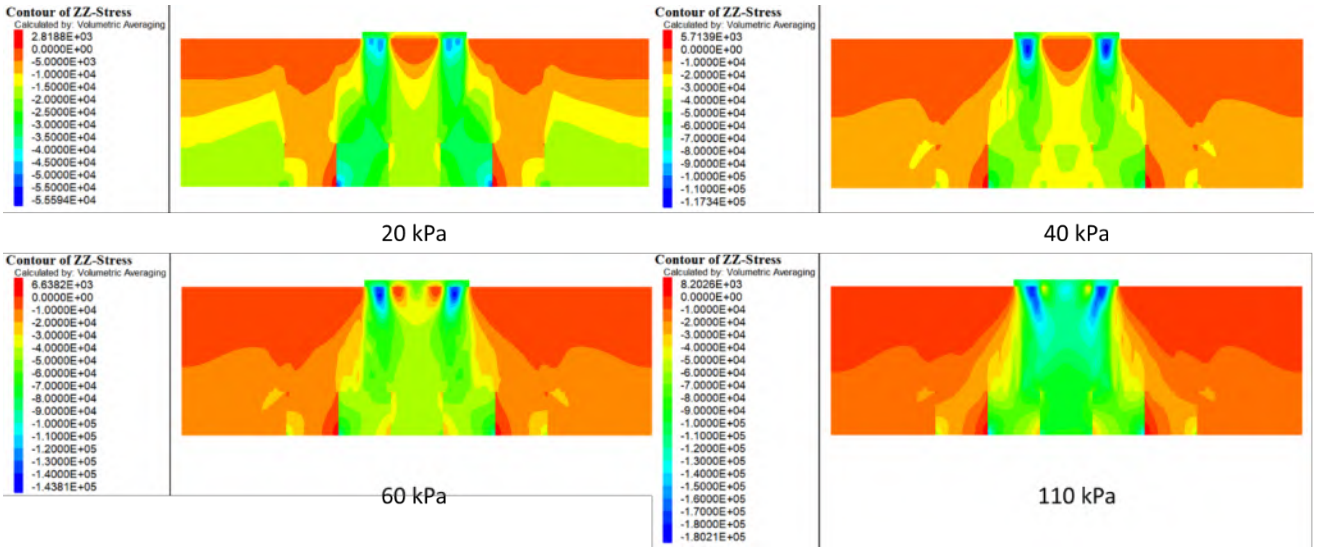

Figure 4.51: Pressure distribution of numerical model under applied loads for Test 27 (three trapdoors- 2B)

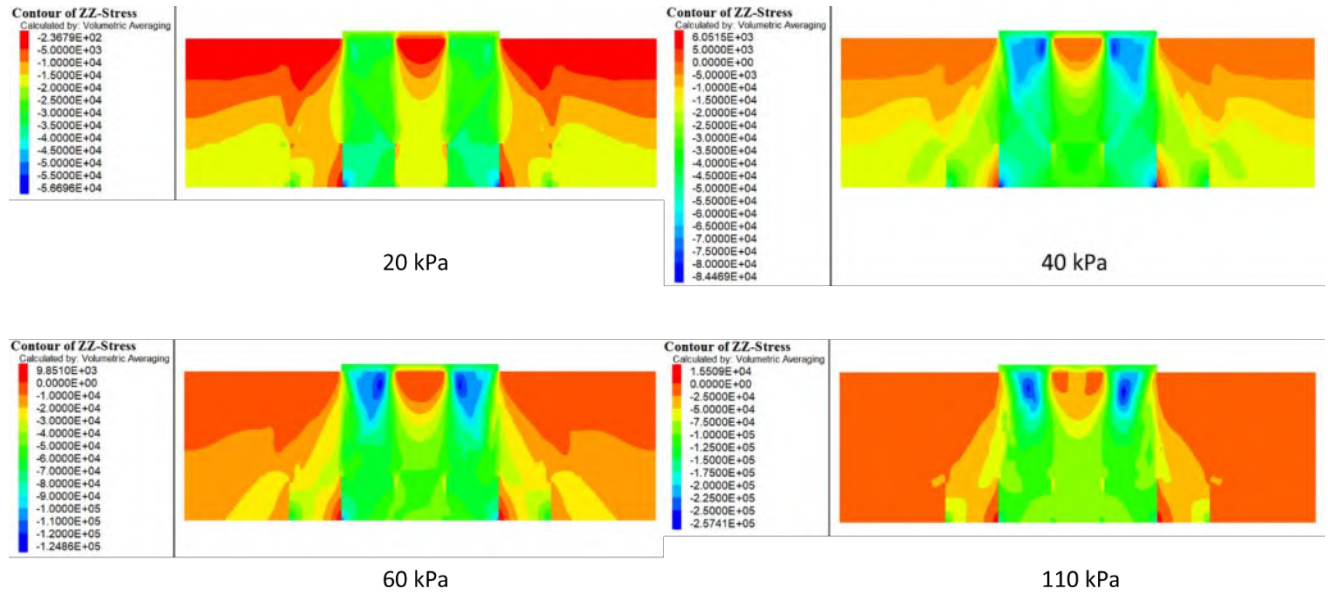

Figure 4.52: Pressure distribution of numerical model under applied loads for Test 28 (three trapdoors- 3B)

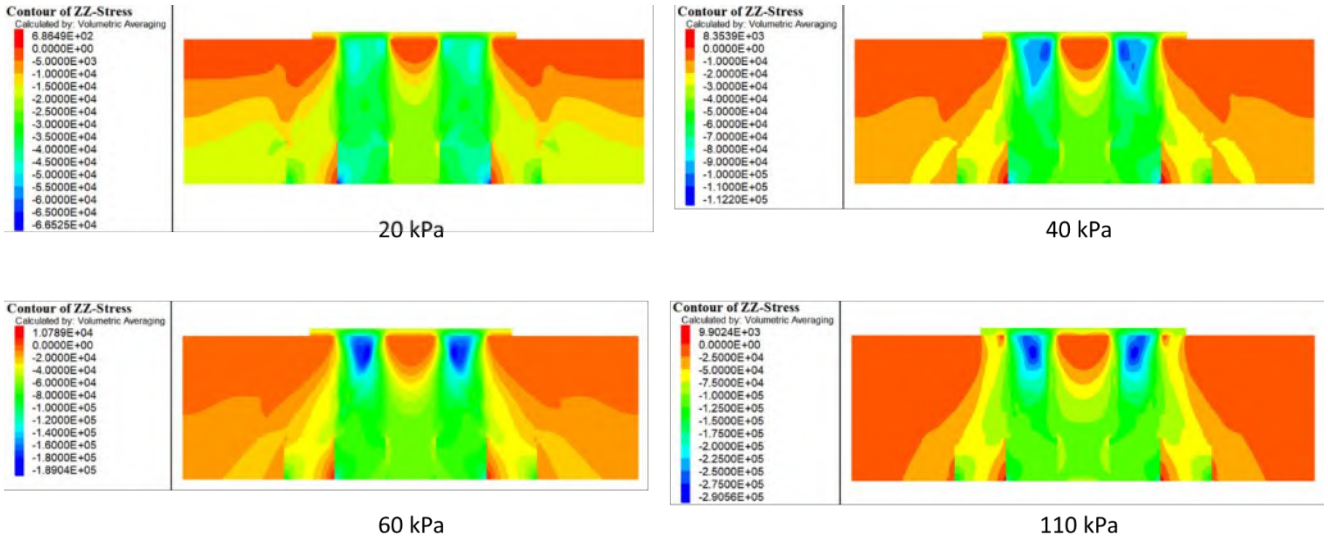

Figure 4.53: Pressure distribution of numerical model under applied loads for Test 29 (three trapdoors- 4B)

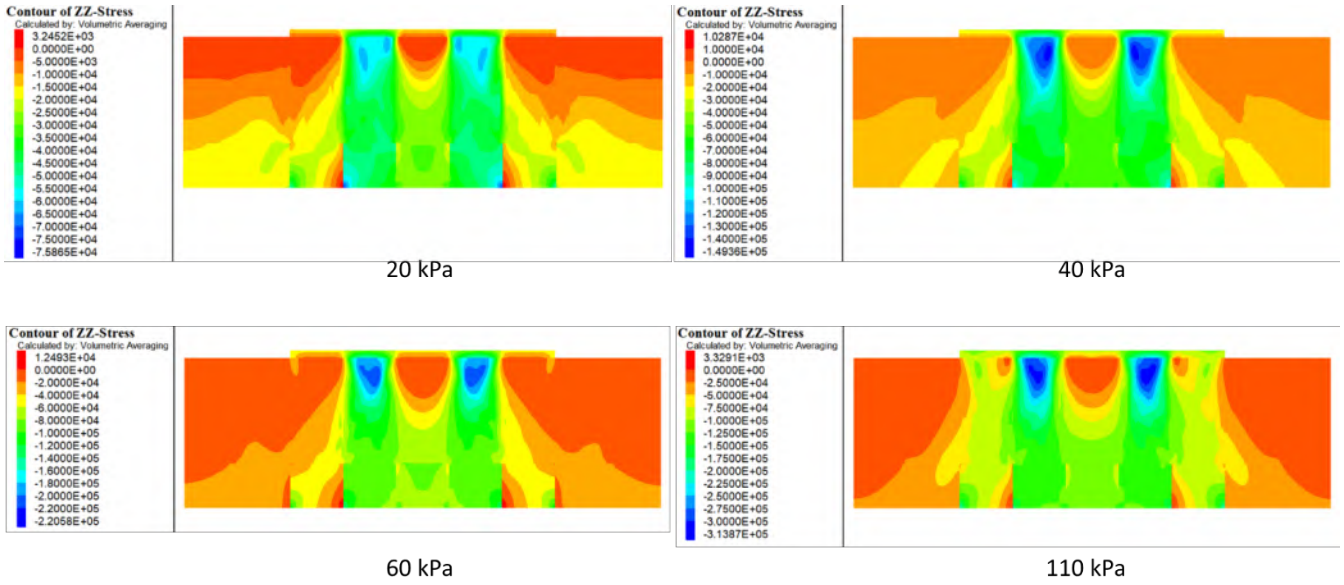

Figure 4.54: Pressure distribution of numerical model under applied loads for Test 30 (three trapdoors- 5B)

4.7 Effect of Geosynthetic Reinforcement

4.7.1 Single Reinforcement

4.7.1.1 During Trapdoor Displacement

The results for the single-trapdoor system reinforced with a geogrid at three different elevations—layer 1 (z = 0.34), layer 2 (z = 0.44), and layer 3 (z = 0.54)—clearly demonstrate the strong influence of reinforcement depth on arch mobilization, stress redistribution, and long-term stability during trapdoor displacement (Figures 4.55 and 4.56).

When the geogrid is positioned in layer 1, immediately above the yielding zone, it engages almost instantly once displacement begins. The vertical stress at the trapdoor center (TC) drops sharply from the initial ~13 kPa to less than 2 kPa within the first 3–4 mm of movement, indicating rapid diversion of load toward the supports. The trapdoor edge (TE) follows a similar decay pattern, reaching negligible residual stresses over the same displacement range. Concurrently, the support location (SE) exhibits a steep stress increase to ~19 kPa, stabilizing quickly and maintaining this value through the remainder of the displacement. This behavior is mirrored in the SRR curve, which falls from near unity to ~0.15 in the first 2–3 mm, confirming that approximately 85% of the overburden load is being transferred to the supports—a clear indication of efficient and stable arch formation.

For layer 2 placement, the geogrid is located higher within the fill, reducing its ability to engage at the earliest stages of settlement. While the general trend remains similar, TC residual stresses are consistently higher than in the layer 1 case, showing that a greater portion of the load remains directly above the yielding zone. TE stress reduction is slower, and SE stress gains are more gradual, peaking slightly lower at ~16.5–17 kPa. The SRR decreases to

~0.17–0.18 after the initial settlement phase, indicating reduced arch efficiency compared to layer 1. The slower stress transfer and lower SE peak suggest that the geogrid is mobilized later due to reduced confinement and a longer load transfer path.

In the layer 3 configuration, where the geogrid is positioned even higher ($z = 0.54$), these effects are amplified. The TC retains the highest residual stresses of all cases, stabilizing above 3 kPa even after full displacement, while TE also shows minimal unloading compared to shallower configurations. SE stress growth is both slower and lower, peaking around ~16 kPa before slightly decreasing at larger displacements, indicating partial loss of arch stability. Correspondingly, the SRR levels off at ~0.30, meaning only about 70% of the load is transferred to the supports. This high plateau value is a clear sign of weaker stress redirection and a less effective arching mechanism.

Overall, the comparison confirms that geogrid placement depth is a critical parameter in reinforced trapdoor systems. deep placement (layer 1) maximizes early tensile mobilization, enhances soil–geogrid interlock, and produces a stiffer and more resilient arch capable of sustaining high load transfer efficiency. As the reinforcement is placed higher (layers 2 and 3), the system's ability to redirect stresses to the supports is progressively reduced, residual stresses above the trapdoor increase, and the SRR plateau rises, reflecting diminished arch performance and greater vulnerability to degradation under large displacements. These findings align with established arching theories and experimental observations, which highlight that reinforcement should be placed as close as possible to the potential settlement plane to achieve optimal load redistribution.

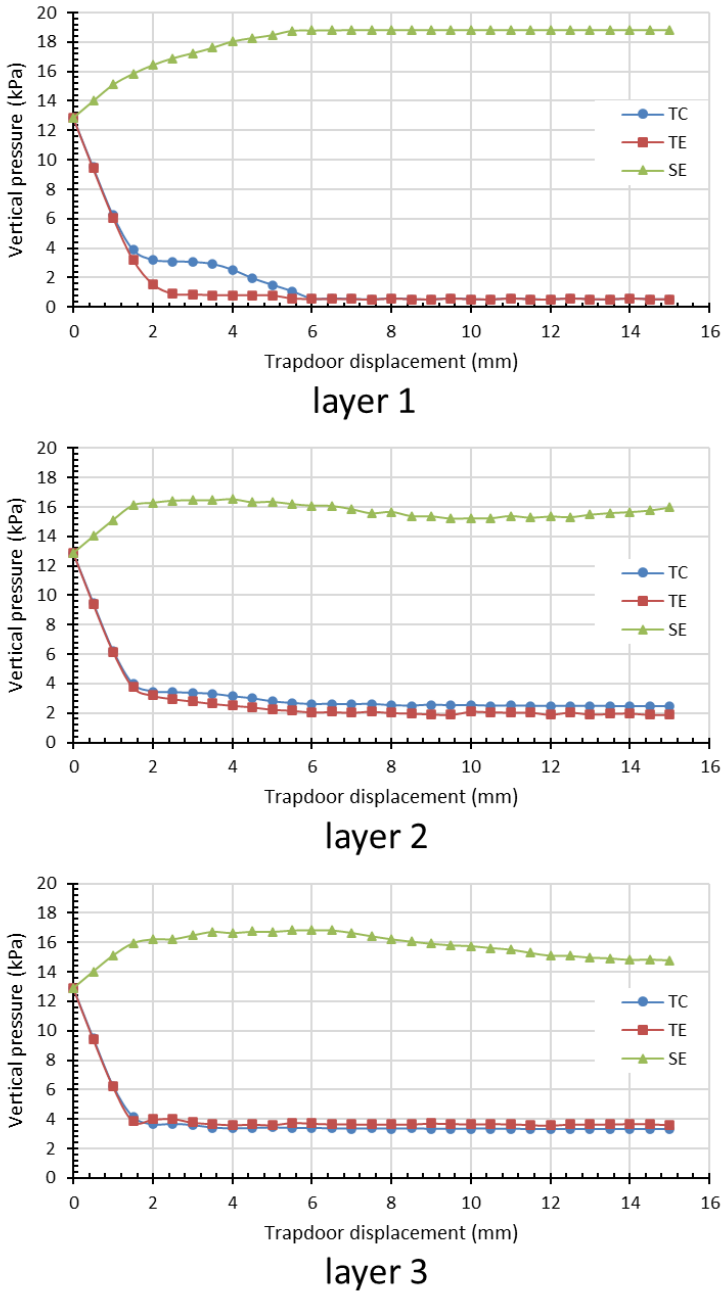

Figure 4.55: Comparison of vertical stress in relation to trapdoor displacement at three monitoring points, for Tests 31-33 (single reinforcement)

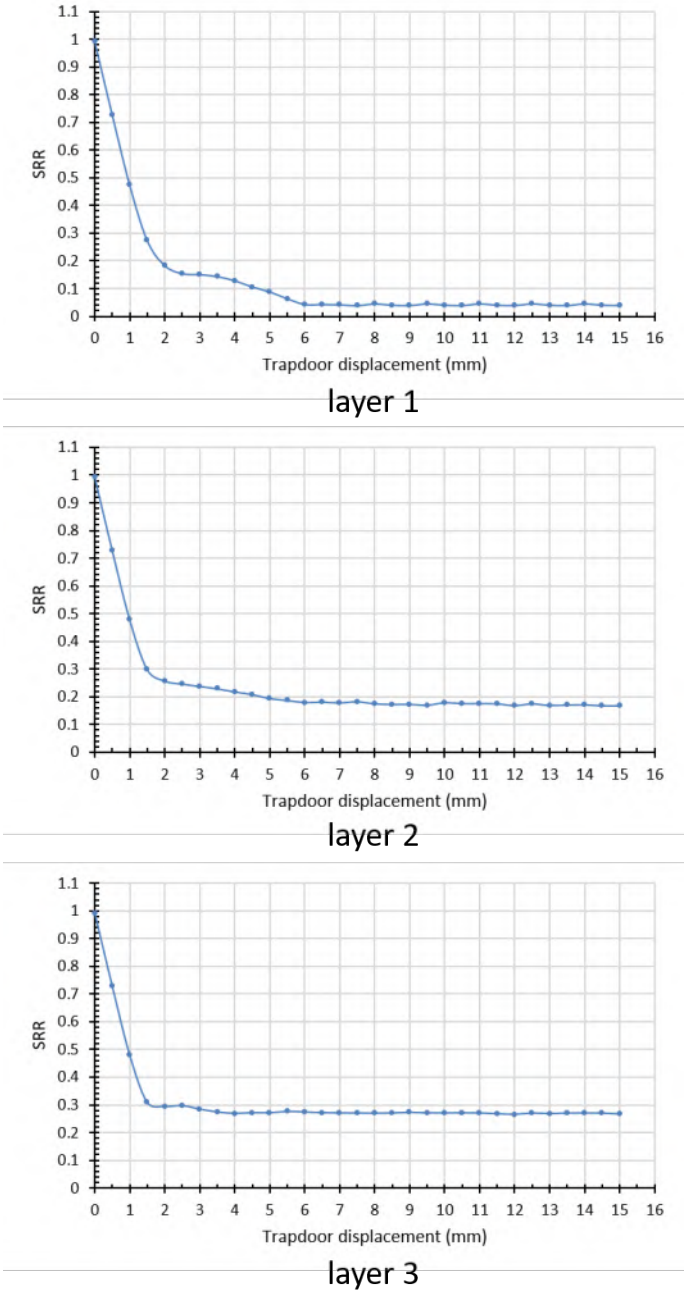

Figure 4.56: Comparison of SRR in relation to trapdoor displacement at five monitoring points, for Tests 31-33 (single reinforcement)

The stress contour evolution for the single-trapdoor system with geogrid reinforcement at three different depths (layer 1 (z = 0.34m), layer 2 (z = 0.44m), and layer 3 (z = 0.54m))provides clear visual confirmation of the depth-dependent differences in arch mobilization and stress redistribution identified in the quantitative results (Figures 4.57, 4.58, and 4.59).

For layer 1, the geogrid lies closest to the trapdoor, allowing immediate engagement as displacement begins. At 0.5–1 mm displacement, distinct stress relief zones appear above the trapdoor, and curved trajectories toward the supports are already visible. By 1.5–2 mm, the stress transfer path is fully established, with pronounced high-stress zones at the supports and minimal stress directly above the yielding area. At 4 mm displacement, the arch is stable and well-developed, with stress concentrations tightly anchored to the supports. Even at 15 mm displacement, the stress pattern remains coherent, indicating that the geogrid effectively sustains the arch against degradation.

In layer 2, the higher geogrid delays the onset of reinforcement engagement. At 0.5–1 mm displacement, stress contours remain relatively uniform above the trapdoor, with only limited lateral diversion. The first clear signs of arch development appear at 1.5–2 mm, but the stress redirection is less pronounced than in layer 1. At 4 mm, the supports carry more load, but the stress relief zone above the trapdoor remains larger than in the deeper placement. By 15 mm, arch degradation is more evident, with stress penetrating deeper into the yielding zone and a reduction in lateral confinement efficiency.

For layer 3, the highest reinforcement placement, initial displacements (0.5–1 mm) produce minimal stress redirection, and the stress field above the trapdoor remains largely vertical. At 1.5–2 mm, small lateral spreading zones appear, but the arch structure is weak. By 4 mm displacement, substantial

stress penetration is visible directly above the trapdoor, with only partial diversion toward the supports. At 15 mm, the stress contours show significant arch degradation, with nearly vertical load paths dominating.

Overall, the contour progression confirms that deep geogrid placement directly above the trapdoor (layer 1) produces the most rapid and stable arch mobilization, with superior confinement and resistance to degradation. Intermediate placement (layer 2) provides moderate performance, while high placement (layer 3) results in delayed mobilization, weaker load transfer, and accelerated arch deterioration under large displacements. These findings are consistent with the measured SRR and vertical stress trends, reinforcing that for maximum efficiency in trapdoor systems, geogrid reinforcement should be positioned as close as possible to the potential settlement plane to engage early and maintain long-term load transfer capacity.

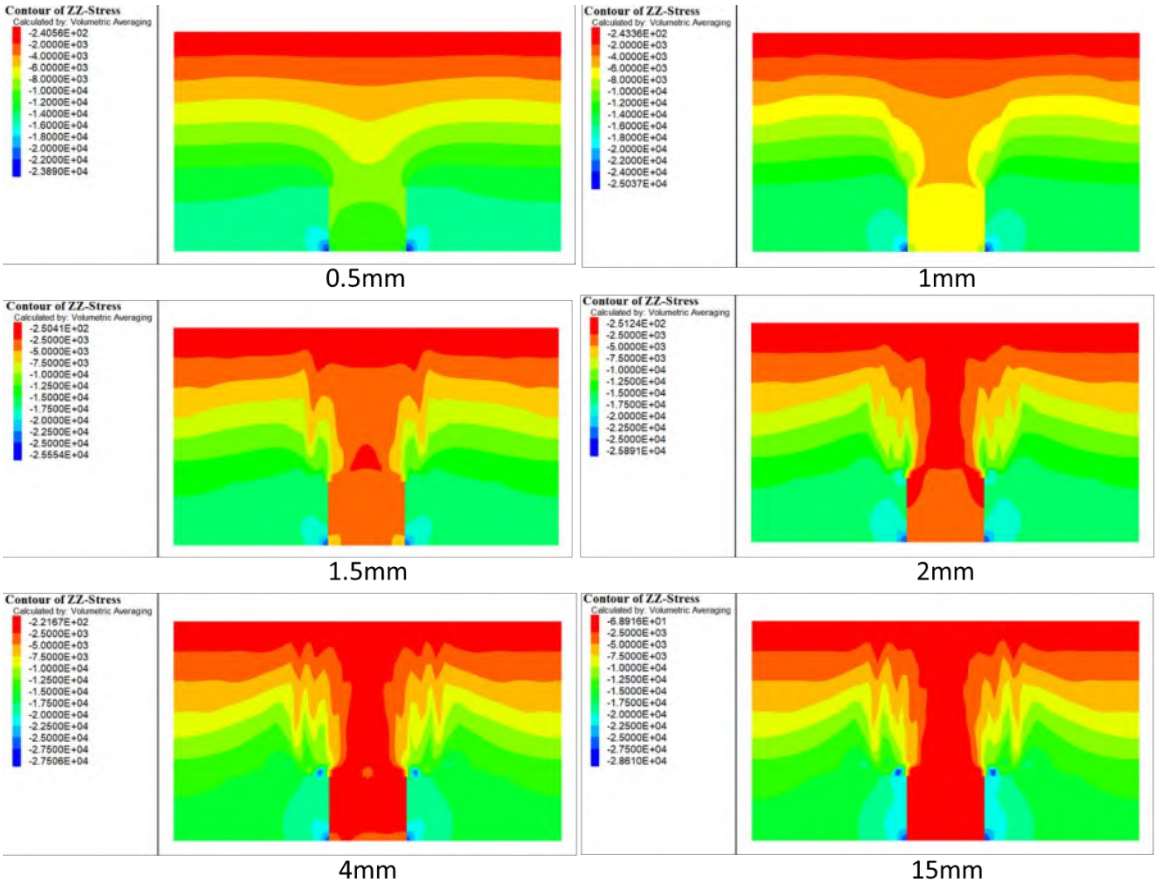

Figure 4.57: Pressure distribution of numerical model during 15mm trapdoor displacements for Test 31 (single reinforcement- layer 1)

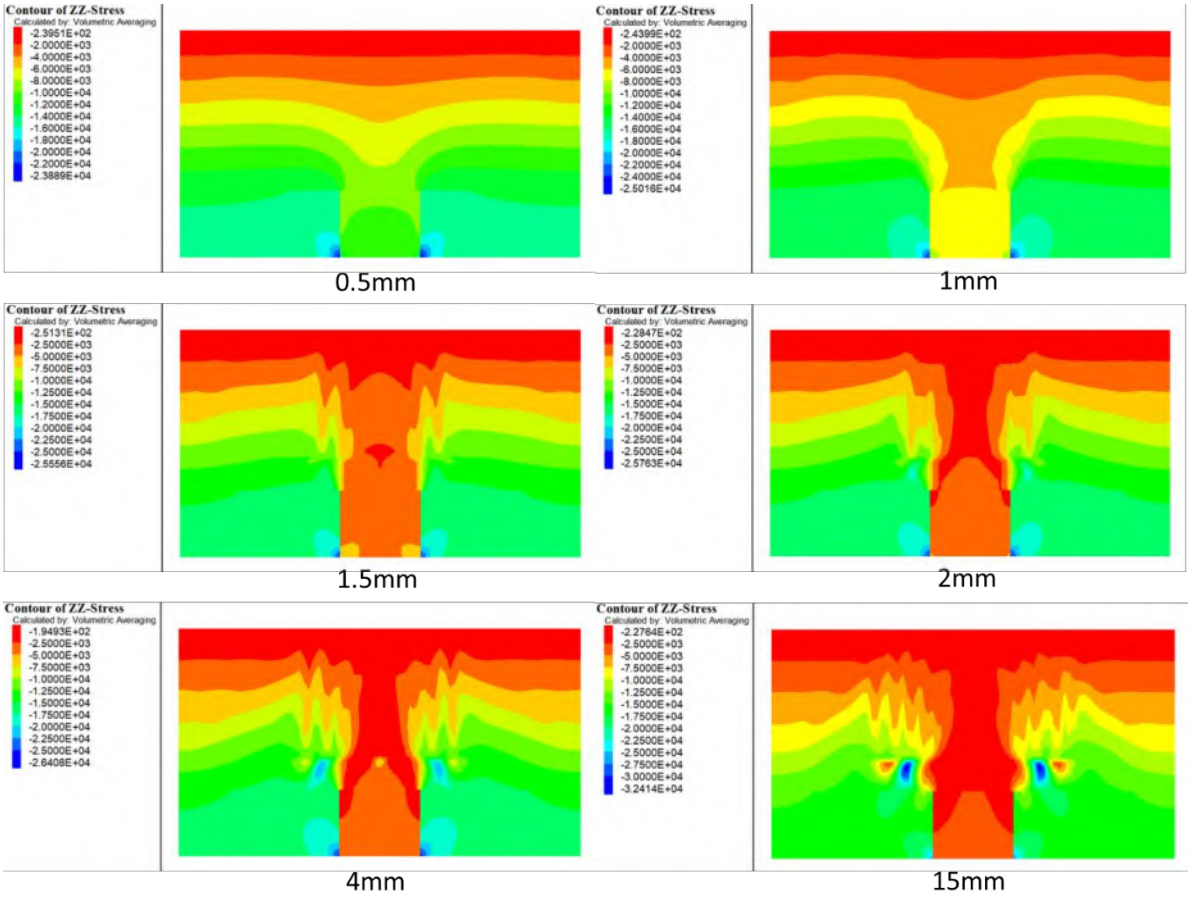

Figure 4.58: Pressure distribution of numerical model during 15mm trapdoor displacements for Test 32 (single reinforcement- layer 2)

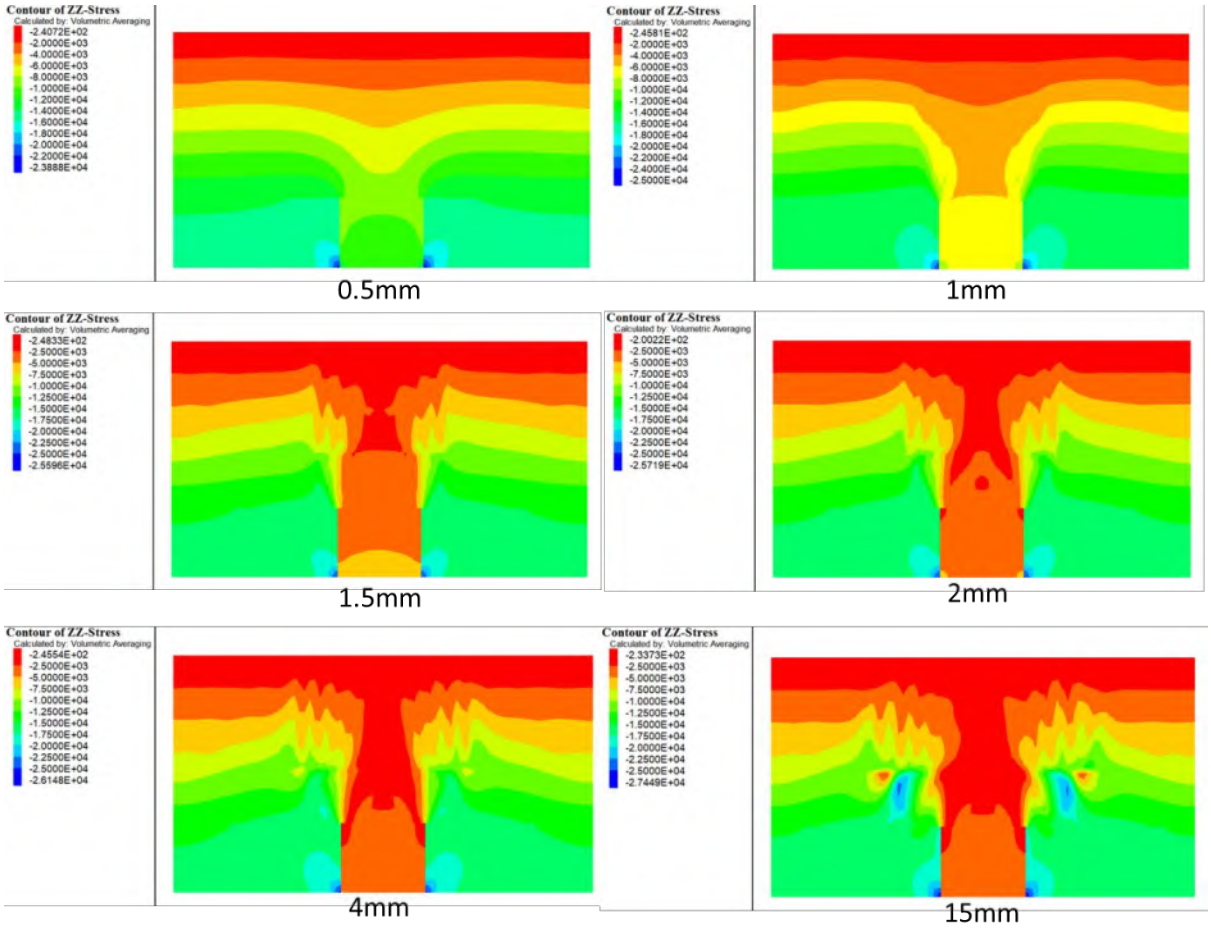

Figure 4.59: Pressure distribution of numerical model during 15mm trapdoor displacements for Test 33 (single reinforcement- layer 3)

4.7.1.2 During Footing Loading

The post-loading analysis for the single-trapdoor system reinforced with a geogrid at three depths—layer 1, layer 2, and layer 3 —demonstrates that while all configurations exhibit similar general trends in vertical stress and SRR evolution, the location of the reinforcement critically affects the timing and nature of the trapdoor center (TC) and support (SE) stress intersection, which serves as a defining marker for arch degradation and the loss of dominant lateral load transfer (Figures 4.60 and 4.61).

In layer 1, with the geogrid located directly above the trapdoor face, SE carries a significantly higher stress than TC through the early and mid-loading stages, reflecting effective redirection of load from the yielding zone toward the supports. This phase continues until the applied load reaches approximately 70 kPa, at which point the TC and SE curves intersect. The intersection marks the start of arch degradation, where the geogrid's tensile contribution and the passive resistance of the surrounding soil can no longer fully sustain the lateral load transfer mechanism. Beyond 70 kPa, TC stresses rise faster than SE stresses, indicating a progressive shift toward direct vertical load transmission to the trapdoor. Nevertheless, SRR continues to climb from ~0.55 at the intersection to ~0.75 at full load, showing that while arch efficiency diminishes after this point, the geogrid–soil system still maintains substantial load transfer capacity.

In layer 2, the intersection occurs later, at around 75 kPa applied load. This suggests that the reinforcement at this intermediate depth, while engaging slightly later than in layer 1, retains its capacity to sustain support-dominated load sharing for a longer portion of the loading range. The stress gap between TC and SE before the intersection is narrower than in layer 1, implying a slightly reduced efficiency in early-stage arch mobilization. After the intersection, TC stresses overtake SE stresses, signaling the gradual breakdown of the arching mechanism. The SRR trend reflects this behavior, rising from ~0.58 at the intersection to ~0.76 at peak load, indicating a strong but slightly delayed attainment of maximum load transfer efficiency compared to layer 1.

In layer 3, the shallowest placement, the TC–SE intersection occurs earliest, at approximately 65 kPa applied load. The geogrid's greater distance from the settlement plane delays its initial mobilization, and the weaker

confinement conditions result in a smaller initial stress advantage for the supports. As a result, the trapdoor region reaches stress parity with the supports much earlier in the loading process. After 65 kPa, TC stresses exceed SE stresses for the remainder of the loading range, indicating that the lateral arching effect is significantly weakened and that direct load transfer through the trapdoor becomes the dominant mechanism. SRR at the intersection is around ~0.50, increasing to ~0.78 at maximum load, but the slower growth compared to layers 1 and 2 suggests a prolonged period of partial arch degradation before peak efficiency is reached.

These observations confirm that the depth of reinforcement placement influences both the timing of the TC–SE intersection and the duration of effective arch performance under applied loading. The intermediate depth (layer 2) achieves the latest intersection (75 kPa), suggesting that it provides the longest sustained phase of support-dominated load transfer. The deepest placement (layer 1) intersects slightly earlier at 70 kPa but benefits from stronger early-stage arch mobilization due to immediate engagement. The shallowest placement (layer 3) performs the weakest, with the earliest intersection (65 kPa) and the longest period of reduced arch stability before maximum load. In design terms, this means that while all three placements ultimately achieve similar SRR values (~0.75–0.77), deeper or intermediate geogrid locations are preferable for maximizing the stability window before arch degradation occurs.

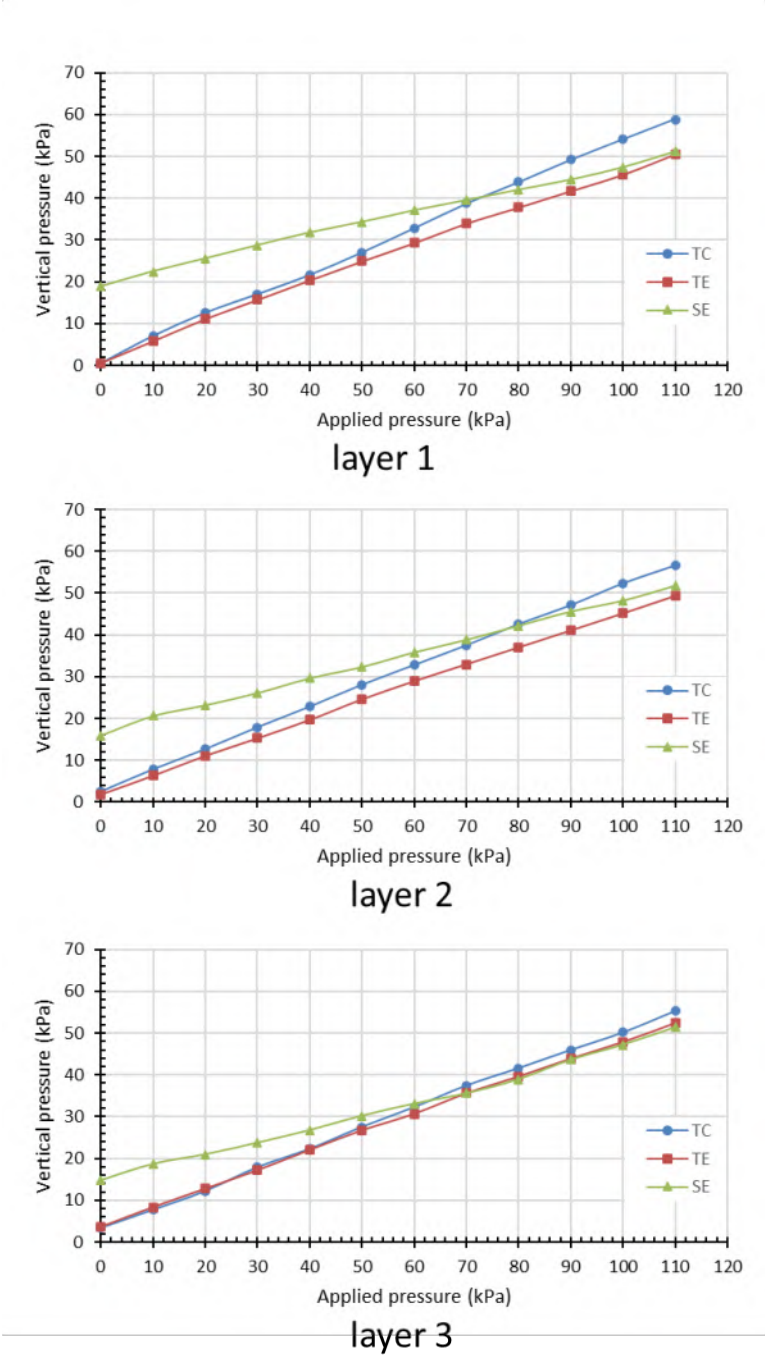

Figure 4.60: Comparison of vertical stress in relation to monotonic static footing pressure in the loading test at three monitoring points , for Tests 31-33 (single reinforcement)

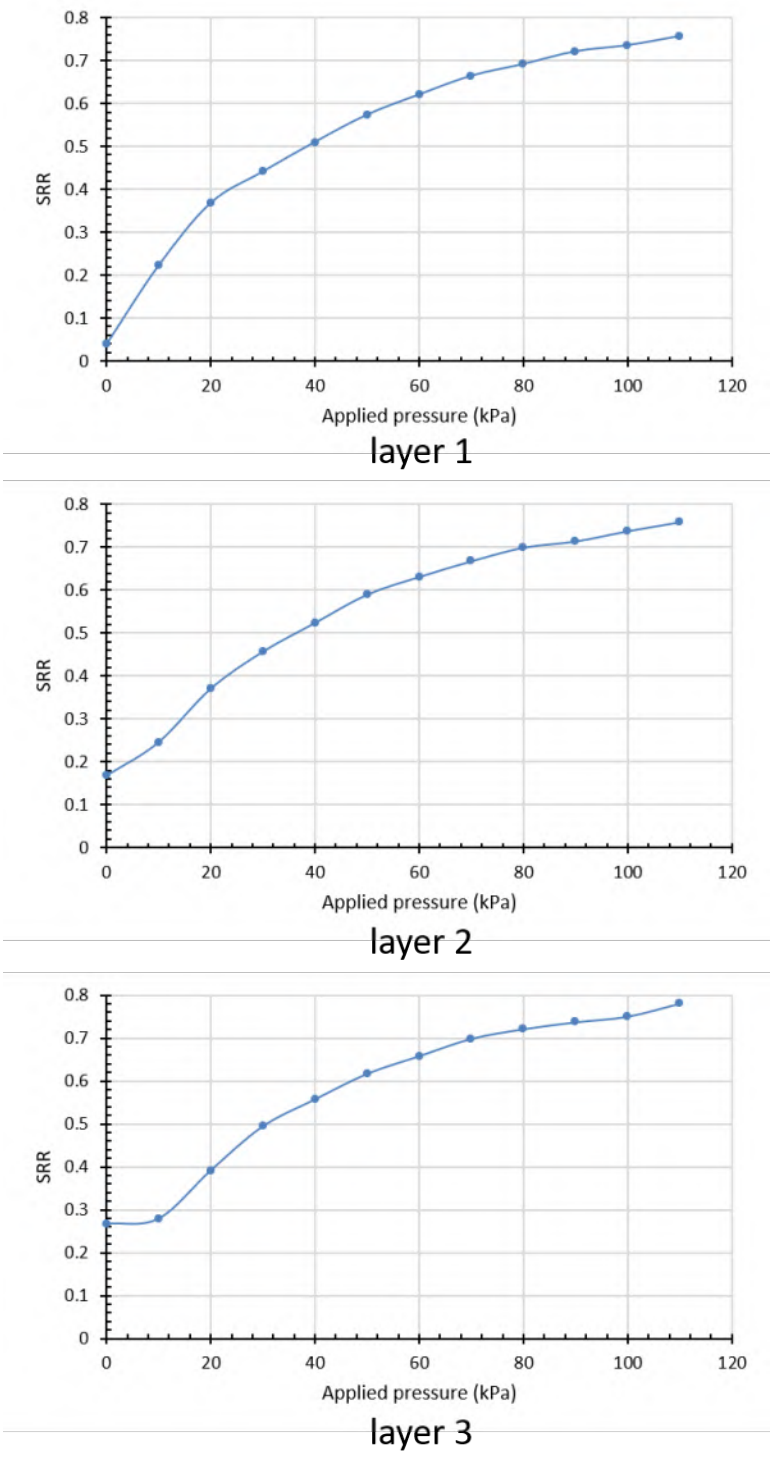

Figure 4.61: Comparison of SRR in relation to monotonic static footing pressure in the loading test at nine monitoring points , for Tests 31-33 (single reinforcement)

The post-loading stress contour sequences for these three cases provide direct visual evidence of the changing load transfer mechanisms leading up to, and following, the TC–SE stress intersection points identified in the vertical stress plots (Figures 4.62-4.64) .

In layer 1, at low load (20 kPa), the contours reveal a clearly defined arching zone above the trapdoor, with curved stress trajectories redirecting vertical load toward the supports. The high-stress zones at the supports dominate, and stress penetration above the trapdoor is minimal. At 40 kPa, the arch is fully mobilized, with strong confinement visible directly above the trapdoor face. By 80 kPa—close to the 70 kPa intersection point—the contours show a notable increase in vertical stress penetration toward the trapdoor center, while support stress zones remain strong but begin to lose dominance. At 110 kPa, after the intersection, stress transfer becomes more vertical, with reduced curvature in the load paths, indicating partial arch degradation and a shift toward trapdoor-dominated load bearing.

For layer 2, the intermediate depth, the early loading stage at 20 kPa shows a functional but less pronounced arch compared to layer 1, with smaller high-stress zones at the supports. At 40 kPa, lateral stress transfer improves, but the influence of the geogrid is less intense due to its greater distance from the settlement plane. At 80 kPa, the contours show a balanced stress distribution, with SE still slightly dominant. By 110 kPa, post-intersection, the stress field exhibits a marked reduction in lateral transfer efficiency, with nearly vertical stress paths over the trapdoor, though some confinement remains due to the reinforcement's engagement.

In layer 3, the shallowest placement, the 20 kPa contours display a relatively uniform vertical stress field, indicating delayed geogrid activation. At 40 kPa, modest lateral stress spreading is visible, but arch definition

remains weak. At 80 kPa—well beyond the 65 kPa intersection point—the contours show that stress above the trapdoor already equals or exceeds that at the supports, confirming that the arching effect has largely degraded earlier in the loading process compared to deeper placements. By 110 kPa, the stress field is dominated by vertical transmission through the trapdoor, with minimal evidence of an effective load transfer pathway to the supports.

The contour evolution supports the key findings from the stress–load curves: deeper reinforcement placement (layer 1) engages earliest, forms the strongest and most stable arches, and delays the TC–SE intersection to higher loads, prolonging the support-dominated phase of load transfer. Intermediate depth (layer 2) achieves the latest intersection but with slightly reduced early-stage confinement. Shallow placement (layer 3) produces the earliest intersection and weakest lateral stress transfer, leading to rapid arch degradation and premature trapdoor dominance under applied surface loads.

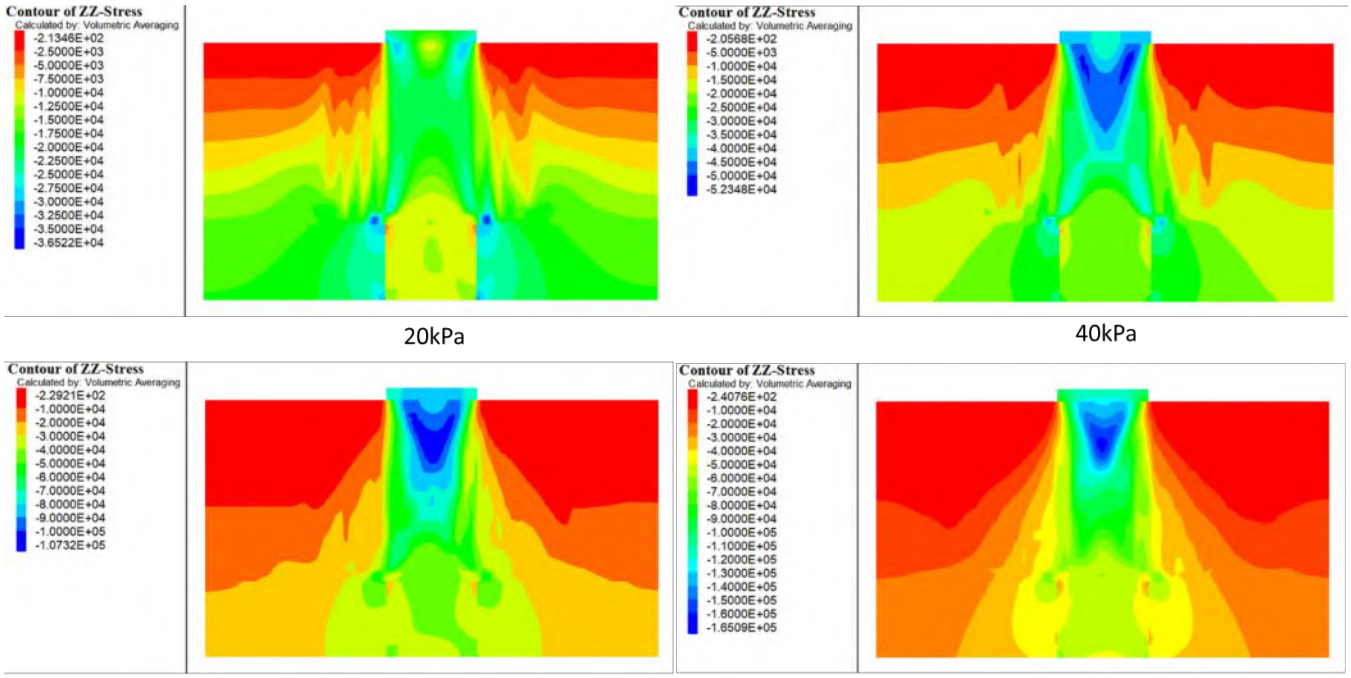

Figure 4.62: Pressure distribution of numerical model under applied loads for Test 31 (single reinforcement-layer 1)

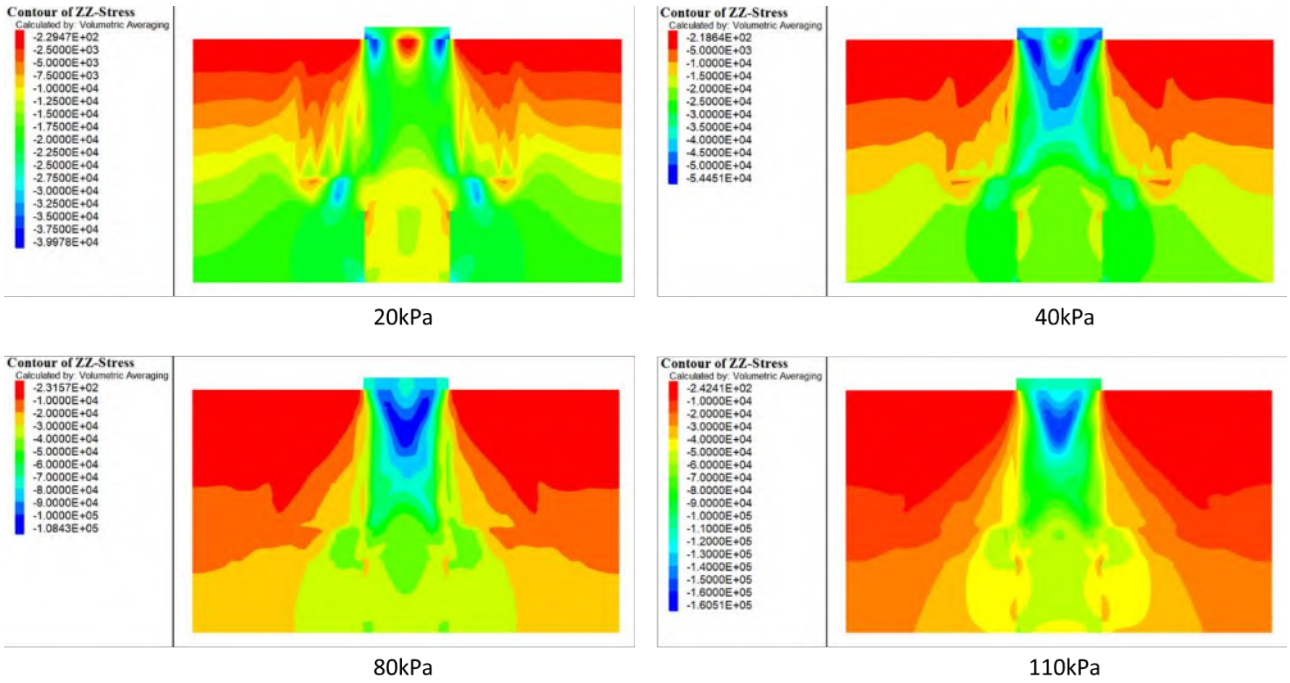

Figure 4.63: Pressure distribution of numerical model under applied loads for Test 32 (single reinforcement-layer 2)

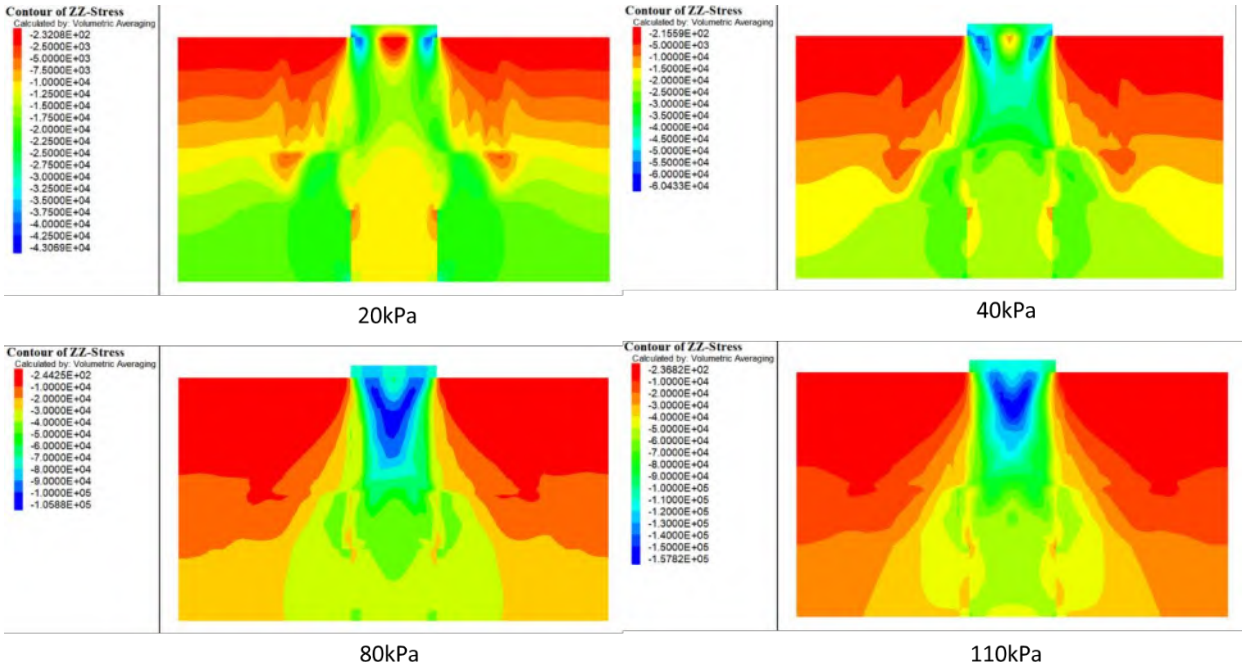

Figure 4.64: Pressure distribution of numerical model under applied loads for Test 33 (single reinforcement-layer 3)

4.7.2 Single Reinforcement Using Geogrid Structure

The numerical simulation for the single-reinforced case in layer 1 (deepest placement, z = 0.34) using a FLAC3D geogrid structural element exhibits a broadly similar load transfer response to the corresponding liner element model, but with measurable differences in stress redistribution during the settlement and loading phases that reflect the distinct mechanical characteristics of the two structural types.

During the trapdoor displacement stage shown in Figure 4.65, both models show rapid mobilization of the soil arching mechanism within approximately 2 mm of movement, with a sharp reduction in stresses at the trapdoor center (TC) and trapdoor edge (TE) and a corresponding increase at the support (SE). In the geogrid-based model, however, residual stresses above the trapdoor are slightly higher (TC and TE ≈ 3 kPa) compared with the liner-based model, where they fall to ≤ 1 kPa. This indicates marginally reduced unloading efficiency when the reinforcement is modeled purely as a tensile membrane. The increased residual stress is attributed to the flexibility of the geogrid element, which, lacking bending and shear stiffness, allows localized sagging and the retention of a small portion of vertical load above the trapdoor rather than enforcing a rigid arch shoulder.

Under applied surface loading shown in Figure 4.66, the general load–stress trend remains consistent between the two modeling approaches. In both cases, SE carries a greater share of the load than TC through the early and mid-loading stages until the TC–SE stress intersection occurs at approximately 70 kPa applied load. This convergence point marks the onset of arch degradation, where vertical load penetration into the trapdoor region increases and lateral load transfer efficiency diminishes. Following the intersection, TC stresses surpass SE stresses, and TE follows TC closely,

indicating a shift toward trapdoor-dominated load bearing. While the timing of the intersection is the same in both models, the geogrid-based simulation exhibits a slightly smaller stress differential between TC and SE before the intersection, suggesting that the arching effect, though still strong, is marginally less pronounced than in the liner-based model.

In summary, while the geogrid and liner models for layer 1 share the same TC–SE intersection load (70 kPa) and capture the same qualitative transition from support-dominated to trapdoor-dominated load transfer, the geogrid element results in higher residual stresses during settlement and a slightly less distinct early-stage stress contrast. These differences highlight the influence of reinforcement structural formulation on arch mobilization and stress redistribution, underscoring the importance of calibrating geogrid tensile stiffness and interface properties to replicate experimental performance accurately.

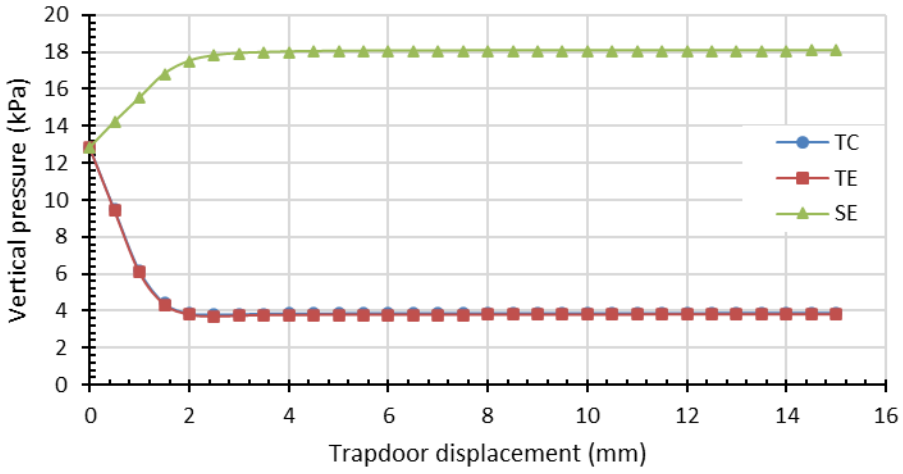

Figure 4.65: Comparison of vertical stress in relation to trapdoor displacement at three monitoring points, for Test 34 (single reinforcement)

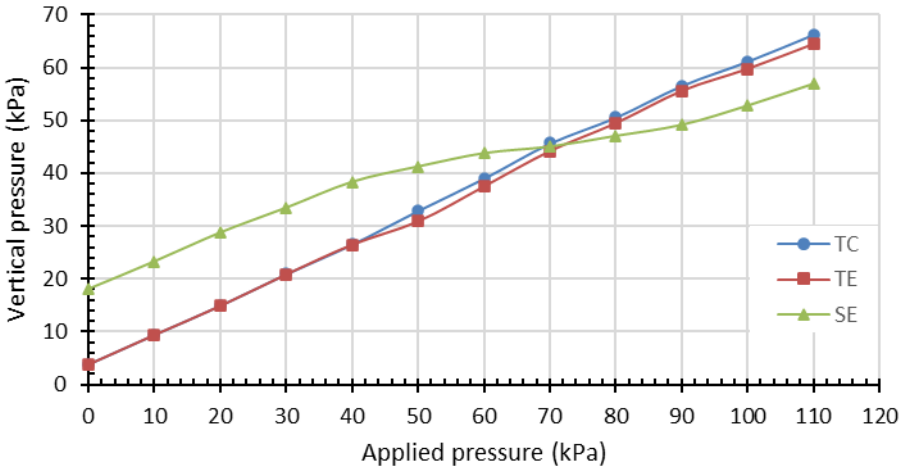

Figure 4.66: Comparison of vertical stress in relation to monotonic static footing pressure in the loading test at three monitoring points , for Test 34 (single reinforcement)

4.7.3 Multiple Reinforcements

4.7.3.1 During Trapdoor Displacement

The displacement-phase results clearly demonstrate that the incorporation of multiple reinforcement courses significantly enhances the mobilization of soil arching and reduces residual vertical stresses above the trapdoor compared with the single-reinforced liner configuration, albeit with diminishing returns beyond two layers (Figures 4.67 and 4.68).

In the single reinforced case, the trapdoor center (TC) and trapdoor edge (TE) stresses exhibit a rapid initial reduction during the first few millimeters of displacement, stabilizing at residual values of approximately 1 kPa by 3–4 mm. Concurrently, the support (SE) stress rises to a plateau of ~18 kPa, reflecting the redirection of vertical load from the yielding zone toward the supports. The Soil Arching Ratio (SRR) stabilizes at ~0.15, indicating that

roughly 85% of the overburden load is effectively transferred to the supports in the steady state.

With double reinforcement, the stress decay at TC and TE is both faster and deeper, with values approaching 0–0.5 kPa within approximately 3 mm of displacement. SE stresses reach their peak magnitude (~17.5 kPa) earlier, at around 2–3 mm, indicating a more rapid establishment of the arching mechanism. The SRR stabilizes at a significantly lower plateau of approximately 0.06–0.07, representing a substantial improvement in arching efficiency compared to the single-RC case. This improvement reflects the enhanced tensile stiffness and confinement provided by the second reinforcement layer, which promotes quicker mobilization of tensile forces and earlier load diversion to the supports.

The triple reinforcement case further accelerates arch mobilization, with TC stresses reaching negligible levels (≈0-0.4 kPa) by 2–3 mm displacement and SRR settling at an even lower plateau of ~0.05. However, SE's ultimate stress plateau remains essentially unchanged (~17 kPa) compared to the double reinforcement case, suggesting that the third layer primarily contributes to marginal reductions in residual stresses over the trapdoor without significantly increasing the total load carried by the supports. This indicates that, once two layers are mobilized, the majority of load transfer capacity is already engaged, and additional layers yield only incremental gains in efficiency.

From a mechanistic perspective, the improved performance with multiple reinforcement can be attributed to the combined effects of increased overall tensile stiffness, improved soil–reinforcement interaction, and the formation of overlapping or compound arches that enhance confinement and reduce stress penetration into the yielding zone. However, the results also

highlight a point of diminishing returns: while the transition from single to double reinforcement produces a marked reduction in SRR (~60–70% lower plateau), the addition of a third layer offers only a modest further improvement.

In design terms, these findings suggest that two reinforcement layers provide the optimal balance between performance enhancement and material use, delivering the majority of achievable gains in arching efficiency, while additional layers may be justified only in scenarios where minimal residual trapdoor stress is critical for serviceability or long-term performance.

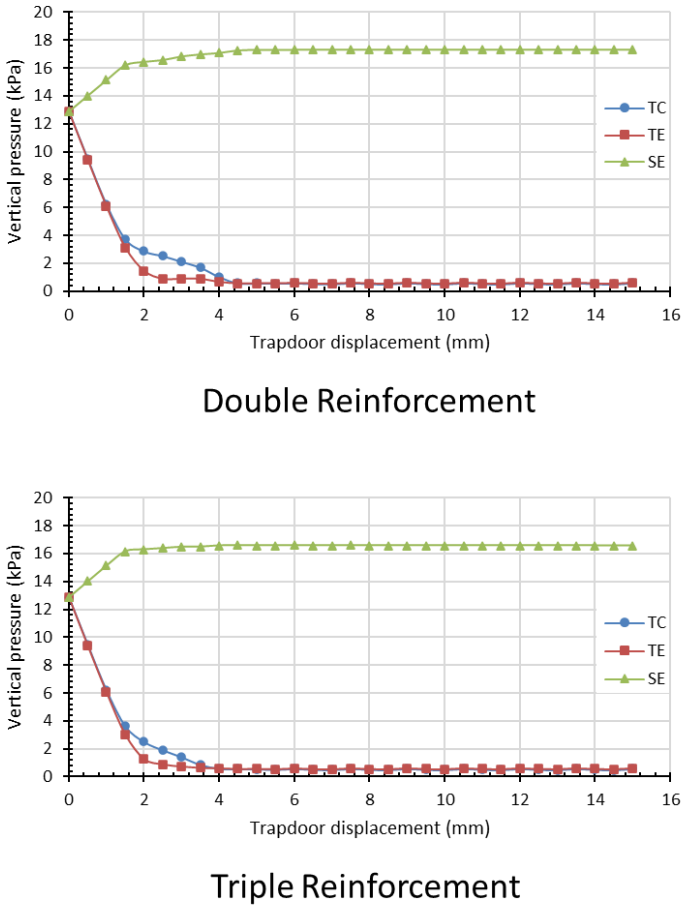

Figure 4.67: Comparison of vertical stress in relation to trapdoor displacement at three monitoring points, for Tests 35 and 36 (multiple

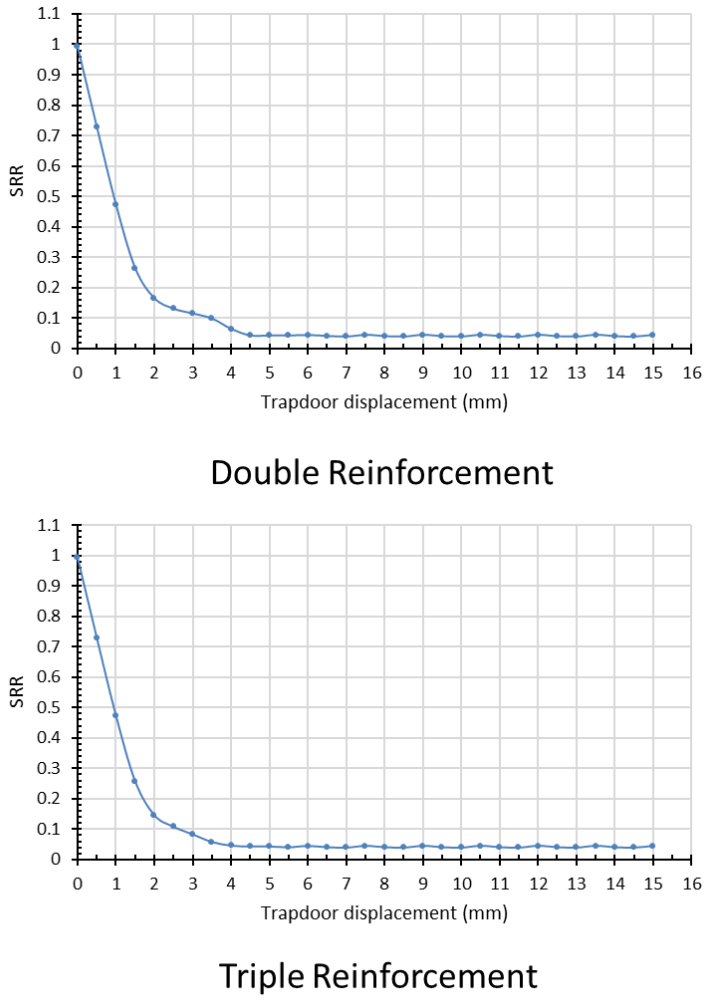

Figure 4.68: Comparison of SRR in relation to trapdoor displacement at three monitoring points, for Tests 35 and 36 (multiple reinforcement)

The contour plots of vertical stress distribution for the double and triple reinforcement configurations further clarify the mechanisms underlying the quantitative trends observed in the displacement–stress and SRR curves.

As shown in Figures 4.69 and 4.70, at the early displacement stages (0.5–1 mm), both configurations exhibit a relatively uniform vertical stress field above the trapdoor, with stress concentration zones at the supports beginning to intensify. However, in the triple reinforcement case, the initial

arch formation is slightly more pronounced, as indicated by the earlier onset of stress attenuation at the trapdoor center (TC) and the more distinct upward curvature of the isostress lines.

By 1.5–2 mm displacement, the influence of multiple reinforcement layers becomes more apparent. In the double reinforcement case, stress transfer to the supports is well established, but vertical stress penetration into the trapdoor zone remains slightly higher compared with the triple configuration. The triple reinforcement case shows a narrower high-stress band above the supports and a larger low-stress cavity directly over the trapdoor, indicating more effective load diversion. This suggests that the third reinforcement layer accelerates the suppression of vertical stress within the yielding zone, leading to earlier and more complete mobilization of the soil arching mechanism.

At intermediate displacements (4 mm), the differences between the two systems become more subtle. Both configurations exhibit fully developed arching with stable load transfer paths toward the supports. However, the triple reinforcement system maintains a marginally larger low-stress region above the trapdoor, reflecting slightly reduced residual stress compared with the double reinforcement case.

By the final stage (15 mm displacement), both double and triple configurations show similar mature arch geometries, with stress contours predominantly aligned to the load transfer paths toward the supports. The triple reinforcement continues to exhibit slightly broader low-stress zones within the central span, but the overall difference in stress distribution relative to the double reinforcement case is minimal—corroborating the earlier finding that the performance gains from adding a third layer are incremental rather than transformational.

In summary, the contour plots confirm that while both double and triple reinforcement layers significantly enhance arching development compared to a single layer, the most substantial improvement occurs when transitioning from one to two layers. The third layer primarily refines the stress field, accelerating the early-stage load transfer and slightly reducing residual stresses, but offers only marginal benefit in the fully mobilized arching stage.

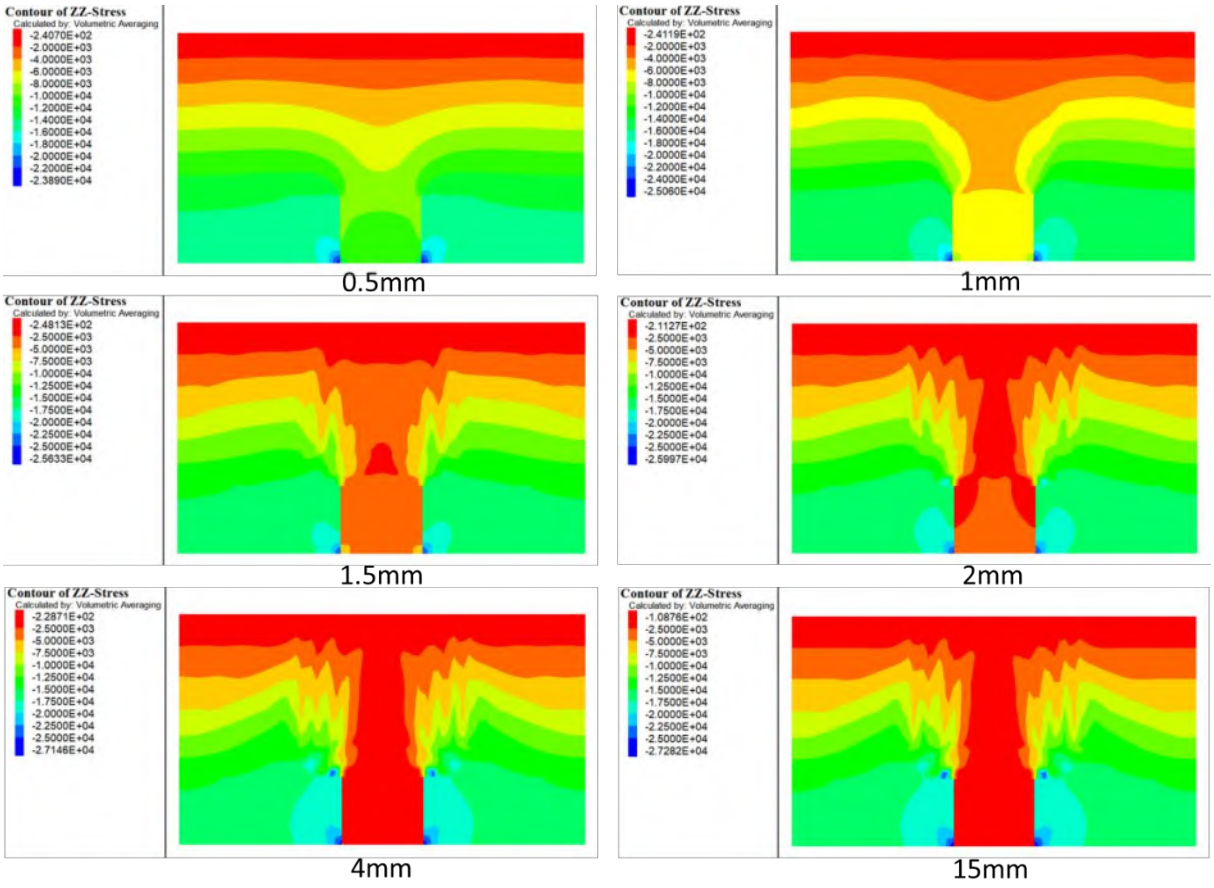

Figure 4.69: Pressure distribution of numerical model during 15mm trapdoor displacements for Test 35 (double reinforcement)

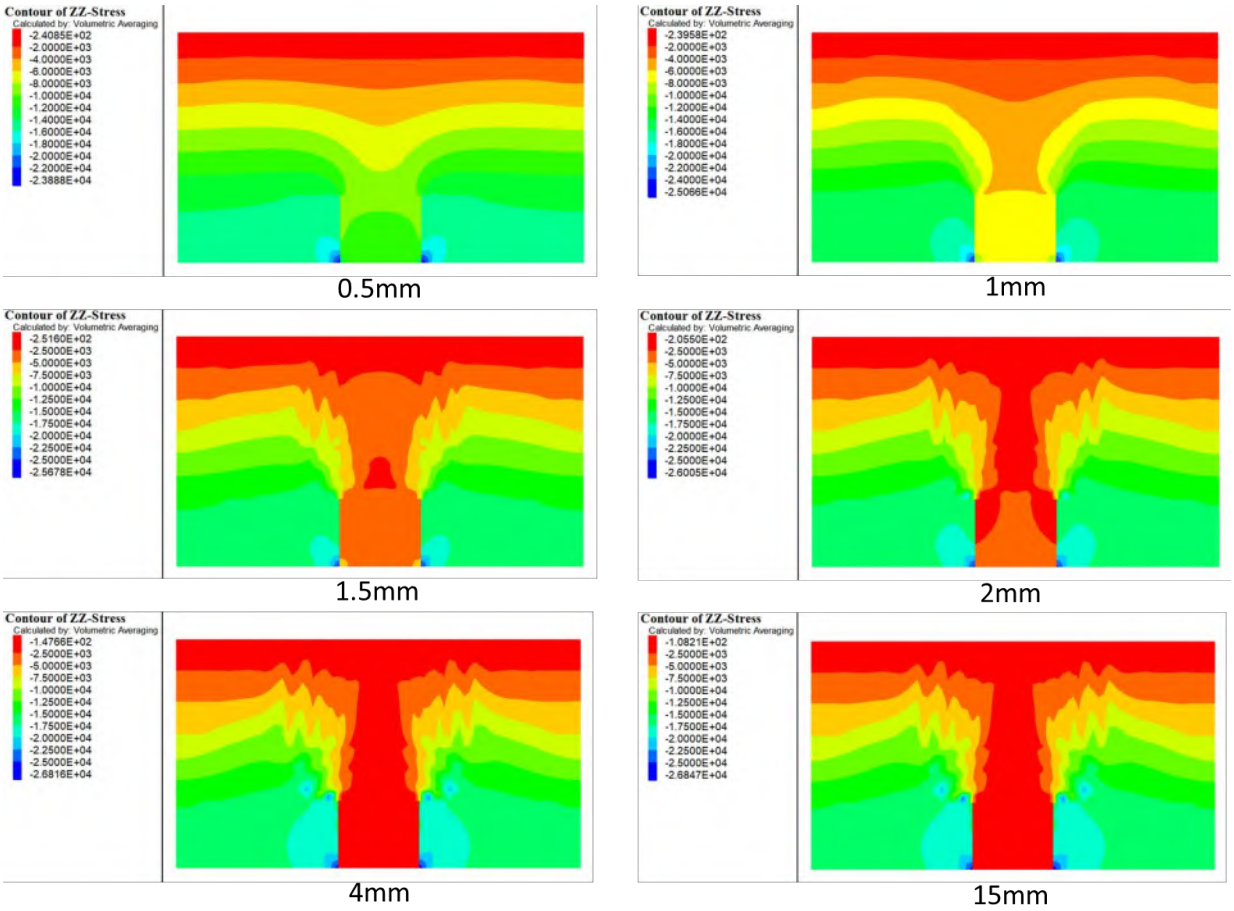

Figure 4.70: Pressure distribution of numerical model during 15mm trapdoor displacements for Test 36 (triple reinforcement)

4.7.3.2 During Footing Loading

The post-loading response for the double and triple reinforcement configurations reveals consistent trends in vertical stress distribution and Soil Arching Ratio (SRR) evolution, while also highlighting subtle distinctions in performance attributable to the number of reinforcement layers (Figures 4.71 and 4.72).

For double reinforcement, the vertical stress distribution curves indicate a steady increase in TC, TE, and SE stresses with applied surface pressure, with SE consistently maintaining the highest stress values due to its role as the primary load-bearing zone. TC and TE follow closely, converging progressively as the applied pressure increases, until intersecting with SE at approximately 108 kPa. This intersection point marks the onset of significant soil arching degradation, where the ability of the reinforcement layers to sustain differential load transfer diminishes and the stress field begins to homogenize across the trapdoor and support zones.

In contrast, the triple-reinforced configuration demonstrates no intersection between TC and SE throughout the loading range up to 110 kPa. In this case, the SE consistently maintains higher vertical stresses than TC, signifying that the arching mechanism remains effectively mobilised and the load transfer to the supports persists even at elevated surface pressures.

The stress arching ratio (SRR) for both configurations exhibits a rapid increase at low pressures, followed by a gradual approach towards a plateau value of approximately 0.70–0.75. However, the triple-reinforced case maintains a slightly greater disparity between TC and SE stresses across the loading spectrum, reflecting sustained lateral load diversion. The absence of intersection in the triple-reinforced model can be attributed to the enhanced composite stiffness provided by the additional reinforcement layer, which promotes the formation of overlapping and mutually stabilising soil arches. This configuration confines the deformation zone above the trapdoor more effectively, thereby delaying or entirely suppressing the breakdown of the arching mechanism. Consequently, the triple-reinforced system extends the stability range under service loading conditions, reducing the likelihood of late-stage arch collapse and limiting stress concentration at the trapdoor, a

performance enhancement of particular significance for structures subjected to sustained or high-intensity loads.

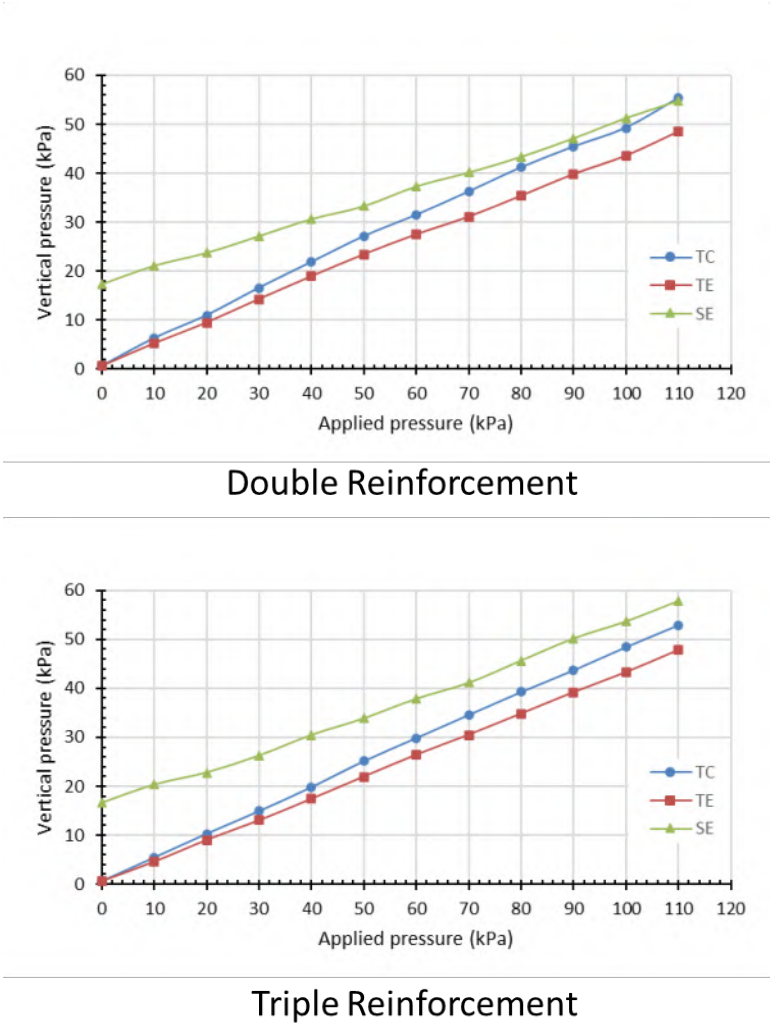

Figure 4.71: Comparison of vertical stress in relation to monotonic static footing pressure in the loading test at three monitoring points , for Tests 35 and 36 (multiple reinforcement)

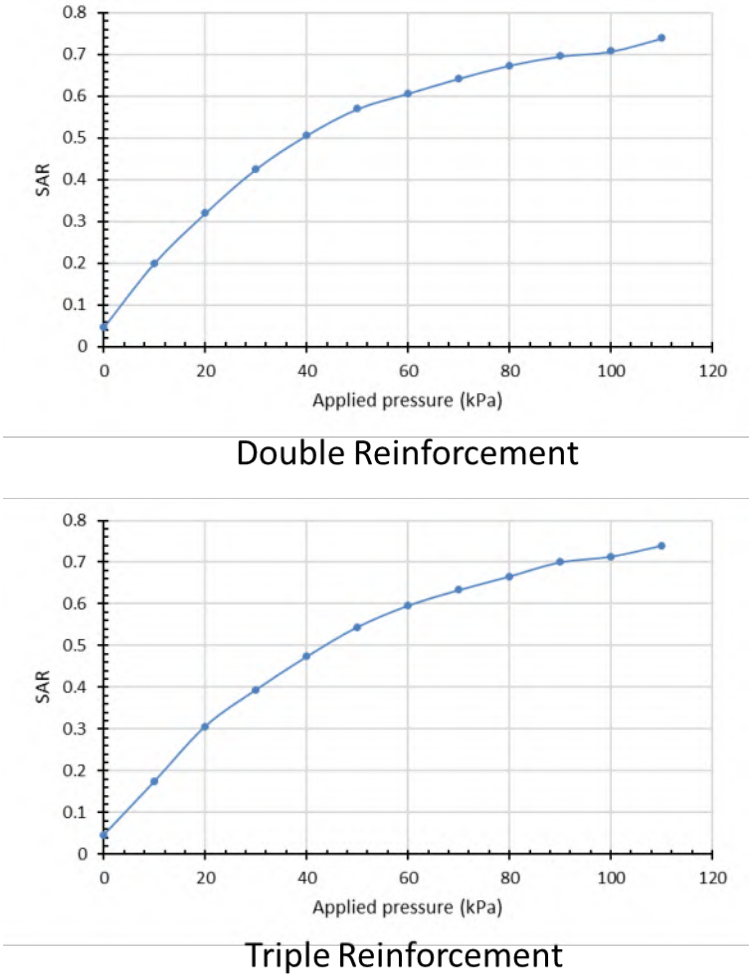

Figure 4.72: Comparison of SRR in relation to monotonic static footing pressure in the loading test at three monitoring points , for Tests 35 and 36 (multiple reinforcement)

The contour plots for the double- and triple-reinforced shown in Figures (4.73 and 4.74) configurations further elucidate the differences in stress redistribution and arching stability observed in the quantitative results. For the double-reinforced case, at the early loading stages (20 kPa and 40 kPa), the stress contours reveal a pronounced diversion of vertical stresses toward the stationary supports, indicating an effectively mobilised soil arch. However, by 80 kPa, the concentration of stresses above the trapdoor becomes more apparent, and at 110 kPa the contours show a significant reduction in lateral load transfer efficiency, consistent with the intersection between TC and SE observed in the vertical stress curves. This reflects a progressive breakdown of the arching mechanism, allowing more load to be transmitted directly to the trapdoor area.

In contrast, the triple-reinforced configuration maintains a more robust and stable arching profile across all loading stages. At 20 kPa and 40 kPa, the stress diversion patterns are similar to those in the double-reinforced model; however, at 80 kPa and even at 110 kPa, the contours show sustained lateral stress concentration towards the supports, with minimal encroachment of high-stress zones into the trapdoor region. This stability directly supports the absence of an intersection point between TC and SE in the triple-reinforced loading curves, indicating that the arching mechanism remains intact throughout the loading process. The additional reinforcement layer enhances the composite stiffness of the system, promoting multiple overlapping arches that resist deformation and confine stress redistribution to the support zones. Consequently, the triple-reinforced model demonstrates an extended service load capacity, improved structural resilience, and a delayed or entirely suppressed onset of arching degradation compared to the double-reinforced arrangement.

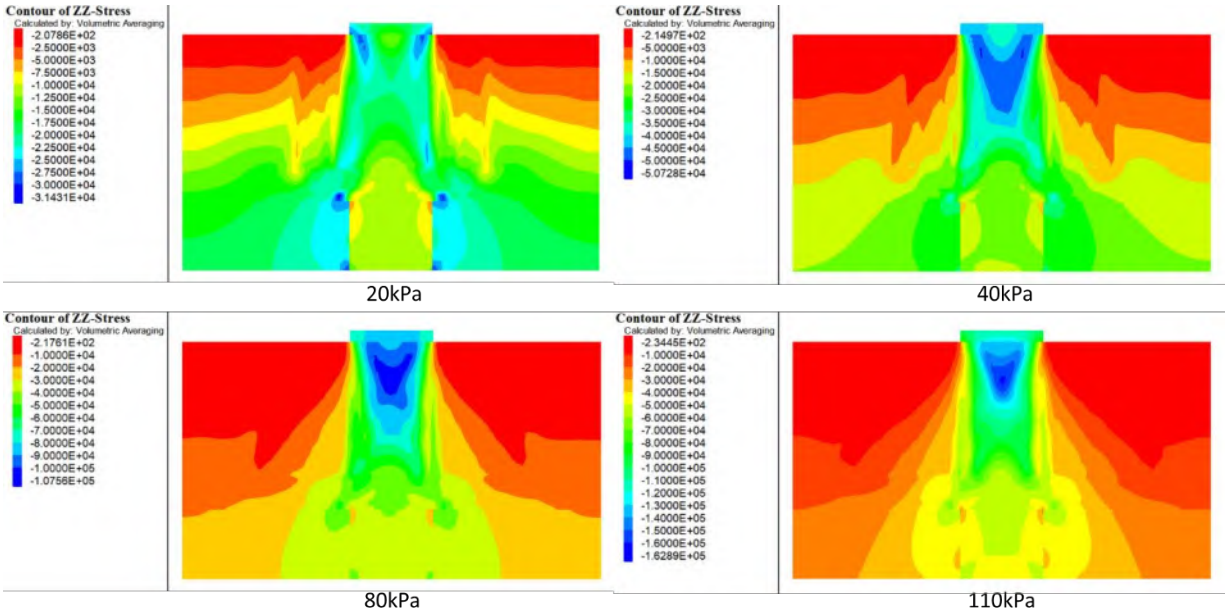

Figure 4.73: Pressure distribution of numerical model under applied loads for Test 35 (double reinforcement)

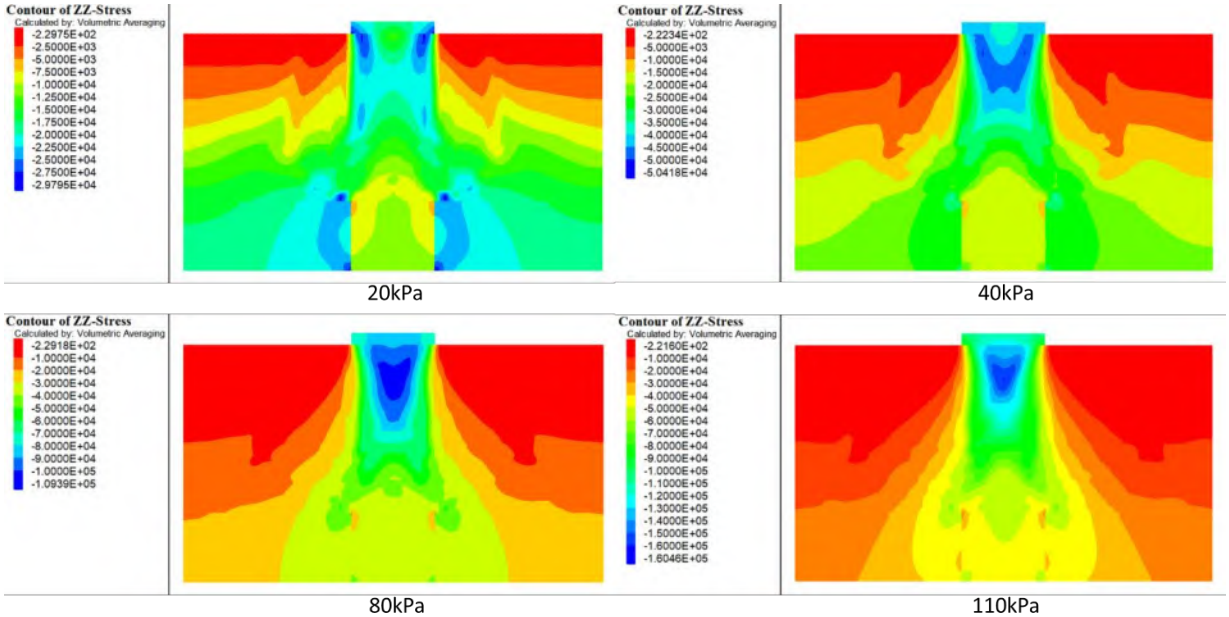

Figure 4.74: Pressure distribution of numerical model under applied loads for Test 36 (triple reinforcement)

Chapter V

Conclusions and Recommendations

Chapter Five: Conclusions and Recommendations

5.1 Conclusions

This research has presented a comprehensive numerical investigation of the performance of load transfer platforms (LTP) constructed over rigid inclusions and subjected to localized subsidence conditions, simulated through a trapdoor mechanism. The key conclusions drawn from this study are summarized as follows:

1. This study is demonstrating the value of employing the finite difference method to analyze the behavior of geosynthetic-reinforced load transfer platforms subjected to localized subsidence. The close agreement between the numerical predictions and the experimental results of Al-Naddaf (2017), with differences generally within 5–8%, is confirming the reliability of the modelling approach. The research is providing a deeper understanding of stress redistribution, soil arching, and reinforcement effects, offering practical guidance for optimizing load transfer platform design in engineering applications.
2. Soil arching is mobilizing rapidly at small trapdoor displacements, transferring up to 70% of vertical stress to adjacent supports at a displacement of 4 mm. Arching efficiency is progressively decreasing as settlement increases, highlighting the importance of controlling deformation to maintain effective load redistribution.
3. The inclusion of geosynthetic reinforcement is significantly improving platform performance. A single reinforcement layer is reducing vertical stress on the trapdoor by approximately 35%, while double and triple layers are achieving reductions exceeding 60%.

4. Increasing the number and width of trapdoors is altering the load transfer mechanism by dividing the embankment into multiple interacting arching zones. This configuration is enhancing stress uniformity and limiting local settlements by up to 40%, demonstrating the importance of considering multi-trapdoor arrangements in design.
5. The footing width and its offset from the trapdoor center are influencing load transfer efficiency. Wider footings and larger offsets are increasing stress transfer to supports by approximately 20–25%, thereby improving stability and reducing deformation above yielding zones.
6. Geosynthetic reinforcement is maintaining soil arching at higher displacements, delaying arch degradation, and improving stress reduction by as much as 65% compared with unreinforced conditions. These results are confirming the reinforcement's effectiveness in sustaining platform performance under increased subsidence or loading.

Overall, this research is contributing to a comprehensive understanding of load transfer platforms over rigid inclusions and is establishing finite difference modelling as a robust tool for predicting their behavior. The findings are equipping engineers with validated guidance for designing platforms that optimize soil arching, minimize settlements, and enhance the long-term serviceability of embankments and similar geotechnical structures.

5.2 Recommendations

5.2.1 Experimental Studies

1. Conduct additional large-scale trapdoor tests to validate the behaviour of load transfer platforms under various soil types, reinforcement layouts, and trapdoor configurations.
2. Investigate the response of geosynthetic-reinforced platforms to cyclic and long-term loading, including traffic-induced and environmental effects, to better assess their serviceability over time.
3. Extend physical testing to include the influence of seismic loading on soil arching and reinforcement performance, evaluating the stability of platforms under earthquake-induced ground motions.

5.2.2 Numerical Studies

1. Develop advanced three-dimensional finite difference models to simulate a broader range of field conditions, including layered soils, variable groundwater levels, and heterogeneous reinforcement properties.
2. Investigate the effect of seismic loading through coupled dynamic analyses, assessing how acceleration and cyclic stress affect stress redistribution, arching, and reinforcement efficiency.
3. Apply probabilistic and sensitivity analyses to quantify the influence of material variability and model assumptions on the predicted performance of load transfer platforms.
4. Enhance numerical procedures for modelling geosynthetic-reinforced platforms, including improved constitutive models for soil and reinforcement, and explore the scalability of results to full-scale engineering projects.

REFERENCES

Abusharar, S.W., Zheng, J.J., Chen, B.G. and Yin, J.H. (2009), "A simplified method for analysis of a piled embankment reinforced with geosynthetics", *Geotextiles and Geomembranes*, Vol. 27 No. 1, pp. 39–52, doi: 10.1016/j.geotexmem.2008.05.002.

Al-Naddaf, M. and Han, J. (2021), "Spring-Based Trapdoor Tests Investigating Soil Arching Stability in Embankment Fill under Localized Surface Loading", *Journal of Geotechnical and Geoenvironmental Engineering*, Vol. 147 No. 9, doi: 10.1061/(asce)gt.1943-5606.0002601.

Al-Naddaf, M.A.M. (2017), "Investigation of Soil Arching Stability Under Static and Cyclic Surface Loading Using Static and Cyclic Surface Loading Using".

Al-Naddaf, M.A.M. (2019), "Investigation of soil arching under different modes of soil movement and surface loading", pp. 1–240.

Alonso, J., Moya, M., Asensio, L., De La Morena, G., Galve, J.P. and Navarro, V. (2022), "A catenary model for the analysis of arching effect in soils and its application to predicting sinkhole collapse", *Geotechnique*, Vol. 72 No. 6, pp. 532–542, doi: 10.1680/jgeot.20.P.235.

Anh Tran, Q., Villard, P. and Dias, D. (2019), "Discrete and Continuum Numerical Modeling of Soil Arching between Piles", *International Journal of Geomechanics*, Vol. 19 No. 2, doi: 10.1061/(asce)gm.1943-5622.0001341.

Bell, A., Jenner, C., Maddison, J. and Vignoles, J. (1994), "Embankment support using geogrids with vibro concrete columns.", *Proc., Proceedings, 5th International Conference on Geotextiles, Geomembranes, and Related Products,* pp. 335–338.

Blanc, M., Rault, G., Thorel, L. and Almeida, M. (2013), "Centrifuge investigation of load transfer mechanisms in a granular mattress above a rigid inclusions network", *Geotextiles and Geomembranes*, Vol. 36, pp. 92–105, doi: 10.1016/j.geotexmem.2012.12.001.

Blanc, M., Thorel, L., Girout, R. and Almeida, M. (2014), "Geosynthetic reinforcement of a granular load transfer platform above rigid inclusions: Comparison between centrifuge testing and analytical modelling", *Geosynthetics International*, Vol. 21 No. 1, pp. 37–52, doi: 10.1680/gein.13.00033.

Bräu, G. (2012), *Recommendations for Design and Analysis of Earth Structures Using Geosynthetic Reinforcements - EBGEO, Second Edition*, *Recommendations for Design and Analysis of Earth Structures Using Geosynthetic Reinforcements - EBGEO, Second Edition*, Berlin, doi: 10.1002/9783433600931.

Briançon, L., Dias, D. and Simon, C. (2015), "Monitoring and numerical investigation of a rigid inclusions-reinforced industrial building", *Canadian Geotechnical Journal*, Vol. 52 No. 10, pp. 1592–1604, doi: 10.1139/cgj-2014-0262.

Briançon, L. and Simon, B. (2012), "Performance of Pile-Supported Embankment over Soft Soil: Full-Scale Experiment", *Journal of Geotechnical and Geoenvironmental Engineering*, Vol. 138 No. 4, pp. 551–561, doi: 10.1061/(asce)gt.1943-5606.0000561.

British Standards Institution. (2010), "Code of practice for strengthened/reinforced soils and other fills.", *Bs 8006-1*.

Broms, B.B. and Wong, I.H. (1985), "Embankment piles", *Proceedings of 3rd International Geotechnical Seminar—Soil Improvement Methods, Singapore: Nanyang Technological Institute,* pp. 167–178.

Card, G.B. and Carter, G.R. (1995), “Case history of a piled embankment in London’s Docklands”, *Engineering Geology of Construction*, pp. 79–84, doi: 10.1016/0148-9062(96)87158-0.

Chen, R.P., Liu, Q.W., Wu, H.N., Wang, H.L. and Meng, F.Y. (2020), “Effect of particle shape on the development of 2D soil arching”, *Computers and Geotechnics*, Vol. 125 No. 103662, doi: 10.1016/j.compgeo.2020.103662.

Chevalier, B., Combe, G. and Villard, P. (2012), “Experimental and discrete element modeling studies of the trapdoor problem: Influence of the macro-mechanical frictional parameters”, *Acta Geotechnica*, Vol. 7 No. 1, pp. 15–39, doi: 10.1007/s11440-011-0152-5.

Collin, J. (2003), : “Column Supported Embankments”, *NHI Ground Improvement Manual–Technical Summary# 10*.

Dang, L.C., Dang, C.C. and Khabbaz, H. (2018), “Numerical Analysis on the Performance of Fibre Reinforced Load Transfer Platform and Deep Mixing Columns Supported Embankments”, *Sustainable Civil Infrastructures*, Springer International Publishing, pp. 157–169, doi: 10.1007/978-3-319-63889-8_13.

Dieguez, C., Ehrlich, M., Mirmoradi, S.H. and Eleutério, J.O. (2020), “Experimental Evaluation of the Effect of Compaction on the Behavior of Geosynthetics-Reinforced Pile-Supported (GRPS) Embankment System”, *Proceeding of 4th Pan American Conference on Geosynthetics*, Rio di Janeiro, Brazil.

Van Eekelen, S.J.M., Bezuijen, A., Lodder, H.J. and Van Tol, A.F. (2012), “Model experiments on piled embankments. Part II”, *Geotextiles and Geomembranes*, Vol. 32, pp. 82–94, doi: 10.1016/j.geotexmem.2011.11.003.

van Eekelen, S.J.M., Bezuijen, A. and van Tol, A.F. (2011), "Analysis and modification of the British Standard BS8006 for the design of piled embankments", *Geotextiles and Geomembranes*, Vol. 29 No. 3, pp. 345–359, doi: 10.1016/j.geotexmem.2011.02.001.

van Eekelen, S.J.M., Bezuijen, A. and van Tol, A.F. (2015), "Validation of analytical models for the design of basal reinforced piled embankments", *Geotextiles and Geomembranes*, Vol. 43 No. 1, pp. 56–81, doi: 10.1016/j.geotexmem.2014.10.002.

Van Eekelen, S.J.M., Bezuijen, A. and Van Tol, A.F. (2013), "An analytical model for arching in piled embankments", *Geotextiles and Geomembranes*, Vol. 39, pp. 78–102, doi: 10.1016/j.geotexmem.2013.07.005.

Van Eekelen, S.J.M. and Brugman, M.H.A. (2016), *Design Guideline Basal Reinforced Piled Embankments*, edited by SJ, E. and MH, B.*Design Guideline Basal Reinforced Piled Embankments*, CRC Press, doi: 10.1201/9781315389806.

El-Gendy, M.M.S., Fayed, A.L. and El-Mossallamy, Y.M. (2020), "Behavior of Embankments Constructed on Soft Soil Deposits Reinforced with Rigid Inclusions", *International Journal of Engineering and Advanced Technology*, Vol. 9 No. 4, pp. 2014–2020, doi: 10.35940/ijeat.d9103.049420.

Ellis, E. and Aslam, R. (2009a), "Arching in piled embankments: comparison of centrifuge tests and predictive methods - part 1 of 2", *Ground Engineering*, Vol. 1, pp. 1–5.

Ellis, E. and Aslam, R. (2009b), "Arching in piled embankments: comparison of centrifuge tests and predictive methods - part 2 of 2", *Ground Engineering*.

Evans, C.H. (1984), “An examination of arching in granular soils”, *Science*.

Gangatharan, R. (2014), “Comparison between piled embankment and load transfer platform - rigid inclusion for soft soil Comparison between piled embankment and load transfer platform - rigid inclusion for soft soil”, No. November, pp. 1–183, doi: 10.13140/2.1.4811.2326.

Gorai, M. (2022), “Geosynthetics - State Engineering Applications Tool The Role and Use of Geo Synthetics in State Engineering and Extensive Projects in India”, *SSRN Electronic Journal*, No. June, doi: 10.2139/ssrn.4152133.

Han, J., Bhandari, A. and Wang, F. (2012), “DEM Analysis of Stresses and Deformations of Geogrid-Reinforced Embankments over Piles”, *International Journal of Geomechanics*, Vol. 12 No. 4, pp. 340–350, doi: 10.1061/(asce)gm.1943-5622.0000050.

Han, J. and Gabr, M.A. (2002), “Numerical Analysis of Geosynthetic-Reinforced and Pile-Supported Earth Platforms over Soft Soil”, *Journal of Geotechnical and Geoenvironmental Engineering*, Vol. 128 No. 1, pp. 44–53, doi: 10.1061/(asce)1090-0241(2002)128:1(44).

He, G.F., Li, Z.G., Yuan, Y., Li, X.H., Hu, L.H. and Zhang, Y. (2018), “Optimization analysis of the factors affecting the soil arching effect between landslide stabilizing piles”, *Natural Resource Modeling*, Vol. 31 No. 2, p. 12148, doi: 10.1111/nrm.12148.

Le Hello, B. and Villard, P. (2009), “Embankments reinforced by piles and geosynthetics-Numerical and experimental studies dealing with the transfer of load on the soil embankment”, *Engineering Geology*, Vol. 106 No. 1–2, pp. 78–91, doi: 10.1016/j.enggeo.2009.03.001.

Hewlett, W.J. and Randolph, M.F. (1988), *Analysis of Piled Embankment*, *Ground Eng*, Vol. 21.

Iglesia, G.R., Einstein, H.H. and Whitman, R. V. (2011), "Validation of Centrifuge Model Scaling for Soil Systems via Trapdoor Tests", *Journal of Geotechnical and Geoenvironmental Engineering*, Vol. 137 No. 11, pp. 1075–1089, doi: 10.1061/(asce)gt.1943-5606.0000517.

Iglesia, G.R., Einstein, H.H. and Whitman, R. V. (2014), "Investigation of Soil Arching with Centrifuge Tests", *Journal of Geotechnical and Geoenvironmental Engineering*, Vol. 140 No. 2, doi: 10.1061/(asce)gt.1943-5606.0000998.

Jenck, O., Dias, D. and Kastner, R. (2005), "Soft ground improvement by vertical rigid piles two-dimensional physical modelling and comparison with current design methods", *Soils and Foundations*, Vol. 45 No. 6, pp. 15–30, doi: 10.3208/sandf.45.15.

Jenck, O., Dias, D. and Kastner, R. (2009), "Discrete element modelling of a granular platform supported by piles in soft soil - Validation on a small scale model test and comparison to a numerical analysis in a continuum", *Computers and Geotechnics*, Vol. 36 No. 6, pp. 917–927, doi: 10.1016/j.compgeo.2009.02.001.

Jones, C., Lawson, C. and Ayres, D. (1992), "Geotextile reinforced piled embankments", *International Journal of Rock Mechanics and Mining Sciences & Geomechanics Abstracts*, Vol. 29, p. A50.

Karl Terzaghi. (1936), "Stress distribution in dry and in saturated sand above a yielding trap-door", *The 1st International Conference on Soil Mechanics and Foundation Engineering*, Cambridge, Massachusetts, pp. 307–311.

Karl Terzaghi. (1943), *Theoretical Soil Mechanics*, *Theoretical Soil Mechanics*.

Kempfert, H.G., Gobel, C., Alexiew, D. and Heitz, C. (2004), "German

recommendations for soil reinforcement above pile-elements", *EUROGeo3, Third Geosynthetic Conference, Munchen*, Vol. 1, pp. 279–283.

King, D.J., Bouazza, A., Gniel, J.R., Rowe, R.K. and Bui, H.H. (2017), "Load-transfer platform behaviour in embankments supported on semi-rigid columns: Implications of the ground reaction curve", *Canadian Geotechnical Journal*, Vol. 54 No. 8, pp. 1158–1175, doi: 10.1139/cgj-2016-0406.

LADANYI B and HOYAUX B. (1969), "Study of the Trap-Door Problem in a Granular Mass", *Canadian Geotechnical Journal*, Vol. 6 No. 1, pp. 1–14, doi: 10.1139/t69-001.

Lai, H. jiang, Zheng, J. jie, Zhang, R. jun and Cui, M. juan. (2016), "Visualization of the formation and features of soil arching within a piled embankment by discrete element method simulation", *Journal of Zhejiang University: Science A*, Vol. 17 No. 10, pp. 803–817, doi: 10.1631/jzus.A1500302.

Lai, H.J., Zheng, J.J., Cui, M.J. and Chu, J. (2020), "'Soil arching' for piled embankments: insights from stress redistribution behaviour of DEM modelling", *Acta Geotechnica*, Vol. 15 No. 8, pp. 2117–2136, doi: 10.1007/s11440-019-00902-x.

Lai, H.J., Zheng, J.J., Zhang, J., Zhang, R.J. and Cui, L. (2014), "DEM analysis of 'soil'-arching within geogrid-reinforced and unreinforced pile-supported embankments", *Computers and Geotechnics*, Vol. 61, pp. 13–23, doi: 10.1016/j.compgeo.2014.04.007.

Low, B.K., Tang, S.K. and Choa, V. (1994), "Arching in piled embankments", *Journal of Geotechnical Engineering*, Vol. 120 No. 11, pp. 1917–1938, doi: 10.1061/(ASCE)0733-9410(1994)120:11(1917).

Magnan, J.P. (1994), “Methods to reduce the settlement of embankments on soft clay: a review”, *Vertical and Horizontal Deformations of Foundations and Embankments, ASCE,* pp. 77–91.

Mánica Malcom, M.Á., Ovando-Shelley, E. and Botero Jaramillo, E. (2016), “Numerical study of the seismic behavior of rigid inclusions in soft Mexico City Clay”, *Journal of Earthquake Engineering*, Vol. 20 No. 3, pp. 447–475, doi: 10.1080/13632469.2015.1085462.

NGG. (2004), “Nordic Guidelines for reinforced soils and fills”, *Nordic Geosynthetic Group of the Nordic Geotechnical Societies, Nordic Industrial Fund*, pp. 1–204.

Patel, A. (2019), “Geotechnical Investigations and Improvement of Ground Conditions”, *Geotechnical Investigations and Improvement of Ground Conditions*, pp. 1–201, doi: 10.1016/C2018-0-01307-9.

der Peet, T.C. (2014), “Arching in basal reinforced piled embankments, numerical validation of the Concentric Arches model”, Delft, the Netherlands.

Van Pham, H. and Dias, D. (2021), “3D Numerical Modeling of Rigid Inclusion-Improved Soft Soils Under Monotonic and Cyclic Loading—Case of a Small-Scale Laboratory Experiment”, *Applied Sciences (Switzerland)*, Vol. 11 No. 4, pp. 1–18, doi: 10.3390/app11041426.

Pham, T.A. (2020), “Load-deformation of piled embankments considering geosynthetic membrane effect and interface friction”, *Geosynthetics International*, Vol. 27 No. 3, pp. 275–300, doi: 10.1680/jgein.19.00030.

Pham, T.A. and Dias, D. (2021), “3D numerical study of the performance of geosynthetic-reinforced and pile-supported embankments”, *Soils and Foundations*, Vol. 61 No. 5, pp. 1319–1342, doi: 10.1016/j.sandf.2021.07.002.

Pham, T.A., Tran, Q.A., Villard, P. and Dias, D. (2024), “Numerical Analysis of Geosynthetic-Reinforced and Pile-Supported Embankments Considering Integrated Soil-Structure Interactions”, *Geotechnical and Geological Engineering*, Vol. 42 No. 1, pp. 185–206, doi: 10.1007/s10706-023-02564-9.

Reid, W.M. and Buchanan, N.W. (1984), “Bridge Approach Support Piling.”, pp. 267–274.

Rui, R., Han, J., Zhang, L., Zhai, Y., Cheng, Z. and Chen, C. (2020), “Simplified method for estimating vertical stress-settlement responses of piled embankments on soft soils”, *Computers and Geotechnics*, Vol. 119 No. 103365, doi: 10.1016/j.compgeo.2019.103365.

Rui, R., Van Tol, A.F., Xia, Y.Y., Van Eekelen, S.J.M. and Hu, G. (2016), “Investigation of soil-arching development in dense sand by 2D model tests”, *Geotechnical Testing Journal*, Vol. 39 No. 3, pp. 415–430, doi: 10.1520/GTJ20150130.

Rui, R., van Tol, F., Xia, X.L., van Eekelen, S., Hu, G. and Xia, Y. you. (2016), “Evolution of soil arching; 2D DEM simulations”, *Computers and Geotechnics*, Vol. 73, pp. 199–209, doi: 10.1016/j.compgeo.2015.12.006.

Rui, R., Ye, Y. qiu, Han, J., Zhai, Y. xin, Wan, Y., Chen, C. and Zhang, L. (2022), “Two-dimensional soil arching evolution in geosynthetic-reinforced pile-supported embankments over voids”, *Geotextiles and Geomembranes*, Vol. 50 No. 1, pp. 82–98, doi: 10.1016/j.geotexmem.2021.09.003.

Russell, D. and Pierpoint, N. (1997), “An assessment of design methods for piled embankments”, *Ground Engineering*, Vol. 30 No. 10, pp. 39–44.

Simon, B. and Terrasol. (2012), “General report S5 Rigid Inclusions and

Stone Columns", *Conference: Recent Research, Advances and Execution Aspects of Ground Improvement*.

T.J.M. den Boogert. (2011), *Piled Embankments with Geosynthetic Reinforcement*.

Wang, K., Cao, J., Wang, X. and Ning, Y. (2021), "Soil arching of piled embankment in equal settlement pattern: A discrete element analysis", *Symmetry*, Vol. 13 No. 9, doi: 10.3390/sym13091627.

Ye, Y. qiu, Han, J. and Rui, R. (2023), "Evaluation of lightweight aggregate to reduce vertical stresses and improve load transfer in pile-supported embankments", *Transportation Geotechnics*, Vol. 43, doi: 10.1016/j.trgeo.2023.101125.

Yun-min, C., Wei-ping, C. and Ren-peng, C. (2008), "An experimental investigation of soil arching within basal reinforced and unreinforced piled embankments", *Geotextiles and Geomembranes*, Vol. 26 No. 2, pp. 164–174, doi: 10.1016/j.geotexmem.2007.05.004.

Zhang, J., Jia, Y., Zheng, Y. and Miao, C. (2021), "Dem simulation of the load transfer mechanism of a grps embankment with a fixed geogrid technique", *Applied Sciences (Switzerland)*, Vol. 11 No. 19, doi: 10.3390/app11198814.

Zhang, S., Liu, Y., Yuan, S., Liu, X., Jiang, G. and Liu, J. (2024), "Performance of composite foundations with different load transfer platforms and substratum stiffness over silty clay", *Journal of Mountain Science*, Vol. 21 No. 5, pp. 1761–1774, doi: 10.1007/s11629-023-8489-4.

Zhang, Z., Ye, G., Tao, F. and Han, J. (2018), "2-D numerical investigation on load transfer in pile-supported fill platforms subjected to cyclic loading", *11th International Conference on Geosynthetics 2018, ICG*

2018, Vol. 3, Seoul, Korea, pp. 2373–2380.

Zhuang, Y. and Wang, K.Y. (2018), "Finite-element analysis of arching in highway piled embankments subjected to moving vehicle loads", *Geotechnique*, Vol. 68 No. 10, pp. 857–868, doi: 10.1680/jgeot.16.P.266.

المستخلص

يُعَدّ إنشاء الردم وأنظمة الأساسات فوق الترب الضعيفة أو القابلة للانضغاط من العمليات التي غالبًا ما تتطلب تقنيات متقدمة لتحسين التربة لضمان الاستقرار وقابلية الخدمة. وقد أثبتت منصات نقل الأحمال المدعمة بالجيوسنثيتك (GRLTP)عند دمجها مع الدعامات الصلبة فعاليتها في إعادة توزيع الإجهادات العمودية وتقليل الهبوطات التفاضلية. ومع ذلك، تُظهر الدراسات السابقة وجود فجوة واضحة فيما يتعلق بالتأثير المشترك لكل من الإجهاد العمودي المطبق، مقدار إزاحة فخ الهبوط(Trapdoor) ، شكل الفخ وترتيبه، أبعاد القاعدة وموقعها، إضافة إلى استخدام التسليح بالجيوسنثيتك على أداء منصات نقل الأحمال تحت ظروف الهبوط الموضعي. نادرًا ما تناولت الدراسات السابقة هذه العوامل مجتمعة ضمن إطار صارم قائم على طريقة الفروق المحدودة.

تتصدى هذه الدراسة لهذه الفجوة البحثية من خلال استخدام طريقة الفروق المحدودة (FDM) المطبقة في برنامج FLAC3Dلتنفيذ تحليل عددي ثلاثي الأبعاد متقدم لمنصات نقل الأحمال فوق دعامات صلبة خاضعة لهبوط ناتج عن فخ هبوط وحمل سطحي. وقد تم إعداد مجموعة من النماذج المُعايرة لدراسة تأثير الإزاحة، وعرض الفخ وتعدده، وحجم القاعدة وموقعها، وعمق وترتيب التسليح. وأظهرت عملية التحقق من النتائج بمقارنتها مع اختبارات مخبرية منشورة توافقًا جيدًا، إذ بلغ معدل الخطأ الجذري التربيعي (RMSE) نحو 3.18%، مما يؤكد دقة النماذج وصلاحيتها.

أظهرت النتائج أن ظاهرة تقوس التربة (Soil Arching) تتطور بسرعة عند إزاحات صغيرة نسبيًا، مما يؤدي إلى إعادة توجيه الإجهادات نحو الدعامات المجاورة. ومع ذلك، فإن كفاءة هذا التقوس تتراجع تدريجيًا مع استمرار الإزاحة أو تحت الأحمال السطحية العالية، حيث تعاود الإجهادات العمودية التركّز فوق مناطق الخضوع. وقد تبيّن أن التسليح يلعب دورًا جوهريًا في تعزيز الاستقرار، حيث حققت طبقة واحدة من الجيوجريد بالقرب من مستوى الهبوط نسبة تقليل إجهاد (SRR) تبلغ حوالي 0.75، مع تقاطع إجهاد TC–SE عند حوالي 70 كيلوباسكال، وهو ما يمثل أداءً جيدًا. علاوة على ذلك، وفرت طبقتان من التسليح تحسينًا أكبر، إذ حققت زيادة في الأداء بنسبة 60% مقارنة بوجود طبقة واحدة، مما رفع قيمة تقاطع الإجهاد TC–SE من 70 إلى 110 كيلوباسكال مع نسبة تكلفة–فائدة ممتازة. ومع ذلك، فإن إضافة طبقة ثالثة من التسليح لم تحقق سوى مكاسب طفيفة مع كفاءة تكلفة–فائدة ضعيفة.

كذلك كشفت الدراسة أن زيادة عدد أفخاخ الهبوط تُغيّر بشكل جوهري آلية نقل الأحمال. ففي الأنظمة المزدوجة والثلاثية للفخاخ، أدت الدعامات الوسيطة إلى تقسيم الردم إلى عدة مناطق متداخلة للتقوس، مما قلل الحمل المباشر على الفخاخ وساهم في توزيع الإجهادات بشكل أكثر انتظامًا عبر الدعامات. كما ساهمت زيادة عرض القواعد وزيادة الإزاحة عن مركز الفخ في تحسين كفاءة نقل الأحمال. وبشكل عام، تقدم هذه النتائج فهمًا شاملًا لسلوك منصات نقل الأحمال تحت ظروف هبوط متعدد الفخاخ، وتوفر رؤى دقيقة لتحسين تصميم الردم المدعوم بالدعامات.

جمهورية العراق

وزارة التعليم العالي و البحث العلمي

جامعة كربلاء

كلية الهندسة

قسم الهندسة المدنية

التحليل بطريقة الفروقات المنتهية لمنصة نقل الأحمال المدعمة بالجيوغريد فوق الدعائم الصلبة

رسالة مقدمة الى مجلس كلية الهندسة / جامعة كربلاء وهي جزء من متطلبات نيل درجة الماجستير في علوم الهندسة المدنية

المؤلف:

الق خليل ابراهيم

باشراف :

أ.م.د. مهدي عباس مهدي النداف

أ.م.د. سيف محمد جواد

ربيع الثاني - 1447 أيلول - 2025